Volume 96 • Number 1• October 2025
Established in 1923 • ISSN 1945-0702

The Chemist

Journal of the American Institute of Chemists

In this Issue

Official journal of
The American Institute of Chemists, Inc.
http://www.theaic.org/pub_thechemist_journals/

The Chemist

Established in 1923, The Chemist is the official publication of The American Institute of Chemists, Inc. (AIC). The Chemist was published quarterly in magazine format up until 2006. The Chemist is currently being set up and formatted as an online journal.

Subscription: $35 per year to members, $100 per year to non-members. Single copy: $50.

The Chemist (ISSN-0009-3025) is published online by The American Institute of Chemists, Inc.

Volume 96 | Issue 1 | 2025

The Chemist

Journal of the American Institute of Chemists

Table of Contents (cont.)

Editorial

Alexander G. Zestos, Ph. D
American University

Nayiri M. Kaissarian, Ph.D
Montgomery College

Dear readers,

As we announce another version of The Chemist, we would like to acknowledge significant advancements in the field of chemical sciences despite the challenges that scientists, researchers, and educators alike have had to endure. Just recently, the Fall 2025 Conference of the American Chemical Society (ACS) was hosted at the Walter E. Washington Convention Center and surrounding venues in Washington, D.C. The return of the American Chemical Society national conference to the nation's capital puts chemistry and related applications to the forefront of the nation's and world's priorities for scientific advancement.

During the American Institute of Chemists (AIC) Chemical Pioneers Symposium in May of this year, Prof. Dale Boger was honored as a 2025 Chemical Pioneer and presented research from his laboratory at the Scripps Research Institute in La Jolla, California. In the headlining article for this year's issue, Dr. Boger highlighted the total syntheses of a series of natural products targeted by virtue of their biological properties. These complex structures inspired divergent synthetic strategies and synthetic methodology designed especially for the natural products of interest. Many of the molecules synthesized include vancomycin, maxamycins, ramoplanin, vinblastine, vincristine, bleomycin A, and several others including more than 100 natural products have been prepared by total syntheses, of which most represent biologically active natural products chosen by virtue of their properties. Many of these products contain cyclic peptides including glycopeptide antibiotics and several DNA binding natural products such as DNA binding, alkylation, and cleaving agents that exhibit antitumor activity.

Other papers in this issue also detail total synthesis including current trends in esters synthesis and the synthesis of dimethyl methylene phosphate, which is an innovative phosphorylated compound with broad-spectrum potential. Several adsorption studies were also part of the issue including humic acid adsorption on natural fiber surface-modified polypropylene and the adsorptive removal of Congo red dye by a synthesized dual ligand. The synthesis and characterization of several natural products were also discussed and detailed in this journal issue including the structural elucidation of ethanol extraction of *Plectranthus zeylanicus* and the antimicrobial and antioxidant properties of extracts from the leaves of Syrian *Juniperus excelsa* M. Bieb. Furthermore, more fundamental articles were also published on metal complexes of ligan 6-amino penicillanic acid (6-APA) including biological activity and molecular docking applications and the reactions of C2H5O2 and C2H5 radicals on acidic and basic surfaces.

As the summer comes to an end and the academic year begins, we wish you the very best going forward and hope to receive your submissions to The Chemist!

The Chemist
Journal of the American Institute of Chemists

Supernatural Products

Dale L. Boger

Department of Chemistry, The Scripps Research Institute, La Jolla, California 92037, USA

(E-mail: boger@scripps.edu)

Abstract: The total syntheses of a series of natural products targeted by virtue of their biological properties are highlighted. Their complex structures inspired the development of new divergent synthetic strategies and synthetic methodology designed especially for the natural products of interest. The subsequent extensions to the divergent total syntheses of key analogues that bear deep-seated structural changes are summarized. They were used to define the structure–function properties of the natural products, to identify their biological target if unknown, to define fundamental features of their interaction with their biological target, and ultimately, to improve their properties, producing supernatural products endowed with features not found expressed by the natural products themselves.

Key Words: natural products, supernatural products, total synthesis, divergent synthesis, medicinal chemistry

1. Introduction

Natural products have provided and continue to define unique opportunities to address problems in biology and medicine. These opportunities have grown as the methods to identify their mechanisms of action and biological targets have improved and as the techniques used to directly determine their target bound structures have advanced [1]. With advances in organic chemistry and especially the total synthesis of complex natural products, the examination of key partial structures, compounds that contain deep-seated structural modifications, their unnatural diastereomers, and even their enantiomers provide a powerful complement to such studies [2–4]. Well-designed modifications in natural products may be used to address the structural basis of their interaction with biological targets, to define fundamental relationships between structure and activity, functional reactivity, and biological properties, or to mitigate liabilities. Because natural products integrate a constellation of properties into compact, highly-functionalized molecules, each structural feature and substituent are often

thought to contribute to the biological activity. This is especially true when their targeted properties are directly related to their emergence in nature where they have undergone natural selection optimization. However, as highlighted herein, there are many examples where even a single atom change can substantially improve on their biological properties [5]. In such work, a challenging feature with natural products is to understand the subtle design elements integrated into their structures and then to rationally extend them to provide more selective, more potent, or more efficacious compounds.

The studies are enabled by the development of divergent synthetic strategies and methods that advance the underlying systematic medicinal chemistry, targeting compounds bearing deep-seated structural changes not accessible by semisynthetic or biosynthetic means. In the work summarized, key structural modifications were designed to also improve defined properties, to endow the natural product with new properties or additional mechanisms of action, or to overcome intrinsic limitations of the natural product itself. The efforts provided supernatural products, a term introduced by my colleague, Ryan Shenvi, with properties superseding the parent natural product [6]. Although introduced with tongue and cheek humor by Shenvi just before Halloween, we have become enamored by the ability of the term "supernatural product" to describe such advances for not only experts in the field but especially for a general audience who may not appreciate the nature or magnitude of the accomplishments [7–9]. The design principles for creating the supernatural products highlighted include those that improve potency, increase selectivity, enhance durability toward raising resistance, broaden the spectrum of activity, improve chemical or metabolic stability, overcome limiting physical properties, add new additional mechanisms of action, enhance PK properties, overcome drug resistance, and/or improve *in vivo* efficacy. While some improvements may be regarded as iterative enhancements, others live up to their characterization as supernatural products.

2. Naturally Occurring Cyclic Peptides Including the Glycopeptide Antibiotics

A long-standing program has focused on the total synthesis and evaluation of naturally occurring biologically active cyclic peptides. The most recognized of the efforts are the total syntheses of naturally occurring glycolpeptide antibiotics including vancomycin and its aglycon, teicoplanin, ristocetin and ramoplanin aglycons, chloropeptin I and II, and the complestatins [10]. Along with these studies, we rationally redesigned the structure of vancomycin to achieve dual binding to both D-Ala-D-Ala and D-Ala-D-Lac, altering a single atom in the binding pocket such that it remains active against vancomycin-sensitive bacteria (e.g., MRSA), but is equally active against vancomycin-resistant bacteria (e.g., VRSA, VRE). The studies first defined the origin of the destabilized binding to the altered D-Ala-D-Lac target in resistant bacteria (100-fold derived from repulsive lone pair/lone pair interaction, 10-fold from lost H-bond) [11]. This led to the design and total syntheses of [Ψ[CH_2NH]Tpg^4]vancomycin and

[Ψ[C(=NH)NH]Tpg[4]] vancomycin and their earlier aglycons, both of which displayed the dual ligand binding affinity and reinstated activity against vancomycin-resistant bacteria while maintaining activity against vancomycin sensitive bacteria. This was followed by the syntheses of peripherally-modified derivatives that we named maxamycins that: (1) contain a binding pocket and two synergistic peripheral modifications, (2) are endowed with three independent mechanisms of action only one of which is dependent on D-Ala-D-Ala binding, (3) display broad spectrum activity (e.g., MRSA, VanA/VanB VRSA and VRE) at remarkable potencies (MICs = 0.01 μg/mL), and (4) are durable antibiotics incapable of raising resistance in vitro and are potentially capable of extensive use for decades without fear of raising resistance [12,13]. With the discovery of the potent and durable activity of the maxamycins, a next generation total synthesis of vancomycin was developed that substantially improved synthetic access (Figure 1) [14].

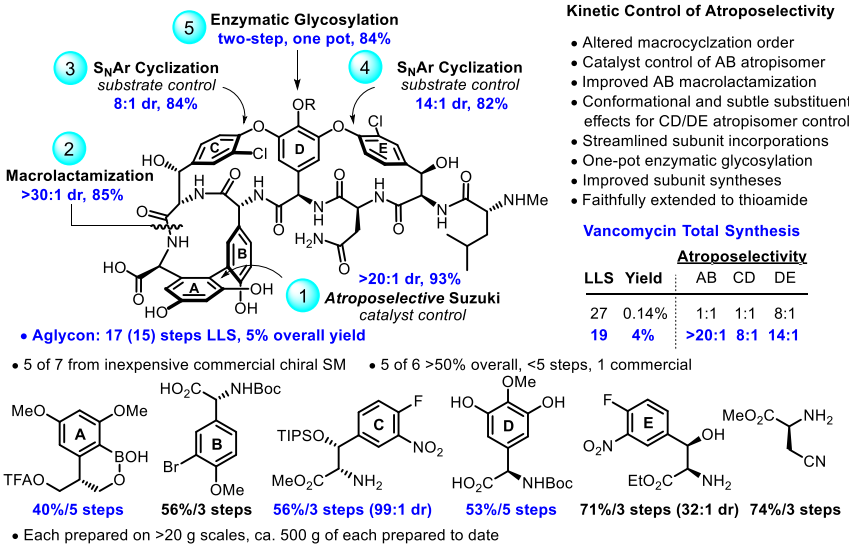

Figure 1. Next Generation Total Synthesis of Vancomycin

This divergent synthetic approach was subsequently further improved and implemented for the total syntheses of any maxamycin from a single late-stage intermediate, permitting traditional medicinal chemistry optimization on the complex glycolpeptide antibiotic [15]. The residue 4-thioamide of this late-stage intermediate, [Ψ[C(=S)NH]Tpg[4]]vancomycin, can be and was directly converted to any pocket-modified derivative that displays the dual ligand binding and paired with any combination of two different peripheral modifications, each introducing independent synergistic mechanisms of action without the use of protecting groups (Figure 2).

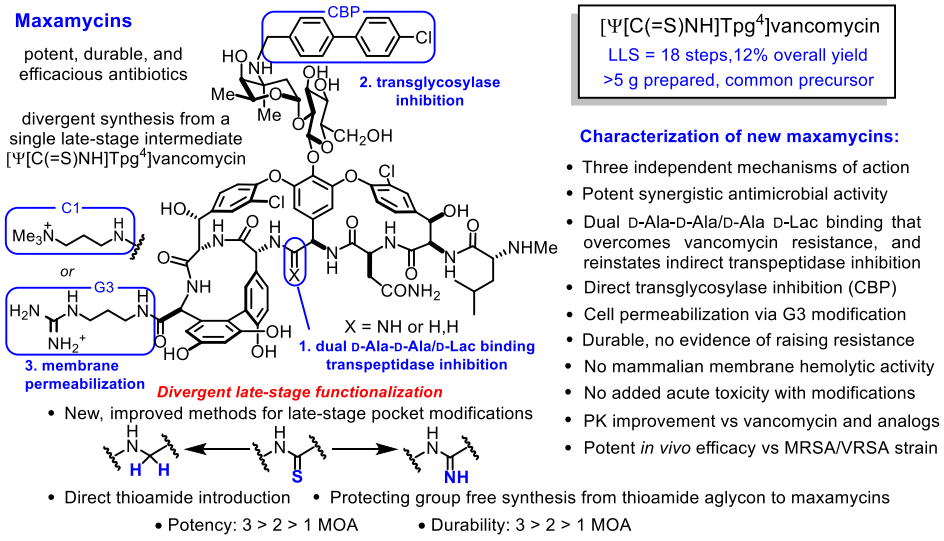

Figure 2. Maxamycins

A class of true supernatural products that supersede the natural product, the maxamycins possess pocket modifications that overcome vancomycin resistance, reinstating transpeptidase inhibition and cell wall synthesis inhibition by binding to the altered target substrate D-Ala-D-Lac, while maintaining binding to the original target D-Ala-D-Ala of vancomycin.

In addition, the peripheral modifications introduce two new synergistic mechanisms of action not seen with vancomycin itself. One peripheral modification (CBP modification) results in the direct competitive inhibition of transglycosylase affecting a separate step in cell wall biosynthesis and the second (G3 modification) induces cell permeability reducing cell wall integrity likely through cell wall teichoic acid binding and induced autolysin release, both of which are independent of one another and of D-Ala-D-Ala/D-Lac binding [15]. The synergic enhancement in activity derived from each modification, each of which increases both potency and durability against raising resistance, requires incorporation into a single molecule, indicating that it arises from the simultaneous expression of all three mechanisms of action at the same time and at the same place in the cell wall (Figure 3).

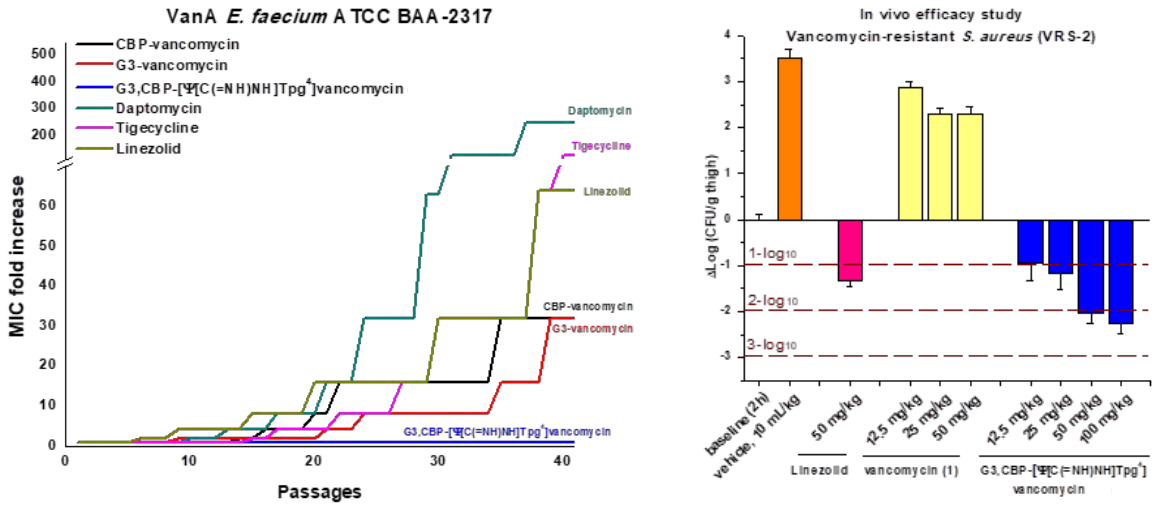

Figure 3. Left: Resistance acquisition upon serial passaging of a VanA VRE strain in the presence of compound and daily MIC determination. Lack of resistance acquisition for the maxamycin G3,CBP-[Ψ[C(=NH)NH]Tpg^4] vancomycin vs CBP-vancomycin, G3-vancomycin, and the frontline therapies daptomycin, linezolid, and tigecycline. Right: *In vivo* efficacy of the G3,CBP-[Ψ[C(=NH)NH]Tpg^4]vancomycin vs linezolid and vancomycin plotted as a dose-dependent bactericidal effect relative to 2 h baseline against the feared multidrug-resistant and vancomycin-resistant *S. aureus* strain VRS-2 in the mouse thigh infection model.

In the first such study, a prototypical maxamycin (G3,CBP-[Ψ[C(=N)NH]Tpg^4]vancomycin) was shown to exhibit efficacious *in vivo* activity against the feared multidrug-resistant (MRSA) and vancomycin-resistant (VRSA) *S. aureus* bacterial strain (VanA VRS-2) for which vancomycin is inactive (Figure 3). Moreover, it was found that the C-terminus modifications (C1 and G3) offset the impact of hydrophobic vancosamine substitution, providing compounds with near ideal *in vivo* PK properties mitigating the short terminal half-life (0.5–1.3 h, $t_{1/2}$), low exposure (AUC), inconsistent volume of distribution (V_d), and rapid clearance (CL) of vancomycin and the poor dose proportionality and problematic long terminal half-life of CBP-vancomycin [15].

A reduction in the complexity of the glycolpeptide structure through addition of two benign aryl chlorides that remove two synthetically challenging atropisomer elements (tetrachlorovancomycin [16] and the corresponding tetrachloromaxamycins [17]) permits an even more streamlined and scalable total synthesis and new opportunities for deep-seated core modifications.

The ramoplanins are naturally occurring lipoglycodepsipeptides that are 2–10-fold more active than vancomycin against Gram-positive bacteria [18]. Ramoplanin A2 disrupts bacterial cell wall biosynthesis, inhibiting the intracellular conversion of lipid intermediate I to lipid intermediate II and the more accessible extracellular transglycosylase-catalyzed incorporation of lipid II into the glycan strand, steps that precede the site of action of vancomycin. Resistance to ramoplanin has not been detected, and cross resistance between ramoplanin and vancomycin has not been ob-

served. Thus, it remains equally active against vancomycin-resistant organisms, including VanA/VanB VRE. Like vancomycin, ramoplanin acts by binding peptidoglycan precursors (lipid II > lipid I), sequestering these substrates from enzyme access, although the structural details of these interactions are not yet defined. In fact, ramoplanin embodies all the characteristics of vancomycin that contribute to its durability against resistance development. However, its instability derived from rapid depsipeptide hydrolysis precludes use for systemic infections and has limited its clinical exploration. Our development of the first and still only convergent total synthesis of the ramoplanin A1–A3 aglycons set the stage for its use in the preparation of key analogues. In these efforts, we demonstrated that synthetic [L-Dap^2]ramoplanin A2 aglycon, which bears a linking amide in place of the sensitive depsipeptide ester in the backbone of the 49-membered macrocycle, is roughly 2-fold more potent ramoplanin A2 and its aglycon, and stable t**6** hydrolytic cleavage (Figure 4) [19].

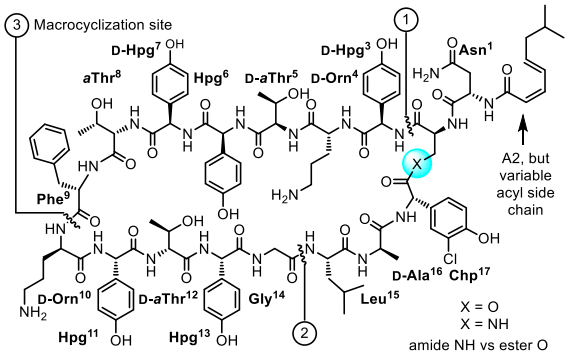

Figure 4. Structure of ramoplanin A2 (X = O) and [L-Dap^2]ramoplanin A2 (X = NH) aglycons and the single heavy atom exchange in the 49-membered macrocycle that mitigates hydrolytic instability that limits the clinical use of ramoplanin.

Here, the single atom exchange in the compound does not impact the interaction of the natural product with its biological target or substantially alter its functional activity, but it mitigates its limiting metabolic instability. In our studies and on this stable amide template, an alanine scan of the complete structure was conducted (15 analogues prepared by total synthesis), establishing the impact and potential role of each residue and providing insights into the nature of its complex with lipid II [20]. Highlights derived from the alanine scan include: (1) the verification of the dominant role of Orn (10) (>500-fold reduction) consistent with an integral role in lipid II diphosphate binding, (2) the more modest impact of Orn (4) (44-fold), suggesting that its role in binding lipid II is not as critical, (3) the disparate importance of each residue in a putative lipid II recognition domain proposed in early work (residues 3–10), (4) the significant impact (>20-fold) of nearly every residue in the dimerization domain (residues 11–14) later defined by Walker reflective of its greater importance, and (5) the lack of importance of the hydrophobic residues 16–17 within the flexible loop that represents the membrane interacting domain (residues 15–17, 1–2). We also showed that the lipid

side chain is essential for antimicrobial activity (200–800-fold reduction) and, in collaboration with Walker, showed it has no impact on lipid II binding or trans-glycosylase inhibition, indicating that its role is likely to anchor the antibiotic to the bacterial cell wall [19]. Complementing these studies on the stable amide-modified ramoplanin and other related studies, Walker used inhibition kinetics and binding assays to establish that ramoplanin preferentially inhibits the transglycosylase versus MurG catalyzed reactions of their substrates lipid II versus lipid I, that it exhibits a greater affinity for lipid II (K_D = 3 nM) than lipid I (K_D = 170 nM), and that it binds with a 2:1 stoichiometry consistent with functional dimerization [21].

Additional studies include efforts culminating in the total syntheses of the series of antitumor agents that act as DNA bisintercalators (sandramycin, luzopeptins A–C, quinoxapeptins A–C, thiocoraline, BE-22179, and triostin A), inhibitors of protein synthesis including cycloisodityrosine, deoxybouvardin, bouvardin/RA-VII, inhibitors of p53/MDM2 binding including chlorofusin and its diastereomers, as well as the natural products K-13, OF4949, piperazinomycin, HUN-7293, and streptide.

3. Vinblastine

The discovery of vinblastine and its antitumor activity led to the identification of tubulin as an especially effective oncology drug target [22]. Vinblastine binds at the tubulin α/β dimer−dimer interface where it destabilizes microtubulin assembly derived from the repetitive head-to-tail tubulin binding. Even by today's standards, vinblastine and the related natural product vincristine are superb clinical drugs. They, and their biological target tubulin, remain the subject of intensive investigations because of their clinical importance in medicine, complex structures, low natural abundance, and unique mechanism of action. Following work that provided total syntheses of vinblastine and vincristine, our studies have probed the importance and role of the vindoline C16 methoxy group, C4 acetate, C5 ethyl substituent, C6–C7 double bond, and vindoline core itself, as well as the upper subunit C20' ethyl substituent, C16' methyl ester, and added C10'/C12' indole substituents [23]. We defined the importance and anchoring role of the C20' Et group and introduced the concept of "added benign complexity (ABC)" with an example that increased functional activity and tubulin binding affinity 10-fold. These and related studies showed that essentially every feature of the vinblastine core structure, every functional group and every substituent productively contributes to its properties. Unlike the removal of structural features or substituents that have a detrimental impact, the additions of new structural features not found in the natural product have been found that enhance target tubulin binding affinity and functional activity while simultaneously disrupting Pgp binding, transport, and functional resistance. Enabled by methodology that we introduced, a series of previously inaccessible vinblastine C20' modifications were disclosed that display remarkable properties: 20' ureas (30-fold increase in potency, reduced resistance due to Pgp efflux) [24], ultra-potent 20' ureas (stunning 100-fold increase in potency derived from further disruption of the tubulin protein–protein interaction) [25], and

vinblastine 20’ amides that completely overcome and mitigate resistance derived from Pgp overexpression and drug efflux (Figure 5) [26].

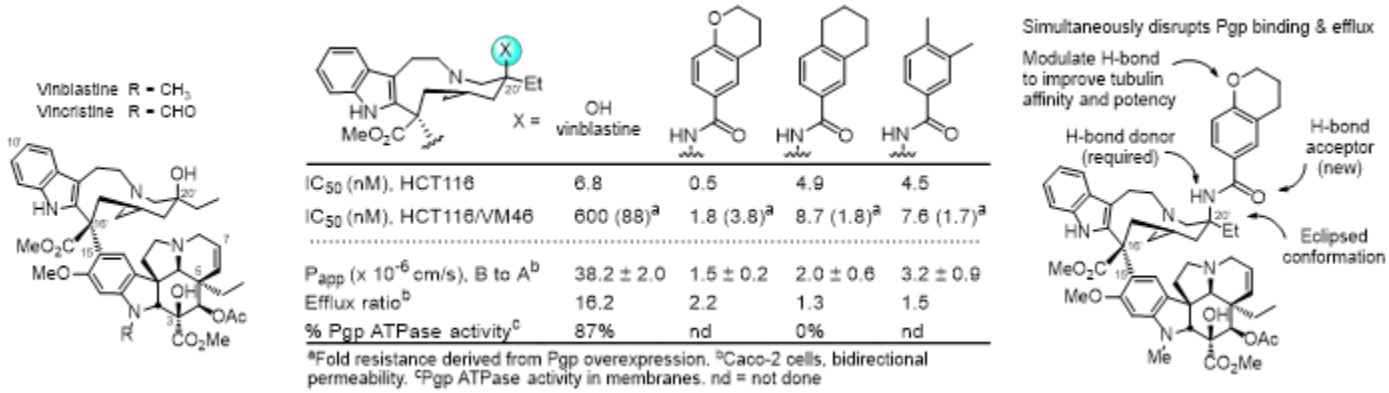

	OH vinblastine			
IC_{50} (nM), HCT116	6.8	0.5	4.9	4.5
IC_{50} (nM), HCT116/VM46	600 (88)[a]	1.8 (3.8)[a]	8.7 (1.8)[a]	7.6 (1.7)[a]
P_{app} (x 10^{-6} cm/s), B to A[b]	38.2 ± 2.0	1.5 ± 0.2	2.0 ± 0.6	3.2 ± 0.9
Efflux ratio[b]	16.2	2.2	1.3	1.5
% Pgp ATPase activity[c]	87%	nd	0%	nd

[a]Fold resistance derived from Pgp overexpression. [b]Caco-2 cells, bidirectional permeability. [c]Pgp ATPase activity in membranes. nd = not done

Figure 5. Left: Structures of vinblastine and vincristine. Right: Representative vinblastine C20' amides that match or exceed the potency of vinblastine, eliminate Pgp binding and efflux, and overcome vinblastine resistance derived from Pgp overexpression.

These studies were based on well-founded rationales, used systematic well-designed analogues (>400 analogues) to answer fundamental questions on the molecular interaction of vinblastine with its biological target (tubulin) or targeting its source of resistance (Pgp), enlisted traditional medicinal chemistry correlations to optimize activities, were accessed by new methodology developed for this purpose, and relied on a series of key functional and on-target assays to produce supernatural products far exceeding the potency and properties on the natural product.

Approaches to improve the biological properties of natural products often strive to identify the essential pharmacophore to simplify the structure or make functional group changes to improve biological target affinity or functional activity, change physical properties, enhance stability, or introduce conformational constraints. Aside from accessible semi-synthetic modifications of existing functional groups, rarely does one consider using chemical synthesis to add molecular complexity to the natural product. In part, this may be attributed to the added challenge intrinsic in the synthesis of an even more complex compound. We discovered synthetically-derived, structurally more complex vinblastines inaccessible from the natural product itself that are a stunning 100-fold more active (IC_{50}’s 50–75 pM vs 7 nM, HCT116) [25], and that are now accessible because of advances in the total synthesis of the natural product (Figure 6).

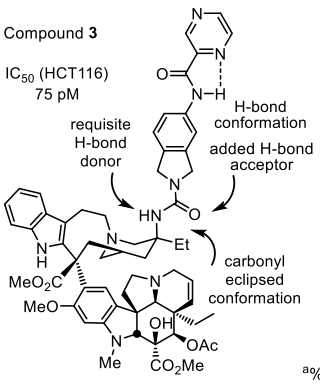

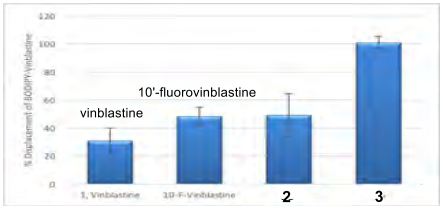

compd	% displacement[a]	IC_{50} (nM) HCT116	IC_{50} (nM) HCT116/VM46	
1, vinblastine	31 ± 9%	6.8	600	(100)[b]
10'-fluorovinblastine	48 ± 7%	0.3	3.5	(12)[b]
2	49 ± 15%	0.6	7.5	(12)[b]
3	101 ± 4%	0.07	0.8	(12)[b]

[a]% Displacement of tubulin-bound BODIPY-vinblastine. [b]Fold difference

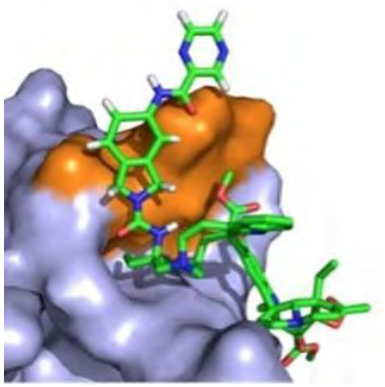

Figure 6. Representative ultrapotent vinblastine and correlation of cell growth inhibition with tubulin binding measured by displacement of tubulin-bound BODIPY-vinblastine. Model of the ultrapotent vinblastine 3 in the tubulin binding site with the interacting a-subunit removed. The extended C20'-urea group continues to bind in a small groove along the extended dimer-dimer interface (in tan), making additional α-tubulin contacts and further disrupting the head-to-tail tubulin α/β dimer−dimer interface.

The newly discovered ultra-potent vinblastines bind tubulin with much higher affinity and further disrupt the tubulin head-to-tail α/β dimer–dimer interaction by virtue of the strategic placement of an added conformationally well-defined, rigid, and extended C20' urea along the continuing head-to-tail tubulin α/β dimer−dimer interface. In this case, the added molecular complexity was used to markedly enhance target binding and functional biological activity (100-fold) [25].

In these efforts, vinblastine served as the inspiration for the discovery of a powerful intramolecular 1,3,4-oxadiazole cascade [4+2]/[3+2] cycloaddition reaction for the synthesis of the vindoline-derived lower subunit [27], development of a diastereospecific Fe(III)-mediated biomimetic coupling of vindoline with catharanthine to provide anhydrovinblastine [28–30], and discovery of a powerful free radical hydrogen atom transfer functionalization of alkenes (Fe(III)–$NaBH_4$/radical traps, [31,32]) that permits the *in situ* C20' functionalization used to install the vinblastine C20' alcohol or corresponding amine for amide and urea derivatization, stimulating further developments in the MHAT field (Figure 7).

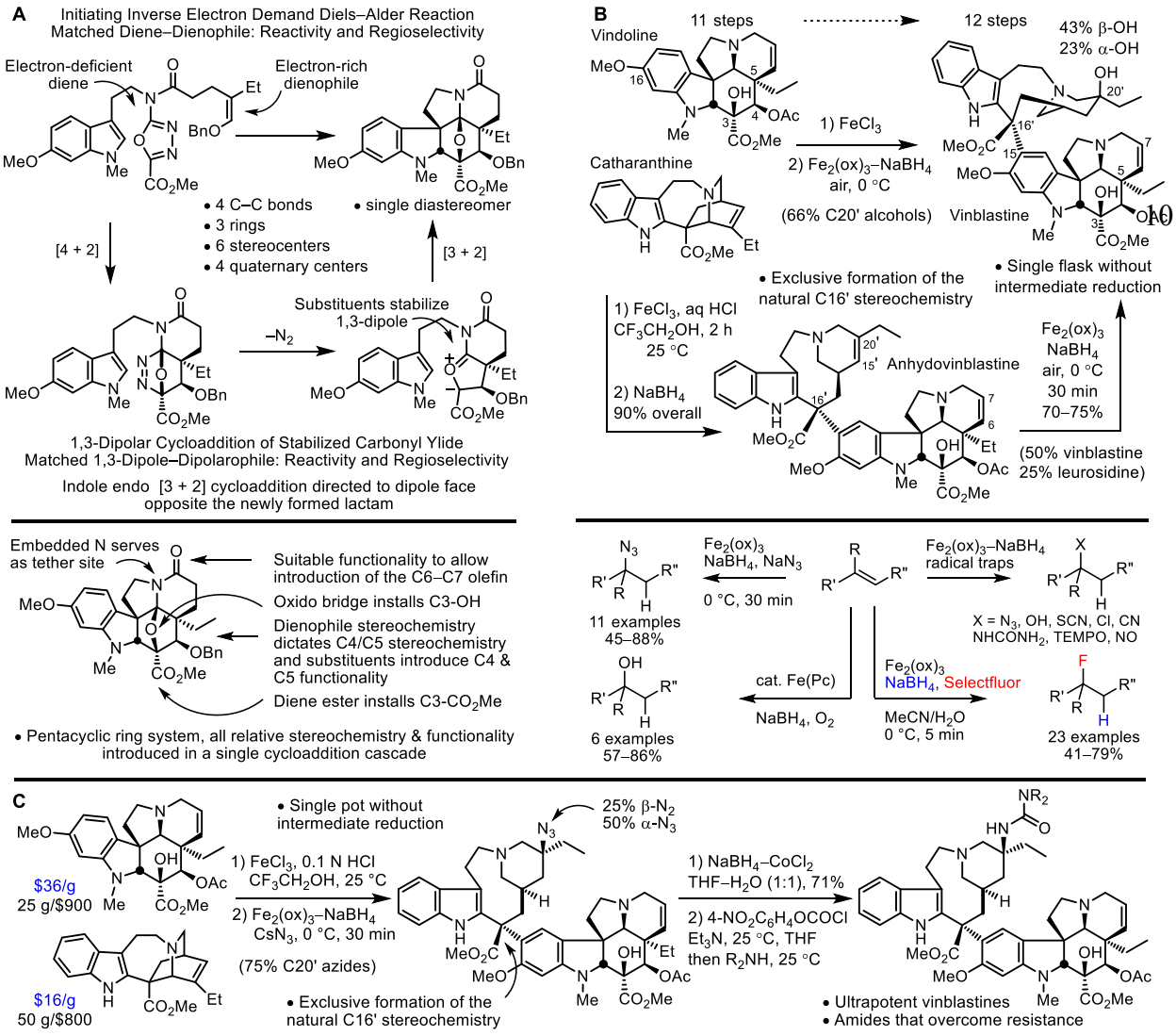

Figure 7. A: Key cycloaddition cascade. B: Fe(III)-promoted coupling of vindoline and catharanthine. Fe(III)-mediated MHAT free radical oxidation for C20' alcohol introduction and generalization of methodology for alkene functionalization. C: Three-step synthesis of ultrapotent vinblastine C20' ureas and amides.

Over 400 analogues of vinblastine were prepared, and it is a tribute to the advances in organic synthesis that such work can now be conducted on a natural product of a complexity once thought refractory to such an approach. Although it could not have been imagined at the stage that we initiated our efforts, the C20' vinblastine analogues are now available in three steps from inexpensive commercially available materials (catharanthine, $16/g; vindoline, $36/g; Figure 7) [25].

4. DNA Binding Natural Products: Total Synthesis, DNA Recognition, and Biological Properties

An early focus of our work targeted DNA binding, alkylation, and cleaving agents that exhibit antitumor activity [33,34]. These studies include work on a class of natural products composed of CC-1065, duocarmycin A and SA, and yatakemycin where we not only conducted total syntheses of each natural product [35–37], defining the absolute stereochemistry and correcting a misassigned structure (yatakemycin), but also characterized their DNA alkylation properties [38–42] (Figure 8).

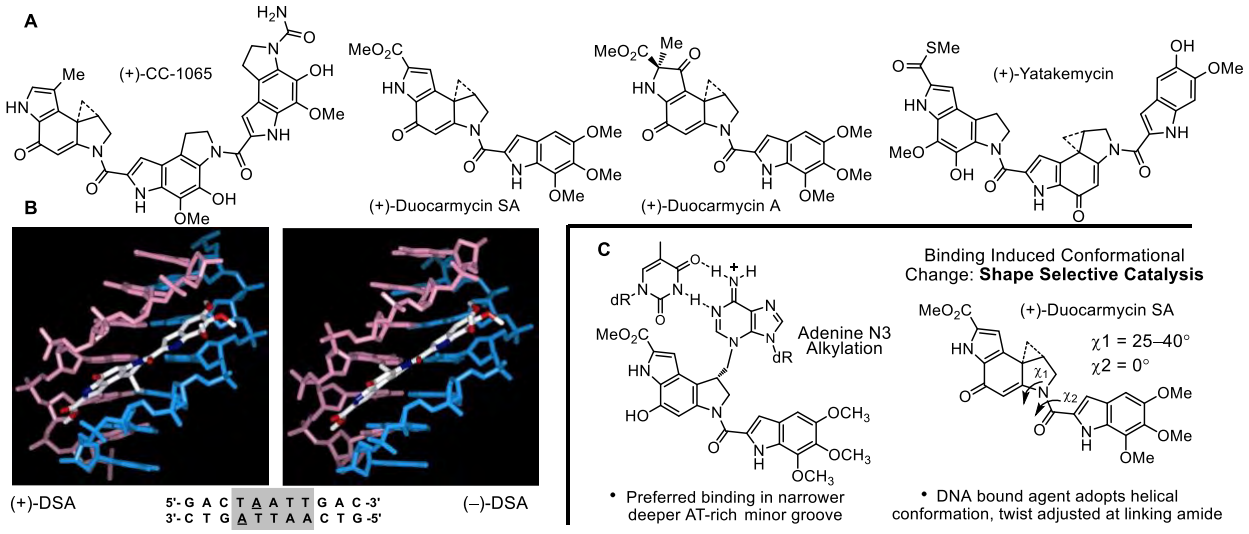

Figure 8. A: Natural product structures. B: NMR-derived structures of natural (+)- and *ent*-(−)-duocarmycin SA bound in the same orientation at an AT-rich site of a deoxyoligonucleotide that illustrate the alkylation sites on complementary DNA stands offset by one base pair. C: Adenine N3 alkylation reaction and DNA binding-induced conformational change that activates the cyclopropane for nucleophilic attack.

In these studies, we defined their DNA alkylation selectivity including that of their biologically active unnatural enantiomers, established their alkylation rates, reversibility, stereoelectronically-controlled reaction regioselectivity, and characterized their adenine N3 adducts. We defined the source of their DNA alkylation selectivity (non-covalent AT-rich binding selectivity – shape selective recognition [43]) and identified the source of catalysis for the DNA alkylation reaction (DNA binding induced conformational change disrupting the stabilizing vinylogous amide conjugation – shape dependent catalysis [44,45]). We provided high-resolution NMR-derived structures of

the natural products bound to DNA [46–48] and established that they are subject to an exquisitely selective "target-based activetion".

More than 2000 analogues of the natural products that contain deep-seated structural changes have been disclosed in our work and were used to define the relationships between structure and reactivity or structure and activity [49], and their contributions to the expression of the DNA alkylation properties and biological activity of the natural products (e.g., "hydrophobic binding-drivenbonding" [50] and a predictive parabolic relationship between reactivity and biological potency [51]). A compilation of the data derived from more than 30 deep-seated modifications in the alkylation subunit, many of which entailed single atom changes, resulted in the establishment of the predictive parabolic relationship between the alkylation subunit reactivity and the resulting cell growth inhibition potency that spanned a 10^4–10^6 range of reactivity and activity[51](Figure9).

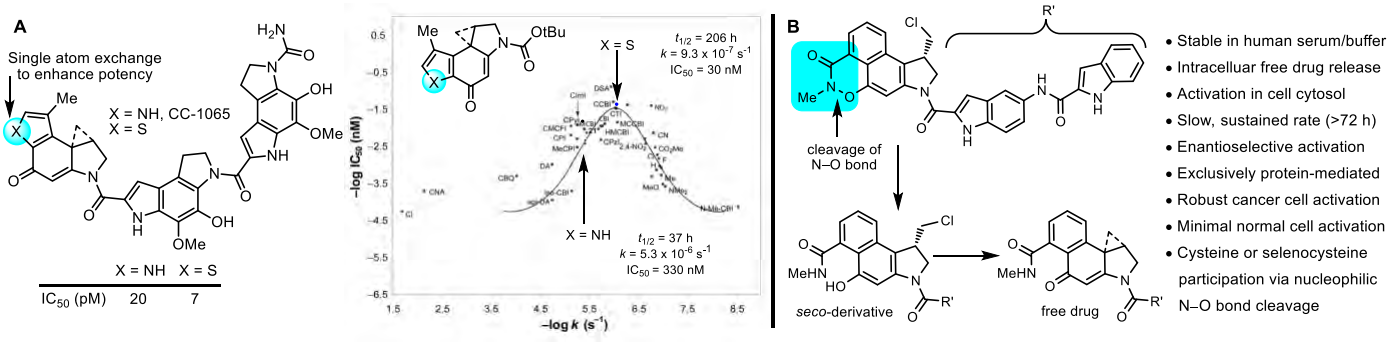

Figure 9. A: Predictive parabolic relationship between structure, reactivity, and biological potency. B: Prodrug design taming the extraordinary potency of the natural products and allowing selective targeting of cancer versus normal cell lines.

Presumably, this fundamental relationship reflects the fact that the compound must be sufficiently stable to reach its biological target yet remain sufficiently reactive to alkylate DNA once it does. The parabolic relationship defined this optimal balance between reactivity and stability, providing a fundamental design feature that was used to improve the potency of CC-1065 by a single heavy atom exchange [52] (Figure 9).

Our recent work led to the discovery of a new class of reductively activated prodrugs specifically designed for this class of natural products, mapping seamlessly onto their core structures [53]. This new class of prodrugs proved especially efficacious *in vivo*, yet are remarkably non-toxic, displaying no myelotoxicity and effectively taming the potent cytotoxic activity of the natural products (Figure 9). Notably, the prototype members of the prodrug class bear structural simplifications that emerged in our studies that improve stability, enhance in vitro potency and *in vivo* efficacy, and simplify synthetic access. Ongoing preclinical studies of one of our lead compounds defined the site (intracellular, cancer vs normal cell lines), slow sustained rate, and mechanism of the exclusively protein-

mediated prodrug cleavage and free drug release mediated by protein cysteine residue [54]. Optimization of these compounds for tolerability, safety, and therapeutic efficacy may provide a breakthrough in the clinical treatment of cancer, defining a new targeted precision therapy.

Bleomycin is a clinically employed antitumor drug that derives its properties through the sequence-selective cleavage of DNA in a process that is both metal ion and O_2 dependent [55−57]. Through development of a modular synthesis capable of modifying each region of the molecule, seminal studies (ca. 70 analogues) that probed each substituent and each subunit in the structure confirmed the origin of DNA cleavage selectivity derived from G triplex-like H-bonding in the minor groove, defined fundamental conformational properties of the linker region contributing to the efficiency of DNA cleavage, identified a conformational swivel point accounting for double-strand DNA cleavage from a single bound site, and provided a high-resolution NMR-derived structure of DNA bound deglycobleomycin A2 [58,59] (Figure 10).

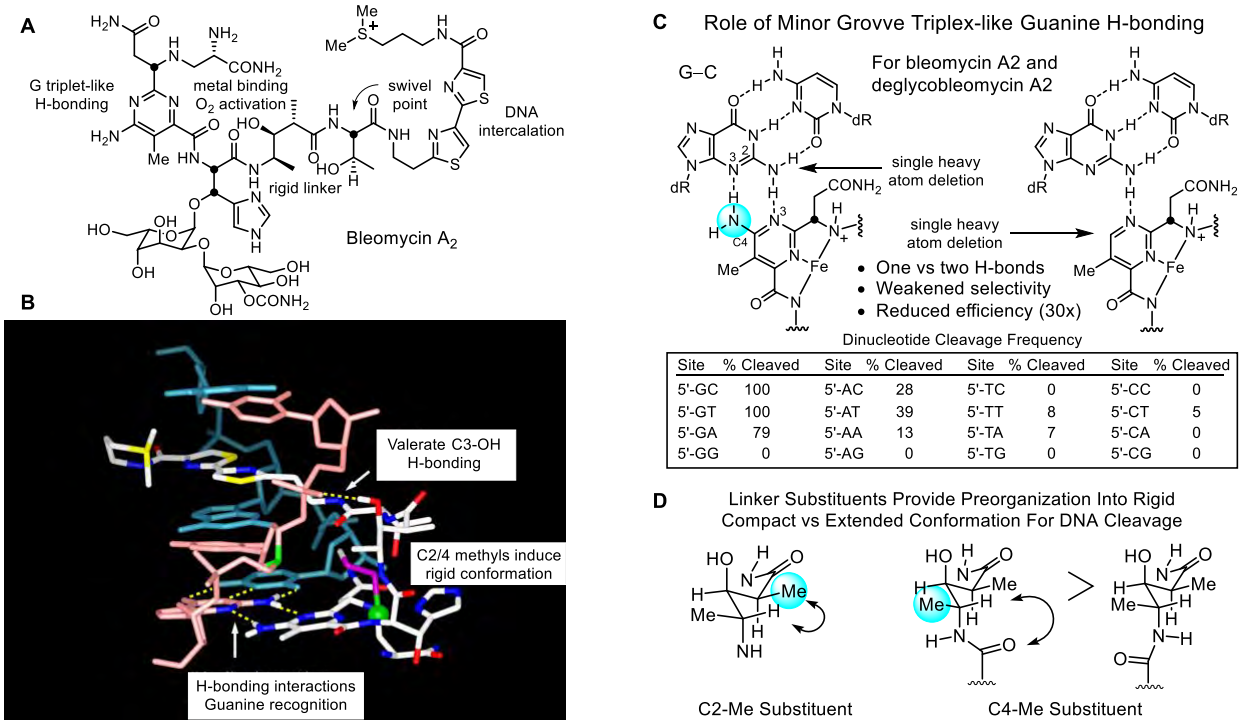

Figure 10. A: Structure of bleomycin A and functional role of subunits. B: NMR-derived structure of bleomycin bound to DNA cleavage site. C: Minor groove triplex-like G recognition and cleavage selectivity. D: Rigid linker region and underlying conformational origin.

Combined, the studies helped define a role not only for each subunit, but also the importance of each substituent in this remarkable molecule.

In the course of our work, we also prepared a >9000-membered screening library of distamycin analogues [60], discovered and

defined the DNA cross-linking properties of ischrysohermidin and established the origin of its selectivity [61], and studied the naturally occurring bis-intercalators (sandramycin, luzopeptins, BE-22179, quinoxapeptins, thiocoraline), defining their DNA binding selectivity, its origins, kinetics of binding, and established a high-resolution NMR-derived structure of sandramycin bound to DNA [62]. In these studies, we introduced a powerful fluorescent intercalator displacement (FID) assay for establishing DNA binding selectivity or affinity [63,64] that complements DNA footprinting and developed a convenient M13-derived alternative to ^{32}P-end-labeling of restriction fragments for DNA cleavage studies[65].

5. Natural Products Total Synthesis, New Synthetic Methodology

In our work, more than 100 natural products have been prepared by total syntheses, of which most represent biologically active natural products chosen by virtue of their properties. Their structures inspired the development of new synthetic methodology designed for the natural products of interest. Many were first total syntheses, defining or correcting the stereochemistry or structure, and often constitute concise, efficient total syntheses easily identifiable with our efforts. Highlights, including those that subsequently probed or defined structure–function properties not described elsewhere, targeted the total syntheses of streptonigrin (1983), juncusol (1984), rufescine and imelutine (1984), colchicine (1985), lavendamycin (1985), PDE-I and PDE-II (1987), prodigiosin and prodigiosene (1988), trikentrin A (1991), combretastatin (1991), (–)-pyrimidoblamic acid (1993), streptonigrone (1993), isochrysohermidin (1993), (+)-P-3A (1994), fredericamycin (1995), grandirubrine and imerubrine (1985), nothapodytine B and (–)-mappicine (1998), ningalin A, lamellarin O, lukianol A, and storniamide A (1999), phomazarin (1999), ningalin B (2000), distamycin (2000), hippadine (2000), rubrulone (2000), fostriecin (2001), (–)-roseophilin (2001), (+)-camptothecin (2002), anhydrolycorinone (2002), minovine (2005), piericidin A1 and B1 (2005), ningalin D (2005), (–)-vindorosine (2006), (–)-vindoline (2006), N-methylaspidospermidine (2006), cytostatin (2006), phostriecin (2010), (+)-fendleridine and (+)-acetylaspidoalbidine (2010), (–)-vindorosine (2010), lycogarubin C and lycogalic acid (2010), (–)-aspidospermine (2012), (+)-spegazzinine (2012), kopsinine (2013), asymmetric synthesis of (+)-P-3A and (–)-pyrimidoblamic acid (2014), (–)-kopsifoline D (2014), (–)-deoxoapodine (2014), (–)-kopsinine (2015), dihydrolysergol and dihydrolysergic acid (2015), methoxatin (2016), streptide (2019), meayamycin (2020), (–)-pseudocopsinine (2020), (–)-minovincinine (2020), (–)-strempeliopine (2021), and (+)-paucidactine D (2025). In this work, new synthetic methodology or synthetic strategies have been introduced. Most recognized of these efforts include the inverse electron demand Diels–Alder reactions of heterocyclic azadienes [66], including the first reported organocatalytic Diels–Alder reaction, the first general method for catalyzing such reactions (solvent H-bonding of HFIP), the successful use of 1,2,3-triazine cycloaddition reactions utilizing powerful substituent effects, and the first synthesis and cycloaddition reactions of 1,2,3,5-tetrazines [67]. We intro-

duced and developed the cycloaddition reactions of acyclic 1-azadienes (N-sulfonyl-1-azabutadienes), identified a unique transition state anomeric effect responsible for their remarkable endo diastereoselectivity, and developed a powerful asymmetric variant of the reactions [66]. We introduced and developed the powerful cascade [4+2]/[3+2] cycloaddition reactions of 1,3,4-oxadiazoles [27], and pioneered the cycloaddition reactions of cyclopropenone ketals ([4+2] cycloaddition) including the discovery of their reversible thermal (80°C) ring opening to π-delocalized singlet vinylcarbenes and subsequent substrate dependent cycloaddition reactions [66] ([1+2], [3+2], and [4+3] cycloadditions). We introduced the use of acyl radical generation from phenyl selenoesters and subsequent intermolecular and intramolecular alkene addition reactions [68], pioneered key palladium-catalyzed reactions including the first examples of a Pd(0)-mediated free amine amination of an aryl halide [69] in 1984, the conduct of unsymmetrical 2,2'-bipyrrole coupling via electrophilic Pd(II) C–H activation [70] in 1987, and introduced an intramolecular Pd(0)-catalyzed indole annulation for (macro)cyclizations [71]. We discovered and disclosed powerful free radical hydrogen atom transfer (HAT) functionalization, cyclization, or reduction reactions of unactivated alkenes (Fe(III)–$NaBH_4$ with radical traps [31]) that has since gained widespread study. We defined the concept of divergent total synthesis [72] in 1984.

6. Conclusions

Enabled by the development of divergent synthetic strategies and methods that advance the underlying systematic medicinal chemistry, the discovery of natural product analogues bearing deep-seated structural changes not accessible by other means is highlighted. Many display biological properties that not only improve those found in the natural product or overcome an intrinsic limitation, but have also been designed to endow them with productive new properties and even additional new mechanisms of action not expressed by the natural product, providing supernatural products.

7. Acknowledgments

Many thanks to the talented group of past and current coworkers for the conduct of the studies and the innovative ideas they introduced. The financial support of the National Institutes of Health (CA041101, CA042056, DA015648) is gratefully acknowledged.

8. References

1. Newman DJ, Cragg GM. *J. Nat. Prod*., 2020, 83, 770–803.
2. Szpilman AM, Carreira EM. *Angew. Chem., Int. Ed.*, 2010, 49, 9592–9628.

3. Hong J. *Chem. - Eur. J.*, 2014, 20, 10204−10212.
4. Huffman BJ, Shenvi RA. J. Am. Chem. Soc., 2019, 141, 3332–3346.
5. Boger DL. *J. Org. Chem.*, 2017, 82, 11961–11980.
6. Wan KK, Shenvi RA. *Synlett*, 2016, 27, 1145–1164.
7. Wu ZC, Boger DL. *Nat. Prod. Rep.*, 2020, 37, 1511−1531.
8. Shenvi RA. *ACS Cent. Sci.*, 2024, 10, 519–528.
9. Katsnelson A. *ACS Cent. Sci.*, 2024, 10, 1125-1128.
10. Okano A, Isley NA, Boger DL. *Chem. Rev.*, 2017, 117, 11952−11993.
11. McComas CC, Crowley BM, Boger DL. *J. Am. Chem. Soc.*, 2003, 125, 9314−9315.
12. Wu ZC, Boger DL. *Acc. Chem. Res.*, 2020, 53, 2587−2599.
13. Okano A, Isley NA, Boger DL. *Proc. Natl. Acad. Sci. U.S.A.*, 2017, 114, E5052–E5061.
14. Moore MJ, Qu S, Tan C, Cai Y, Mogi Y, Keith DJ, Boger DL. *J. Am. Chem. Soc.*, 2020, 142, 16039−16050.
15. Moore MJ, Qin P, Keith DJ, Wu ZC, Jung S, Chatterjee S, Tan C, Qu S, Cai Y, Stanfield RL, Boger DL. *J. Am. Chem. Soc.*, 2023, 145, 12837−12852.
16. Moore MJ, Qin P, Yamasaki N, Zeng X, Keith DJ, Jung S, Fukazawa T, Graham-O'Regan K, Wu ZC, Chatterjee S, Boger DL. *J. Am. Chem. Soc.*, 2023, 145, 21132−21141.
17. Qin P, Moore MJ, Jung S, Fukazawa T, Yamasaki N, Chatterjee S, Wu ZC, Boger DL. *J. Org. Chem.*, 2024, 89, 12701−12710.
18. Walker S, Hu Y, Chen L, Rew Y, Shin D, Boger DL. *Chem. Rev.*, 2005, 105, 449–476.
19. Chen L, Yuan Y, Helm JS, Hu Y, Rew Y, Shin D, Boger DL, Walker S. *J. Am. Chem. Soc.*, 2004, 126, 7462–7463.
20. Nam J, Shin D, Rew Y, Boger, DL. *J. Am. Chem. Soc.*, 2007, 129, 8747–8755.
21. Fang X, Tiyanont K, Zhang Y, Wanner J, Boger DL, Walker S. Mol. *BioSystems*, 2006, 2, 69–76.
22. The Alkaloids, eds. A Brossi, M. Suffness, Academic, San Diego, 1990, vol 37.
23. Sears JE, Boger DL. *Acc. Chem. Res.*, 2015, 48, 653–662.
24. Leggans E K, Duncan KK, Barker TJ, Schleicher KD, Boger DL. *J. Med. Chem.*, 2013, 56, 628−639.
25. Carney DW, Lukesh III JC, Brody DM, Brutsch MM, Boger DL. *Proc. Natl. Acad. Sci. U.S.A.*, 2016, 113, 9691–9698.
26. Lukesh III JC, Carney DW, Dong H, Cross RM, Shukla V, Duncan KK, Yang S, Brody DM, Brütsch MM, Radakovic A, Boger DL. *J. Med. Chem.*, 2017, 60, 7591−7604.
27. Sears JE, Boger DL. *Acc. Chem. Res.*, 2016, 49, 241–251.
28. Ishikawa H, Colby DA, Seto S, Va P, Tam A, Kakei H, Rayl TJ, Hwang I, Boger DL. *J. Am. Chem. Soc.*, 2009, 131, 4904–4916.
29. Ishikawa H, Colby DA, Boger DL. *J. Am. Chem. Soc.*, 2008, 130, 420–421.
30. Gotoh H, Sears JE, Eschenmoser A, Boger DL. *J. Am. Chem. Soc.*, 2012, 134, 13240–13243.
31. Leggans EK, Barker TJ, Duncan, KK, Boger DL. *Org. Lett.*, 2012, 14, 1428–1431.
32. Barker TJ, Boger, DL. *J. Am. Chem. Soc.*, 2012, 134, 13588–13591.
33. Wolkenberg SE, Boger DL. *Chem. Rev.*, 2002, 102, 2477−2496.
34. Tse WC, Boger DL. *Chem. Biol.*, 2004, 11, 1607−1617.
35. Boger DL, Boyce CW, Garbaccio

RM, Goldberg JA. *Chem. Rev.*, 1997, 97, 787–828
36. Boger DL. *Acc. Chem. Res.*, 1995, 28, 20−29.
37. Tichenor MS, Boger DL. *Nat. Prod. Rep.*, 2008, 25, 220−226.
38. Boger DL, Johnson DS. *Proc. Natl. Acad. Sci. U.S.A.*, 1995, 92, 3642−3649.
39. Boger DL, Johnson DS. *Angew. Chem., Int. Ed. Engl.*, 1996, 35, 1438−1474.
40. Boger DL, Johnson DS, Yun W. *J. Am. Chem. Soc.*, 1994, 116, 1635−1656.
41. Boger DL, Johnson DS, Yun W, Tarby CM. *Bioorg. Med. Chem.*,1994, 2, 115−135.
42. Parrish JP, Kastrinsky DB, Wolkenberg SE, Igarashi Y, Boger DL. *J. Am. Chem. Soc.*, 2003,125,10971−10976.
43. Boger DL, Bollinger B, Hertzog DL, Johnson DS, Cai H, Mésini P, Garbaccio RM, Jin, Q, Kitos PA. *J. Am. Chem. Soc.*, 1997, 119, 4987–4998.
44. Boger DL, Garbaccio RM. *Acc. Chem. Res.*, 1999, 32, 1043−1052.
45. Boger DL, Garbaccio RM. *Bioorg. Med. Chem.*, 1997, 5, 263−276.
46. Eis PG, Smith JA, Rydzewski MJ, Case DA, Boger DL, Chazin WJ. *J. Mol. Biol.*, 1997, 272, 237−252.
47. Smith JA, Bifulco G, Case DA, Boger DL, Gomez-Paloma L, Chazin WJ. *J. Mol. Biol.*, 2000, 300, 1195−1204.
48. Schnell, JR, Ketchem RR, Boger DL, Chazin WJ. *J. Am. Chem. Soc.*, 1999, 121, 5645–5652.
49. MacMillan KS, Boger DL. *J. Med. Chem.*, 2009, 52, 5771−5780.
50. Wolfe AL, Duncan KK, Lajiness JP, Zhu K, Duerfeldt AS, Boger DL. *J. Med. Chem.*, 2013, 56, 6845−6857.
51. Parrish JP, Hughes TV, Hwang I, Boger DL. *J. Am. Chem. Soc.*, 2004, 126, 80−81.
52. Tichenor MS, MacMillan KS, Stover JS, Wolkenberg SE, Pavani MG, Zanella L, Zaid AN, Spalluto G, Rayl TJ, Hwang I, Baraldi PG, Boger DL. *J. Am. Chem. Soc.*, 2007, 129, 14092−14099.
53. Wolfe AL, Duncan KK, Parelkar NK, Brown D, Vielhauer GA, Boger DL. *J. Med. Chem.*, 2013, 56, 4104−4115.
54. Chakraborty N, Momirov J, Radakovic A, Chatterjee, S, Kirchhoff AM, Kolb AL, West TJ, Sanchez BB, Martinez-Bartolome S, Saviola A, McClatchy D, Yates III JR, Chen JS, Lairson LL, Felding BH, Boger DL. *ACS Chem. Biol.*, 2025, 20, 442−454.
55. Bleomycin: Chemical, Biochemical, and Biological Aspects, ed. SM Hecht, Springer–Verlag, New York, 1979.
56. Hecht SM. *Acc. Chem. Res.*, 1986, 19, 383−391.
57. Stubbe J, Kozarich JW. *Chem. Rev.*, 1987, 87, 1107−1136.
58. Boger DL, Cai H. *Angew. Chem., Int. Ed.*, 1999, 38, 448−476.
59. Wu W, Vanderwall DE, Teramoto S, Lui SM, Hoehn ST, Tang XJ, Turner CJ, Boger DL, Kozarich JW, Stubbe J. *J. Am. Chem. Soc.*, 1998, 120, 2239−2250.
60. Stover JS, Shi J, Jin W, Vogt PK, Boger DL. *J. Am. Chem. Soc.*, 2009, 131, 3342–3348.
61. Boger DL, Baldino CM. *J. Am. Chem. Soc.*, 1993, 115, 11418–11425.
62. Boger DL, Saionz KW. *Bioorg. Med. Chem.*, 1999, 7, 315–322.
63. Boger DL, Fink BE, Brunette SR, Tse WC, Hedrick MP. *J. Am. Chem. Soc.*, 2001, 123, 5878−5891.
64. Tse WC, Boger DL. *Acc. Chem. Res.*, 2004, 37, 61–69.
65. Boger DL, Munk SA, Zarrinmayeh H,

Ishizaki T, Haught J, Bina M. *Tetrahedron*, 1991, 47, 2661−2682.
66. Zhang J, Shukla V, Boger DL. *J. Org. Chem.*, 2019, 84, 9397–9445.
67. Wu ZC, Boger DL. *J. Org. Chem.*, 2022, 87, 16829−16846.
68. Boger DL, Mathvink RJ. *J. Org. Chem.*, 1992, 57, 1429–1443.
69. Boger DL, Panek JS. *Tetrahedron Lett.*, 1984, 25, 3175–3178.
70. Boger DL, Patel M. *J. Org. Chem.*, 1988, 53, 1405–1415.
71. Breazzano SP, Poudel YB, Boger DL. *J. Am. Chem. Soc.*, 2013, 135, 1600–1606.
72. Boger DL, Brotherton, CE. *J. Org. Chem.*, 1984, 49, 4050–4055.

The Chemist
Journal of the American Institute of Chemists

Synthesis, Structural Characterization, and Antimicrobial Evaluation of Dimethyl Methylene Phosphate: An Innovative Phosphorylated Compound with Broad-Spectrum Potential

Alae Aachari*, Mohamed Khamar, Essediya Cherkaoui , Siham Bachar

Civil Engineering and Environmental Laboratory, Water and Environmental Materials Team, Higher School of Technology in Salé, Mohammed V University in Rabat
11060 Salé, Morocco

**Corresponding author (E-mail: alae_aachari@um5.ac.ma; alaeaac@gmail.com)*

Abstract: Dimethyl Methylene Phosphate was synthesized and its chemical and antimicrobial properties were investigated. Its structure was corroborated by advanced spectroscopic methods (IR, NMR and UV-Visible spectroscopy), underscoring the important role played by the phosphate group. The compound showed potent antibacterial activity with inhibition zones against Gram-negative bacteria such as *Alcaligenes faecalis* reaching 47 mm. Furthermore, UV-Visible quantitative analysis showed the maximum absorption at 260 nm, affirming its electronic properties. The results establish its potential as a broad-spectrum antimicrobial agent, warranting further exploration into its biological applications and mechanisms of action.

Key Words: Dimethyl Methylene Phosphate (DMP), IR spectroscopy, NMR spectroscopy, antimicrobial activity, phosphate compounds

1. Introduction

Phosphate-containing compounds play a pivotal role in both biological and chemical systems, serving as integral components in cellular energy transduction, signal transduction pathways, and as scaffolds for advanced drug development. The escalating crisis of antimicrobial resistance has underscored the urgency of discovering innovative compounds capable of targeting resistant pathogens effectively.

Dimethyl Methylene Phosphate (DMP), a novel phosphorylated compound, represents a significant advance in this domain. Its

distinctive structural features, particularly the phosphoryl (P=O) bond, enable unique interactions with bacterial membranes, potentially disrupting essential cellular functions. In this study, we report the synthesis of DMP, provide a comprehensive evaluation of its antimicrobial activity, and investigate its structural and chemical properties using advanced spectroscopic techniques. These findings aim to shed light on the potential of DMP as a new tool in the fight against antimicrobial resistance.

2. Experimental

Chemical Part

The synthesis protocol for Dimethyl Methylene Phosphate

Dimethyl Methylene Phosphate (DMP) was synthesized using pulegone as a precursor. In a typical procedure, pulegone (0.35 g, 2.25 mmol) was dissolved in diethyl ether, and diethylamine was added dropwise while stirring to ensure homogeneity. The resulting mixture was phosphorylated by the gradual addition of phosphoric acid (12 mL) under controlled conditions at 60°C for 3 hours. Upon completion, the reaction mixture was cooled to ambient temperature, promoting crystallization of the product. Purification was achieved via recrystallization employing a diethyl ether/benzene solvent system, yielding DMP in high purity as confirmed by analytical techniques.

Characterization methods

- **IR Spectroscopy**: The IR spectrum of DMP exhibited key absorption bands corresponding to its functional groups: 2985 cm^{-1} (C-H stretching), 1250 cm^{-1} (P=O stretching), and 1023 cm^{-1} (P-O-C stretching). These findings confirm the successful incorporation of phosphorylated functional groups.

- **NMR Spectroscopy**:
  - *^{1}H NMR*: Notable signals included a triplet at 0.9 ppm (methyl protons), a singlet at 2.1 ppm (methyl group adjacent to C=O), and multiplets between 4.0-5.0 ppm, attributed to methylene groups interacting with polar moieties.
  - *^{13}C NMR*: The spectrum revealed peaks characteristic of distinct carbon environments: 0-50 ppm (aliphatic carbons), 120-150 ppm (aromatic carbons), and 160-180 ppm (carbonyl carbons).
  - *^{31}P NMR*: A single, sharp peak at 10 ppm confirmed the presence of a single phosphorus environment, indicative of the compound's organo-phosphate nature.

- **UV-Visible Spectroscopy**: DMP exhibited maximum absorption at 260 nm, with an extinction coefficient (ε) of 0.127 $L \cdot mol^{-1} \cdot cm^{-1}$. This absorption is consistent with the electronic transitions associated with the phosphorylated moiety, providing

further evidence of the compound's structural framework.

Biological Part

Antimicrobial evaluation

The antimicrobial efficacy of Dimethyl Methylene Phosphate (DMP) was evaluated using the disk diffusion method across six clinically-relevant bacterial strains: *Escherichia coli*, *Staphylococcus aureus*, *Pseudomonas aeruginosa*, *Bacillus subtilis*, *Klebsiella pneumoniae*, and *Alcaligenes faecalis*. Sterile disks impregnated with DMP at concentrations of 1, 2, 5, and 10 mg/mL were applied to Mueller-Hinton agar plates inoculated with bacterial suspensions. Following 24 hours of incubation at 37°C, inhibition zones were measured, providing quantitative data on the compound's antimicrobial potential.

3. Results and Discussion

- ✓ **Chemical Characterization**

The chemical structure of DMP was confirmed through a comprehensive suite of analytical techniques:

- **IR Spectroscopy**: The spectrum (Figure 1) revealed prominent absorption bands at 1250 cm^{-1} (P=O stretching) and 1023 cm^{-1} (P-O-C stretching), consistent with the functional groups characteristic of organophosphates.
- **NMR Spectroscopy**: The ^{1}H NMR spectrum displayed key signals, including a triplet at 0.9 ppm (methyl protons), a singlet at 2.1 ppm (methyl adjacent to C=O), and multiplets at 4.0–5.0 ppm (methylene groups). The ^{13}C NMR spectrum exhibited peaks at 0–50 ppm (aliphatic carbons), 120–150 ppm (aromatic carbons), and 160–180 ppm (carbonyl carbons). A sharp ^{31}P NMR signal at 10 ppm confirmed the presence of a single phosphorus environment.
- **UV-Visible Spectroscopy**: DMP exhibited a maximum absorption peak at 260 nm, attributed to electronic transitions within the phosphate moiety, which underscores its optical and electronic properties.

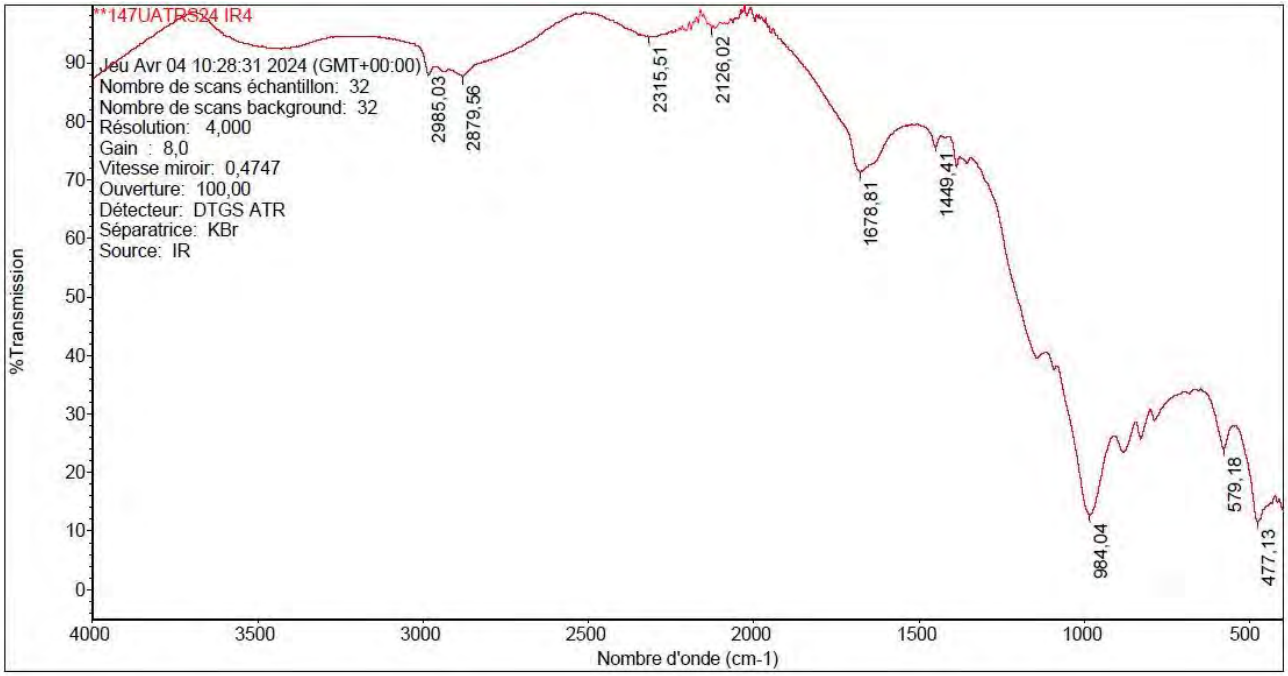

Figure 1. IR Spectrum of Dimethyl Methylene Phosphate

- ✓ **Concentration and Solubility:** Quantitative analysis determined DMP's solubility at 0.25 mol/L in ethanol, indicating excellent solubility in polar solvents. This property enhances its applicability in biological systems, where solubility significantly impacts bioavailability and efficacy.
- ✓ **Antimicrobial Activity:** The antimicrobial activity of DMP was assessed across various bacterial strains, with inhibition zones summarized in Table 1. At a concentration of 10 mg/mL, DMP exhibited remarkable efficacy against Gram-negative bacteria, including *Alcaligenes faecalis* (47 mm) and *Escherichia coli* (46 mm). Gram-positive bacteria, such as *Staphylococcus aureus* and *Bacillus subtilis*, exhibited moderate inhibition zones of 38 mm and 32 mm, respectively. The enhanced activity against Gram-negative strains likely results from DMP's ability to penetrate the outer membrane, destabilizing the bacterial cell envelope and interfering with essential intracellular targets. Figure 2 illustrates the significant inhibition zone observed for *A. faecalis*, further demonstrating the compound's broad-spectrum activity. The interaction of the phosphate group with bacterial membranes likely disrupts structural integrity, leading to cellular lysis and death.

Figure 2. The Inhibition Zone for Six Bacterial Strains (0.25 mol/L Dimethyl Methylene Phosphate on Mueller-Hinton Agar)

Table 1. Antimicrobial Activity of Dimethyl Methylene Phosphate

Bacterial Strain	Inhibition Zone (mm)
Escherichia coli	46 ± 2
Staphylococcus aureus	38 ± 1.5
Pseudomonas aeruginosa	30 ± 1
Bacillus subtilis	32 ± 1.5
Klebsiella pneumoniae	34 ± 1
Alcaligenes faecalis	47 ± 2

- ✓ **Mechanism of Action:** The proposed mechanism involves membrane disruption and enzymatic interference. Phosphorylated compounds, such as DMP, integrate into bacterial lipid bilayers, increasing membrane permeability and impairing critical cellular processes. This mechanism provides a plausible explanation for DMP's significant activity against resistant pathogens, including *Pseudomonas aeruginosa*.
- ✓ **Comparative Analysis:** Compared to existing antimicrobial agents, DMP demonstrates several advantages, including high chemical stability, excellent solubility, and consistent efficacy across a range of concentrations. Its robust performance against nosocomial pathogens positions it as a promising candidate for combating antimicrobial resistance. These properties make DMP a valuable addition to the repertoire of anti-

microbial agents with potential clinical applications.

4. Conclusion

Dimethyl Methylene Phosphate (DMP) represents a breakthrough in the development of antimicrobial agents. Its significant activity against both Gram-positive and Gram-negative bacteria, combined with its favorable chemical properties, underscores its potential as a versatile therapeutic candidate. This study establishes a robust foundation for further exploration, including optimization of its structure and elucidation of its molecular interactions in biological systems.

Future research should prioritize *in vivo* evaluations, comprehensive safety assessments, and detailed mechanistic studies to support its progression toward clinical applications. The incorporation of DMP into pharmaceutical formulations could provide innovative solutions to combat multi-drug-resistant infections, addressing one of the most pressing challenges in modern healthcare.

5. Acknowledgments

The authors thank Civil Engineering and Environmental Laboratory, Water and Environmental Materials Team, Higher School of Technology in Salé, Mohammed V University in Rabat for providing laboratory resources, including chemical and biology supplies, which supported this research. This study did not receive external funding.

6. References

1. Rodriguez JB, Gallo-Rodriguez C. The role of the phosphorus atom in drug design. *ChemMedChem*, 2019, 14(2),190-216. https://doi.org/10.1002/cmdc.201800693
2. Rafiee Z, Khalafi-Nezhad A, Shahidzadeh M. Multicomponent synthesis of new thiazolylpyrazole derivatives: Green and reusable catalyst, optimized reaction conditions, and DFT study. *J. Organomet. Chem.*, 2018, 869, 165-172. https://doi.org/10.1016/j.toxlet.2018.03.028
3. Silva VB, Santos YH, Hellinger R, Mansour S, Delaune A, Legros J, Zinoviev S, Nogueira ES, Orth ES. Organophosphorus chemical security from a peaceful perspective: Sustainable practices in its synthesis, decontamination and detection. *Green Chem.*, 2022, 24(2), 585-613.
4. Gupta A, Sharma S, Goyal S, Sharma A, Sharma D. Sustainable and green synthesis of quinoline derivatives: A review. *Green Chem.*, 2022, 24(2), 472-504. https://doi.org/10.1039/D1GC02705K

5. Vega MA, Maldonado JR, Rodríguez A, Ortega MG. A new series of hybrid compounds with promising antimalarial activity: Synthesis, biological evaluation, and in silico studies. *Bioorg. Med. Chem.*, 2023, 72, 116961. https://doi.org/10.1016/j.bmc.2023.117512
6. Castro-Sánchez E, Drumright LN, Gharbi M, Farrell S, Holmes AH. Mapping antimicrobial stewardship in undergraduate medical, dental, pharmacy, nursing and veterinary education in the United Kingdom. *PLoS One*, 2016, 11(2), e0150056. https://doi.org/10.1371/journal.pone.0150056
7. Koskela H. Use of NMR techniques for toxic organophosphorus compound profiling. *J. Chromatogr. B*, 2010, 878(17-18), 1365-1381. https://doi.org/10.1016/j.jchromb.2009.10.030
8. Haque R, Buhler DR in Annual Reports on NMR Spectroscopy, Academic Press, 1972, vol 4, Nuclear Magnetic Resonance Spectroscopy in Pesticide Chemistry, pp 237-309. https://doi.org/10.1016/S0066-4103(08)60346-4
9. Pashirova T, Salah-Tazdaït R, Tazdaït D, Masson P. Applications of microbial organophosphate-degrading enzymes to detoxification of organophosphorous compounds for medical countermeasures against poisoning and environmental remediation. *Int. J. Mol. Sci.*, 2024, 25(14),7822. https://doi.org/10.3390/ijms25147822
10. Silva-Santana G, Ferreira Silva CM, Botelho Olivella JG, Ferreira Silva I, Oliveira Fernandes LM, Sued-Karam BR, Silva Santos C, Souza C, Mattos-Guaraldi AL. Worldwide survey of *Corynebacterium striatum* increasingly associated with human invasive infections, nosocomial outbreak, and antimicrobial multidrug-resistance, 1976–2020. *Arch. Microbiol.*, 2021, 203,1863-1880. https://doi.org/10.1007/s00203-021-02246-1

The Chemist
Journal of the American Institute of Chemists

An Overview of Current Trend in Esters Synthesis

T. J. Ogundoro, O. Atolani

Department of Chemistry, Obafemi Awolowo University, Ile-Ife, Nigeria
Department of Chemistry, University of Ilorin, Ilorin, Nigeria

(E-mail: tjogundoro@pg-student.oauife.edu.ng; atolani.o@unilorin.edu.ng)

Graphical Abstract:

Abstract: Esterification is a fundamental organic reaction that forms the basis of ester synthesis, a process integral to numerous industrial, pharmaceutical, and biochemical applications. This review provides a detailed evaluation of the esterification process, focusing on the synthesis of esters, the factors influencing the reaction, their diverse applications, and the associated toxicity. Generally, the synthesis of esters is achieved through the reaction of carboxylic acids with alcohols in the presence of catalysts. Here, emphasis is laid on both traditional and advanced methodologies, including enzymatic catalysis and the utilization of alternative energy sources like microwave and ultrasonic irradiation. Factors such as the nature of the reactants, catalyst type and concentration, temperature, and solvent choice are well discussed, highlighting their impact on reaction efficiency and selectivity. Furthermore, this review provides broad range of ester applications, from their role as intermediates in drug synthesis and components of flavors

and fragrances to their use as solvents, plasticizers, and lubricants in various industries. However, the potential toxicity of some esters, particularly in pharmaceutical and environmental contexts, is also evaluated. While many esters are considered safe, certain esters exhibit toxicity that necessitates careful evaluation and regulations particularly for pharmacological and environmental concerns.

The insights provided herein serve as a guide for future studies and applications of esters in various scientific and industrial domains.

Key Words: esters synthesis, transesterification, microwave, esters toxicity

1. Introduction

Esterification is a foundational reaction in organic chemistry, producing esters, a versatile class of compounds widely used across industries. These carbonyl-containing molecules, both acyclic and cyclic, serve as essential building blocks in organic transformations, finding applications in fine chemicals, polymers, pharmaceuticals, cosmetics, and personal care products [1]. Esters have been integral to industrial chemistry since their first synthesis by German chemist Leopold Gmelin [2]. They remain one of the most abundant functional groups in both synthetic and natural compounds, emphasizing their central role in chemical synthesis and their extensive applications.

Typically, esters are synthesized through the esterification reaction, wherein carboxylic acids and alcohols react in the presence of a catalyst. Other methods, such as reactions with carboxylic anhydrides or halides, are also employed for ester production [2]. This synthesis is increasingly significant due to esters' unique applications in various fields, including biodegradable polymers, thermoplastics, pharmaceuticals, agrochemicals, cosmetics, and food additives. For instance, esters like polylactic acid and polyethylene terephthalate are pivotal in producing biodegradable plastics, while others add flavors to foods or fragrances to personal care products [3]. Additionally, ester derivatives, such as benzyl benzoate, methyl benzoate, and benzyl acetate, demonstrate therapeutic and antimicrobial properties, further highlighting their importance in pharmaceuticals [4].

This review aims to provide an in-depth analysis of current advancements and emerging trends in ester synthesis, with particular attention to new catalytic strategies and green synthesis approaches. These recent methodologies address critical industrial needs for more efficient, sustainable, and application-specific ester production processes. By examining these advancements, we highlight the innovative pathways that researchers are exploring to enhance ester synthesis, expanding its practical and commercial potential across multiple fields.

2. Synthesis of Esters

Esters are structurally versatile compounds with significant industrial relevance, synthesized primarily via esterification processes that vary in terms of reactivity, catalyst requirements, and environmental impact [5]. Traditional esterification methods in-volve the reaction of carboxylic acids with alcohols, acid anhydrides with alcohols, or acid chlorides with alcohols. Each route presents unique advantages and challenges, with current research focusing on enhancing efficiency, reducing energy consumption, and minimizing environmental footprint.

The classical esterification of carboxylic acids with alcohols is one of the most utilized methods due to the accessibility of carboxylic acids and alcohols. This reaction, however, is limited by its equilibrium nature and typically requires a strong acid catalyst, such as sulfuric acid, to protonate the carboxyl group, thereby enhancing electrophilicity. Traditional approaches to drive this equilibrium toward ester formation involve high reaction temperatures and the continuous removal of water [6]. Recent advancements have introduced heterogeneous acid catalysts such as sulfonated carbon, zeolites, and mesoporous silicas which provide advantages in terms of recyclability and reduced catalyst contamination [7]. Furthermore, studies on microwave and ultrasonic-assisted esterification have demonstrated enhanced reaction kinetics and increased yields under milder conditions, which supports a reduction in energy consumption while maintaining high reaction efficiencies. These physical activation methods are gaining prominence in green chemistry frameworks, particularly for large-scale applications.

Esterification via acid anhydrides with alcohols offers a more reactive pathway than carboxylic acid-alcohol esterification. The electrophilic nature of acid anhydrides permits reaction under milder conditions and often without the need for a strong acid catalyst [8]. Acetic anhydride is frequently utilized in both laboratory and industrial contexts due to its reactivity and lower cost. This reaction pathway also minimizes the water by-product, facilitating higher yields and purer ester products. However, the generation of acetic acid as a by-product necessitates downstream separation, increasing processing costs. To address these limitations, recent studies have explored the use of biodegradable anhydrides and alternative green solvents to reduce the environmental impact of this synthesis route. Additionally, ionic liquids have shown promise as dual-function reaction media and catalysts, enhancing the sustainability of acid anhydride esterification in synthetic applications.

The reaction of acid chlorides with alcohols represents one of the most efficient routes for ester synthesis, characterized by rapid reaction kinetics due to the high electrophilicity of acid chlorides. This method, which does not require a catalyst, typically yields high-purity esters at ambient temperatures, making it favorable in synthetic applications where reaction speed and efficiency are critical [9]. However, the by-product hydrogen chloride gas poses challenges, such as equipment corrosion and the need for neutralization. To mitigate these issues, novel activating agents like N,N'-carbonyldiimidazole (CDI) and dicyclo-hexylcarbodiimide (DCC) have been investigated as substitutes for acid chlorides, enabling ester formation while reducing the environmental and safety concerns associated with hydrogen chloride [10]. Additionally, recent advancements in green

chemistry have focused on replacing conventional acid chlorides with more benign electrophiles, thereby reducing toxic by-products while maintaining high reactivity.

To align ester synthesis with green chemistry principles, recent research has explored alternative reaction media and catalytic systems that reduce or eliminate traditional organic solvents. Methods such as transesterification using renewable feedstocks (e.g., vegetable oils) have been employed to produce biodiesel and other biodegradable esters, providing an eco-friendly approach to ester synthesis. The application of deep eutectic solvents (DES) and supercritical fluids as reaction media has been shown to increase reaction efficiency while facilitating catalyst recovery and recycling [11]. These solvents exhibit unique physicochemical properties that support high selectivity and yield, making them suitable for large-scale ester production with minimized environmental impact. Additionally, the use of metal-organic frame-works (MOFs) and supported ionic liquid phases (SILPs) as catalytic materials is emerging as a promising strategy for enhancing catalyst reusability and optimizing reaction conditions.

Fischer Esterification

Fischer esterification is a traditional and widely used method for synthesizing esters, involving the reaction of carboxylic acids and alcohols in the presence of a catalyst under heated conditions (Figure 1). Typically, this process uses refluxing excess alcohol with organic acids, catalyzed by a concentrated mineral acid, at an elevated temperature for several hours [12].

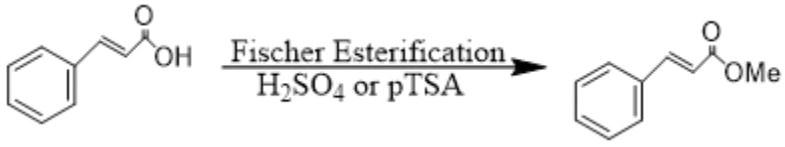

Figure 1. Synthetic Route to Fischer Esterification

Recent research has focused on optimizing Fischer esterification to enhance reaction efficiency, sustainability, and industrial applicability. Heterogeneous acid catalysts, such as sulfonated polymers and zeolites, have been developed as alternatives to traditional homogeneous acids like sulfuric acid. These catalysts offer higher catalytic efficiency, recyclability, and reduced environmental impact. For instance, studies [13] reported the use of sulfonated graphene oxide, resulting in improved yields and reusability. Additionally, ionic liquids and deep eutectic solvents (DES) have been reviewed as eco-friendly solvents that enhance esterification rates and minimize hazardous reagent use. Nonetheless, the process has some limitations, such as the high boiling point, slow reaction rate, and occasionally low yields [6]. Studies have shown that conventional ester synthesis typically requires between 1 to 4 hours for completion. Research revealed that synthesizing methyl esters requires over 1 hour to achieve complete conversion under standard reflux conditions [14].

Table 1. Advantages and Disadvantages of Fischer Esterification

Aspect	Advantages	Disadvantages
Reaction Conditions	Uses relatively mild conditions (acid catalyst, heat)	Requires strong acid (e.g., H_2SO_4), which can lead to side reactions
Reagents	Uses inexpensive and readily available carboxylic acids and alcohols	Reaction is reversible, requiring excess reactants or removal of water to drive equilibrium
Mechanism	Simple, well-understood acid-catalyzed mechanism	Can be slow, requiring prolonged heating
Product Purity	Produces esters with good purity when optimized	Purification may require extraction and distillation
Atom Economy	Produces water as the only by-product	Loss of reactants due to equilibrium limitations
Versatility	Can be applied to a wide range of carboxylic acids and alcohols	Some substrates (e.g., sterically hindered ones) may react poorly
Catalyst	Acid catalyst is catalytic and reusable	Acidic conditions may lead to unwanted side reactions (e.g., dehydration of alcohols)
Scalability	Suitable for both small- and large-scale synthesis	Removal of water in large-scale reactions can be challenging

Steglich Esterification

Steglich esterification involves the conversion of acids and alcohols into esters under neutral and mild conditions (Figure 2).

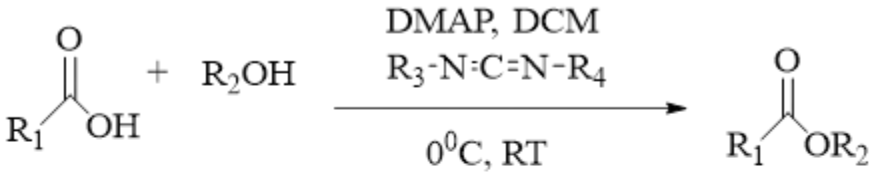

Where;

R1, R2 = alkyl, aryl
R3 = R4 = DCC
R3 = R4 = DIC
R3 = EDC
R4 = 3-dimethyiamino propyl

Figure 2. Synthetic Method for Steglich Esterification

It is considered one of the most efficient methods for ester synthesis [15]. This reaction typically employs carbodiimide coupling reagents, such as N,N'-dicyclohexylcarbodiimide (DCC), N,N'-diisopropylcarbodiimide (DIC), and N-ethyl-N'-(3-dimethylaminopropyl)carbodiimide (EDC). For example, DCC reacts with a carboxylic acid in the presence of dimethylaminopyridine (DMAP) to facilitate ester formation.

The reaction mechanism involves the initial interaction between the carboxylic acid and carbodiimide to form an intermediate, known as O-acyl urea. The acyl group from this intermediate is then transferred by DMAP, which interacts with the alcohol to produce an ester. Here, DMAP acts as an activating agent to transfer the acyl group [16]. Steglich esterification has been used to synthesize several natural products, including anaenamides, cephalosporins, laterocidine, havellockate, and higginasianin [15].

Table 2. Advantages and Disadvantages of Steglich Esterification

Aspect	Advantages	Disadvantages
Reaction Conditions	Mild, room temperature conditions	Requires anhydrous conditions to prevent side reactions
Reagents	Compatible with acid-sensitive functional groups	Uses expensive reagents like DCC (N,N′-Dicyclohexylcarbodiimide) and DMAP (4-Dimethylaminopyridine)
Mechanism	Avoids strong acid/base catalysts	Carbodiimides can lead to side products like urea derivatives
Product Purity	Produces high yields and high selectivity	DCC by-products (dicyclohexylurea) must be carefully removed
Atom Economy	Does not require excess alcohol or acid to drive reaction	Produces additional by-products (e.g., dicyclohexylurea)
Versatility	Works well for sterically hindered or acid-sensitive substrates	Less effective for simple, non-functionalized carboxylic acids and alcohols
Catalyst	Uses DMAP as an effective nucleophilic catalyst	DMAP is toxic and requires careful handling
Scalability	Suitable for lab-scale synthesis and peptide coupling	DCC can be hazardous on large scales due to urea precipitation

Enzymatic Esterification

Enzymes are non-toxic biocatalysts that accelerate the rate of reactions [17]. They are used in reversible reactions and are highly versatile in the catalysis of various types of reaction using mild conditions. Enzymes have gained considerable attention in synthetic chemistry due to their versatility, high specificity, chemo-selectivity, stereo-selectivity, regio-selectivity, their broad substrate array as well as their high reaction yield ability in organic chemistry. Notably, enzymes can selectively catalyze the formation of esters at specific positions on a molecule and can produce a single enantiomer (chiral molecule) preferentially. Enzymes are environmentally friendly due to the use of mild conditions and biodegradability. They avoid the use of hazardous chemicals, reduce waste generation, and often allow for aqueous or solvent-free reactions, aligning with the principles of green chemistry [18]. As a result of enhanced regioselectivities, synthesis of sucrose esters gives a higher purity form. In enzymatic esterification, the enzyme binds to the substrates (the alcohol and the acid) at its active site, stabilizing the transition state and lowering activation energy to accelerate the reaction. The process typically proceeds through the formation of an acyl-enzyme intermediate, followed by the nucleophilic attack of the alcohol, leading to the release of the ester and regeneration of the enzyme. Enzymes as a catalyst have gained importance and significant use in the biotechnology sector globally today. Enzymatic esterify-cation has been experiencing a resurgence in interest and innovation due to its potential for more sustainable and efficient chemical synthesis [19]. The use of enzymes as a catalyst in the synthesis of esters are economically friendly. Although enzymes are expensive, their recyclability and the reduced need for purification steps offset the costs. Enzymes are often reused multiple times without significant loss of activity, contributing to the overall cost-efficiency of the process [20]. Enzymatic esterification is one of the friendly and biological ways of producing biodiesel, compared to that of chemical means in term of temperature, reaction time, purification, desired product, recovery and lot more [21]. Several types of enzymes, including lipases, esterases, pro-teases, carboxylesterases, and phosphor-lipases, can promote ester formation. Among these, lipases are the most commonly used due to their ability to catalyze esterification and transesterification of a wide range of substrates, as well as their high stability, versatility, and relatively low cost [22].

Lipase, also known as triacylglycerol ester hydrolase, is a hydrolase enzyme widely utilized in organic synthesis and biotechnology due to its broad temperature and pH stability, high enantioselectivity, and substrate specificity [23]. Lipases catalyze the hydrolysis of lipids into fatty acids and glycerol and can facilitate reactions involving alcohols and carboxylic acids, esters and alcohols, esters and acids, and acyl group transfer from esters to nucleophiles. Although lipases are found across various organisms, industrial applications primarily utilize those derived from yeast and fungi.

Lipases are instrumental in biodiesel production from waste cooking oil. In ester syn-thesis, lipase functions at equilibrium (Figure 3) and requires a small amount of water to maintain catalytic activity. When anhydrous organic solvents are used, product ester hydrolysis can occur, affecting yield [24].

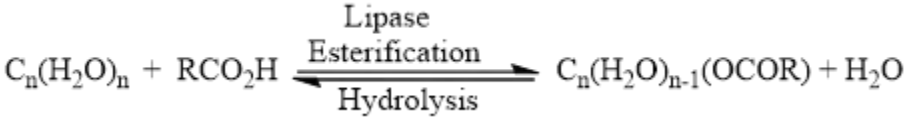

Figure 3. Esterification Reaction Using Lipase Catalyst

Esterase is another enzyme used in esterification, recognized for its specificity and efficiency under mild conditions. As a member of the hydrolase enzyme class, esterases act on ester bonds and can operate in both esterification (forward) and hydrolysis (reverse) reactions. In esterase-catalyzed esterification, the enzyme catalyzes the formation of an ester from a carboxylic acid and an alcohol [25]. Unlike lipases, which hydrolyze long-chain, insoluble carboxylic acids, esterases typically hydrolyze short-chain acids and play a significant role in the metabolism of various biomolecules. Esterases act on substrates like fats, oils, and other ester-containing compounds. They are used in the synthesis of flavors, fragrances, pharmaceuticals, and biofuels [26]. The mechanism involves nucleophilic attack by the hydroxyl group of the alcohol on the carbonyl carbon of the acid, forming a tetrahedral inter-mediate that subsequently collapses to release water and form the ester bond. The enzyme stabilizes the transition state, lowering the activation energy and enhancing the reaction rate [27].

Protease, another enzyme involved in esterification, traditionally cleaves peptide bonds but can also catalyze ester bond formation under specific non-aqueous or low-water conditions, broadening its utility in organic synthesis and biotechnology [28]. This versatility makes proteases valuable in syn-thetic applications where traditional hydrolysis activity is minimized.

Carboxylesterases, another hydrolase sub-class, hydrolyze carboxylic esters into alcohols and carboxylates and are essential for drug metabolism and detoxification. They play a significant role in pharmaceutical research, where they transform ester-containing drugs into active or inactive forms [29]. In addition, carboxylesterases are used in agrochemical detoxification, bioreme-diation, and the synthesis of fine chemicals and bio-fuels [30]. Their catalytic mechanism involves a nucleophilic attack on the carbonyl carbon of the ester, forming a tetrahedral intermediate and an acyl-enzyme complex. Subsequent hydrolysis of this complex by water releases the carboxylate product and regenerates the enzyme.

Table 3. Advantages and Disadvantages of Enzymatic Esterification

Aspect	Advantages	Disadvantages
Reaction Conditions	Mild, environmentally-friendly conditions (room temperature, aqueous or organic solvents)	Requires strict control of pH and temperature to maintain enzyme activity
Reagents	Highly selective for specific substrates, reducing side reactions	Enzymes can be expensive and may require co-factors
Mechanism	Biocatalytic, avoids harsh acids or bases	Reaction rates are often slower compared to chemical methods
Product Purity	High chemo-, regio-, and stereoselectivity	Product isolation may require additional purification steps
Atom Economy	Minimal by-products, greener alternative	Some reactions may require excess reactants to drive equilibrium
Versatility	Works well with sensitive functional groups and complex molecules	Not suitable for all types of esterification, especially those requiring extreme conditions
Catalyst	Enzymes (e.g., lipases, esterases) are reusable and biodegradable	Enzymes may lose activity over time and require special storage conditions
Scalability	Potential for industrial-scale applications in pharmaceuticals and food industries	Large-scale enzymatic processes can be costly and may require immobilized enzymes for efficiency

Microwave- Assisted Esterification

Microwave-assisted esterification is a versatile and energy-efficient synthetic route for ester synthesis, offering advantages such as reduced reaction times, cost-effectiveness, and positive environmental impacts [31]. Microwaves are electromagnetic waves with frequencies ranging from 300 MHz to 300 GHz, used widely in organic synthesis. This technique relies on dipolar polarization and ionic conduction, with low energy input, allowing for efficient energy transfer through electromagnetic waves [32]. During microwave-assisted esterification, the reaction medium is irradiated, causing polar molecules, such as alcohol, to align with the oscillating magnetic field. This alignment,

coupled with molecular dipole interactions with the electric field, generates heat through molecular friction, thereby accelerating reaction rates.

Table 4. Advantages and Disadvantages of Microwave-Assisted Esterification

Aspect	Advantages	Disadvantages
Reaction Conditions	Rapid heating, leading to shorter reaction times	Requires specialized microwave equipment
Reagents	Can work with conventional esterification reagents (e.g., acids, alcohols, catalysts)	Some reagents may degrade under microwave irradiation
Mechanism	Enhances reaction rates and yield through localized heating	Not all substrates absorb microwave radiation effectively
Product Purity	Often leads to higher yields and fewer side products	Can cause overheating, leading to unwanted by-products
Atom Economy	Reduces the need for excess reagents and solvents	Some reactions may still require catalysts or excess reactants
Versatility	Works for a variety of esterification methods, including Fischer and enzymatic esterification	Scale-up can be challenging due to non-uniform heating in larger volumes
Catalyst	Can reduce or eliminate the need for strong acids/bases	Some catalysts may degrade under microwave conditions

Microwave-assisted synthesis has proven effective for biodiesel production and has been successfully applied to the synthesis of esters like methyl levulinate, ethyl ferulate, and methyl salicylate, as shown in Figure 4. Esterification reactions using microwave irradiation can be conducted in various setups, including batch systems and continuous flow reactors [33].

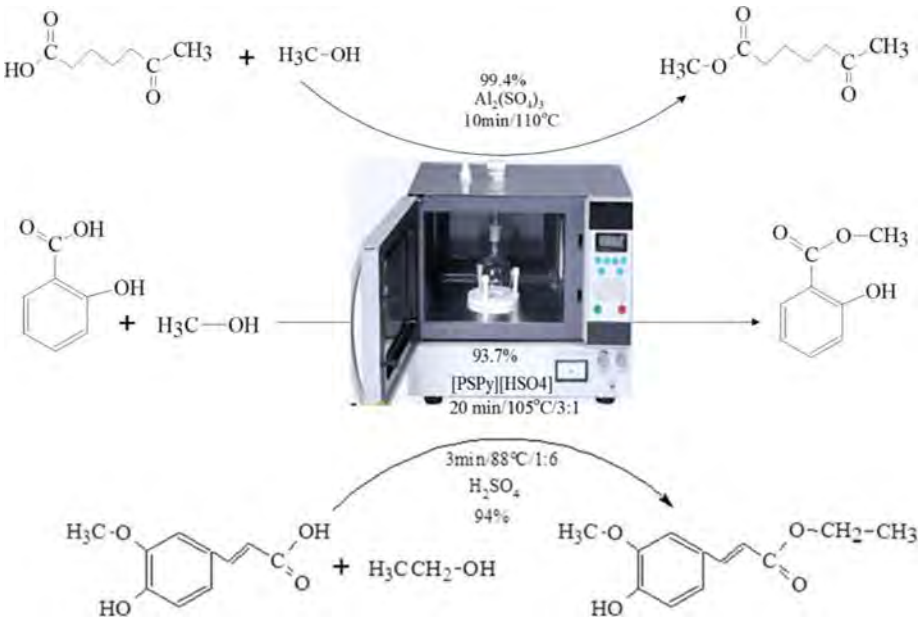

Figure 4. Microwave Irradiation for the Production of Methyl Levulinate, Ethyl Ferulate and Methyl Salicylate [6]

This technique addresses limitations associated with conventional esterification methods, making it a valuable approach for synthesizing ester compounds.

Table 5, below, provides a comparative analysis of reaction times and yields for synthesizing various esters using microwave irradiation versus conventional heating methods, highlighting the efficiency and benefits of microwave-assisted synthesis in terms of both reaction speed and product yield.

Table 5. Reaction Time of Microwave Irradiation Compared to the Conventional Heating in the Synthesis of Some Esters

Esters	Temperature (°C)	Microwave	Irradiation	Conventional	Heating
		Time (h)	% Yield	Time (h)	% Yield
1	120	0.5	85	5	63
2	90	4	96	4	90
3	70	3	79	3	60
4	60	1	94.84	1	69
5	60	1	80	10	30
6	90	0.5	90	3	65

Studies show that microwave irradiation significantly reduces the reaction time compared to conventional heating. [34] reported the synthesis of methyl levulinate (1) at 120°C, takes only 0.5 h with 85% yield using micro-wave irradiation, while conventional heating requires 5 h and yields only 63% [34]. This trend is similarly observed for ascorbyl palmitate (5), where microwave irradiation at 60°C yields 80% in just 1 h, whereas conventional heating requires 10 h and produces a much lower yield of 30% [35].

The effectiveness of microwave irradiation is further demonstrated in the synthesis of ethyl ferulate and citronellyl acetate. At 90°C, ethyl ferulate (6) synthesis takes only 0.5 h with microwave heating, yielding 90%, whereas it requires 3 h with conventional heating and achieves a lower yield of 65% [6]. Similarly, for citronellyl acetate (4) at 60°C, microwave irradiation yields 94.84% in 1 h, compared to 69% yield with conventional heating over the same time period [36].

However, esters like sorbityl laurate and geraniol ester, the reaction times are similar across both methods, suggesting that micro-wave irradiation does not always drastically reduce reaction time. For sorbityl laurate (2), both methods require approximately 4 h, though microwave heating provides a slightly higher yield of 96% compared to 90% with conventional heating [37]. Also, the synthesis of geraniol ester (3) at 70°C takes 3 h with both methods, though the yield with micro-wave irradiation (79%) is higher than that of conventional heating (60%) [38].

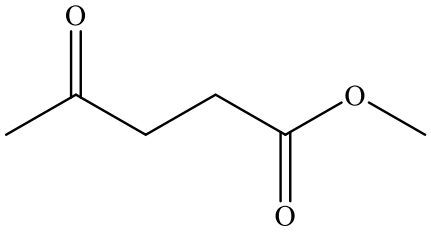

Methyl levulinate

1

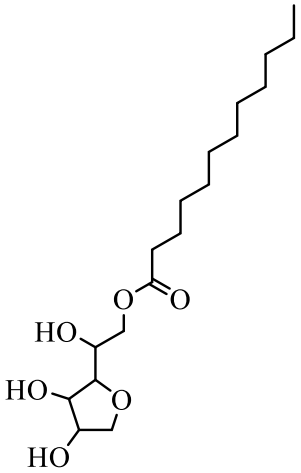

Sorbityl Lautrate

2

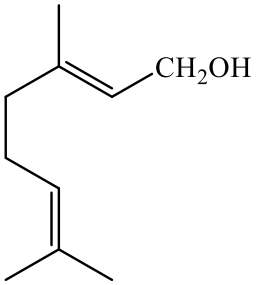

Geraniol ester

3

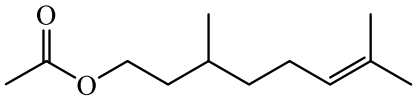

Citronellyl acetate

4

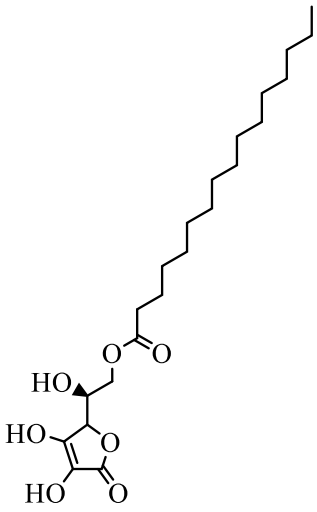

Ascorbyl palmitate

5

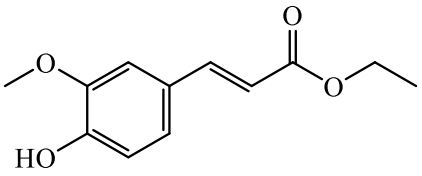

Ethyl ferulate

6

Microbubble Esterification

Microbubble technology is an innovative method for enhancing esterification efficiency, particularly in biodiesel production from vegetable oils, as well as in synthesizing esters for pharmaceuticals and fragrances. Microbubbles, generated using a micro-bubble generator, have diameters between 10 and 100 micrometers [39]. This technique can be implemented through methods such as ultrasonics, gas sparging through porous materials, and mechanical agitation. Studies have shown that

microbubbles significantly improve mass transfer at the gas-liquid interface, providing a stable surface area where reactants can easily diffuse to the reactive sites [6]. The small size and high surface area of microbubbles allow for uniform distribution and effective mixing within the liquid medium, optimizing reaction conditions. For example, reactions between carboxylic acids and alcohols, such as oleic acid with methanol or ethyl acetate production, demonstrate higher yields in shorter reaction times when using microbubble reactors [40].

Table 6. Advantages and Disadvantages of Microbubble-Assisted Esterification

Aspect	Advantages	Disadvantages
Reaction Conditions	Enhances mass transfer and interfacial area for better reaction efficiency	Requires specialized microbubble generation equipment
Reagents	Can reduce the need for excess reagents due to improved reactant dispersion	Some solvents and reactants may not form stable microbubbles effectively
Mechanism	Increases reaction kinetics by improving gas-liquid or liquid-liquid interactions	Limited knowledge and optimization for certain esterification reactions
Product Purity	Can lead to higher yields and fewer side products by promoting uniform mixing	Potential bubble collapse or instability may affect reaction control
Atom Economy	Reduces reagent waste and enhances efficiency	Additional gas input may be needed for bubble formation
Versatility	Works for various esterification types, including enzymatic and catalytic methods	Not widely studied or commercialized for all esterification reactions
Catalyst	Can improve catalyst dispersion and reactivity	Some catalysts may be deactivated by bubble interactions or gas phase effects
Scalability	Promising for industrial applications due to enhanced efficiency	Large-scale implementation requires advanced reactor design and cost considerations

Acid- and Base-Catalyzed Esterification

Esterification of alcohols with carboxylic acids in the presence of an acid catalyst is known as acid-catalyzed esterification. This process (Figure 5) involves the protonation of the carboxylic acid, which increases the electrophilicity of the carbonyl carbon, making it more susceptible to nucleophilic attack by alcohol.

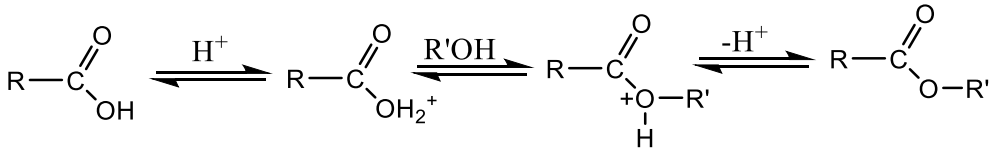

Figure 5. Acid-Catalyzed Esterification

Following nucleophilic attack and subsequent proton transfer, the product undergoes dehydration to form the ester. Common acid catalysts include sulfuric acid (H_2SO_4) and hydrochloric acid (HCl), and the reaction mixture is typically heated under reflux to facilitate the reaction [41].

Base-catalyzed esterification refers to the reaction between an ester and an alcohol in the presence of a base catalyst to form a new ester (Figure 6). This reaction is widely used in the synthesis of fatty acid esters and in biodiesel production from natural products [42-44].

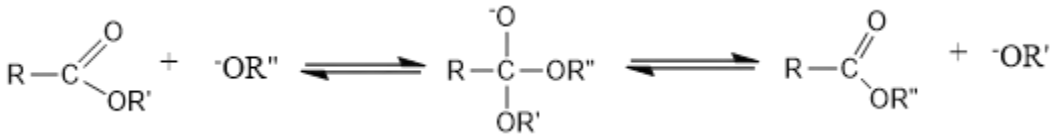

Figure 6. Base-Catalyzed Esterification

In this process, the base deprotonates the alcohol, generating an alkoxide ion, a strong nucleophile that attacks the carbonyl carbon of the ester. This forms a tetrahedral intermediate, which then undergoes further rearrangement to produce a new ester and an alkoxide ion. Base-catalyzed esterification generally proceeds faster than acid-catalyzed esterification [45]. However, one limitation of base-catalyzed transesterification is the risk of saponification, where fatty acids react with the base to form soap, leading to phase separation issues in the reaction mixture.

Table 7. Comparison Between Acid-Catalyzed and Base-Catalyzed Esterification

Aspect	Acid-Catalyzed Esterification	Base-Catalyzed Esterification
Reaction Conditions	Requires strong acids (e.g., H_2SO_4, HCl) and heat	Requires strong bases (e.g., NaOH, KOH), usually under milder conditions
Reagents	Uses carboxylic acid and alcohol	Uses carboxylate salts and alkyl halides or esters
Mechanism	Protonation of carboxyl group increases electrophilicity	Nucleophilic attack by carboxylate anion on alkyl halide/ester
Product Purity	May require extensive purification due to side reactions and reversibility	Often produces high-purity esters but may require excess reactants
Atom Economy	Produces water as a by-product	Produces inorganic salts (from base neutralization)
Versatility	Works well for a broad range of carboxylic acids and alcohols	Limited to substrates that can undergo nucleophilic substitution
Catalyst	Acid catalyst is catalytic and reusable but can cause side reactions	Base catalyst often consumed in neutralization, increasing waste
Scalability	Suitable for large-scale synthesis but requires water removal	Scalable, but strong bases can lead to unwanted side reactions

Reaction Mechanism of Esterification

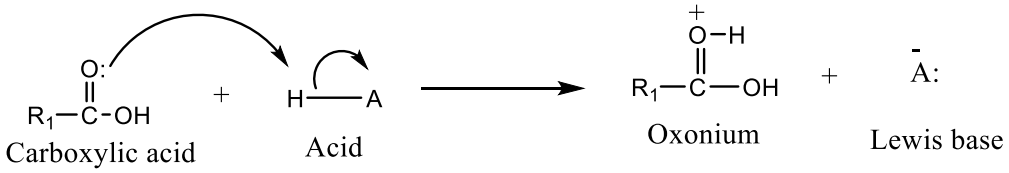

Protonation of carbonyl group of the carboxylic acid by catalyst

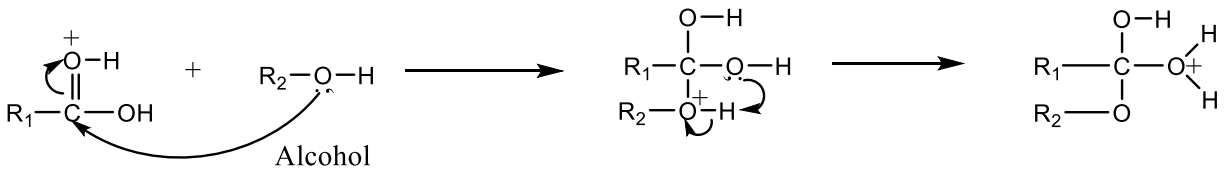

Nucleophilic attack on carbonyl by acohol and cleavage of pi bond

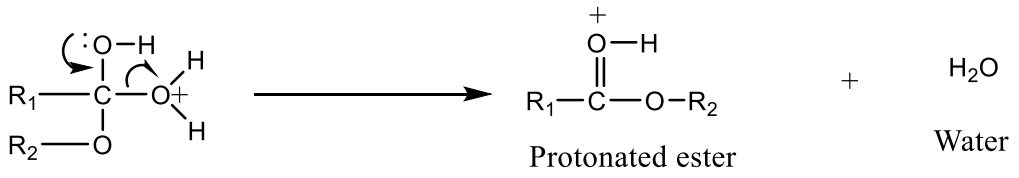

Elimination of water followed by a pi bond formation between C and O

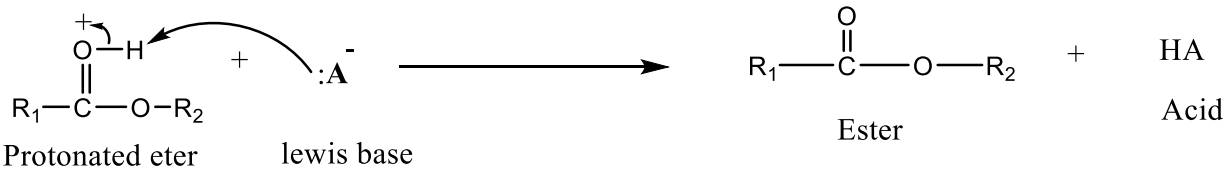

Deprotonation of protonated esters given rise to the desired ester

Membrane Technology Esterification

Membrane technology has gained significant attention for its role in the synthesis and purification of esters. This technique utilizes selectively permeable membranes to enhance various stages in ester production, including separation, purification, and catalysis [46]. It has proven especially valuable in applications such as biodiesel synthesis. Membrane technology enables the continuous removal of by-products (e.g., water) from esterification reactions, shifting the reaction equilibrium toward product formation and increasing both yield and reaction rate. It also allows selective removal of impurities and unreacted starting materials, resulting in high-purity ester products. Membrane technology is suitable for both laboratory-scale synthesis and industrial production of esters, offering advantages in energy efficiency, sustainability, and cost-effectiveness. Various mem-brane technologies are used in ester syn-thesis, including pervaporation, membrane distillation, membrane bioreactors, nano-filtration, and catalytic membranes, each classified by mode of action and application in the esterification process.

Pervaporation, a widely used membrane technology in ester synthesis, selectively removes water from the esterification reaction mixture [47]. This method is especially useful for separating close-boiling-point mixtures and low-concentration compounds. In pervaporation, a hydrophilic membrane separates reactants from the permeate side, where water vapor is continuously removed. literature reported successful synthesis of ethyl acetate via the esterification of acetic acid and ethanol, using polyvinyl alcohol (PVA) and polyacetate membranes with high selectivity for water removal [48]. This selective removal of water shifted the equilibrium toward ester formation, achieving higher yields.

Membrane distillation employs a hydro-phobic membrane to separate water based on differences in vapor pressure and is frequently used in high-temperature reactions [49]. Research has demonstrated the application of polytetrafluoroethylene (PTFE) membranes in the esterification of lactic acid with methanol [50]. This study found that PTFE membranes offer stability

and selectivity, making them suitable for continuous water removal at elevated temperatures, significantly enhancing both reaction rate and ester yield.

Membrane bioreactors (MBRs) are commonly used in enzymatic esterification, combining enzymatic catalysis with membrane separation to provide controlled reaction environments and efficient product recovery [51]. Enzymes immobilized on the membrane surface offer a high surface area for reactions, while the membrane selectively removes water, resulting in high conversion rates and purity of the ester products.

Nanofiltration membranes, characterized by nanometer-range pore sizes, are also frequently used in ester synthesis for their ability to separate small molecules [52]. These membranes retain the ester product while allowing the passage of water and unreacted alcohol, which increases ester concentration and yield [53].

Catalytic membranes, incorporating catalytic sites within the membrane matrix, integrate reaction and separation into a single unit and have shown significant promise in ester synthesis. [54] reported the use of a sulfonated polyether ether ketone (SPEEK) catalytic membrane for the esterification of oleic acid with methanol. The SPEEK membrane provided catalytic sites for the reaction and allowed for continuous water removal, enhancing the overall efficiency and yield of the esterification process.

Table 8. Advantages and Disadvantages of Membrane Technology-Assisted Esterification

Aspect	Advantages	Disadvantages
Reaction Conditions	Operates under mild conditions, reducing thermal degradation	Requires specialized membrane materials and equipment
Reagents	Can enhance reaction efficiency by selectively removing water or by-products	Membrane fouling can occur, reducing efficiency over time
Mechanism	Improves ester yield by shifting equilibrium via selective permeation of water or alcohol	Some esterification reactions may not be compatible with membrane separation
Product Purity	Produces high-purity esters by continuously removing undesired by-products	Membrane selectivity and efficiency depend on operating conditions
Atom Economy	Reduces excess reactant usage and minimizes waste	Membrane replacement and maintenance add to process costs
Versatility	Can be integrated with enzymatic, acid- or base-catalyzed esterification	Not all esterification reactions benefit significantly from membrane separation
Catalyst	Can reduce catalyst degradation by maintaining optimal reaction conditions	Some catalysts may be incompatible with membrane materials
Scalability	Suitable for industrial applications, particularly in biodiesel and pharmaceutical synthesis	Large-scale implementation can be costly due to membrane fabrication and operational constraints

Non-Catalytic Thermal Esterification

Non-catalytic thermal esterification is another synthetic route for ester production conducted without the use of catalysts, relying solely on thermal energy to facilitate the reaction between carboxylic acids and alcohols [55]. In this approach, heat provides the activation energy required for the reaction to proceed.

Non-catalytic thermal esterification employs alcohol in either supercritical or subcritical states [56]. In the supercritical state, alcohols, such as methanol, are heated above their critical temperature and pressure, resulting in a fluid with properties between those of a

liquid and a gas, which enhances solubility and reaction rates. Supercritical fluids promote efficient mixing, diffusion, and reaction kinetics, resulting in desirable yields. For example, [57] reported the synthesis of methyl oleate from oleic acid using supercritical methanol. Another study documented the production of fatty acid methyl esters (biodiesel) from waste beef tallow using supercritical methanol, demonstrating that the supercritical approach enables a green synthetic pathway with high conversion rates. At supercritical temperatures, methanol's dielectric constant is reduced, forming a single-phase mixture that favors the esterification reaction.

In the subcritical state, alcohol is heated to high temperatures without reaching its critical point, allowing it to act as a liquid or gas [58]. Subcritical fluids offer reduced solubility and diffusion rates, potentially resulting in slower reaction kinetics but with operational advantages. For instance, esterification of fatty acids with ethanol in subcritical water can produce ethyl esters [59]. Additionally, reported the synthesis of fatty acid methyl esters from fatty acids derived via subcritical water hydrolysis of fresh and waste cooking oil. This study highlighted that subcritical water hydrolysis enhances esterification by increasing the ionic product, thus facilitating the reaction, and reducing the need for extensive feedstock purification.

The mechanism of action in non-catalytic thermal esterification involves nucleophilic acyl substitution [6]. At elevated temperatures (150–250°C), the hydroxyl group (-OH) from the carboxylic acid and the hydrogen atom (H) from the alcohol combine to form water (H_2O). The continuous removal of water from the reaction shifts the equilibrium toward ester formation.

Non-catalytic thermal esterification offers several advantages, including the elimination of catalyst-related costs, reduced contamination, and fewer purification steps. These benefits are particularly valuable in biodiesel and fragrance production, where catalyst residues can complicate product quality. However, this method also has limitations, such as the need for high temperatures (often above 200°C), which increases energy consumption and can limit reaction rates, particularly with bulky or less reactive substrates [6].

Table 9. Advantages and Disadvantages of Non-Catalytic Thermal Esterification

Aspect	Advantages	Disadvantages
Reaction Conditions	Avoids the need for acid or base catalysts, reducing side reactions	Requires high temperatures (often above 200°C), leading to high energy consumption
Reagents	Simple reaction setup using only carboxylic acids and alcohols	Some reactants may degrade or undergo unwanted side reactions at high temperatures
Mechanism	Driven by heat, shifting equilibrium towards ester formation	Reaction is often slow and may require prolonged heating
Product Purity	Avoids catalyst contamination, leading to cleaner products	Risk of polymerization or decomposition of reactants at high temperatures
Atom Economy	Produces only water as a by-product, making it environmentally friendly	High temperatures can lead to side-product formation, reducing efficiency
Versatility	Suitable for esterification of simple and stable carboxylic acids and alcohols	Not ideal for thermally sensitive or sterically hindered substrates
Catalyst	No need for catalysts, reducing costs and complexity	Requires excess reactants or continuous water removal to drive equilibrium
Scalability	Can be applied in industrial settings for bulk ester production	High energy demand makes it less sustainable compared to catalytic methods

Factors Affecting the Synthesis of Esterification

Esterification is a widely studied organic synthesis process due to its applications in pharmaceuticals, industry, cosmetics, food, beverages, and personal care products. However, several factors impact the reaction chemistry of esterification. The mode of reaction during synthesis significantly affects esterification. According to [6], esterification involves the equimolar reaction of a carboxylic acid with an alcohol. However, the equilibrium constant for this reaction is influenced by both temperature and the ratio of reactants. Typically, only two-thirds of the acid reacts in an equimolar mixture; thus, increasing the alcohol concentration enhances product yield. However, an excess of alcohol can reduce the catalyst concentration, which may hinder the forward reaction and lead to catalyst deactivation due to binding at the active site [60].

The structure of the reactants also affects esterification chemistry (Figure 7). Alcohols are classified as primary, secondary, or

tertiary, based on the position of the hydroxyl group.

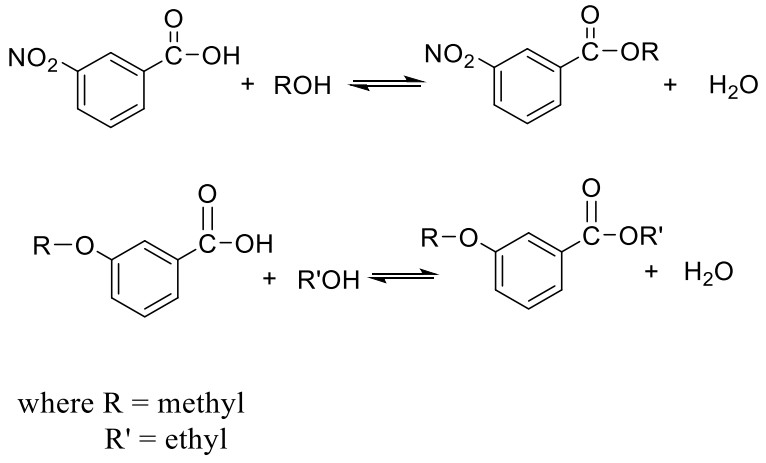

where R = methyl
R' = ethyl

Figure 7. Presence of Some Functional Group Affecting Reaction Mode in Esterification Reaction

This classification impacts ester yield and by-product formation. Primary alcohols are reported to yield high ester levels within a short reaction time, secondary alcohols yield an average ester percentage, and tertiary alcohols tend to produce a low yield and require a longer reaction time due to steric hindrance around the hydroxyl group [6].

Water is another critical factor influencing esterification chemistry. Water shifts the reaction equilibrium toward the reactants, which can reduce ester yield. However, continuous removal of water from the reaction mixture promotes the forward reaction, resulting in a higher ester yield. Water presence can also lead to ester hydrolysis, impacting the reaction rate. Acid-catalyzed esterification is particularly sensitive to water, as it can lower catalytic activity and slow down the reaction rate [61].

Catalysts play a vital role in esterification by lowering activation energy, increasing reaction rates, and influencing reaction conditions [62]. The choice of catalyst affects process efficiency, selectivity, and sustainability. Solvents also impact reaction rates; excessive solvent use, especially polar or hydrophilic solvents, can reduce ester yield. Polar solvents may interact with the enzyme's water layer, altering its activity, whereas non-polar solvents enhance enzyme dispersion at active sites, resulting in a higher reaction rate and yield [63]. Additionally, polar solvents can stabilize ionic intermediates and transition states, which can benefit the reaction rate. In acid-catalyzed esterification, polar solvents dissolve the carboxylic acid, alcohol, and catalyst, facilitating the reaction. However, an excess of polar solvent may slow down the reaction.

Transesterification

Transesterification is a reaction method that involves the conversion of oils and fatty acids into alkyl esters. The process involves a reaction of triglycerides with an alcohol (alkane) to form alkyl ester of fatty acids and glycerol. It is a versatile reaction that is widely used in the production of biodiesel, polymers, and fine chemicals [64]. Transesterification, also known as alcoholysis, entails the reaction of lipids and low carbon alcohol in the presence of a homogeneous or heterogeneous catalyst [65]. It is also used in the production of hardened vegetable oil as it reduced its viscosity and improved its fuel properties. Methanol and ethanol are usually employed in the transesterification process, but methanol is preferred because of it is economically friendly nature and steady availability. As many underutilized seed oils are emerging, the transesterification to fatty acid methyl or ethyl esters prior to analysis have been widely adopted [66,67]. The application of the transesterification techniques extended to analysis of triacylglycerol (fats and oils) from animal sources [68]. Transesterification process can be carried out through homogenous or heterogeneous acid or base catalysts. Generally, it is believed that homogeneous catalysis undergoes a fast reaction when compared to the heterogenous catalyst; yet, it cannot be reused, which serves as a major setback. However, the use of heterogenous catalysis in continuous biodiesel production results in high activity, high selectivity, ease of separation from product and catalyst reusability, although its reaction often takes longer [69]. Despite the time taken for the reaction to complete, heterogeneous plays a major role in overcoming the challenges faced by homogeneous catalysis. This includes the ability to regenerate and recycle the products, quick separation and purification of product. There are some factors affecting the transesterification process which include the type of catalyst used and concentration, mole ration, reaction time, temperature, and free fatty acid [70].

General equation for transesterification reaction

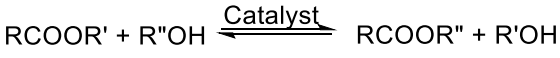

(1)

Transesterification of triglyceride

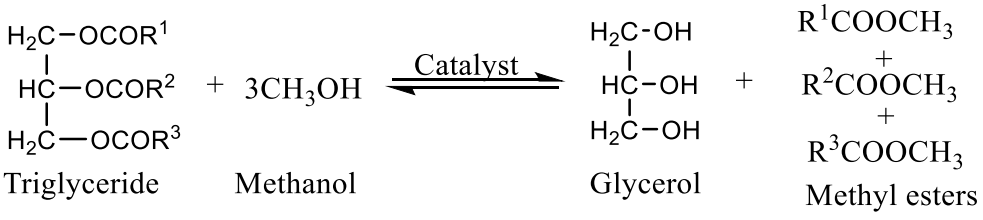

(2)

Application of Esters

Ester compounds are one of the major compounds used across different industries due to their distinctive chemical properties. Synthetic esters are extensively used as intermediates in the formation of a variety of organic compounds. Literature revealed its

application in the pharmaceutical industry, food and beverage industries, biochemistry, material sciences and so on.

Reactive capacity of esters, particularly in esterification and hydrolysis reactions, makes them invaluable in the synthesis of pharmaceuticals, where they are used to create prodrugs [71]. These prodrugs improve the solubility of active pharmaceutical ingredients. Esters enhance the pharmacokinetic properties of active drugs. An example is the ester enalapril, a prodrug that is hydrolyzed *in vivo*, then converts to the active form of enalaprilat, used to treat hypertension and heart failure. Also, aspirin (acetylsalicylic acid), an ester that undergoes hydrolysis to produce salicylic acid, provides both anti-inflammatory and analgesic effects when used. These ester modifications improve solubility, stability, and absorption of drugs, enhancing their therapeutic efficacy [72].

In the food and beverage industry, according to [73], ester compounds are widely used as flavoring agents due to their ability to impart fruity and floral aromas. Different ester compounds such as ethyl acetate, isoamyl acetate, ethyl butyrate, methyl butyrate were studied. They impart fruity and floral scents to enhance the aroma and taste of a wide range of products. Natural and synthetic esters are added to candies, beverages, and baked goods to achieve desired flavor profiles. In fragrances, esters are major components in the formulation of perfumes and cosmetics, contributing to the pleasant scents [74].

Esters have also been found useful in biochemistry, especially in biological processes for the formation of essential biomolecules. Esters are found in DNA and RNA as phosphodiester bonds, linking nucleotides together to form the backbone of genetic materials [75]. Literature has revealed acetylcholine, a neurotransmitter used in muscle contraction and neural signaling [76].

Ester compounds have also been widely used in material science, particularly in the production of polymers. Polyesters, such as polyethylene terephthalate (PET), are synthesized through the polycondensation of diols and dicarboxylic acids or their ester derivatives. These materials are used in the production of textiles, packaging, and plastic bottles due to their durability and flexibility [77]. Additionally, esters serve as plasticizers in the manufacturing of plastics, enhancing the flexibility and workability of polymers like polyvinyl chloride (PVC) [78].

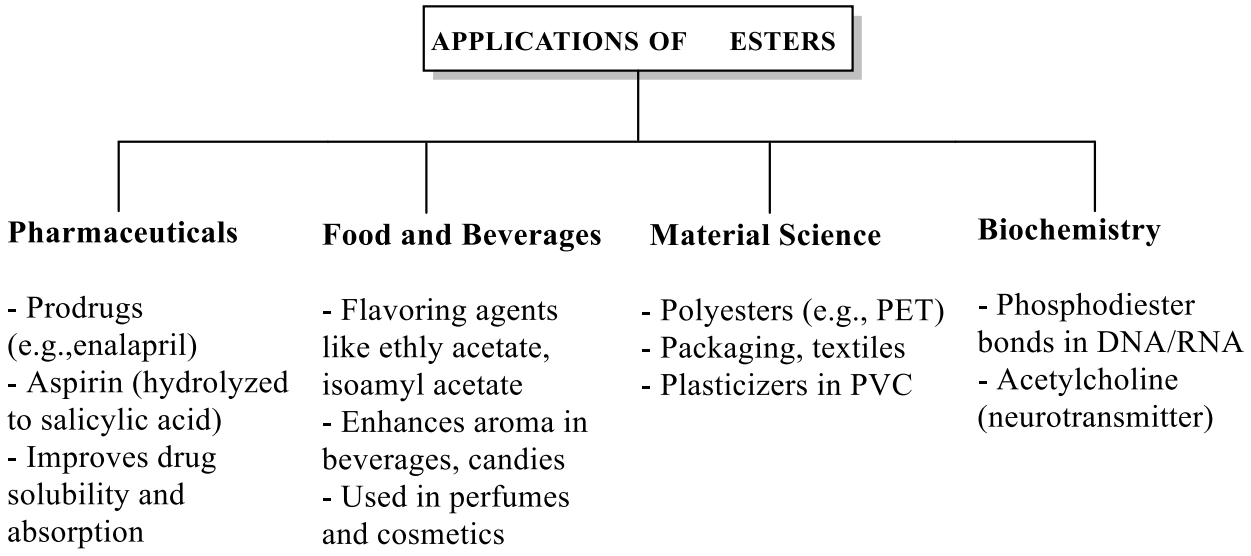

Esters Toxicity

Esters are widely used across industries, including food flavoring, fragrances, pharmaceuticals, and as solvents, making it essential to understand their toxicity profiles. Generally, esters exhibit low toxicity compared to other organic compounds, which makes them relatively safe for many applications. However, toxicity can vary significantly depending on ester structure and functional groups. Common esters, like ethyl acetate and methyl acetate, are low in toxicity and are frequently used in the food and beverage industries without significant health concerns when regulated appropriately [79].

However, the metabolic breakdown of esters can produce potentially toxic metabolites. For example, methanol (a breakdown product of methyl esters) is highly toxic and can lead to serious health effects, including blindness and central nervous system damage. Additionally, aromatic esters such as benzyl acetate can metabolize into benzyl alcohol and acetic acid, which may exhibit toxicity depending on exposure dose and duration [80].

Long-term exposure to certain phthalate esters, widely used as plasticizers, is linked to adverse health effects such as endocrine disruption, reproductive toxicity, and developmental toxicity in humans and animals. Phthalates like diethyl phthalate disrupt hormone functions, posing risks to reproductive health and development, especially in infants, following prolonged exposure [81]. Regulatory bodies are working to limit the use of certain phthalates in consumer products, especially those intended for children and pregnant women, to reduce potential risks.

In industries, exposure to high concentrations of ester vapors may lead to respiratory irritation, dizziness, headaches, and, in severe cases, central nervous system depression [82]. Thus, implementing protective measures, like proper ventilation and

personal protective equipment, is essential to minimize these risks. Many esters are biodegradable and environmentally low risk, but breakdown products like certain phthalates can accumulate and impact aquatic ecosystems [83].

In response to concerns about ester toxicity, several studies have proposed solutions to reduce toxicity by modifying ester structure, controlling exposure, enhancing biodegrade-ability, and strengthening regulatory frame-works. Structural modifications can enhance compound safety by focusing on esters that yield non-toxic metabolites. [84] reported that switching from methyl to ethyl or isopropyl esters in various applications reduces toxic metabolite formation, particularly avoiding methanol release, which has neurotoxic effects. Additionally, research shows that improving ester biodegradability has led to the development of alternative plasticizers, such as citrate and adipate esters, which are less toxic and more environ-mentally friendly than phthalates, decom-posing readily without harmful byproducts [85]. Advanced ventilation systems and the use of PPE effectively reduce inhalation risks for workers exposed to volatile ester compounds, as high concentrations of ester vapors can cause respiratory and neurological issues.

3. Conclusion

This study provides a comprehensive overview of esterification, synthesis methods, influencing factors, applications, and toxicity of esters. Esterification, a fundamental reaction in organic chemistry, plays a critical role in the synthesis of esters, which are widely utilized across industrial, pharmaceutical, and biochemical sectors. Esters are synthesized through the reaction of carboxylic acids and alcohols in the presence of catalysts, highlighting the versatility and efficiency of this chemical process. Advanced methods, including enzyme-catalyzed esterification and the use of alternative energy sources like microwave and ultrasonic irradiation, have further broadened the scope of ester synthesis, offering environmentally-friendly and efficient pathways.

Several factors influence esterification, such as the nature of the reactants, catalyst type and concentration, temperature, and solvent choice. Understanding these factors is essential for optimizing reaction conditions to achieve high yields and selectivity. Esters have a wide range of applications across various sectors. In the pharmaceutical industry, esters are used as intermediates in the synthesis of drugs and prodrugs. The flavor and fragrance industries rely heavily on esters for their pleasant aromas and flavors. Additionally, esters serve as solvents, plasticizers, and lubricants in industrial ap-plications, underscoring their multifunctional nature.

The toxicity of esters is an important con-sideration in pharmaceutical and environ-mental applications. While many esters are generally regarded as safe, some can exhibit toxicity, necessitating thorough evaluation and regulation. Understanding the toxicological profiles of esters is crucial for

mitigating potential risks and ensuring safe usage.

Research in esterification and ester synthesis is a dynamic and evolving field, driven by the ongoing pursuit of more efficient, sustainable, and environmentally-friendly synthetic methods. The diverse applications of esters, alongside an awareness of their toxicity, enhance the significance of this class of compounds in modern science and industry. Future research and innovation in ester chemistry will undoubtedly lead to new discoveries and advancements.

4. References

1. Tan M, Peters BB, Andersson P, Zhou T. Recent advances in the metal catalyzed asymmetric alkene hydrogenation of cyclic conjugated carbonyl compounds. *Org. Chem. Front.*,2024. doi.org/10.1039/D4QO00227J
2. Rigo D, Masters AF, Maschmeyer T, Selva M, Fiorani G. Isopropenyl esters (iPEs) in green organic synthesis. *Chem.—A Eur. J.*, 2022, 28(40),e202200431. doi.org/10.1002/chem.202200431
3. Bali R, Shet H. Transition metal-based nanoparticles catalyzed esterification reactions. *Bombay Technol.*,2021. doi.org/10.36664/bt/2021/v68i1/160703
4. Şahin S, Kaya B, Güldü A. Scabies:A growing concern for public health. *Anatolian J. Fam. Med.*, 2024, 7(1), 9-12.doi: 10.5505/ajfamed.2024.10820
5. Belousov AS, Esipovich AL, Kanakov EA, Otopkova KV. Recent advances in sustainable production and catalytic transformations of fatty acid methyl esters. *Sustainable Energy Fuels*, 2021, 5(18), 4512-4545. doi.org/10.1039/D1SE00830G
6. Khan Z, Javed F, Shamair Z, Hafeez A, Fazal T, Aslam A, Zimmerman WB, Rehman F. Current developments in esterification reaction: A review on process and parameters. *J. Ind. Eng. Chem.*, 2021, 103,80-101. doi.org/10.1016/j.jiec.2021.07.018
7. Yu X, Williams CT. Recent advances in the applications of mesoporous silica in heterogeneous catalysis. *Catal. Sci. Technol.*, 2022, 12(19), 5765-5794. doi.org/10.1039/D2CY00001F
8. Ramakrishnan A, Romeijn SG, Bouwman E. Palladium-catalyzed synthesis of carboxylic acid anhydrides from alkenes. *J. Catal.*, 2023, 428,115192. doi.org/10.1016/j.jcat.2023.115192
9. Zheng Y, Huang C, Li Y, Yang Y, Xu R. Review on performance and preparation of catalysts for oxidative esterification of aldehydes or alcohols to esters. *ChemCatChem*, 2024, 16(4),e202300976. doi.org/10.1002/cctc.202300976
10. Castiello C, Junghanns P, Mergel A, Jacob C, Ducho C, Valente S, Rotili D, Fioravanti R, Zwergel C, Mai A. GreenMedChem: The challenge in the next decade toward eco-friendly compounds and processes in drug design. *Green Chem.*, 2023, 25(6), 2109-2169. doi: 10.1039/D2GC03772F
11. Isci A, Kaltschmitt M. Recovery and recycling of deep eutectic solvents in

biomass conversions: A review. *Biomass Convers. Biorefin.*, 2021, 1-30. doi: 10.1007/s13399-021-01860-9

12. Steele JH, Bozor MX, Boyce GR. Transmutation of scent: An evaluation of the synthesis of methyl cinnamate, a commercial fragrance, via a Fischer esterification for the second-year organic laboratory. *J. Chem. Educ.*, 2020, 97(11), 4127-4132. doi.org/10.1021/acs.jchemed.0c00861
13. Roy AS, Poulose AC, Bakandritsos A, Varma RS, Otyepka M. 2D graphene derivatives as heterogeneous catalysts to produce biofuels via esterification and transesterification reactions. *Appl. Mater. Today*, 2021, 23, 101053. doi.org/10.1016/j.apmt.2021.101053
14. Štrukil V, Margetić D. Mechanochemistry in heterocyclic synthesis. *Heterocycles: Synth., Catal., Sustainability, Charact.*, 2022, 339-369. doi.org/10.1002/9783527832002.ch10
15. Munawar S, Zahoor AF, Hussain SM, Ahmad S, Mansha A, Parveen B, Ali KG, Irfan A. Steglich esterification: A versatile synthetic approach toward the synthesis of natural products, their analogues/derivatives. *Heliyon*, 2024, 10(1).
16. Tsakos M, Schaffert ES, Clement LL, Villadsen NL, Poulsen TB. Ester coupling reactions–An enduring challenge in the chemical synthesis of bioactive natural products. *Nat. Prod. Rep.*, 2015,32(4),605-632. doi.org/10.1039/C4NP00106K
17. Anwar A, Imran M, Iqbal HM. Smart chemistry and applied perceptions of enzyme-coupled nano-engineered assemblies to meet future biocatalytic challenges. *Coord. Chem. Rev.*, 2023, 493,215329. doi.org/10.1016/j.ccr.2023.215329
18. Kuthiala T, Thakur K, Sharma D, Singh G, Khatri M, Arya SK. The eco-friendly approach of cocktail enzyme in agricultural waste treatment: A comprehensive review. *Int. J. Biol. Macromol.*, 2022, 209, 1956-1974. doi.org/10.1016/j.ijbiomac.2022.04.173
19. Romero EO, Saucedo AT, Hernández-Meléndez JR, Yang D, Chakrabarty S, Narayan AR. Enabling broader adoption of biocatalysis in organic chemistry. *JACS Au*, 2023,3(8),2073-2085. doi.org/10.1021/jacsau.3c00263
20. Bachosz K, Zdarta J, Bilal M, Meyer AS, Jesionowski T. Enzymatic cofactor regeneration systems: A new perspective on efficiency assessment. *Sci. Total Environ.*, 2023, 868, 161630. https://doi.org/10.1016/j.scitotenv.2023.161630
21. Pandit C, Banerjee S, Pandit S, Lahiri D, Kumar V, Chaubey KK, Al-Balushi R, Al-Bahry S, Joshi SJ. Recent advances and challenges in the utilization of nanomaterials in transesterification for biodiesel production. *Heliyon*, 2023, 9(4).
22. Ali S, Khan SA, Hamayun M, Lee IJ. The recent advances in the utility of microbial lipases: A review. *Microorganisms*, 2023, 11(2),510. doi.org/10.3390/microorganisms11020510
23. Jaiswal KS, Rathod VK. Process intensification of enzymatic synthesis of flavor esters: A review. *Chem.*

Rec., 2022, 22(3), e202100213. doi.org/10.1002/tcr.202100213
24. Freitas DS, Quesado V, Rocha D, Noro J, Martins M, Cavaco-Paulo A, Silva C. Lipase-catalysed polymerization of eutectic mixtures. *ChemSusChem*, 2023, 16(11), e202202374. doi.org/10.1002/cssc.202202374
25. Cheng J, Du H, Zhou MS, Ji Y, Xie YQ, Huang HB, Zhang SH, Li F, Xiang L, Cai QY, Li YW. Substrate-enzyme interactions and catalytic mechanism in a novel family VI esterase with dibutyl phthalate-hydrolyzing activity. *Environ. Int.*, 2023, 178, 108054. doi.org/10.1016/j.envint.2023.108054
26. Rajendran D, Chandrasekaran N. Unveiling the modification of esterase-like activity of serum albumin by nanoplastics and their cocontaminants. *ACS Omega*, 2023, 8(46),43719-43731. doi.org/10.1021/acsomega.3c05447
27. Zhao J, Xu Y, Ding Z, Wu Q, Li W, Sun B, Li X. Discovery and mechanism explanation of a novel green biocatalyst esterase Bur01 from *Burkholderia ambifaria* for ester synthesis under aqueous phase. *Int. J. Biol. Macromol.*, 2024, 132630. doi.org/10.1016/j.ijbiomac.2024.132630
28. Gupta MN, Uversky VN in Structure and Intrinsic Disorder in Enzymology, Academic Press, 2023, The Various Facets of Protein Promiscuity: Not Just Broad Specificity of Proteins, pp 241-277.
29. Masson P, Shaihutdinova Z, Lockridge O. Drug and pro-drug substrates and pseudo-substrates of human butyrylcholinesterase. *Biochem. Pharmacol.*, 2023, 115910. doi.org/10.1016/j.bcp.2023.115910
30. Bhagat S, Joshi A, Jain A in Microbiome-Assisted Bioremediation, Academic Press, 2024, Processes and Mechanism Involved in Effective Bioremediation of Xenobiotic Substances from Agricultural Fields, pp 81-101. doi.org/10.1016/B978-0-443-21911-5.00017-9
31. Wang W, Hu A, Liu S, Yan J, Li Y, Zheng J. Physicochemical properties and structure of starch ester/copolymer/complex synthesized by combination of microwave and acid (anhydride): A review. *Trends Food Sci. Technol.*, 2023. doi.org/10.1016/j.tifs.2023.06.033
32. Mishra RK, Yadav A, Mishra V, Mishra SN, Singh DS, Verma DK. Fundamental theory of electromagnetic spectrum, dielectric and magnetic properties, molecular rotation, and the green chemistry of microwave heating equipment. *Green Chem. Synth. Microwaves Ultrasound*,2024,21-67. doi.org/10.1002/9783527844494.ch2
33. Kiss NZ, Henyecz R, Keglevich G. Continuous flow esterification of a H-phosphinic acid, and transesterification of H-phosphinates and H-phosphonates under microwave conditions. *Molecules*, 2020, 25(3), 719. doi.org/10.3390/molecules25030719
34. Samanta R, Chakraborty R. Sustainable continuous synthesis of methyl levulinate in a rotating catalytic-bed recycle reactor: Reaction kinetics, process scale-up, engine performance, and exhaust emission. *Ind. Eng. Chem. Res.*, 2024. doi.org/10.1021/acs.iecr.4c01485
35. Zhang XJ, Qi FY, Qi JM, Yang F, Shen JW, Cai X, Liu ZQ, Zheng YG.

Efficient enzymatic synthesis of L-ascorbyl palmitate using *Candida antarctica* lipase B-embedded metal-organic framework. *Biotechnol. Prog.*, 2022,38(1),e3218. doi.org/10.1002/btpr.3218

36. Zarei N, Golmakani MT, Keramat M, Majdinasab M, Karami A. Process intensification for the autocatalytic esterification of citronellol using microwave radiation. *LWT—Food Sci. Technol.*, 2021, 145, 111358. doi.org/10.1016/j.lwt.2021.111358
37. Delavault A, Opochenska O, Schönrock S, Hollenbach R, Ochsenreither K, Syldatk C. Intensification of enzymatic sorbityl laurate production in dissolved and neat systems under conventional and microwave heating. *ACS Omega*, 2024, 9(15), 17163-17173. doi.org/10.1021/acsomega.3c10004
38. Venturi V, Presini F, Trapella C, Bortolini O, Giovannini PP, Lerin LA. Microwave-assisted enzymatic synthesis of geraniol esters in solvent-free systems: Optimization of the reaction parameters, purification and characterization of the products, and biocatalyst reuse. *Mol. Diversity*, 2024, 28(3), 1665-1679. doi: 10.1007/s11030-023-10682-y
39. Prajapati JV, Agrawal YK. Synthesis, characterization and application of microbubbles: A review. *Int. J. Pharm. Sci. Res.*, 2012, 3(6), 1532.
40. Ahmad N, Javed F, Awan JA, Ali S, Fazal T, Hafeez A, Aslam R, Rashid N, Rehman MSU, Zimmerman WB, Rehman F. Biodiesel production intensification through microbubble mediated esterification. *Fuel*, 2019, 253,25-31. doi.org/10.1016/j.fuel.2019.04.173
41. Tang X, Niu S. Preparation of carbon-based solid acid with large surface area to catalyze esterification for biodiesel production. *J. Ind. Eng. Chem.*, 2019,69,187-195. doi.org/10.1016/j.jiec.2018.09.016
42. Atolani O, Areh ET, Oguntoye OS, Zubair MF, Fabiyi OA, Oyegoke RA, Tarigha DE, Adamu N, Adeyemi OS, Kambizi L, Olatunji GA. Chemical composition, antioxidant, anti-lipo-oxygenase, antimicrobial, anti-parasite and cytotoxicity of *Polyalthia longifolia* seed oil. *Med. Chem. Res.*, 2019a,22(12). https://link.springer.com/article/10.1007/s00044-019-02301-z
43. Atolani O, Areh ET, Oguntoye OS, Zubair MF, Fabiyi OA, Oyegoke RA, Tarigha, DE, Adamu N, Adeyemi OS, Kambizi L, Olatunji GA. Chemical characterization, antioxidant, cytotoxicity, anti-*Toxoplasma gondii* and antimicrobial potentials of the *Citrus sinensis* seed oil for sustainable cosmeceutical production. *Heliyon*, 2020a,6(2),e03399. https://doi.org/10.1016/j.heliyon.2020.e03399
44. Oguntoye SO, Ezennaya OL, Yusuff OK, Atolani O. Eco-friendly formulation, characterizations, bioactivity studies and *in silico* evaluation of cosmetic prepared from the seed oils of *Carica papaya*, *Dacryodes edulis* and *Raphia hookeri. The Chemist*, 2023,94(2). doi.org/10.1002/ejlt.201900207
45. Nie J, Shen J, Shim YY, Tse TJ, Reaney MJ. Synthesis of trimethylolpropane esters by base-catalyzed transesterification. *Eur. J. Lipid Sci. Technol.*, 2020, 122(3), 1900207. doi.org/10.1002/ejlt.201900207
46. Govindaraju R, Chen SS, Wang LP, Chang HM, Pasawan M. Significance of membrane applications for high-quality biodiesel and byproduct

(glycerol) in biofuel industries. *Curr. Pollut. Rep.*, 2021, 7, 128-145. doi: 10.1007/s40726-021-00182-8

47. Liu G, Jin W. Pervaporation membrane materials: Recent trends and perspectives. *J.Membr.,Sci.*, 2021,636,119557. doi.org/10.1016/j.memsci.2021.119557
48. Raza W, Wang J, Yang J, Tsuru T. Progress in pervaporation membranes for dehydration of acetic acid. *Sep. Purif. Technol.*, 2021, 262, 118338. doi.org/10.1016/j.seppur.2021.118338
49. Ding M, Xu H, Yao C, Chen W, Song N, Zhang Q, Lin T, Xie Z. Understanding the membrane fouling control process at molecular level in the heated persulfate activation-membrane distillation hybrid system. *Water Res.*, 2023, 229, 119465. doi.org/10.1016/j.watres.2022.119465
50. Aktij SA, Zirehpour A, Mollahosseini A, Taherzadeh MJ, Tiraferri A, Rahimpour A. Feasibility of membrane processes for the recovery and purification of bio-based volatile fatty acids: A comprehensive review. *J. Ind. Eng. Chem.*, 2020, 81, 24-40. doi.org/10.1016/j.jiec.2019.09.009
51. Mazzei R, Gebreyohannes AY, Papaioannou E, Nunes SP, Vankelecom IF, Giorno L. Enzyme catalysis coupled with artificial membranes towards process intensification in biorefinery—A review. *Bioresour. Technol.*, 2021,335,125248. doi.org/10.1016/j.biortech.2021.125248
52. Zhang Z, Fan K, Liu Y, Xia S. A review on polyester and polyesteramide thin film composite nanofiltration membranes: Synthesis, characteristics and applications. *Sci. Total Environ.*, 2023,858,159922. doi.org/10.1016/j.scitotenv.2022.159922
53. Li S, Wang X, Guo Y, Hu J, Lin S, Tu Y, Chen L, Ni Y, Huang L. Recent advances on cellulose-based nanofiltration membranes and their applications in drinking water purification: A review. *J. Cleaner Prod.*, 2022, 333,130171. doi.org/10.1016/j.jclepro.2021.130171
54. Greve A, Stein H, Osterland T, Hinrichsen O. SPEEK-based temperature-resistant catalyst for etherification and esterification reactions. *Appl. Catal. O: Open*, 2024, 206951. doi: 10.1007/s40726-021-00182-8
55. Majumdar N. Carboxylic acids as building blocks in catalytic asymmetric reactions. *ACS Catal.*, 2022, 12(14),8291-8324. doi.org/10.1021/acscatal.2c02410
56. Rizal KM, Ariyanto E, Yuliwati E, "Biodiesel Production Optimization from Triolein Through Esterification Process Using Dwsim Software Simulation", International Conference on Engineering, Construction, Renewable Energy, and Advanced Materials, July 2024.
57. Minami E, Kawamoto H. Methyl esterification of oleic acid in supercritical methanol with methyl formate. *J. Jpn. Pet. Inst.*, 2021, 64(4),188-196. doi.org/10.1627/jpi.64.188
58. Zhao B, Wang H, Xu S, Qian L, Li H, Gao J, Zhao G, Ray MB, Xu CC. Influence of extraction solvents on the recovery yields and properties of bio-oils from woody biomass liquefaction in sub-critical water, ethanol or water–ethanol mixed sol-

vent. *Fuel*, 2022,307,121930. doi.org/10.1016/j.fuel.2021.121930

59. Akkarawatkhoosith N, Bangjang T, Kaewchada A, Jaree A. Biodiesel production from rice bran oil fatty acid distillate via supercritical hydrolysis–esterification–transesterification in a microreactor. *Energy Rep.*, 2023, 9,5299-5305. doi.org/10.1016/j.egyr.2023.04.348
60. Pandian S, Saravanan AS, Sivanandi P, Santra M, Booramurthy VK. Application of heterogeneous acid catalyst derived from biomass for biodiesel process intensification: A comprehensive review. *Refin. Biomass Residues Sustainable Energy Bioprod.*,2020,87-109. doi.org/10.1016/B978-0-12-818996-2.00004-1
61. Shi J, Zhang L, Cheng Z. Design of water-tolerant solid acids: A trade-off between hydrophobicity and acid strength and their catalytic performance in esterification. *Catal. Surv. Asia*, 2021, 25, 279-300. doi: 10.1007/s10563-021-09334-8
62. Mandari V, Devarai SK. Biodiesel production using homogeneous, heterogeneous, and enzyme catalysts via transesterification and esterification reactions: A critical review. *BioEnergy Res.*, 2022, 15(2), 935-961. doi: 10.1007/s12155-021-10333-w
63. Baek Y, Lee S, Son J, Lee T, Oh JM, Lee SH, Kim HU, Seo SW, Park SJ, Yoo HY, Park C. Efficient production of naringin acetate with different acyl donors via enzymatic transesterification by Lipases. *Int. J. Environ. Res. Public Health*, 2022, 19(5), 2972. doi.org/10.3390/ijerph19052972
64. Wang B, Wang B, Shukla SK, Wang R. Enabling catalysts for biodiesel production via transesterification. *Catalysts*, 2023,13(4),740. doi.org/10.3390/catal13040740
65. Chandra Kishore S, Perumal S, Atchudan R, Sundramoorthy AK, Alagan M, Sangaraju S, Lee YR. A review of biomass-derived heterogeneous catalysts for biodiesel production. *Catalysts*, 2022, 12(12), 1501. doi.org/10.3390/catal12121501
66. Atolani O, Oguntoye H, Areh ET, Adeyemi OS, Kambizi L. Chemical composition, anti-toxoplasma, cytotoxicity, antioxidant, and anti-inflammatory potential of *Cola gigantea* seed oil. *Pharm. Biol.*, 2019b,57(1),154–160. doi.org/10.1080/13880209.2019.1577468
67. Zubair MF, Ibrahim SO, Stephen K, Hamid AA, Ibukun O. and Atolani O. Synthesis and chemical characterization of alkyd resins using maleic and phthalic anhydrides and seed oil of *Luffa aegyptiaca*. *J. Turk. Chem. Soc.,Sect.A*,2023. https://dergipark.org.tr/tr/pub/jotcsa/issue/78393/1256237
68. Adeyemi KD, Ogundele VO, Atolani O. Dietary supplementation of *Allium cepa* skin alters intramuscular fat, muscle cholesterol, and fatty acids in rabbits. *J. Sci. Food Agric.*, 2022a, 102(9),3683-3692. doi.org/10.1002/jsfa.11715
69. Faruque MO, Razzak SA, Hossain MM. Application of heterogeneous catalysts for biodiesel production from microalgal oil—A review. *Catalysts*,2020,10,1025. doi.org/10.3390/catal10091025
70. Kayode B, Hart A. An overview of transesterification methods for producing biodiesel from waste vegetable oils. *Biofuels*, 2019, 10(3), 419-437.

doi.org/10.1080/17597269.2017.1306683
71. Nguyen A, Böttger R, Li SD. Recent trends in bioresponsive linker technologies of prodrug-based self-assembling nanomaterials. *Biomaterials*, 2021,275,120955. doi.org/10.1016/j.biomaterials.2021.120955
72. Das B, Baidya AT, Mathew AT, Yadav AK, Kumar R. Structural modification aimed for improving solubility of lead compounds in early phase drug discovery. *Bioorg. Med. Chem.*, 2022, 56, 116614. doi.org/10.1016/j.bmc.2022.116614
73. Abbas F, Zhou Y, O'Neill Rothenberg D, Alam I, Ke Y, Wang HC. Aroma components in horticultural crops: Chemical diversity and usage of metabolic engineering for industrial applications. *Plants*, 2023, 12(9),1748. doi.org/10.3390/plants12091748
74. Rocha F, Ratola N, Homem V in The Handbook of Environmental Chemistry, Springer International Publishing, 2023, Fragrances in the Environment: Properties, Applications, and Emissions,pp1-36.doi: 10.1007/698_2023_983
75. Pathania AS, Shah R, Singh J, Singh D, Chopra DS, Singh N, Singh RS in Polymer-Drug Conjugates, Academic Press, 2023, Bonding Through Phosphodiester Moiety: Its Implications in Pharmaceutical Modifications,pp245-278. doi.org/10.1016/B978-0-323-91663-9.00009-6
76. Balla H, Borsodi K, Őrsy P, Horváth B, Molnár PJ, Lénárt Á, Kosztelnik M, Ruisanchez É, Wess J, Offermanns S, Nyirády P, Benyó Z. Intracellular signaling pathways of muscarinic acetylcholine receptor-mediated detrusor muscle contractions. *Am. J. Physiol.: Renal Physiol.*, 2023, 325(5), F618-F628. doi.org/10.1152/ajprenal.00261.2022
77. Joseph TM, Azat S, Ahmadi Z, Jazani OM, Esmaeili A, Kianfar E, Haponiuk J, Thomas S. Polyethylene terephthalate (PET) recycling: A review. *Case Stud. Chem. Environ. Eng.*,2024,100673. doi.org/10.1016/j.cscee.2024.100673
78. Godwin AD in Applied Plastics Engineering Handbook, William Andrew Publishing, 2024, Plasticizers, pp 595-618. doi.org/10.1016/B978-0-323-88667-3.00031-X
79. Reshna KR, Gopi S, Balakrishnan P in Flavors and Fragrances in Food Processing: Preparation and Characterization Methods, American Chemical Society, 2022, Introduction to Flavor and Fragrance in Food Processing, pp 1-19. doi: 10.1021/bk-2022-1433.ch001
80. Li AJ, Pal VK, Kannan K. A review of environmental occurrence, toxicity, biotransformation and biomonitoring of volatile organic compounds. *Environ.Chem.Ecotoxicol.*, 2021,3,91-116. doi.org/10.1016/j.enceco.2021.01.001
81. Arrigo F, Impellitteri F, Piccione G, Faggio C. Phthalates and their effects on human health: Focus on erythroncytes and the reproductive system. *Comp. Biochem. Physiol., Part C:Pharmacol.Toxicol.Endocrinol.*, 2023,270,109645. doi.org/10.1016/j.cbpc.2023.109645
82. Radparvar S. The clinical assessment and treatment of inhalant abuse. *Perm.J.*, 2023,27(2),99. doi.org/10.7812/TPP/22.164
83. Li JY, Guo JL, Yi JF, Liu LY, Zeng LX, Guo Y. Widespread phthalate

esters and monoesters in the aquatic environment: Distribution, bioconcentration, and ecological risks. *J. Hazard. Mater.*, 2024, 135201. doi.org/10.1016/j.jhazmat.2024.135201

84. Joshi DR, Adhikari N. An overview on common organic solvents and their toxicity. *J. Pharm. Res. Int.*, 2019, 28(3),1-18. doi.org/10.9734/jpri/2019/v28i330203

85. Qadeer A, Anis M, Warner GR, Potts C, Giovanoulis G, Nasr S, Archundia D, Zhang Q, Ajmal Z, Tweedale AC, Kun W, Shuhang W. Global environmental and toxicological data of emerging plasticizers: Current knowledge, regrettable substitution dilemma, green solution and future perspectives. *GreenChem.*,2024. doi.org/10.1039/D3GC03428C

The Chemist
Journal of the American Institute of Chemists

Adsorptive Removal of Congo Red Dye by a Synthesized Dual Ligand (Carboxylate and N-donor) Coordination Compound

V. O. Adimula [a*], R. A. Anifowose [a], E. O. Adeniyi [a], A. D. Obafemi [a], S. E. Elaigwu [b], S. Owalude [b], A. C. Tella [b]

[a] *Department of Industrial Chemistry, University of Ilorin, Ilorin, Nigeria*
[b] *Department of Chemistry, University of Ilorin, Ilorin, Nigeria*

**Corresponding author (E-mail: vincentadimula@gmail.com; Tel: +2348036973282)*

Abstract: The adsorption of Congo red dye from water by a synthesized Cu(II) coordination compound formulated as [Cu(BTCA)(AMB)] is herein reported (BTCA= 1,2,4,5-bezene tetra carboxylic acid; AMB= 4-aminomethylbenzoic acid). Characterization of the compound was achieved by X-ray diffraction (XRD), Fourier-transform infrared (FTIR) spectroscopy, scanning electron microscopy (SEM), and thermogravimetric analysis (TGA). The adsorption performance of the compound was assessed through batch adsorption experiments. Kinetic and isotherm models were employed to elucidate the adsorption mechanism and establish a comprehensive understanding of the interaction between the compound and Congo red dye molecules. The SEM analysis results before and after adsorption showed the presence of the dye molecules on the adsorbent. Adsorption data were seen to be best for the pseudo-second order kinetics model. Thermodynamic parameters indicated that the adsorption process is spontaneous by ΔG values ranging from -0.38 KJ/mol to -2.15 KJ/mol.

Key Words: coordination compound, adsorption, Congo red dye, characterization, pseudo second order

1. Introduction

Coordination polymers have been noted to be a group of functional materials that have found applications in multiple processes. The study of coordination polymers has expanded rapidly in the past decade due to its susceptibility to attain a variety of architectures built up from an extended range of molecular building blocks with varying interactions. Coordination compounds with backbones, constructed from metal ions as connectors

and ligands as linkers, have been utilized in various processes due to their interesting characteristics [1]. Coordination networks having porous features have advanced nanoporous compounds for processes, which include catalysis, adsorption, and gas separation, among others, due to their tunable pore sizes, large surface areas, high porosities, and good thermal and mechanical stabilities [2,3].

The study of coordination compounds involves the study of metals, which perform a variety of roles in many biological, catalytic, and materials applications and are essential parts of coordination chemistry. To harness their reactivity and fully utilize their potential in various domains, it is crucial to comprehend the behavior and characteristics of metal centers in coordination compounds [3]. Their electrical structure determines the bonding and reactivity of metal centers. Metal ions frequently display varying oxidation states which cause coordination compounds to develop with various electronic configurations [4]. The stability and spectroscopic characteristics of metal complexes are influenced by the distribution of electrons in the metal d orbitals [5]. Specific coordination geometries, such as octahedral, square planar, or tetrahedral, are adopted by metal centers in coordination complexes. These geometries are determined by the type of ligands used and the metal ion's electronic state [3].

Dyes, such as Congo red, are reportedly utilized as coloring agents for materials such as leather, textile, and paper, among others [5-7]. The reactiveness of some dyes makes them suitable for use due to their brightness and fastness when used [4,5]. These dyes, however, present the problem of toxicity and carcinogenicity when used, causing harm directly to aquatic life and humans, thus, generating conditions that include lung cancer and neurological disorders. The removal of these toxins from the environment is hindered by the structural complexity of synthetic dyes and their highly water-soluble nature [7-9].

We herein report the sorption of Congo red dye from water by a synthesized Cu(II) complex containing mixed 1,2,4,5-bezene tetra carboxylic acid (BTCA) and 4-aminomethyl benzoic acid (AMB) ligands, as adsorbents for the removal of Congo red dye from aqueous solution. The compound was successfully characterized and formulated as [Cu(BTCA)(AMB)].

2. Experimental

Materials and Methods

The reagents used for this study were of analytical grade and used without further purification. The absorbance measurements were taken using a SHIMADZU UV-1650 UV-Vis spectrophotometer. Scanning electron microscopy (SEM) was carried out using a JEOL JSM-7600F Scanning Electron Microscope.

Synthesis of the [Cu(BTCA)(AMB)]

The compound was synthesized using a solvent-based method. Solutions of the ligands (BTCA and AMB; 1 mmol each) were dissolved in 10 mL each of dimethyl

formamide and distilled water separately and transferred into a round-bottom flask containing the dissolved Cu^{2+} salt. The mixture was stirred thoroughly to ensure homogeneity and refluxed for 2 h at 120°C with constant stirring. The precipitate formed was thereafter isolated by filtration, washed with 50:50 DMF and distilled water, dried, and stored.

Batch Adsorption Studies

Adsorption of Congo red (CR) dye onto [Cu(BTCA)(AMB)] was studied using a Congo red stock solution of 1000 mg/L. This was prepared by dissolving 0.25 g of the Congo red dye in 250 ml of deionized water. Absorbance of the Congo red solution was then observed using a UV-Visible spectrophotometer to obtain the wavelength of maximum absorption which was found to be 500 nm. Lower concentrations of the dye (5–30 mg/L) were prepared from the stock solution by serial dilution with deionized water and absorbance readings taken with the UV–Visible spectrophotometer at a λ_{max} value of 500 nm [6]. The graph of absorbance against concentration was plotted to give the calibration curve (Figure 1).

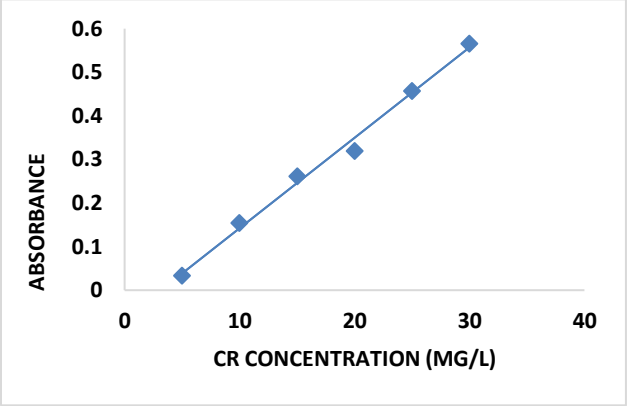

Figure 1. Calibration Curve for Congo Red Dye Adsorption onto [Cu(BTCA)(AMB)]

The effect of concentration, temperature, time, pH, and the dose of adsorbent on the adsorption process was investigated. To determine the quantity adsorbed (q_e in mg/g) at equilibrium, equation 1 was utilized:

$$q_e = \left(\frac{C_o - C_e}{m}\right) v \quad (1)$$

where Co and Ce (mg/L) are the initial and final concentrations of the adsorbates, respectively, v is the volume of the solution used (L), and m is the mass (g) of the adsorbents.

The effect of concentration was studied using 5–30 mg/L of the adsorbate, while the effect of temperature was studied at the temperature range of 30–70°C. The effect of pH was investigated by varying the pH between 2 and 13 using 0.1 M HCl or 0.1 M NaOH, while the effect of adsorbent dosage was studied using 0.01–0.05 g of the adsorbents, and the investigation of effect of time was done at time interval of 60–300 min [7].

3. Result and Discussion

Result of SEM Analysis

Figure 2a and 2b depict the SEM images of [Cu(BTCA)(AMD)] before and after adsorption.

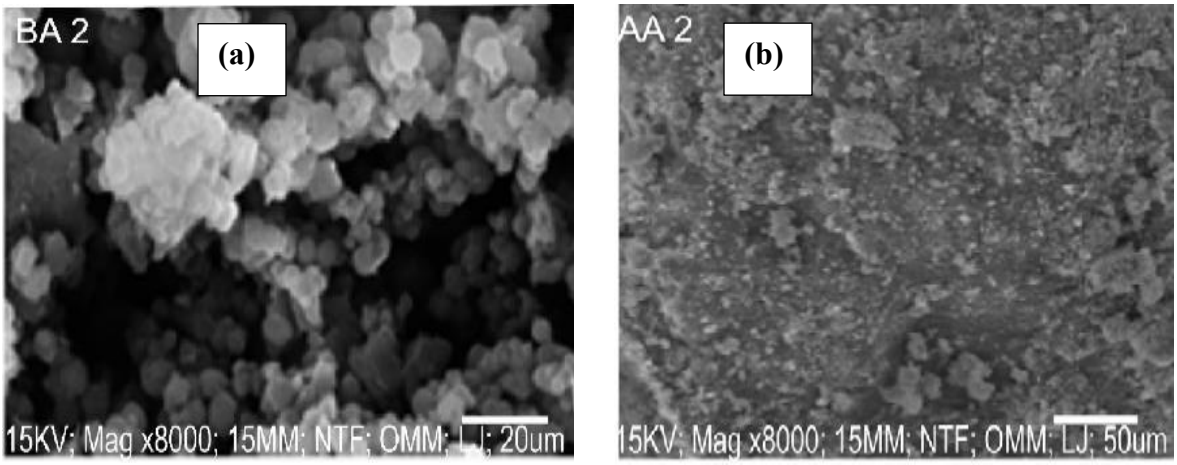

Figure 2. SEM Images of [Cu(BTCA)(AMD)] a) Before Adsorption; b) After Adsorption

The surface morphology showed the presence of voids in-between the particles before adsorption while the image after adsorption shows the incorporation of the dye into the voids in-between the particles (Figure 2b).

Result of PXRD Analysis

The PXRD pattern of the [Cu(BTCA)-(AMD)] compound, before and after adsorption, are presented in Figure 3 (a and b).

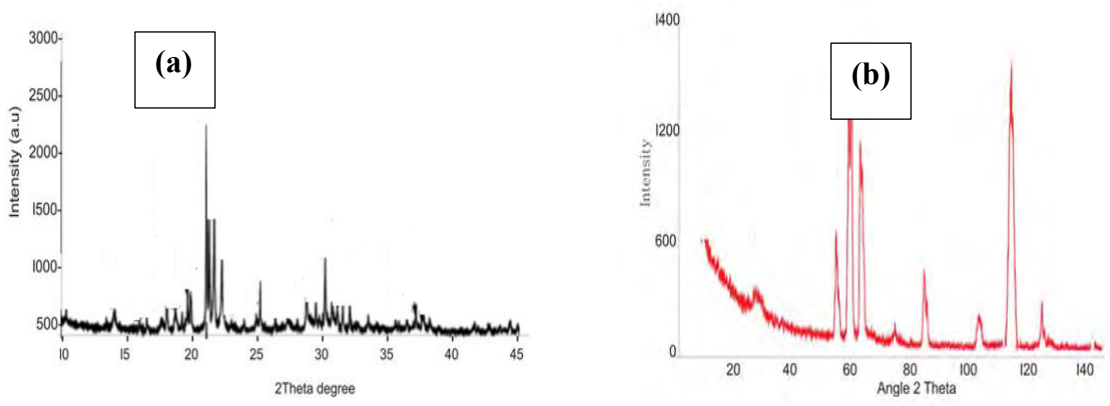

Figure 3. PXRD Analysis Result of a) Before Adsorption; b) After Adsorption

A comparison of the patterns showed a reduction in intensity of peaks generally for the PXRD pattern after adsorption of CR dye. This is attributed to the presence of the dye molecules on the adsorbent [8-10].

Result of TGA Analysis

The TGA of the compound showed two stages of decomposition within a temperature range of 0–650°C [9-11]. The first stage of decomposition results to about 12% weight loss, ranging from a temperature of 0–290°C. The second decomposition stage, which starts from 290°C and ends at 500°C, results in a weight loss of 79%. Figure 4 shows the TGA curve of the sample.

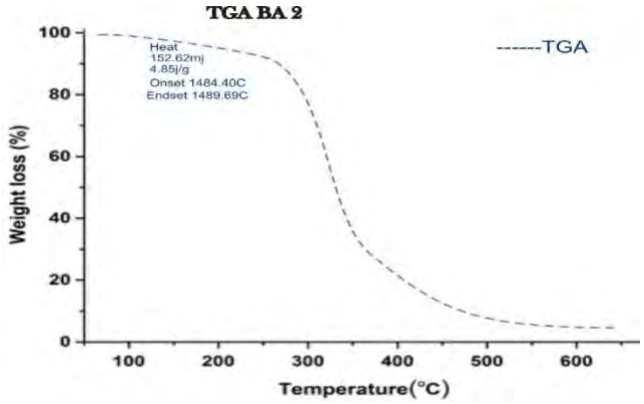

Figure 4. TGA Curve of [Cu(BTCA)(AMD)]

Result of FTIR Analysis

Using a Shimadzu FTIR spectrophotometer, the functional groups present in the [Cu(BTCA)(AMD)] compound, before and after adsorption, were obtained by studying the spectral as shown in Figure 5. Peaks observed at 3496.99 cm^{-1} and 3444.96 cm^{-1} were attributed to the presence of hydroxyl (O-H) and amino group (N-H), respectively. The peak observed at 1710 cm^{-1} was attributed to the carbonyl group of the carboxylate. The diagnostic region of the compound, before and after adsorption, were observed to be similar. However, the presence of the Congo red dye on the compound, after adsorption, causes a significant difference in the fingerprint region (Figure 5, a and b).

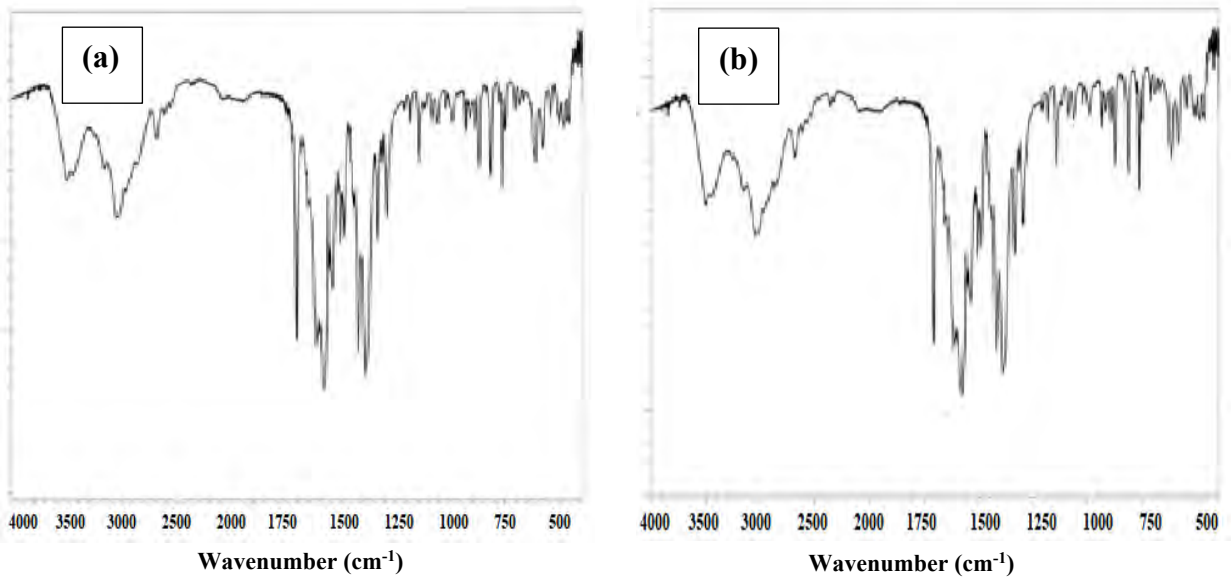

Figure 5. FTIR Spectroscopy Analysis of [Cu(BTCA)(AMB)] a) Before Adsorption; b) After

The peak observed at 732 cm^{-1} in the spectra after adsorption was attributed to the characteristic FTIR band of the ν(S-O) group in the Congo red dye. This peak was observed to be absent in the spectra before adsorption study.

Adsorption Study

Effect of Congo Red Dye Concentration

The findings from investigating the effect of Congo red dye concentration on the adsorption process using the adsorbents is presented in Figure 6.

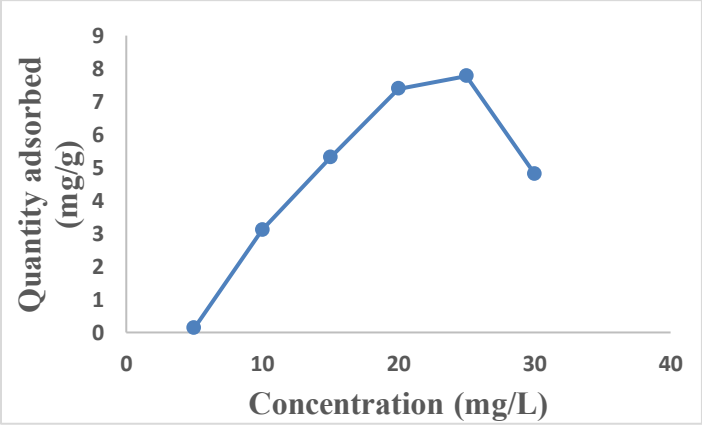

Figure 6. Effect of Concentration on the Adsorption of Congo Red Dye by [Cu(BTCA)(AMB)]

It was observed that as the concentration of the dye increased, the amount of Congo red dye adsorbed onto the adsorbents also increased, reaching its maximum at 25 mg/L. As the dye concentration increased, the adsorption sites on the adsorbents became saturated, resulting in the subsequent release of the dye as the process continued. This phenomenon occurred because there was intensified competition among Congo red dye molecules for the available adsorption sites on the adsorbent, causing an initial surge in the adsorption rate, followed by a gradual deceleration of the process. This behavior can be attributed to the fact that at lower dye concentrations, there is a higher ratio of solute to vacant adsorbent sites, leading to increased quantity adsorbed [8].

Effect of Time

The impact of time on the adsorption of Congo red dye onto the [Cu(BTCA)(AMB)] material, as presented in Figure 7, suggests that as the contact time increased, the efficiency of adsorption gradually rose and reached its maximum value after 120 minutes, after which it remained constant.

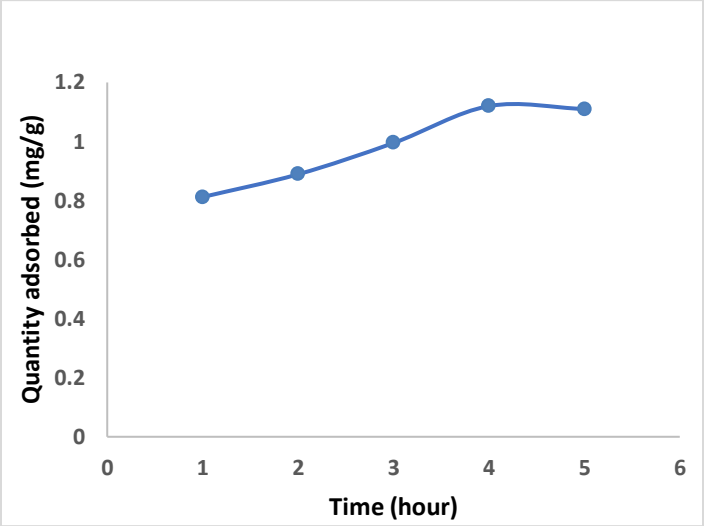

Figure 7. Effect of Time on the Quantity of Congo Red Dye Adsorbed

This experiment was conducted at a pH of 7.0 with a dye concentration of 25 mg/L. A dosage of 0.01 g of adsorbent was used for durations ranging from 60 to 360 minutes to determine the equilibrium time for the adsorption process. The initial increase in adsorption is attributed to the presence of available adsorption sites on the materials, which gradually became occupied over time [9-12].

Effect of pH

The impact of change in pH on the adsorption of Congo red dye by [Cu(BTCA)(AMB)] is presented in Figure 8. Equilibrium concentrations of dye at 25 mg/L over 240 min were employed. Adjusting the pH within the range of 2.0 to 11.0 using either 0.1 M HCl or 0.1 M NaOH [9] indicated that at lower pH (between 3.0 and 6.0), sorption of Congo red dye onto [Cu(BTCA)(AMB)] decreases.

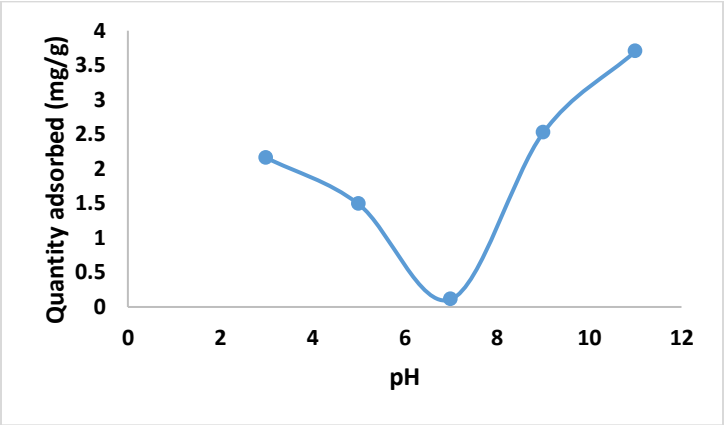

Figure 8. Effect of pH on the Quantity of Congo Red Adsorbed

This phenomenon is attributed to an acid-base interaction between the dye molecules and the surface of the [Cu(BTCA)(AMB)]. Conversely, at higher pH values (ranging from 8.0 to 12.0), the Congo red dye adopts an anionic nature due to the presence of hydroxyl ions in its solution. This leads to an increased adsorption of the dye onto the surface of the adsorbent [9,13,14].

Effect of Temperature

The effect of temperature change on the adsorption process was monitored using 0.01 g of the adsorbent for this study. The temperature was varied within the range of 30 to 70°C, and each experiment lasted for 4 hours.

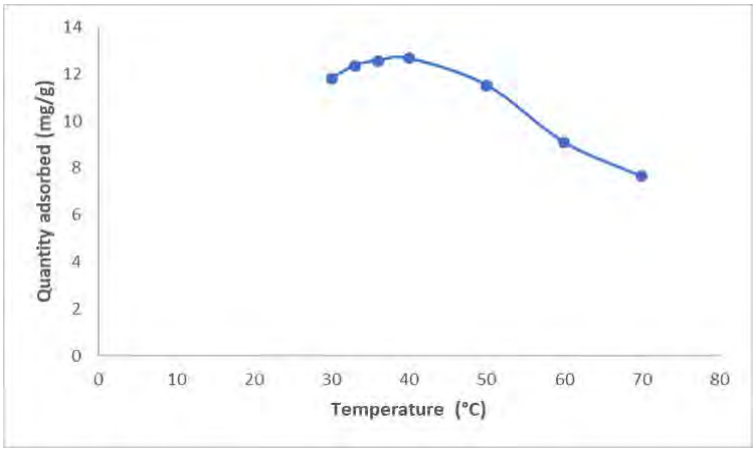

Figure 9. Effect of Temperature on the Quantity of Congo Red Dye Adsorbed

The findings presented in Figure 9 revealed that the quantity adsorbed increases after an increase in the temperature to 40°C and later decreases at a further increase in temperature. The decline in quantity adsorbed may be attributed to the increased kinetic energy acquired by the dye molecules at temperatures beyond 40°C [15-17].

Effect of Adsorbent Dose

The impact of varying the dosage of adsorbents on the adsorption of Congo red dye was examined in this study (Figure 10). Specifically, a constant equilibrium dye concentration of 25 mg/L was maintained, and the study was done at a temperature of 40°C.

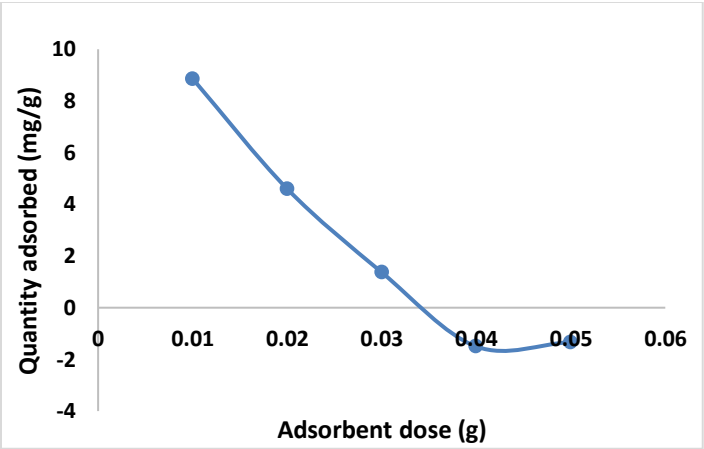

Figure 10. Effect of Adsorbent Dose on the Quantity of Congo Red Adsorbed on the Adsorbents

The quantity of adsorbent used in the experiment was adjusted, ranging from 0.01 to 0.05 g. It was observed that as the amount of adsorbent increased, the quantity adsorbed

decreased. This can be attributed to an agglomeration of the adsorbent particles due to the increased quantity of adsorbents employed [10,14,18].

Adsorption Isotherms Studies

To assess the adsorption of congo red dye over [Cu(BTCA)(AMB)], three different models, Langmuir, Freundlich, and Temkin, were employed in an effort to determine which isotherm model best describes the adsorption process [8]. The parameters obtained from subjecting the adsorption data to the various isotherm models are given in Table 1.

Table 1. Isotherm Parameters for Congo Red Dye Adsorption on [Cu(BTCA)(AMB)]

Isotherms	Equation	Constants	Values
Langmuir	$\frac{Ce}{qe} = \frac{1}{KaQm} + \frac{Ce}{Qm}$	Qm (mg g^{-1})	-0.693
		ka	-0.09
	$R_l = \frac{1}{1 + KaCo}$	R_L	0.8
		R^2	0.116
Freundlich	$\ln qe = \ln K_f + \frac{1}{n} lnCe$	K_f	0.089
		n	0.635
		R^2	0.359
Temkin	$\mathrm{Qe} = \mathrm{BlnA} + \mathrm{BlnCe}$	A	0.553
		B	2.930
		R^2	0.9487

The Langmuir adsorption isotherm (equation 2) was studied by plotting a graph of Ce/Qe against

$$\frac{Ce}{qe} = \frac{1}{KaQm} + \frac{Ce}{Qm} \quad (2)$$

Ce (Figure 11), where Ce is the final concentration, and Qe is the quantity of Congo red adsorbed.

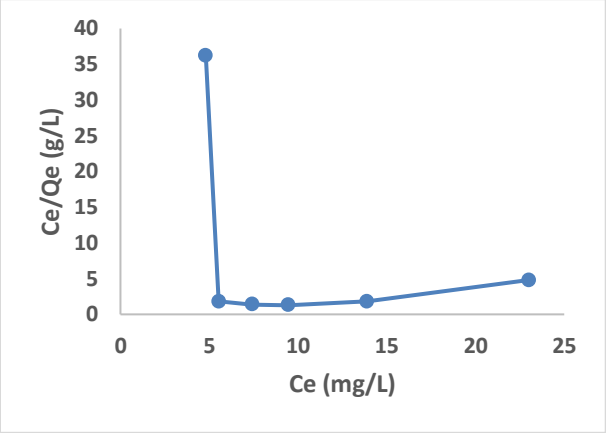

Figure 11. Langmuir Isotherm Model Plot for the Adsorption of Congo Red Dye by [Cu(BTCA)(AMB)]

The linear form of the Langmuir isotherm model gave the values of Ka [the Langmuir adsorption constant (L/mg)] and Qm [theoretical maximum adsorption capacity (mg/g)] obtained from the intercept and slope of the plot of the graph [9]. Adsorption is speculated to be a monolayer adsorption with no interaction between the adsorbate molecules.

The linear form of the Langmuir model and the equation used in calculating the separation factor (R_L) (equation 3) are given in equations below:

$$R_l = \frac{1}{1+KaCo} \tag{3}$$

where Ka (L/mg) is the Langmuir constant, and Co (mg/L) is the initial concentration. The adsorption process can be determined as favorable when the R_L value lies between 0 and 1. The Qm value was found to be -0.6922 and the constant Ka to be -0.09. The R_L was calculated to be -0.8, which falls below 0 and indicates unfavorable adsorption, while the R^2 value was obtained as 0.1166.

The relationship of the amount adsorbed per unit mass or mole with concentration is demonstrated by the Freundlich model (equation 4) given as:

$$\ln qe = \ln K_f + \frac{1}{n} lnCe \tag{4}$$

The Freundlich isotherm model parameters such as the 1/n and as K_f [(mg g^{-1})/(mg L^{-1})] were obtained from the intercept and slope of the linear plot of lnQe versus ln Ce (Figure 12), respectively.

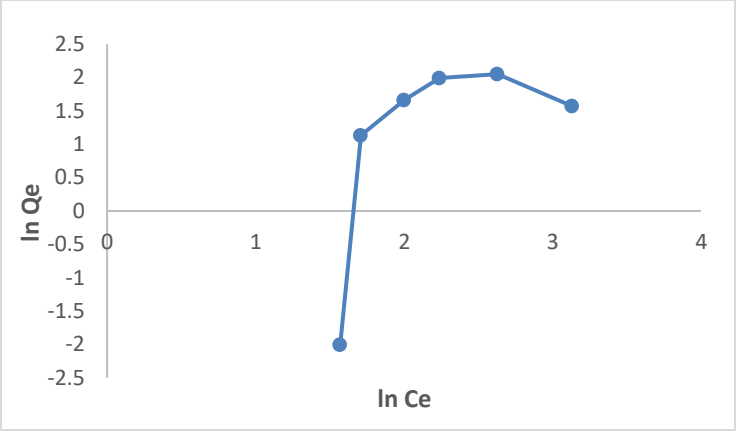

Figure 12. Freundlich Isotherm Model Plot

The K_f, Freundlich constant is the adsorption capacity, that is the adsorptive power, and the 1/n, heterogeneity factor, indicates the energy of adsorption. The 1/n value of 1.527 obtained indicates the unfavorable adsorption of Congo red dye for adsorption onto the adsorbents, while lower R^2 value of 0.359 for the adsorbents indicates that the Freundlich model less fits the experimental data

The Temkin isotherm model (equation 5) was used to estimate the heat of the adsorption and the adsorbent–adsorbate interaction.

$$Q_e = BlnA + BlnC_e \quad (5)$$

It is evaluated using the equation given below by plotting the graph of Qe against ln Ce (Figure 13), and the constants A (g/L) and B (J/mole) corresponding to the maximal equilibrium binding energy and heat of adsorption, respectively, were calculated using the linearized Temkin equation.

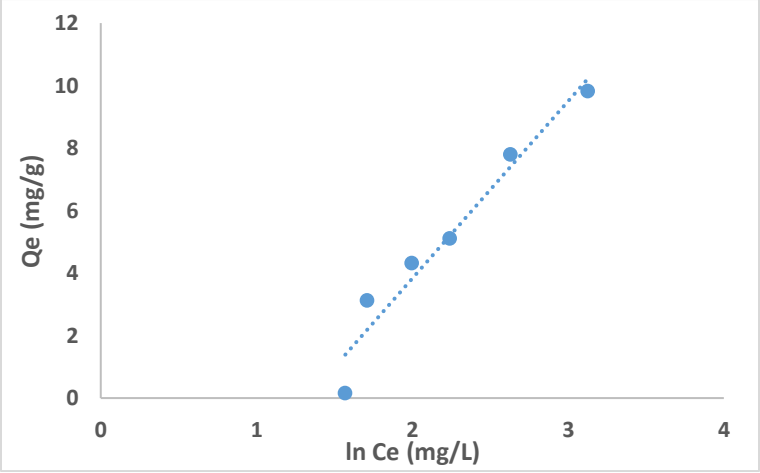

Figure 13. Plot of Temkin Isotherm Model

The obtained values of A and B are given as 0.553 and 2.930, respectively. The R^2 value of 0.9487 obtained indicated the best-fit of the Temkin adsorption isotherm to the adsorption data obtained for uptake of Congo red dye by [Cu(BTCA)(AMB)]. This suggests the occurrence of adsorbent–adsorbate interactions in the adsorption process [16].

Adsorption Kinetics

The experimental adsorption data for the adsorption of Congo red dye by [Cu(BTCA)(AMB)] was analyzed using the kinetic models of pseudo-first order, pseudo-second order, intraparticle diffusion model and Elovich diffusion model. Parameters obtained were summarized in Table 2.

Table 2. Kinetic Parameters for Congo Red Adsorption by [Cu(BTCA)(AMB)]

Models	Equations	Parameters	values
Pseudo-first order	$\ln(q_e - q_t) = \ln(q_e) - K_1 t$	k_1	0.0091
		q_e (cal)	0.79
		R^2	0.748
Pseudo-second order	$\frac{t}{q_t} = \frac{1}{K_2\, q_e^2} + (\frac{1}{q_e})t$	K_2	0.018
		q_e (cal)	1.25
		R^2	0.99
Intra-particle diffusion	$q_t = K_{idiff}\, t^{1/2} + C$	C	0.5318
		K_{idiff}	0.0349
		R^2	0.949
Elovich	$q_t = \frac{1}{\beta}\ln(\alpha\beta) + \frac{1}{\beta}\ln(t)$	B	4.87
		R^2	0.9389

Pseudo First Order Kinetics (Lagergren Model)

The Lagergren model (equation 6) parameters for the uptake of Congo red dye by the [Cu(BTCA)(AMB)] absorbent was derived by plotting ln ($q_e - q_t$) against time from the linearized form of the equation given below.

$$\ln (q_e - q_t) = \ln(q_e) - K_1 t \quad (6)$$

Values of k_1 and q_e were determined from the slope and intercept. The q_e value was obtained as 0.79, and k_1 was obtained as 0.0091. The discrepancy between the intercept and the actual experimental Qe value signifies that this model does not accurately describe the experimental data, indicating that the adsorption rate does not conform to this equation [16].

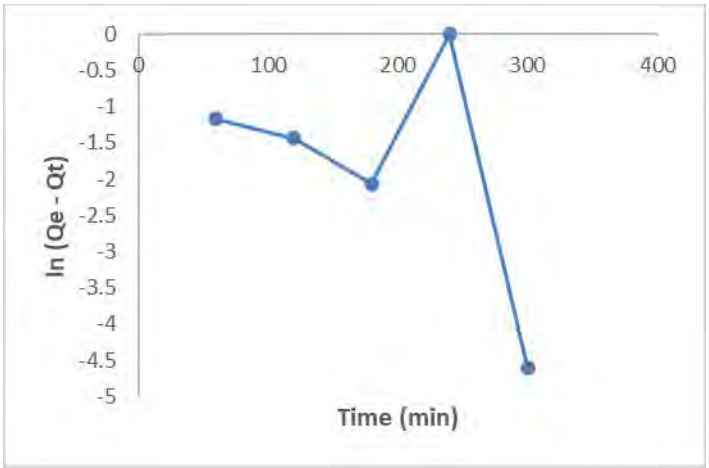

Figure 14. Pseudo First Order Kinetics Plot for Congo Red Adsorption by [Cu(BTCA)(AMB)]

Pseudo-Second Order Kinetic Model

The adsorption data for uptake experiment of Congo red dye by [Cu(BTCA)(AMB)] was analyzed using the pseudo-second-order kinetic model. A linear relationship was observed from the plot t/Qt versus t (Figure 15), exhibiting a notably strong correlation coefficient (R^2) value.

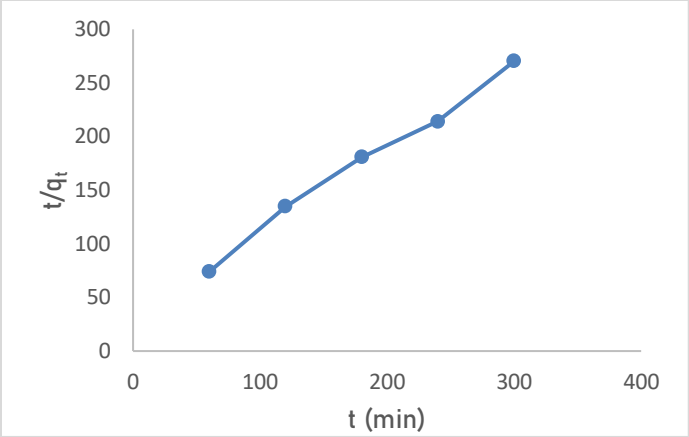

Figure 15. Pseudo-Second Order Kinetics Plot for Congo Red Adsorption by [Cu(BTCA)(AMB)]

Both the equilibrium adsorption capacity (Qe) and the rate constant (k_2) were computed by extracting these values from the slope and intercept, respectively. The Qe and k_2 values were calculated to be 1.27 and 0.018, respectively. The pseudo-second-order model proves its applicability to the adsorption experiment due to the high correlation coefficient (R^2) value of 0.99 obtained, and also indicates it best explains the adsorption process [17]. The linearized form of the pseudo-second order rate equation (7) is given as:

$$\frac{t}{q_t} = \frac{1}{K_2\, q_e^2} + \left(\frac{1}{q_e}\right)t \tag{7}$$

Intraparticle Diffusion Model

The intraparticle diffusion model is often represented by a plot of the amount of adsorbate adsorbed (Qt) against the square root of time ($t^{1/2}$) using the equation (8) below:

$$q_t = K_{idiff}\, t^{1/2} + C \tag{8}$$

The values of K_{diff} [the intraparticle diffusion rate constant ($mg/g/min^{1/2}$)] and C (thickness of the boundary layer) were calculated from the slope and intercept of the plot of q_t versus $t^{1/2}$ (Figure 16) and obtained as 0.0349 and 0.5318, respectively. The R^2 value was found to be 0.949 which indicates that the experimental data can be explained by the intraparticle diffusion adsorption kinetics model [15,16].

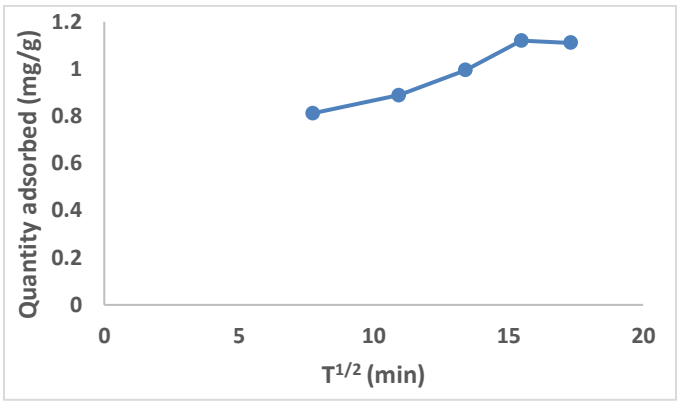

Figure 16. Intraparticle Diffusion Model Plot

Elovich Kinetics Model

The adsorption of Congo red onto the adsorbent surfaces was analyzed using the Elovich model. This model accounts for the non-linear behavior that is frequently seen during the early phases of adsorption. The Elovich equation, plot of q_t against ln(t), presented a slope of (1/ β) and an intercept of (1/β) ln (αβ). The value of β was calculated to be 4.87, and α to be 0.16 (Figure 17).

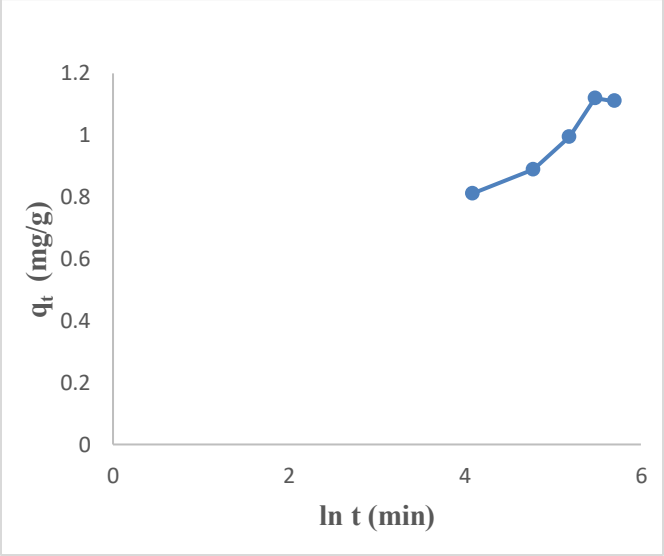

Figure 17. Elovich Kinetic Model Plot

However, it's worth noting that the correlation coefficients (R^2) were found to be high with a value of 0.9389, indicating that this model is suitable for an assessment of the

adsorption process [17]. The linearized equation (9) for the Elovich kinetic model is given as:

$$q_t = \frac{1}{\beta}\ln(\alpha\beta) + \frac{1}{\beta}\ln(t) \quad (9)$$

The data presented in Table 2 suggests that the Congo red dye adsorption experiment best-fits the pseudo-second-order kinetics with a correlation coefficient value of 0.99. This fit was superior compared to alternative kinetic models across the entire adsorption process. Consequently, it can be inferred that the pseudo-second-order equation provides a more accurate description of the adsorption kinetics of Congo red dye on the adsorbent. This suggests that occurrence of chemical interaction between the adsorbate and the adsorbent as suggested by the Temkin isotherm model earlier analyzed [14,16,18-20].

Adsorption Thermodynamics

To obtain the thermodynamics data of the adsorption study of Congo red dye on the adsorbent, an investigation of the thermodynamics was done at five different temperatures ranging from 30° to 70°C. The change in Gibbs free energy (ΔG°), change in entropy (ΔS°) and change in enthalpy (ΔH°) were calculated based on the equations 10, 11 & 12 [11]:

$$K_c = \frac{C_a}{C_e} \quad (10)$$

$$\Delta G = \Delta H - T\Delta S \quad (11)$$

$$\text{Log Kc} = \frac{\Delta S}{2{:}303 \text{ x R}} - \frac{\Delta H}{2{:}303 \text{ x R x T}} \quad (12)$$

In the equations above, Kc is the equilibrium constant, Ca and Ce represent the quantity of Congo red dye adsorbed on the adsorbent and the final concentration of the solution, respectively. T is the temperature in kelvin and R= molar gas constant which is 8.314 J $K^{-1}mol^{-1}$.

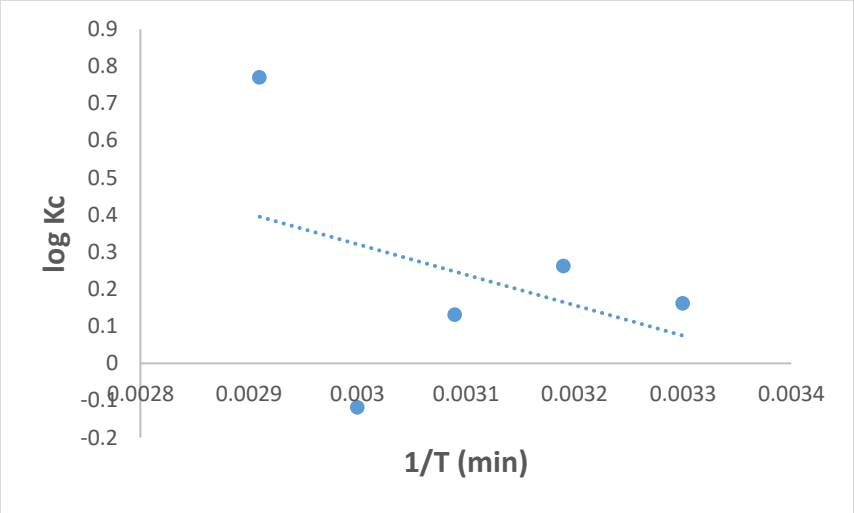

Figure 18. Thermodynamic Plot for Congo Red Dye Adsorption by [Cu(BTCA)(AMB)]

The Gibbs free energy change (ΔG°) values for the adsorption experiment at different temperatures were obtained as negative values (Table 3), indicating that the sorption process was spontaneous [13,15]. The change in enthalpy value calculated was obtained as 15.721 KJ/mol, and the change in entropy was 53.15 J/mol. The positive value of these two thermodynamic parameters depicts an endothermic process [13]. Since the range of the free energy is less than 20 KJ/mol, the thermodynamic investigation could be concluded as a physical sorption process which is spontaneous and endothermic [9,11].

Table 3. Thermodynamic Parameters for Congo Red Dye Adsorptions on to [Cu(BTCA)(AMB)]

Temperature (K)	ΔG° (KJ/mol)	ΔH° (KJ/mol)	ΔS° (J/mol)
303	-0.38	15.721	53.15
313	-0.91		
323	-0.14		
333	-1.92		
343	-2.51		

4. Conclusion

This research focused on the synthesis and characterization of a Cu (II) coordination compound containing mixed carboxylate and nitrogen donor ligands for dye adsorption. The study aimed to contribute to the field of environmental remediation and wastewater treatment by investigating the potential of this compound as an effective dye adsorbent.

Throughout this research, a systematic approach was followed, starting with the synthesis of the Cu (II) coordination compound through a well-defined procedure. This involved the selection of suitable ligands and optimization of reaction conditions to obtain a stable and efficient adsorbent. Optimum conditions for Congo red dye adsorption were observed to be 25 mg/L dye concentration, time of 4 h, at alkaline pH, temperature of 40°C, and adsorbent dosage of 0.01 g. Equilibrium adsorption isotherms, kinetic studies, and thermodynamic analyses were performed to elucidate the adsorption behavior and mechanisms. The results indicated that the Temkin isotherm model and pseudo-second order kinetic model best-fit the adsorption data obtained in this experiment. The thermo-dynamic studies carried out showed a rapid dye removal process indicating that the [Cu(BTCA)(AMB)] adsorbent is a promising material for remediation of dye polluted water.

5. References

1. Pang Y, Zhao C, Li Y, Li Q, Bayongzhong X, Peng D, Huang T. Cadmium adsorption performance and mechanism from aqueous solution using red mud modified with amorphous MnO_2. *Sci. Rep.*, 2022, 12(1), 4424.
2. Ishak S, Rosly NZ, Abdullah AH, Alang-Ahmad SA. Fabrication of calix[4]arene/ polyurethane for the adsorptive removal of cationic dye from aqueous solutions. *Environ. Monit. Assess*., 2023, 195(11), 1303. doi: 10.1007/s10661-023-11909-z
3. Jianlong W, Xuan G. Adsorption kinetic models: physical meanings, applications, and solving methods. *J. Hazard. Mater.*, 2020., 390, 122156.
4. Holm J, Hillenbrand R, Steuber V, Bartsch U, Moos M, Lubbert H, Montag D, Schachner M. Structural features of a close homologue of L1 (CHL1) in the mouse: A new member of the L1 family of neural recognition molecules. *Eur. J. Neurosci.*, 1996, 8(8), 1613-1629.
5. Adimula VO, Elaigwu SE, Owalude SO, Clayton HS, Rotifa AA, Adeniyi E, Tella AC. Synthesis and characterization of the cu(ii)-quinoxaline, 3,3-thiodipropionate mixed ligand coordination polymer for the removal of methylene blue from aqueous solution. *Chem. Eng. Commun.*, 2024, 211(8), 1175-1190.
6. Tella AC, Bamgbose JT, Adimula VO, Omotoso M, Elaigwu SE, Olayemi VT, Odunola OA. Synthesis of metal–organic frameworks (MOFs) MIL-100(Fe) functionalized with thioglycolic acid and ethylenediamine for removal of eosin B dye

from aqueous solution. *SN Appl. Sci.*, 2021, 3(1). https://doi.org/10.1007/s42452-021-04163-w
7. Tella AC, Oladipo AC, Adimula VO et al. Synthesis and crystal structures of a copper(II) dinuclear complex and zinc(II) coordination polymers as materials for efficient oxidative desulfurization of dibenzothiophene. *New J. Chem.*, 2019, 43, 14343-14354.
8. Tella AC, Oladipo AC, Adimula VO et al. Synthesis and crystal structures of zinc(II) coordination polymers of trimethylenedipyridine (tmdp), 4-nitrobenzoic (Hnba) and 4-biphenylcarboxylic acid (Hbiphen) for adsorptive removal of methyl orange from aqueous solution. *Polyhedron*, 2020, 192, 114819.
9. Tella AC, Owalude SO, Olatunji SO et al. Synthesis of zinc-carboxylate metal-organic frameworks for the removal of emerging drug contaminant (amodiaquine) from aqueous solution. *J. Environ. Sci.*, 2018, 64, 264-275.
10. Adimula VO, Tella AC, Owalude SO, Oladipo AC, Olayemi VT, Adeniyi E, Ismail B, Mumtaz A, Khan AM. Synthesis, characterization and catalytic studies of bimetallic heteronuclear com-plexes for the reduction of nitro-aromatic compounds. *Inorg. Nano-Met. Chem.*,2022.doi: http://10.1080/24701556.2022.2078364
11. Sagita CP, Nulandaya L, Kurniawan YS. Efficient and low-cost removal of methylene blue using activated natural kaolinite material. journal of multidisciplinary. *Appl. Nat. Sci.*, 2021, 1(2), 69-77.
12. Liu Z, He W, Zhang Q, Shapour H, Bakhtari MF. Preparation of a GO/MIL-101(Fe) composite for the removal of methyl orange from aqueous solution. *ACS Omega*, 2021, 6(7), 4597-4608.
13. Ma X, Wang L, He Q, Sun Q, Yin D, Zhang Y. A review on recent developments and applications of green sorbents-based solid phase extraction techniques. *Adv. Sample Prep.*, 2023, 6, 100065.
14. Meng W, Ma Z, Shu J, Li B, Su P, Wang R, Chen M, Liu Z, Ai K. Efficient adsorption of methylene blue from aqueous solution by hydrothermal chemical modification phosphorus ore flotation tailings. *Sep. Purif. Technol.*, 2022, 281, 119496.
15. Mohammed B, Youssef M, Gulsun AE, Farid Z, Sanae L. Recent advances in adsorption kinetic models: Their application to dye types. *Arabian J. Chem.*, 2021, 14(4), 103031.
16. Mu X, Liu X, Ye X, Zhang W, Li L, Ma P, Song D. Branched poly(ethylenimine) carbon dots-MnO_2 nanosheets based fluorescent sensory system for sensing of malachite green in fish samples. *Food Chem.*, 2022, 394, 133517.
17. Munir M, Nazar MF, Zafar MN, Zubair M, Ashfaq M, Hosseini-Bandegharaei A, Khan S, Ahmad A. Effective adsorptive removal of methylene blue from water by didodecyldimethylammonium bromide-modified brown clay. *ACS Omega*, 2020, XXXX, XXX, XXX−XXX. https://dx.doi.org/10.1021/acsomega.0c01613
18. Nachiyar CV, Rakshi AD, Sandhya S, Britlin Deva Jebasta N, Nellore J.

Developments in treatment technologies of dye-containing effluent: A review. *Case Stud. Chem. Environ. Eng.*, 2023, 7, 100339. https://doi.org/10.1016/j.cscee.2023.100339.

19. Revellame ED, Fortela DL, Sharp W, Hernandez R, Zappi ME. Adsorption kinetic modeling using pseudo-first order and pseudo-second order rate laws: A review. *Cleaner Eng. Technol.*, 2020, 1, 100032. https://doi.org/10.1016/j.clet.2020.100032.
20. Rohaley GAR, Hegmann E. The importance of structure-property relationship for the designing of biomaterials using liquid crystal elastomers. *Mater. Adv.*, 2022, 3, 5725-5734.

The Chemist
Journal of the American Institute of Chemists

Structural Elucidation of Ethanol Extraction of *Plectranthus zeylanicus*

Divya Sant and Karickal Raman Haridas*

School of Chemical Sciences, Kannur University, SAT Campus, Edat PO. 670327 Kannur, Kerala, India
**Corresponding author (Email: krharidas2001@gmail.com)*

Abstract: *Plectranthus zeylanicus,* is an aromatic herb in the family of Lamiaceae. It is widely used in Sri Lanka for making herbal medicines. *Plectranthus zeylanicus* is often called *Coleus zeylanicus*, and is locally known as *iruveli* in India. It is used in Aayurvedic medicines and effective in the treatment of asthma, cough, vomiting, diarrhea, throat infection, dysentery, fever, chronic ulcers, dental and eye diseases. This plant contains enzymes and flavonoids. The leaf and stem of the plant were subjected to solvent extraction and the ethyl acetate fraction is purified for obtaining a single compound. The compound was characterized by UV Visible, FT-IR, ^{1}H NMR, and LC-MS studies and investigated for its possible structure.

Key Words: *Plectranthus zeylanicus,* UV Visible, ^{1}H NMR , FT-IR and LC-MS

1. Introduction

Plant based medicines (Aayurveda) are safer alternatives to many synthetic medicines. They have fewer side effects, and the body can absorb these bio-compounds easily [1-4]. Even though this natural medicine is considered to have many advantages, the main drawback is that it needs more curing time, and larger amounts of the plants are essential for the drug's preparation [5-9]. The main alternate solution for such problems is to concentrate the particular components of the plant which cures and to synthesize the same chemically [10-11]. So, we may have to consider the whole plant extract and it's chemical components, which are actually responsible for healing [12]. While choosing the synthesis of the same chemically, we can minimize its excess use and presence of other components in the plant which may cause complications [13]. That is, we may suggest the medicinal compound in pure form through chemical

synthesis without destroying the natural sources.

Plectranthus zeylanicus (PZ) is a perennial herb, cultivated in Sri Lanka and in India. This plant is known as *karpuravalli* and *iruveli* in Malayalam and *kannikkaurkk*a in Sanskrit. Because of the presence of bioactive secondary metabolites, *PZ* is used in many traditional drugs [14-16]. The plants as a whole or as various extracts are used for the treatment of dysentery, eye disorders, vomiting, dermatitis, throat infection, cough, fever, and ulcers. The major component of this plant is α-terpeneol [17]. More than 100 compounds of this plant were detected, presented in small amounts. That is, only 60% of the components were identified. P-cymene, geraniol and geranyl acetate were found. 6β, 7β- dihydroxyroyleanone were also identified. It contains aromatic chemical compounds and essential oils, and has anti-inflammatory, antifungal, antimicrobial and disinfectant activities. These plants are very important for the perfume and medical industry [18].

Mayuri Napagoda et al. [19] have isolated dichloromethane extract of PZ and obtained the compound 7α-acetoxy-6β-hydroxyroyleanone. In another study, Mayuri Napagoda et al. [21] revealed 5 lipoxygenase(5-Lo) inhibition of PZ, which has an important role in preventing disorders like asthma or atherosclerosis. They have studied the anti-inflammatory activity of the isolated phytoconstituent *in-vitro*. They also studied its antibacterial and antifungal activities and claimed this as a remedy for inflammatory disorders and microbial infections.

Sudhara G. De Soyaza et al. [20] studied the antimicrobial activity of silver nanoparticle prepared from *PZ*. They have studied the hexane extract of this plant and indicate the potent inhibition of 5-lipoxygenase enzyme. They have also claimed the presence of diterpenoids, pentacyclic triterpenes, fatty acids, phytosterols, etc., in the extract.

In this paper, we describe the extraction of *PZ* using ethanol solution. The green plants planted in our farm were collected, washed and dried in shade [21-23]. The plant was identified by a botanical expert. They were subjected to polarity index extractions, using organic solvents. For the specific study, we collected the ethanol extract. Our aim was to extract the phytochemical components, separate and purify and reproduce them in high concentration and use them in the affected areas [24-26].

2. Experimental

Materials

Plectranthus zeylancius (Figure 1), Hexane, Ethyl Acetate (E Merck, India), Ethanol (commercial grade). All solvents were distilled before use.

Fig 1. Image of *Plectranthus zeylancius*

Instruments

UV spectra were recorded on an Ultraviolet-visible spectrophotometer (Jasco V-650), FT-IR spectrum was produced by Fourier transform infrared spectrometer (FT-IR) (Jasco model 4100) using KBr pellets. Liquid Chromatography Mass Spectrum was obtained by Agilent 6100 Series Quadrupole. The NMR spectral study was carried out at 400 (^{1}H) and 100 (^{13}C) MHz on a Bruker-400 MHz spectrometer instruments. The chemical shift values are reported relative to Me_4Si (^{1}H) and $CDCl_3$ (^{13}C) as internal standards. The value of coupling constant (J) was stated in Hertz (Hz).

Procedure

The dried and powdered sample was used for the analysis. It was extracted using solvents of increasing polarity. First, hexane was used. The components soluble in hexane were separated out. The second extraction was carried out with ethyl acetate and the compounds were separated. In the third step, we selected ethanol as a solvent. 30 g of the powder of stem and leaf of *PZ* was transferred to the round bottom flask and extracted using ethanol as a solvent for a time span of three hours. It was filtered and the ethanol extract was collected. The solvent was removed. The dry army green coloured compound, thus obtained, was subjected to TLC and then purified by column chromatography. A single component was obtained (Figure 2) and used for further study.

Fig 2. Image of the Extracted Compound

The structural elucidation was carried out using UV, IR, NMRs and LC-MS spectra and information from literature.

3. Results and Discussion

As a whole, we have obtained a very low yield of 800 mg pure compound from 30 g of starting material. For the structure elucidation of the compound, the following spectra were recorded.

Extract	Colour	Yield	Melting point (°C)	Nature
Ethanol extract	Army Green	800mg	> 360	Powder

Spectral Details

Figure 3 shows the UV-visible spectrum of ethanol extract of *PZ.* It shows three peaks at 286, 310 and 664 nm. The first peak (286 nm) indicates the presence of unsaturation (π-π* transitions) and the second peak (310 nm) for a carbonyl group (n- π*transitions). The peak obtained in the visible region (664 nm) is of its colour.

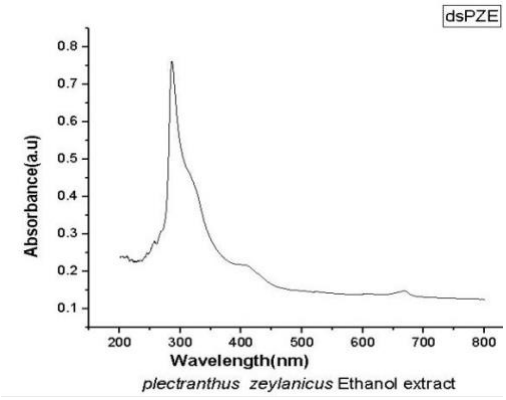

Fig 3. UV-Visible Spectrum of Ethanol Extract of *PZ*

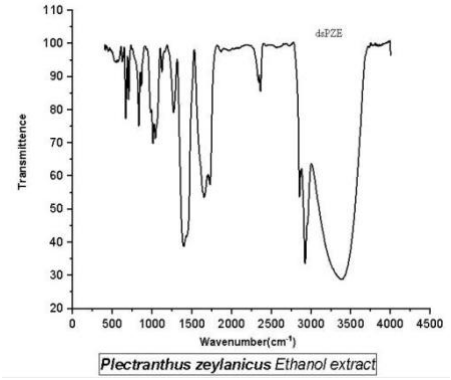

Fig 4. IR Spectrum of Ethanol Extract of *PZ*

Figure 4 shows the IR spectrum of ethanol extract of *PZ*. The peaks (cm^{-1}) obtained are at 3557 (OH), 3345 (C-H str of C=C), 2918 (C-H str of CH_3), 2849 (C-H str of CH), 1716 (C=O), 1644 (C=C bend), 1603 (C-N), 1383 (C-H bend), 1262 (C-O aromatic), 1116(C-Oaliphatic).

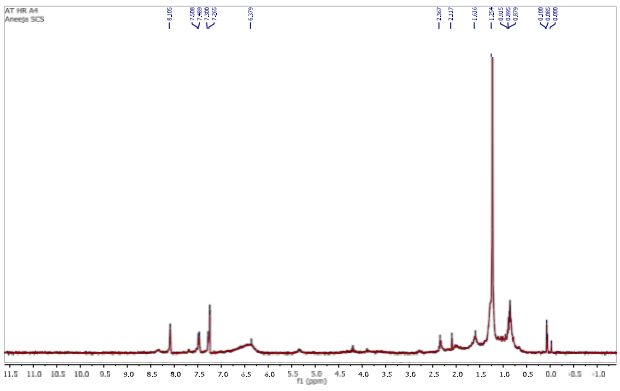

Fig 5. ^{1}H NMR Spectrum of the Compound

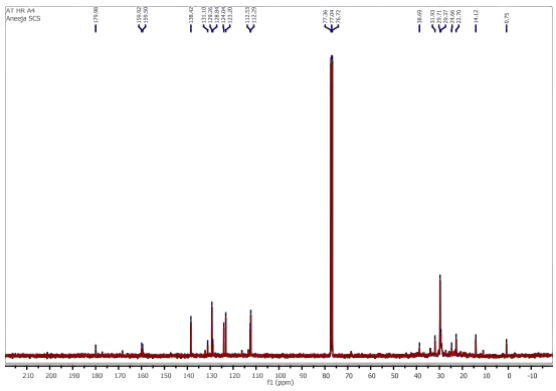

Fig 6. ^{13}C- NMR Spectrum of the Compound

Figures 5 and 6 give the NMR spectra of the compound. The^{1}H- NMR spectrum of the compound shows the peaks (ppm) at 8.10 (s) (CHO), 7.48 (d), (ar H), 7.26 (solvent $CDCl_3$) 6.37 (s) (CH=C), 2.36 (s), 2.11 (s), 1.61 (s), 1.25 (s), 0.89 (t), 0.08 (t) (aliphatic hydrogen). From ^{13}C-NMR spectroscopy, we obtained peaks (ppm) at 170.98 (C=O), 150.5, 130.4, 128.8, 123.2 (ar C), 112.2 (C=C), 36.6, 31.9, 29.37, 24.66, 22.7, 14.5 (aliphatic C).

Figure 7 shows LC-MS spectrum of the ethanol extract of the *PZ***.** The maximum molar weight obtained is 305. The most abundant peak is observed at 185. The fragmentation pattern is given in Table 1.

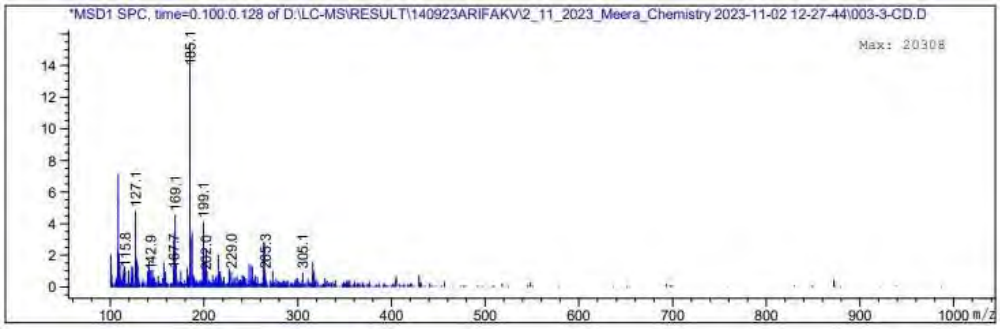

Fig 7. LC-MS Spectrum of the Ethanol Extract of the *PZ*

Table 1. The LC-MS Fragmentation Pattern of Ethanol Extract of the *PZ*

Mol. peaks	Mol. peaks Subtraction	Mass lost	Inference
414			Molecular ion peak
305	414-305	109	Loss of 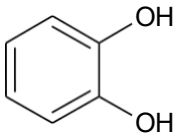
265	305-265	40	Loss of -H_2C-CH=CH-
219	305-219	86	Loss 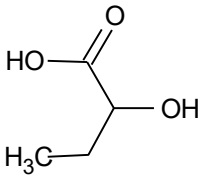
200	229-200	29	Loss of C_2H_5
183	265-183	17	Loss of OH
167.7	199-167.7	31	Loss of OCH_3
144	199-144	55	Loss of 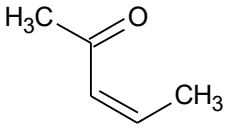
116	159-116	43	Loss of C_3H_7

As per the UV spectrum, we have a C=O and unsaturation in the molecule. From IR spectrum, we have C=C, CH_3, CH, C=O, C-N, OH and C-O groups. The mass spectrum gives the possibility of groups that are shown in Table 1.

From the literature values of various extracts of *PZ*, the following structure (Figure 8) is almost suited for our extract.

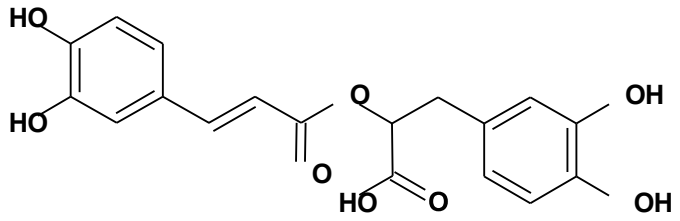

Fig 8. Structure of the Ethanol Extract of the *PZ*

The positions of the substituents are maintained at the same place. The phenolic groups may be substituted with alkyl chains. As per the mass spectrum, the molar mass is 414 (M^+ peak) and the proposed structure has the molar mass of 416.

4. Conclusion

Phytomedicines are more important in curing various chronic diseases. Plant bodies contain many chemical components in different ratios. When we analyze the therapeutic application of phytochemicals, the structural details are necessary. In this paper, the extraction of *Plectranthus zeylancius* using ethanol has been carried out. Spectroscopic techniques such as UV, IR, NMR and LCMS were used for structural elucidation. The peaks in the UV-visible spectrum show the presence of an unsaturation and carbonyl group. IR spectrum indicates the presence of C-H str of C=C, C-H str of CH_3, C-H str of CH, C=O, C=C bend, C-N, C-H bend, C-O aromatic, C-O aliphatic groups. NMR spectroscopy also suggests the existence of aliphatic and aromatic carbons and CHO group. Considering the UV, IR, NMR and LCMS spectroscopic details, the structure of the compound obtained is shown above.

5. References

1. Arambewela L, Wijesinghe A in Sri Lankan Medicinal Plant Monographs and Analysis, 1st ed., National Science Foundation, Colombo, Sri Lanka: klm, 2006, vol 11.
2. Chiang N, Fredman G, Bäckhed F, Oh SF, Vickery T, Schmidt BA, Serhan CN. Infection regulates pro-resolving mediators that lower antibiotic requirements. *Nature*, 2012, 484, 524–528. doi: 10.1038/nature11042.
3. Serhan CN. Novel pro-resolving lipid mediators in inflammation are leads for resolution physiology. *Nature*, 2014, 510,92–101. doi: 10.1038/nature13479.
4. Koeberle A, Werz O. Natural products

as inhibitors of prostaglandin E2 and pro- inflammatory 5-lipoxygenase-derived lipid mediator biosynthesis. *Biotechnol. Adv.*, 2018, 36, 1709–1723.doi: 10.1016/j.biotechadv.2018.02.010.
5. Grayer RJ, Eckert MR, Lever A, Veitch NC, Kite GC, Paton AJ. Distribution of exudate flavonoids in the genus Plectranthus. *Biochem. Syst. Ecol.*,2010,38,335–341.doi: 10.1016/j.bse.2010.01.014.
6. Lukhoba CW, Simmonds MSJ, Paton AJ. Plectranthus: A review of ethnobotanical uses. *J. Ethnopharmacol.*, 2006, 103, 1–24. Doi 10.1016/ j.jep.2005.09.011.
7. Dassanayake MD, Fosberg FR in A Revised Handbook to the Flora of Ceylon, 1st ed., Amerind Publ. Co., Ltd., New Delhi, India, 1981, vol 3, pp 150–151.
8. Abubakar AR, Haque M. Preparation of medicinal plants: Basic extraction and fractionation procedures for experimental purposes. *J. Pharm. BioAllied Sci.*, 2020, 12, 1–10.
9. Jayaweera DMA in Medicinal Plants (Indigenous and Exotic) Used in Ceylon, Part 2, 1st ed., National Science Council, Colombo, Sri Lanka, 1982, pp 108–109.
10. Deena MJ, Sreeranjini K, Thoppil JE. Antimicrobial screening of essential oils of *Coleus aromaticus* and *Coleus zeylanicus*. *Int. J. Aromather.*, 2002, 12, 105–107. doi: 10.1016/S0962-4562(02)00035-8.
11. Kotagiri D, Beebi SK, Chaitanya KV. Secondary metabolites and the antimicrobial potential of five different Coleus species in response to salinity stress. *BioRxiv.org*, 2017, 220368. doi: 10.1101/220368.
12. Mehrotra R, Vishwakarma RA, Thakur RS. Abietane diterpenoides from *Coleus zeylanicus*. *Phytochemistry*, 1989,28,3135–3137.doi: 10.1016/0031-9422(89)80293-6.
13. Jirovetz L, Jirovetz K, Buchbauer G, Fleischhacker W, Shafi PM, Saidutty A. Analyses of the essential oil of the leaves of the medicinal plant *Coleus zeylanicus* from India. *Sci. Pharm.*, 1998, 66, 223–229.
14. Teixeira AP, Batista O, Simoes MF, Nascimento J, Duarte A, de la Torre MC, Rodriguez B. Abietane diterpenoids from *Plectranthus grandidentatus*. *Phytochemistry*, 1997, 44, 325–327. doi: 10.1016/S0031-9422(96)00467-0.
15. Bernardes CES, Garcia C, Pereira F, Mota J, Pereira P, Cebola MJ, Reis CP, Correia I, Piedade MFM, da Piedade MEM, Rijo P. Extraction, optimization and structural and thermal characterization of the antimicrobial abietane 7α-acetoxy-6β- hydroxyroyleanone. *Mol. Pharmaceutics*, 2018, 15, 1412–1419.doi: 10.1021/acs.molpharmaceut.7b00892.
16. Deena MJ, Sreeranjini K, Thoppil JE. Antimicrobial screening of essential oils of *Coleus aromaticus* and *Coleus zeylanicus*. *Int. J. Aromather.*, 2002, 12, 105–107. doi.org/10.1016/S0962-4562(02)00035-8.
17. Fonseka DLCK, Wickramaarachchi WWUI. *Plectranthus ambonicus* and *Plectranthus zeylanicus*: As promising medicinal plants. *Int. J. Sci. Res. (IJSR)*,2018,7.doi: 10.21275/ART2019161.
18. Napagoda M, Gerstmeier J, Butschek H, Lorenz S, De Soyza S, Qader M, Nagahawatte A, Gaya Bandara Wijayaratne WMD, Schneider B, Svatoš A, Jayasinghe L, Koeberle A, Werz O. *Plectranthus zeylanicus*: A rich source of secondary metabolites with antimicrobial, disinfectant and

anti-inflammatory activities. *Pharmaceuticals*, 2022, 15(4), 436. doi: 10.3390/ph15040436.
19. Napagoda M, Gerstmeier J, Wesely S, Popella S, Lorenz S, Scheubert K, Svatoš A, Werz O. Inhibition of 5-lipoxygenase as anti-inflammatory mode of action of *Plectranthus zeylanicus Benth* and chemical characterization of ingredients by a mass spectrometric approach. *J. Ethnopharmacol.*, 2014, 151, 800–809. doi: 10.1016/j. jep.2013.11.004.
20. De Soyzal SG, Gaya Bandara Wijayaratne WMD, Napagoda1 M, Witharana S. Antimicrobial potential in biogenic silver nanoparticles synthesized from *Plectranthus zeylanicus*. *J. Mol. Nanotechnol. Nanomed.*, 2017, 1(1), kkm1800105.
21. Turner NA, Sharma-Kuinkel BK, Maskarinec SA, Eichenberger EM, Shah PP, Carugati M, Holland TL, Fowler VG, Jr. Methicillin-resistant *Staphylococcus aureus*: An overview of basic and clinical research. *Nat. Rev. Microbiol.*, 2019, 17, 203–218. doi: 10.1038/s41579-018-0147-4.
22. Anand U, Jacobo-Herrera N, Altemimi A, Lakhssassi N. A comprehensive review on medicinal plants as antimicrobial therapeutics: Potential avenues of biocompatible drug discovery. *Metabolites*,2019,9,258.doi: 10.3390/metabo9110258.
23. Cowan MM. Plant products as antimicrobial agents. *Clin. Microbiol. Rev.*., 1999, 12, 564–582. doi: 10.1128/CMR.12.4.564.
24. Chandra H, Bishnoi P, Yadav A, Patni B, Mishra A.P, Nautiyal AR. Antimicrobial resistance and the alternative resources with special emphasis on plant-based antimicrobials—A review. *Plants*, 2017, 6, 16. doi: 10.3390/plants6020016.
25. Rijo P, Esteves M, Simões MF, Silva A, Duarte A, Rodriguez B. Antimicrobial activity of 7α-acetoxy-6β-hydroxyroyleanone 12-O-benzoyl esters. *Planta Med.*, 2008, 74, PB81. doi: 10.1055/s-0028-1084426.
26. Pereira F, Figueiredo T, de Almeida R, Antunes C, Garcia C, Reis C.P, Ascensão L, Sobral RG, Rijo P. Unveiling the mechanism of action of 7α-acetoxy-6β- hydroxyroyleanone on an MRSA/VISA strain: Membrane and cell wall interactions. *Biomolecules*, 2020,10,983.doi: 10.3390/biom10070983.

The Chemist
Journal of the American Institute of Chemists

Humic Acid Adsorption on Natural Fiber Surface-modified Polypropylene

Bashir Brika[1*], Wael Elhrari[2,3], Mahasn Kubbt[1], Hoda Jelani[1], Abdulrouf Trish[2,3]

[1] Libyan Advanced Center for Chemical Analysis, Libyan Authority for Scientific Research, Tripoli, Libya (Tel. +218 91 0610178)
[2] Libyan Polymer Research Center, Tripoli, Libya
[3]Research, Consultation and Training Center, Sirte University, Sirte, Libya

**Corresponding author (E-mail: bashirforlibya@gmail.com)*

Abstract: Polypropylene, a commercially abundant polymer, has widely been used for industrial applications but due to its low surface charge, the use of polypropylene as an adsorbent to remove humic substances from water and aqueous solution has never been explored. The objective of this study is to explore opportunities for removal humic acid (HA) from aqueous solutions using a composite of polypropylene with inexpensive and abundant natural materials such as palm date leaf fibers and seaweed (Posidonia). Composites with different percentages were prepared by a melt extrusion method and were then used individually as a granular adsorbent for the removal of humic acid aqueous solution. Batch adsorption experiments were conducted under various conditions of process parameters (initial HA concentration, pH, contact time, and adsorbent weight) to examine the HA removal efficiency. The experimental results showed that optimal conditions for humic acid removal were initial humic acid concentration (20 mg/l), low pH (2.0), low adsorbent weight (0.2 g) and contact time of 50 minutes. At these conditions the best removal of humic acid was achieved by polypropylene seaweed composite (68%). From this study, it can be concluded that seaweed mixed with polypropylene (at low concentration) could be an effective and low-cost, natural and abundant material for the removal of humic acid from water sources.

Key Words: polypropylene, polypropylene natural fiber composite, surface modification, humic acid

1. Introduction

Natural organic matters (NOM), which are a mixtures of decomposition product of plants and animals, are major constituents commonly present in water that require removal [1,2]. Humic acid (HA) accounts for a significant portion (40-90%) of the NOM [3] and has a harmful effect on the water quality, such as undesirable color (yellowish to brownish) and taste; serves as food for bacterial growth; binds with heavy metals and other organic substances to yield high concentrations of these substances and enhance their transportation in the water; reacts with chlorine during water treatment leading to the evolution of chlorinated organic compounds, some of them know as human carcinogens (trihalomethanes) [3-7]. As a result, humic acid is considered as impurities and needs to be measured for water studies.

In the past years, several methods have been employed for removal of humic acid from aqueous solution. adsorption is one of the most-effective methods in removal of humic acid. Several kinds of adsorbents have been employed for humic acid adsorption including zeolite [8], polypyrrole-coated granules [9], chitosan [10-13], clay [14], activated carbon [15-17], and resins [18]. However, some of the previously mentioned adsorbent compounds have some shortcomings; for example, activated carbon is expensive and requires high operating cost and require frequent regeneration [3]. In recent years, many efforts have been focused on low-cost and abundant natural minerals sorbents for water and wastewater treatment adsorbents.
The conventional filtration process, which uses sand as the filter media, has been found to be ineffective in removing humic substances. In water filtration, there has been a considerable interest in the use of granular media that can enhance the removal of humic substances [19]. One option is to replace the sand with modified polyolefin as the filter media.

Polyolefin's and polypropylene have a very low surface charge due to the non-polarity nature of the polymer and thus because the surface tension of these polymers ranges between 30 and 40 dynes/cm, the polymers would not attract any polar chemicals and hence the removal of these compounds would not be achieved. The polarity can be changed of this family of polymers by ionizing the surface. However, this is not a permanent surface change as it tends to reverse with time. For this reason, natural materials such as natural fibers (palm date leaf) and seaweed (Posidonia) were chosen in this study to be melt mixed with polypropylene and investigate the humic acid removal by the modified polypropylene.

To date, no study related to adsorption of humic acid by natural fiber-modified polypropylene has appeared in the literature. The aims of this study are (1) to determine the ability of modified polypropylene to adsorb humic acid from aqueous solutions and (2) to examine the effect of different parameters such as contact time, adsorbate concentration, adsorbent weight and initial pH value on the adsorption process. It is hoped that this modest effort may substitute the deficiency in the literature on the modification of polypropylene using natural fibers materials such as palm date leaf and seaweed.

2. Materials and Methods

Materials

A commercially available polypropylene in the form of granular pellets from LUKOIL and used as the matrix [(Polypropylene Buplen 6631), melt index = 1-3 g/10 min (230°C, 2.16 Kg), density of 898-905 kg/m^3]. The natural fibers (palm date leaf) and seaweed (Posidonia) were provided from the Libyan Polymer Research Center, while humic acid was purchased from agricultural equipment market.

Preparation of Modified Polypropylene

The method of production that was chosen for the modified polymer was extrusion as this method could lead to a large production volume and the physical size could be maintained relatively easily.

Dried polypropylene pellets were melted, mixing once with palm date leaf fibers and once with seaweed fiber powder by using HAAKE mini twin-screw extruder CTW, with average screw speed of 35 rpm, and barrel temperature of 190°C. Blend samples of different percentages (1, 3 and 5 w%) were prepared and then were grinded and prepared for analysis and adsorption experiments.

Characterization Techniques

The contact angle measurements were carried out using ramè-hart instrument co. Model 200-F4 at room temperature. Two μL volume drops of water were deposited on the surface of the samples using a syringe. Pictures of the water drops were acquired through a digital camera positioned on a static contact angle analyzer. The θ of the contact angle was measured automatically from the image setup. Each contact angle value is an average of five measurements.

Unmodified and modified forms of the polypropylene were characterized using Fourier-transformed infra-red spectroscopy (630 FTIR, Agilent). Measurements were taken in transmission mode at the range of 4000-580 cm^{-1} with resolution of 4 cm^{-1}.

Batch Adsorption Experiments

Humic acid solution was prepared by dissolving a certain amount of humic acid in a known volume of deionized water. The solution was stirred for 2 h and filtered through a Whatman membrane filter (0.45 μm) before conducting the adsorption tests.

A series of batch adsorption experiments were conducted to examine the adsorption isotherm, and the effect of solution pH values on the adsorption behaviors. In the adsorption experiments, a number of 100-ml flasks contained 20 ml of the humic acid solution with an initial pH value of 6 and an initial humic acid concentration in the range of 10-100 mg/l, respectively, were used. A 0.2-gram amount of the modified polypropylene was added to each of the flasks and the contents were stirred on a shaker at 120 rpm and at room temperature

(25°C) for 1 h for adsorption to take place and reach equilibrium. The initial and final humic acid concentration in the solutions in each of the flasks was determined with an UV-visible spectrometer (Photolab 7600 UV-vis, Xylem Analytics, Germany) at 254 nm in 1 cm quartz cell.

All experiments were performed in triplicate and average values were used for calculations. The percentage of HA removal (%) was calculated from initial HA concentration (C_0, mg/L), and final HA concentration (C_e, mg/L) according to equation 1:

$$R\ (\%) = \frac{(C0-Ce)}{C0} X\ 100 \quad (1)$$

The amount of humic acid adsorbed on the modified polypropylene at adsorption equilibrium, *qe* (mg/g) was calculated from the equation 2:

$$qe = \frac{(C0-Ce)V}{m} \quad (2)$$

where C_0 and C_e are the initial and equilibrium humic concentrations, respectively (mg/L), V is the total volume of the suspension (L), and m the adsorbent mass (g).

Adsorption Isotherms

The adsorption capacity is the value that gives information about the feasibility of the adsorbents for removing the humic acid as a pollutant from water.

The two classical models of Langmuir and Freundlich were tested to describe the adsorption equilibrium of HA onto both modified polypropylene with 1% palm leaf fibers and modified polypropylene with 1% seaweed. The Langmuir mode in the linearized form can be written as follows [20]:

$$\frac{1}{qe} = \frac{1}{qmax * Kl * Ce} + \frac{1}{qmax} \quad (3)$$

$$Intercept = \frac{1}{qmax} \quad (4)$$

$$Slope = \frac{1}{qmax * Kl} \quad (5)$$

where *q*e is the amount of humic acid adsorbed per unit weight of the modified polypropylene granules at equilibrium concentration (mg g^{-1}), Ce is the final concentration in the solution (mg l^{-1}), *q*max is the maximum adsorption at monolayer

coverage (mg g^{-1}), and *Kl* is the adsorption equilibrium constant (l $mg^{-1)}$.

The experimental isotherm data are also modeled with log-linearized Freundlich model in the format [20]:

$$\log qe = \frac{1}{n}\log Ce + \log Kf \quad (6)$$

were *qe* and *Ce* have the same definitions as in equation 3, K*f* is a Freundlich constant representing the adsorption capacity (mg g) (l g^{-1}) ^{n}, and *n* is a constant depicting the adsorption intensity (dimensionless).

3. Results and Discussion

Characterization of Modified Polypropylene

Surface polarity

The surface polarity or the repulsion of water was determined by means of the water droplet method and subsequent measurement of the contact angle of the water to the substrate.

A one microliter droplet of distilled water was placed on the surface of the substrate to be measured. A photo was then taken with a stereomicroscope that was connected to a computer. The contact angle of the water droplet with the surface of the substrate was thus measured and reported as angle theta (θ).

Data presented in Table 1 states that the presence of palm date leaf fiber and seaweed vastly reduces the surface tension, thus increases the polarity of the polypropylene. Furthermore, the lowest average contact angle or the highest polar surface was achieved with 1% seaweed followed by 1% palm date leaf fiber. Therefore, these two composites were used in the adsorption experiments.

Table 1. Average Contact Angle Data vs. Polymer Composition

Polymer	Co-extrudate	Co-extrudate (%)	Average Contact angle (θ)
Polypropylene	---	---	95.3
Polypropylene	Palm date fiber	1 %	64.3
Polypropylene	Palm date fiber	3 %	66.9
Polypropylene	Palm date fiber	5 %	74.3
Polypropylene	Seaweed	1 %	63.5
Polypropylene	Seaweed	3 %	73.1
Polypropylene	Seaweed	5 %	72.9

FTIR

To obtain a clear understanding of the polypropylene structure characteristics, and the effects of natural fibers modifications, FTIR analysis was carried out. The obtained FTIR spectrum is shown in Figure 1.

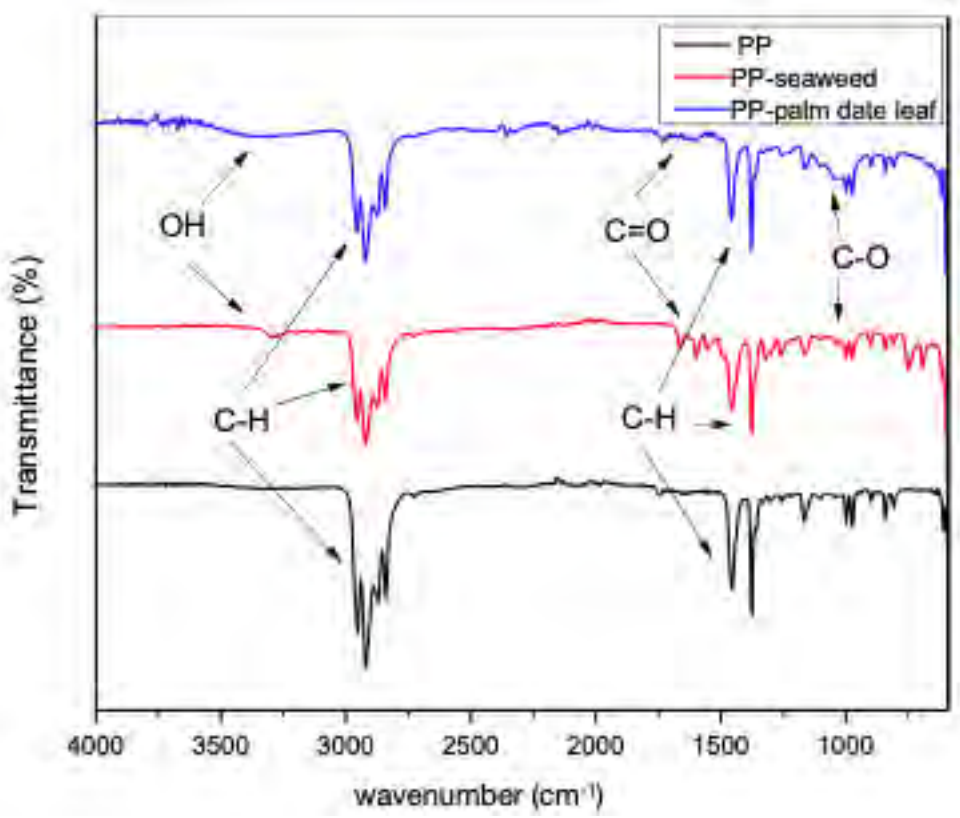

Figure 1. FTIR Spectrum of Polypropylene and Polypropylene Palm Date Leaf Fibers and Polypropylene Seaweed

Figure 1 shows the FTIR spectrum of polypropylene, before modification (original) and after modification with a 1% of palm dates leaf fibers, and with a 1% of seaweed. From Figure 1, FTIR spectra of polypropylene showed characteristic bands of polypropylene, stretching vibration of –C-H at 2959-2823 cm^{-1} and bending vibrations of $–CH_2$ and CH_3 at 1471-1417 cm^{-1} and 1383-1349 cm^{-1}. When polypropylene was mixed with palm date leaf fibers and seaweed, new bands appeared that are characteristics of natural fiber and correspond to cellulose and lignin. O-H stretching vibration at 3448-3169 cm^{-1} and carbonyl stretching C=O and C-O at 1770-1567 cm^{-1} and 1084-1043 cm^{-1}, respectively.

Adsorption of Humic Acid into Modified Polypropylene

Effect of adsorbent weight on humic acid removal

To investigate the effect of the modified polypropylene as an adsorbent on the efficiency of the humic acid adsorption process, the experiments were carried out with different weights of modified polypropylene ranging from 0.1, 0.2, 0.3 and 0.4 g; the other conditions were fixed for the adsorption process (initial humic acid concentration 20 mg/L, solution pH 2, temperature 25°C, and adsorption time 60 min, 120 rpm). Results are presented in Table 2.

Table 2. Effects of Adsorbent Weight of Palm Date Leaf Fibers and Seaweed on HA Removal

No	Weight (gram)	HA removal			
		R% (Palm fibers)	SD	R% (Seaweed)	SD
1	0.1	28.06	0.011	48.14	0.021
2	0.2	33.67	0.013	47.86	0.014
3	0.3	32.27	0.012	42.80	0.13
4	0.4	30.87	0.011	41.20	0.015

As was expected from the literature, when the adsorbent's weight increased, the humic acid removal increased [21,22], but the results showed that the increase was not clearly noticeable and there was a fluctuation in the readings, especially in the case of the seaweed samples. However, the highest humic acid removal on both modified polypropylene samples was achieved when a weight of 0.2 g/20 mL was used at 25°C. From the results, it is clear that an increase in the adsorbent weight above 0.2 g had no important effect on the adsorption efficiency of humic acid from the aqueous solution. Additionally, regarding the efficiencies of two modifications, it is clearly noticed that more efficient removal of humic acid was achieved with polypropylene modified with seaweed than with polypropylene modified with palm date leaf fibers.

Effect of pH on humic acid removal

The effect of pH on the adsorption of humic acid onto modified polypropylene was studied by varying the pH of the solution from 2.0 to 5. The results are shown in Table 3 and Figure 2.

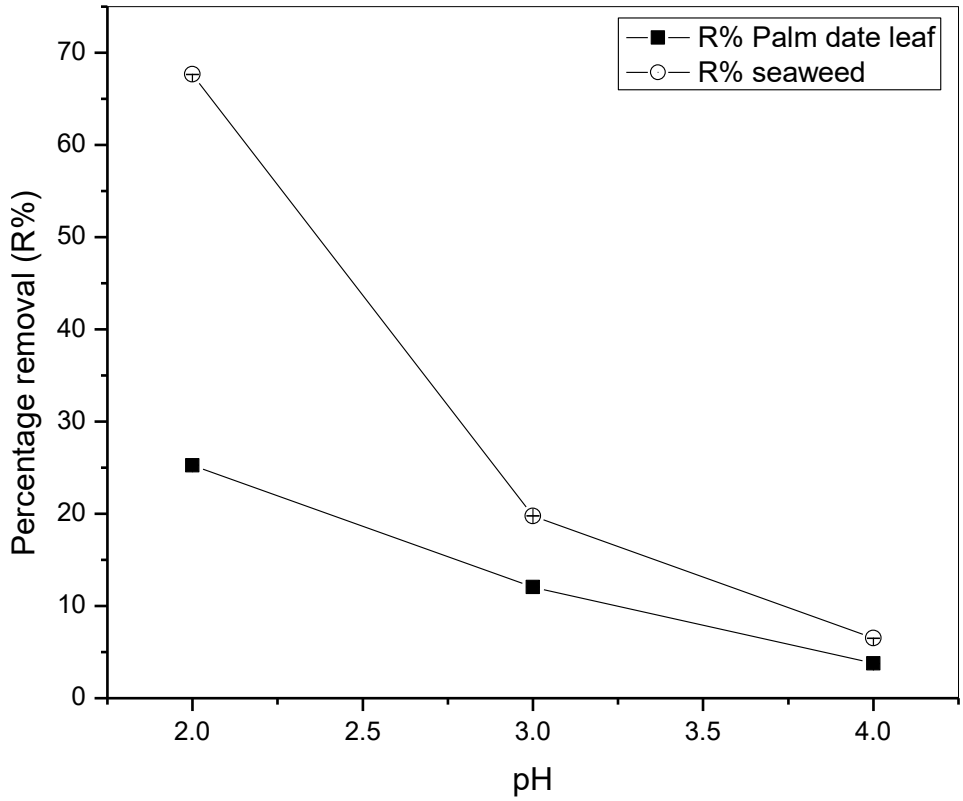

Figure 2. Effects of pH on HA Removal Using (■) Palm Fibers, and (○) Seaweed (HA concentration = 20 mg/l, weight= 0.2 g, T = 25 °C, V solution = 20 ml, t = 60 min, 120 rpm)

It was observed that the maximum adsorption was achieved at pH 2.0. As the pH of the solution was increased from 2.0 to 4.0, the percentage removal of humic acid on modified polypropylene with palm date leaf fibers decreased from 25.25 to 3.76% at an initial concentration of 20 mg/L, while in the case of modified polypropylene with seaweed the humic acid percentage removal decreased from 67.77% at pH 2.0 to 6.5% at pH 4.0. On the other hand, results showed that there was almost no reduction in humic acid removal above pH 4.0. This can be explained by the following: as pH increases, both the adsorbent surface and the humic acid lose their protons and become negatively charged, and, consequently, repel each other. The decrease in humic acid adsorption with increasing pH suggests that electrostatic interaction plays a role in the adsorption process [23].

Table 3. Effects of pH on HA Removal on Modified Polypropylene with Palm Leaf Fiber and Seaweed

No	pH	HA removal			
		R% (palm fibers)	SD	R% (seaweed)	SD
1	2.0	25.25	0.022	67.66	0.018
2	3.0	12.05	0.019	19.77	0.021
3	4.0	3.76	0.011	6.50	0.016

The high adsorption of HA at lower pH values can be attributed to the external hydrogen bonds formed between phenolic hydroxyl groups of HA and hydrogen bonding sites on the modified polypropylene [24]. The large increase in adsorption between pH 3 and 2 could also be attributed to a reduction in the size of the humic acid molecules at low pH [25]. Smaller molecular size enables more molecules to be adsorbed on the adsorbent's surface.

Effect of initial humic acid concentration

In order to investigate the effect of initial humic acid concentration, experiments were carried out at room temperature (25°C) and at the initial pH 2.0. Initial humic acid concentrations ranging from 10 to 50 mg/L were prepared; 0.2 g of modified polypropylene was added to 20 ml of humic acid solution and agitated magnetically at 120 rpm for 60 min. Obtained results of humic acid removal are shown in Table 4 and Figure 3.

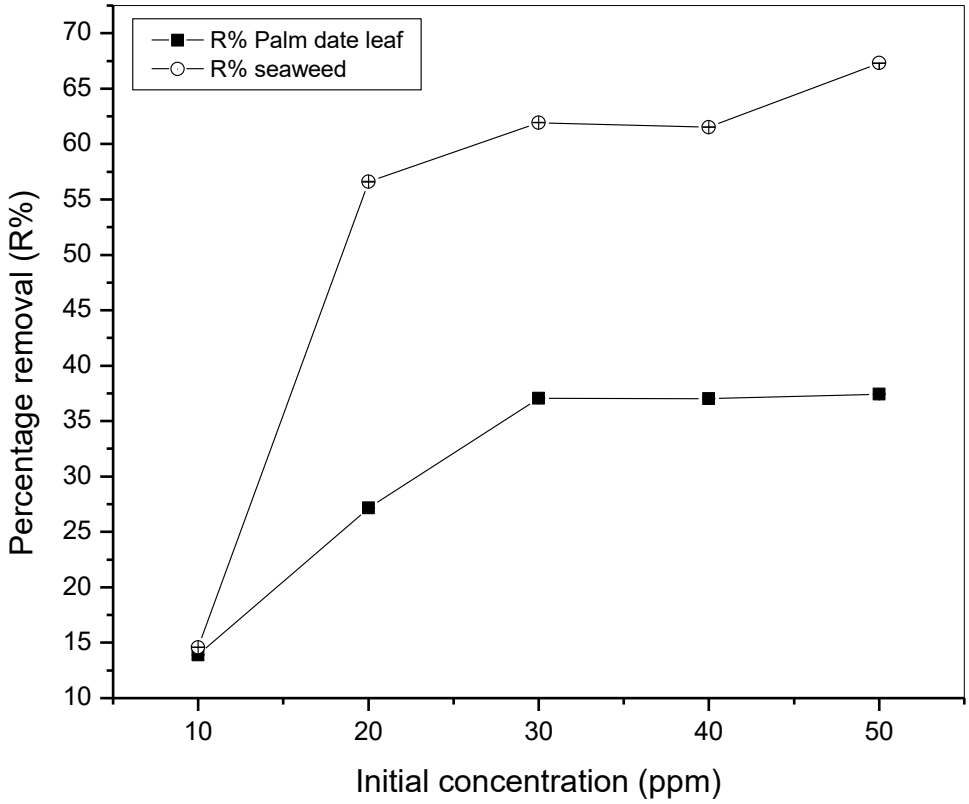

Figure 3. Effects of Initial Concentration on HA Removal Using (■) Palm Fibers, and (○) Seaweed

Table 4. Effect of Initial Humic Acid Concentration on HA Removal

No	Concentration (ppm)	HA removal			
		R% (palm date leaf fibers)	SD	R% (seaweed)	SD
1	10	13.90	0.023	14.58	0.019
2	20	27.15	0.014	56.60	0.022
3	30	37.05	0.021	61.94	0.017
4	40	37.03	0.011	61.52	0.018
5	50	37.43	0.016	67.30	0.019

It can be observed that as the concentration increased from 10 to 50 mg/L, humic acid removal percentage increased from 13.9 to 37.43% in the case of modified polypropylene with palm date leaf fibers, while in the case of modified polypropylene with seaweed, humic acid removal percentage increased from 14.58 to 67.3%. This is attributed to the increase in the mass driving force which allows more humic acid molecules to pass from the solution to the surface of the modified polypropylene. It is clear that the initial humic acid concentration plays an important role in the adsorption process.

Effect of contact time

The effect of agitation time on the adsorption of humic acid onto modified polypropylene was determined within the following contact time intervals: 5, 10, 20, 30, 40, 50, 60 and 120 minutes. Experiments were performed at room temperature (25°C), at a fixed modified polypropylene weight of 0.2 g, pH 2 and initial humic acid concentration of 20 mg/L. Samples were stirred for 120 minutes. The results of humic acid removal as a function of time are presented in Table 5 and Figure 4. The results showed that the time of 50 minutes was sufficient to achieve the maximum adsorption for both modified polypropylene types. As can be seen in the Figure 4, the adsorption process can be divided into two phases: the humic acid removal was initially rapid (fast) and then slowed down until it reached equilibrium at around 50 min for polypropylene modified with palm date leaf fibers and polypropylene modified with seaweed.

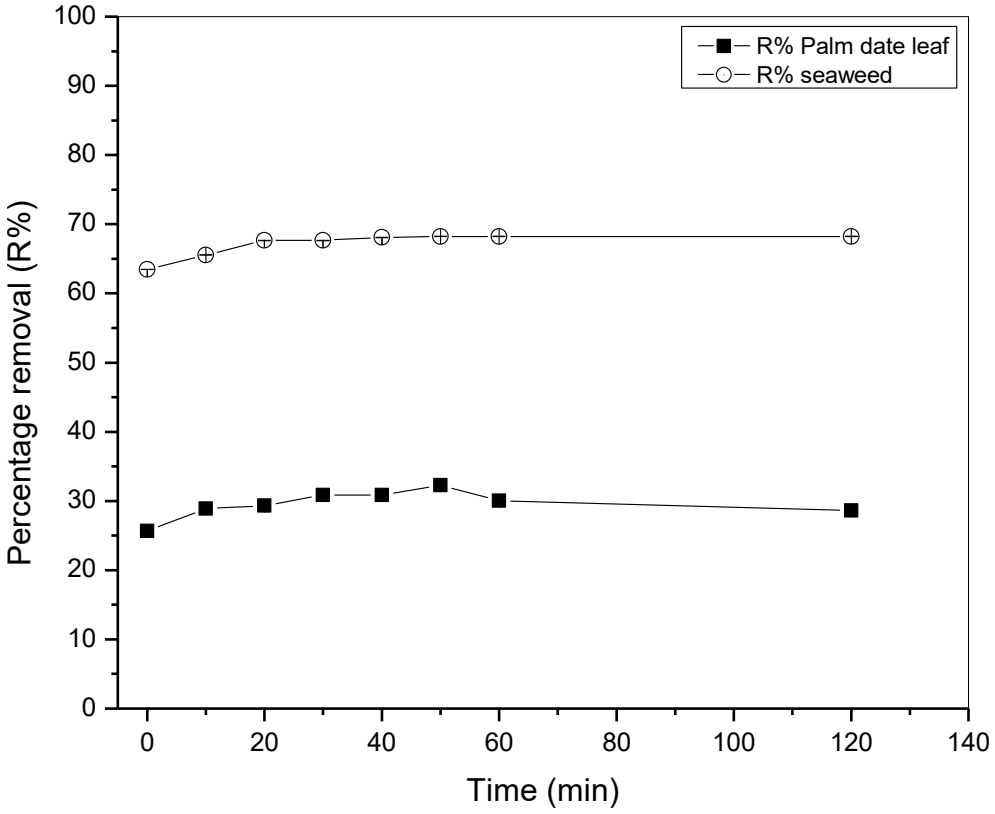

Figure 4. Effects of Contact Time on HA Removal by (○) 1% Seaweed and (■) 1% Palm Fibers

This can be attributed to the fact that in the beginning, a large number of vacant surface sites are available for humic acid. After a while, the remaining vacant surface sites are hardly occupied due to repulsive forces between the humic acid molecules in the aqueous solution and those on the adsorbent surface [26-28].

Table 5. Effects of Contact Time on HA Removal on Modified Polypropylene (a) with 1% Palm Date Leaf, (b) with 1% Seaweed

No	Time (minutes)	R% (Palm fibers)	SD	R% (Seaweed)	SD
1	0	25.67	0.017	63.45	0.012
2	10	28.90	0.011	65.56	0.016
3	20	29.32	0.011	67.66	0.023
4	30	30.87	0.018	67.66	0.021
5	40	30.87	0.019	68.08	0.012
6	50	32.27	0.011	68.23	0.014
7	60	30.03	0.015	68.23	0.025
8	120	28.62	0.012	68.23	0.019

Adsorption Isotherm Models

Two non-linear adsorption isotherm models were used to describe the humic acid adsorption onto tested modified polypropylene: Langmuir and Freundlich. The equilibrium adsorption data were processed by adsorption equations at temperatures of 20°C, 30°C, 40°C and 50°C, and the obtained adsorption parameters for humic acid adsorption onto two modified polypropylene adsorbents are presented in Table 6. The results show that the Langmuir isotherm model represents somehow well the experimental sorption data, since similar range of correlation coefficients (r^2) were obtained. Namely, the r^2 values for the Langmuir adsorption model were in the range from 0.513 to 0.986 at 20°C, and from 0.704 to 0.890 at 30°C. The calculated isotherm parameters revealed that HA adsorption onto polypropylene modifications (palm date leaf fiber and seaweed) followed the order: Langmuir. Therefore, HA adsorption onto polypropylene modified with (a) palm date leaf fiber and (b) seaweed can be characterized as monolayer adsorption.

Table 6. Langmuir Isotherm Model for HA Adsorption by Tested Modified Polypropylene

Isotherm	Parameter	Temperature (°C)							
		20		30		40		50	
		PP +1% palm fibers	PP +1% seaweed	PP +1% palm fibers	PP +1% seaweed	PP +1% palm fibers	PP +1% seaweed	PP +1% palm fibers	PP +1% seaweed
Langmuir	q_{max} (mg/g)	0.0169	33.11	0.0618	0.244	0.131	0.0179	0.0401	1.511
	KL (L/mg)	0.0056	0.0661	16.81	0.113	22.58	0.0730	23.85	0.0402
	R^2	0.9857	0.5131	0.7044	0.8902	0.5556	0.4405	0.6447	0.2608

It can be seen from Table 6 that the Langmuir maximum adsorption capacity q_{max} was found to be 33.11 mg/g for polypropylene modified with 1% seaweed at 20°C. On the other hand, the modified polypropylene with 1% palm date leaf fiber prepared in this work showed a low adsorption capacity of 0.0169 mg/g at the same conditions.

4. Conclusion

While polypropylene has not been studied for humic acid removal due to its polarity, it is possible to modify its surface with some local natural materials to extend the application of polypropylene as an adsorbent to remove charged organic compound such as humic acid from water and wastewater.

In this study, the removal of humic acid from aqueous solution using commercially available polyolefin (polypropylene) modified with natural fibers materials (palm date leaf fiber and seaweed) was investigated. The following conclusions are extracted from this study:

- Adsorption of humic acid onto modified polypropylene granules was pH dependent and a significant amount of humic acid could be adsorbed under acidic pH conditions.

- Higher adsorption capacity and removal efficiency values were obtained with polypropylene modified with seaweed at low concentration (1%). The quantity of adsorbed humic acid ranged from 0.0169 mg g^{-1} for polypropylene modified with palm date leaf fiber to 33.11 mg g^{-1} for polypropylene modified with seaweed, which means that the adsorption capacity of seaweed is far greater than that of palm date leaf fiber.

- The equilibrium data were analyzed using Langmuir and Freundlich equations. According to obtained results and values of the correlation coefficients (r^2), it could be concluded that the Langmuir model reasonably describes the humic acid adsorption onto modified polypropylene with seaweed. This means that humic acid adsorbed on polypropylene modified with 1% seaweed in form of a monolayer.

- In general, the results of the present investigation reveal that polypropylene modified with local natural fibers materials such as seaweed may be used as a low-cost, recycled polyolefin, a natural and abundant source for the removal of humic acid from aqueous solutions.

5. References

1. Liu AG, Gonzalez DR. Adsorption/desorption in a system consisting of HA, heavy metals, and clay minerals. *J. Colloid Interface Sci.*, 1999, 218, 225-232.
2. Schnitzer M, Khan SU in Humic Substances in the Environment, Marcel Dekker, New York, 1972.
3. Danae Doulia Ch, Leodopoulos K, Gimouhopoulos, Rigas F. Adsorption of humic acid on acid-activated Greek bentonite. *J. Colloid Interface Sci.*, 2009, 340, 131-141.
4. WHO in Health Criteria and Other Suporting Information, WHO, Geneva, 1996, vol 2, Guidelines for Drinking Water Quality.
5. Habuda-Stanić M, Tutić A, Kučić Grgić D, Zeko-Pivač A, Burilo A, Paixão S, Teixeira V, Pagaimo M, Pala A, Ergović Ravančić M, Šiljeg M. Adsorption of humic acid from water

using chemically modified bituminous coal-based activated carbons. *Chem. Biochem. Eng. Q.*, 2021, 35(2), 189-203.
6. Kitis M, Kaplan SS, Karakaya E, Yigit NO, Civlekoglu G. Adsorption of natural organic matter from waters by iron coated pumice. *Chemosphere*, 2007, 66, 130-138. http://dx.doi:10.1016/j.chemosphere.2006.05.002.
7. Deng S, Bai R. Adsorption and desorption on humic acid on aminated polyacrylonitrile fibers. *J. Colloid Interface Sci.*, 2004, 280, 36-43.
8. Capassoa S, Salvestrinia S, Coppolaa E, Buondonnoa A, Colellab C. *Appl. Clay Sci.*, 2005, 28, 159.
9. Bai RB, Zhang X. Polypyrrole coated granules for humic acid removal, *J. Colloid Interface Sci.*, 2001, 243, 52-60. http://dx.doi:10.1006/jcis.2001.7843
10. Wan Ngah WS, Musa A. Adsorption of humic acid onto chitin and chitosan. *J. Appl. Polym. Sci.*, 1998, 69, 2305-2310.
11. Zhang X, Bai R. Mechanisms and kinetics of humic acid adsorption onto chitosan-coated granules. *J. Colloid Interface Sci.*, 2003, 264, 30-38.
12. Chang MY, Juang RS. Adsorption of tannic acid, humic acid, and dyes from water using the composite of chitosan and activated clay. *J. Colloid Interface Sci.*, 2004, 278, 18-25. doi: 10.1016/j.jcis.2004.05.029. PMID: 15313633.
13. Yan WL, Bai R. Adsorption of lead and humic acid on chitosan hydrogel beads. *Water Res.*, 2005, 39, 688-698.
14. Abraham BT, Anirudhan TS. Adsorption equilibria of Hg (II) on clays in presence of organic materials. *J. Sci. Ind. Res*, 1999, 58, 883-892.
15. Lorenc-Grabowska E, Gryglewicz G. Adsorption of lignite-derived humic acids on coal-based mesoporous activated carbons. *J. Colloid Interface Sci.*, 2005, 284, 416-23. doi: 10.1016/j.jcis.2004.10.031. PMID: 15780277.
16. Han S, Kim S, Lim H, Choi W, Park H, Yoon J, Hyeon T. New nanoporous carbon materials with high adsorption capacity and rapid adsorption kinetics for removing humic acids. *Microporous Mesoporous Mater.*, 2003, 58, 131-135.
17. Daifullah AAM, Girgis BS, Gad HMH. A study of the factors affecting the removal of humic acid by activated carbon prepared from biomass material. *Colloids Surf., A*, 2004, 235, 1-10. https://doi.org/10.1016/j.colsurfa.2003.12.020
18. Cheng KL. Separation of humic acid with XAD resins. *Microchim. Acta*, 1977,68,389-396. https://doi.org/10.1007/BF01196224
19. Teermann IP, Jekel MR. Adsorption of humic substances onto ß-FeOOH and its chemical regeneration. *Water Sci. Technol.*, 1999, 40(9), 199-206.
20. Bousba S, Meniai AH. Removal of phenol from water by adsorption onto sewage sludge based adsorbent. *Chem. Eng. Trans.*, 2014, 235-240. doi: 10.3303/CET1440040
21. Noorimotlagh Z, Ravanbakhsh M, Valizadeh MR, Kyzas GZ, Ahmafi M, Rahbar N, Jaafarzadeh N. Optimization and genetic programming modeling of humic acid adsorption onto prepared activated carbon and modified by multi-wall carbon nanotubes. *Polyhedron*, 2020, 179, 114354.
22. Sepehr MN, Sivasankar V, Zarrabi M, Kumar MS. Surface modification of pumice enhancing its fluoride adsorption capacity: An insight into kinetic and thermodynamic studies. *Chem. Eng. J.*, 2013, 228, 192. https://doi.org/10.1016/j.cej.2013.04.08

9
23. Al-Essa K, Khalili F. Adsorption of humic acid onto Jordanian kaolinite clay: Effects of humic acid concentration, pH, and temperature. *Sci. J. Chem.*, 2018, 6(1), 1-10.
24. Anirudhan T, Ramachandran M. Surfactant modified bentonite as adsorbent for the removal of humic acid from wastewaters. *Appl. Clay Sci.*, 2007,35,276-281. doi: 10.1016/j.clay.2006.09.009
25. Vermeer AWP, van Riemsdijk WH, Koopal LK. *Langmuir*, 1998, 14, 2810-2819.
26. Lin J, Zhan Y. Adsorption of humic acid from aqueous solution onto unmodified and surfactant modified chitosan/zeolite composites. *Chem. Eng. J.*, 2012, 200-202, 202-213. doi: 10.1016/ j.cej.2012.06.039
27. Uslu H. Adsorption equilibria of formic acid by weakly basic adsorbent Amberlite IRA-67: Equilibrium, kinetics, thermodynamic. *Chem. Eng. J.*,2009,155,320-325. doi: 10.1016/j.cej.2009.06.040
28. Suresh S, Sundaramoorthy S in Green Chemical Engineering: An Introduction to Catalysis, Kinetics, and Chemical Processes, CRC Press, 2014. ISBN 978-1-4665-5885-4

The Chemist
Journal of the American Institute of Chemists

Preparation and characterization of Complexes (Cr^{+3}, V^{+3}, Ti^{+3}) with ligand 6-amino penicillanic acid (6-APA): Evaluation of the Biological Activity and molecular docking applications

Zainab Adnan Kadhum[1], Mohammed Hamid Said[2], Aseel M. Aljeboree[3*]

[1,2,3] *Department of Chemistry, College of Sciences for Girls University of Babylon, Hilla, Iraq*

[1] *(E-mail: zeena4920@gmail.com)*

[3*] *Corresponding author (E-mail: annenayad@gmail.com)*

Abstract: In this study, we have synthesized and characterized three complexes of titanium (III), vanadium (III), and chromium (III) with 6-aminopenicillin acid as a ligand. The complex prepared was a 1:2 ratio (metal:ligand). The characterized complexes were prepared by using different techniques, including Fourier transform infrared (FT-IR), atomic absorption spectroscopy, ultraviolet-visible spectrophotometry, conductivity, mass spectroscopy for complexes of titanium (III), and X-ray diffraction (XRD) patterns of three complexes. In FTIR spectra, the absorption band in ligand 6-APA observed at 1773 cm^{-1} was attributed to the υ β(C=O); this band changed in the spectra of the complexes. The results indicate that there is no crystalline structure of the three complexes. The solid state of the complex showed an octahedral geometric structure (d^2sp^3). Finally, antibacterial effectiveness was determined for the complexes against two distinct bacteria strains (*Staphylococcus aureus* and *Pseudomonas aeruginosa*). Using two concentrations (1×10^{-6} M, 1×10^{-3} M), it was discovered that the complexes had high inhibitory activity against the bacteria (*Staphylococcus aureus*, *Pseudomonas aeruginosa*). Consequently, the chemicals produced could serve as viable alternatives to commonly used medications. To investigate the molecular interactions of the 6-aminopenicillin acid, molecular docking studies were conducted to evaluate their binding affinity with Salmonella global domain 191 proteins.

Key Words: Molecular docking, β-Lactam, 6-amino penicillanic acid, antibacterial, ligand, complex

1. Introduction

As a result of the vast diversity of transition metal coordination chemistry, prospects for the design of coordination compounds, in more recent times, have been a subject of great interest [1]. The pharmacological activity of these metal compounds depends on the metal ions, ligands, and the structure of the compounds [2]. These factors are partly responsible for the ability of these coordination compounds to locate the proper target site of activity and, consequently, their pharmacological activity [3]. It is known that certain metal ions penetrate through bacteria cell walls, in the form of complexes, into the cell and inactivate certain enzymes, thus killing such bacteria [4]. Through the synthesis of organic ligands containing various donating groups, coordination chemistry is constantly expanding, and it grows in importance, particularly when these ligands possess biological significance [5]. Amino acids are a distinct class of organic compounds and serve as components of chiral compounds (except glycine), so they play a crucial role in biochemical processes within living organisms [6].

β-Lactam antibiotics have been successfully used in the treatment of infectious diseases for many years, and compounds containing a β-Lactam ring are a class of important compounds in the medicinal and pharmaceutical field. Since the discovery of β-Lactam antibiotics in 1907 by Scantest and its clinical introduction as an anti-bacterial agent in the early 1950s [7], β-lactam antibiotics have remained the most popular drugs for treating bacterial infections of many diseases [8]. Since that time, the biological applications of these compounds have attracted remarkable attention, particularly 6-aminopenicillin [9]. 6-Aminopenicillin acid is the most widely used class of antimicrobial agents [10]. This acid has been shown to exert pronounced biological effects on various bacterial strains [11].

Ibtisam M. Ali et al. (2021) utilized Schiff bases and 6-amino penicillanic acid (6-APA) to create azomethine ligands (HL1, HL2, HL3, and HL4). These ligands were complexed with four fresh ligands of copper (II), nickel (II), and iron (II) metal ions, forming octahedral complexes. The synthesized ligands and their complexes exhibited strong biological activity [14]. N. Ghufran Kareem et al. (2021) prepared a novel azo-azomethine ligand [6{2-hydroxy-4-((3-nitrophenyl)diazenyl)-1-phenyl}imine penicillanic acid] (HNDIP) through the interaction of [2-hydroxy-4-(3-nitrophenyl)diazenyl] benzaldehyde with 6-aminopenicillanic acid (6-APA). The ligand was then complexed with Cu(II), Ni(II), Co(II), Zn(II), and Fe(II) metal ions. These complexes were identified using FTIR, UV-Vis, molar conductance, magnetic sensitivity theory, and atomic absorption analysis [15]. In another study, Haneen Saadi et al. (2023) prepared three novel ligands by reacting 6-amino penicillin acid (6-APA) with aromatic amines to synthesize triazene ligands L1, L2, and L3. The complexes were then prepared by reacting these ligands with copper (II), cadmium (II), and zinc (II). The resulting bonds facilitated the formation of dimeric complexes [17].

Titanium is the ninth most abundant element in the earth's crust and the fourth most abundant element. Its elemental abundance is about five times less than iron and 100 times greater than copper [18,19]. Vanadium is a trace metal that is found naturally, both in soil and water [20]. Vanadium compounds have been prepared in many oxidation states, three of which are vana-

dium(III), (IV), and (V) [21].The catalytic activity of vanadium compounds and their role in biological systems chromium (Cr), a chemical element of Group 6 (VIb) of the periodic table, is a hard steel-gray metal that takes a high polish and is used in alloys to increase strength and corrosion resistance. Chromium was discovered in 1797 by the French chemist Nicolas-Louis Vauquelin and isolated as a metal a year later [22]. In another study, Tabark Mohammed et al. (2024) synthesized three novel ligands by reacting 6-amino penicillin acid (6-APA) with aromatic amines to produce triazene ligands L1, L2, and L3. The complexes were subsequently prepared by reacting these ligands with chromium (III), vanadium (III), and titanium (III) metals. The resulting bonds facilitated the formation of dimeric complexes with octahedral geometry. The synthesized ligands and their complexes demonstrated good biological activity [23]

Staphylococcus aureus is a gram-positive spherically-shaped bacterium, a member of the Bacillota phylum, and is a usual member of the microbiota of the body, frequently found in the upper respiratory tract and on the skin. It is often positive for catalase and nitrate reduction and is a facultative anaerobe, meaning that it can grow without oxygen [24]. Although *S. aureus* usually acts as a commensal of the human microbiota, it can also become an opportunistic pathogen, being a common cause of skin infections including abscesses, respiratory infections such as sinusitis, and food poisoning [25]. *Pseudomonas aeruginosa* is a common encapsulated, gram-negative, aerobic–facultatively anaerobic, rod-shaped bacterium that can cause disease in plants and animals, including humans [26]. It is a species of significant medical importance, known for being a multidrug-resistant pathogen. It is recognized for its widespread presence and advanced mechanisms of antibiotic resistance, which are associated with serious illnesses, including hospital-acquired infections such as ventilator-associated pneumonia and various sepsis syndromes. *P. aeruginosa* can selectively prevent certain antibiotics from penetrating its outer membrane, contributing to its high resistance to multiple antibiotics. According to the World Health Organization, *P. aeruginosa* represents one of the greatest threats to human health in terms of antibiotic resistance [27].

2. Experimental

Chemicals

6-Amino penicillanic Acid, Purity 99.98%, Chemical Formula $C_8H_{12}O_3N_2S$, Company Sigma-Aldrich, Ethanol C_2H_5OH, Purity 99.98%, Chromium (III) Chloride $CrCl_3$, Purity 97.98%, Titanium (III) Chloride $TiCl_3$, Purity 97.88%, Vanadium (III) Chloride VCl_3, Purity 97.98%, Company BDH.

Study Mole Ratio

The mole-ratio way was followed to determine the metal:ligand [M:L] ratio in

absolute ethanol as solvent. The data suggested that the metal-to-ligand ratio [M:L] was [2:1] for complexes.

Synthzesis of Metal-Ligand Complexes

The complex was prepared by the following procedure: 1:2 ratio (metal:ligand) 0.50 gm (0.002 mole) of 6-APA was mixed with 20 ml of absolute ethanol. It was completely dissolved by heating at a temperature of (30-40°C), and then 0.001 mole of the salts $TiCl_3$, VCl_3 and $CrCl_3$ (0.28 ml, 0.27 g, 0.25 g) were, respectively, dissolved successively with 5 mL of ethanol and serially added, step by step, to the 6-APA solution, with a noticeable color change upon addition. The mixture was stirred continuously for two hours after the reaction was completed. The complex solution was dried at 25°C. The precipitate colors of the complexes that were formed differed from the original materials, and pure ethanol was used for washing and recrystallization to get rid of impurities, as shown in Table 1 and Figure 1. To describe the synthesis of the three complexes by the chemical equations 1-3.

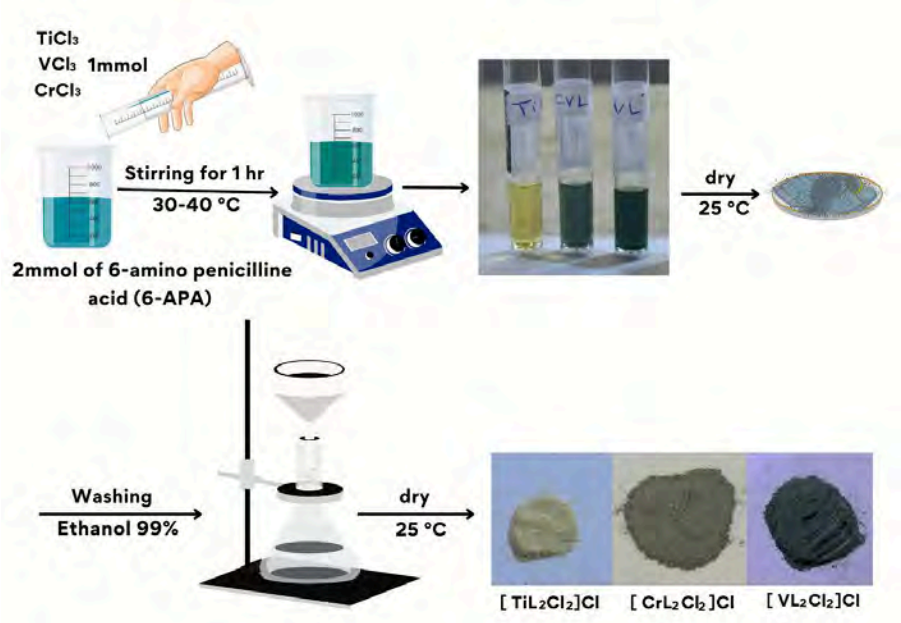

Figure 1. Preparation of Metal-Ligand Complexes

$$TiCl_3 + 2L \longrightarrow [Ti(L)_2Cl_2]\,Cl \quad (1)$$

$$VCl_3 + 2L \longrightarrow [V(L)_2Cl_2]\,Cl \quad (2)$$

$$CrCl_3 + 2L \longrightarrow [Cr(L)_2Cl_2]\,Cl \quad (3)$$

Table 1. The Physical Properties of the Ligand and Its Complexes

Symbol	Chemical Formula	M. Wt (g/mole)	Color	M. P °C
L	$C_8H_{12}O_3N_2S$	216.25	Colorless	**198**
$[TiL_2\ Cl_2]\ Cl$	$[Ti(C_8H_{12}O_3N_2S)_2Cl_2]\ Cl$	586.72	Yellow	**205**
$[VL_2\ Cl_2]\ Cl$	$[V\ (C_8H_{12}O_3N_2S\ )_2Cl_2]\ Cl$	589.79	Olive	**199**
$[CrL_2\ Cl_2]\ Cl$	$[Cr(C_8H_{12}O_3N_2S)_2Cl_2]\ Cl$	590.85	Dark green	**209**

Evaluation of Antibacterial Activity

The *in vitro* biological screening effects of the investigated compounds were tested against the bacteria (*Staphylococcus aureus*, *Pseudomonas aeruginosa*). This was carried out by the disk diffusion technique, using agar nutrient as the medium [28]. The stock solution (1×10^{-6} M,1×10^{-3} M) of new complexes was prepared by dissolving the compounds in DMSO. In a standard procedure, a well was created in an agar medium that had been inoculated with microorganisms. Using a micropipette, the test solution was added to the well, and the plate was then incubated for 24 hours at 37°C. During this incubation period, the test solution was diffused and impacted the growth of the inoculated microorganisms. Afterward, the diameter of the inhibition zone was measured.

Molecular Docking (*Salmonella typhi*) As an Against Typhoid Fever-Causing Agent

Molecular docking was utilized to estimate the binding mechanism between 6-amino-penicillin acid and the *Salmonella typhi* enzymes that are involved in bacterial membrane proteins (PDB ID: 5I5F). The crystallographic structure of the 6-aminopenicillin acid was obtained from the Material Project database in CIF format. Subsequently, the transformation of these crystallographic structures into 3D was performed by Avogadro software and saved as an a. mol2 data file. One type of protein from *Salmonella typhi* was selected (PDB ID: 5I5F) to evaluate the effect of 6-aminopenicillin acid on the protein selected for molecular docking.

3. Results and Discussion

Sample Characterization

FT-IR spectrum

The FTIR spectra provided valuable information regarding the nature of the functional group attached to the metal atom [29]. The most important infrared spectral bands that provided conclusive structural evidence for the coordination of the ligand to the central metal ions are given in Table 1. The FT-IR spectrum of the ligand shows characteristic bands at 3525 cm^{-1} due to the (N-H) functional group [30]. The (N-H) and

band in the free ligand shift for the complex; these shifts confirm the coordination of the ligand via the nitrogen of the amine group to metal ions [31]. The absorption band in ligand 6-APA observed at 1773 cm^{-1} is attributed to the υβ(C=O); this band changed in the spectra of their complexes [32]. New bands are attributed to the appearance of υ(M-N) and (M-O) vibrations in all complexes. It was established that the ligand functions as a bidentate ligand, coordinating with metal ions through the oxygen atom of the carbonyl group in β-lactam and the nitrogen atoms of the imine groups. Table 2 presents the main absorption values observed in the spectra of the prepared compounds, while Figure 2 displays the FT-IR spectrum of these compounds.

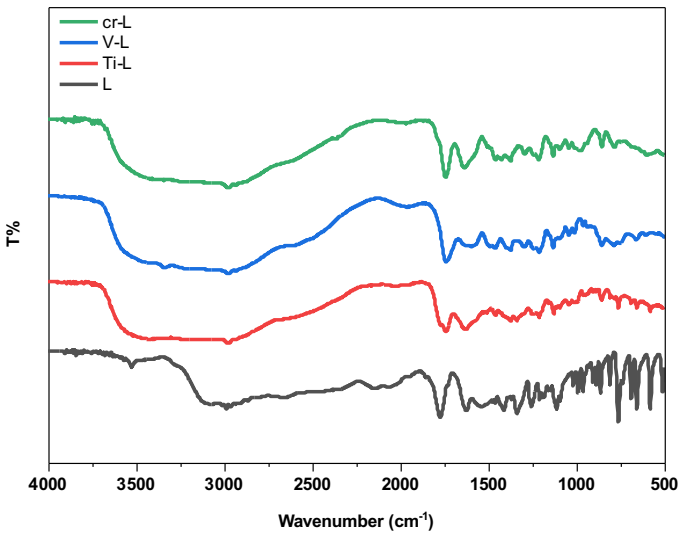

Figure 2. FT-IR Spectrum of Ligand 6-APA and Complexes

Table 2. The FT-IR Spectrum of the Ligand and Its Complexes

Compound	O-H cm^{-1}	N-H cm^{-1}	C=O (b-lactam) cm^{-1}	C-N cm^{-1}	M-O, M-N cm^{-1}
L	3400	3525	1773	1300	**-**
$[CrL_2Cl_2]Cl$	3409	3420	1742	1337	**495** **412**
$[TiCL_2Cl_2]Cl$	3380	3338	1738	1371	**463** **405**
$[VL_2Cl_2]Cl$	3437	3340	1742	1371	**495** **410**

Electronic spectra

In ethanol absolute solution, the electronic spectrums of complexes were determined to be between 200-1100 nm at room temperature [33]. The UV-visible spectra of the ligand include absorption peaks at wavelengths 280 nm n-π* transition for the non-bonding pair of electrons of a nitrogen amine group. The UV-Vis spectrum of complexes exhibits two peaks due to the (C.T) [34]. The UV-Vis data of ligands and complexes are reported in Figure 3 and Table 3.

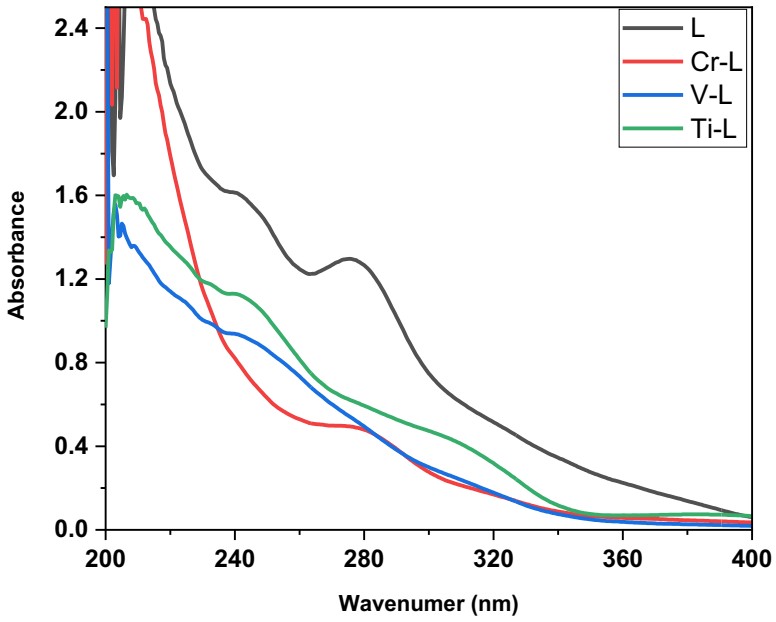

Figure 3. UV Absorption Spectrum of Ligand 6-APA and Its Complexes with Ti(III), V(III), and Cr(III)

Table 3. Electronic Spectra Data of Ligand and Metal Complexes

Complexes	Absorption band nm ʎ	Assignment
L	**280**	n-π*
$[TiCL_2Cl_2]Cl$	**230, 310**	n -π*, C.T
$[VL_2Cl_2]Cl$	**250, 315**	n-π*, C.T
$[CrL_2Cl_2]Cl$	**270, 300**	n-π*, C.T

Mass spectroscopy for the complex of Ti(III)

A peak in the complex of Ti(III) mass spectrum appeared at 585.7, attributed to the parent molecular ion. Figure 4 shows the mass spectrum for (Complex), corresponding to the proposed molecular formula (586.74).

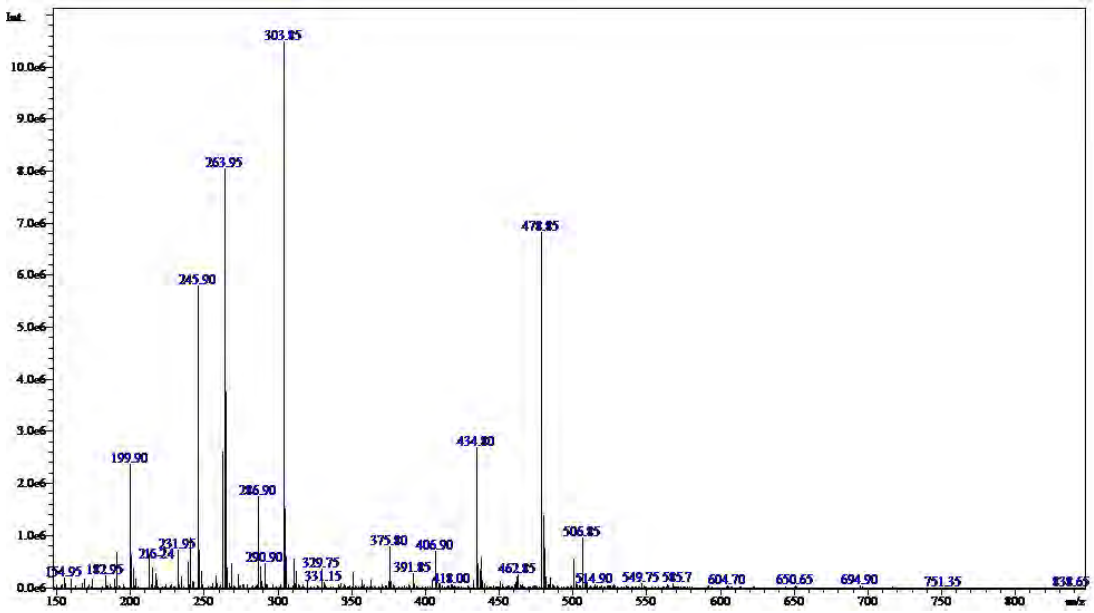

Figure 4. Shows the Mass Spectrum for the Complex of Ti(III)

The spectrum recorded other peaks corresponding to the Complex molecule's fragments. These peaks are listed in Table 4, where 549.75 for $[Ti(APA)_2Cl_2]^+$, 514.9 for $[Ti(APA)_2Cl]^+$, 478.85 for $[Ti(APA)_2]^+$, 434.8 for $(APA)_2$ and 216.24 for (APA).

Table 4. Mass Fragments for Complex of Ti(III)

M\Z	ABUNDANCE
585.7	5
549.75	8
514.9	10
478.85	68
434.3	30
303.85	98
216.24	15

XRD

The X-ray diffraction (XRD) patterns of three complexes (L-V, L-Cr, and L-Ti) were analyzed. The results indicate that none of the three complexes exhibit a crystalline structure, as illustrated in Figure 5. Peaks observed at 2θ values of 19.12° and 26.24° suggest a transition from an amorphous state.

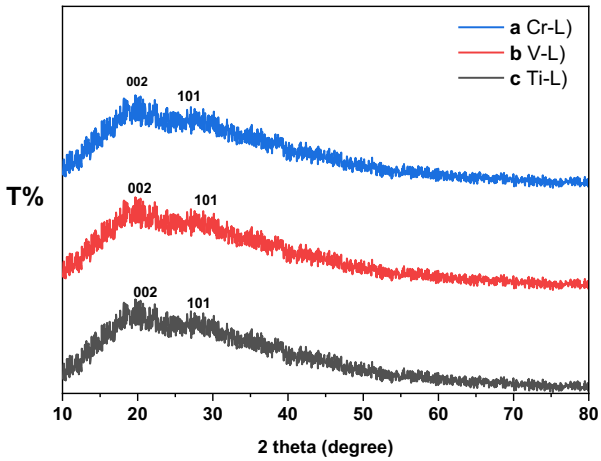

Figure 5. X-ray Diffraction (XRD) Patterns of Three Complexes a) Cr-L , b) V-L , c) Ti-L

The broad peak noted in the complexes confirms the involvement of ligand grafting with the metal. The broadness of the XRD patterns indicates the dispersion of the metal within the ligand. Additionally, the shifting of peaks to 2θ values of 22.12° and 28.12° suggests the presence of non-crystalline planes. A comparative analysis of the three complexes reveals shifts in the diffraction peaks and a reduction in crystallinity.

Magnetic Susceptibility

For coordination complexes, the Magnetic Susceptibility properties of all complexes were measured and compared with the literature, which has been reached from the vacuum of these complexes and was found to be an octahedral shape.

Atomic Absorption

The atomic absorption of the transition metal complexes was measured, and the experimental results closely matched the theoretical values. This consistency supports the accuracy of the proposed formulas and the mixing ratios between the metals and ligands in the complex structure.

Molar Conductivity

Looking at the molar conductivity results using ethanol absolute as a solvent at a concentration (0.003M), it has been found that all complexes are conductive (the behavior of these complexes was conductive) [35]. According to these results and those obtained from the IR study, an octahedral geometry around Ti (III), V(III), and Cr(III) ions can be suggested, as shown in Table 5 and Figure 6.

Table 5. Magnetic Susceptibility, Atomic Absorption, and Conductivity at the Molar Level for Coordination Complexes

Complexes	μeff(B.M)		Hybridization and Shape	Atomic absorption		Molar conductivity
	Cal.	Exp.		Cal.	Exp.	μs/cm
$[TiL_2Cl_2]Cl$	1.73	1.5	d^2sp^3 Octahedral	8.15%	9.8%	44 μs/cm
$[VL_2Cl_2]Cl$	2.8	2.3	d^2sp^3 Octahedral	8.63%	10.2%	39 μs/cm
$[CrL_2Cl_2]Cl$	3.8	3.2	d^2sp^3 Octahedral	8.8%	10.7%	43 μs/cm

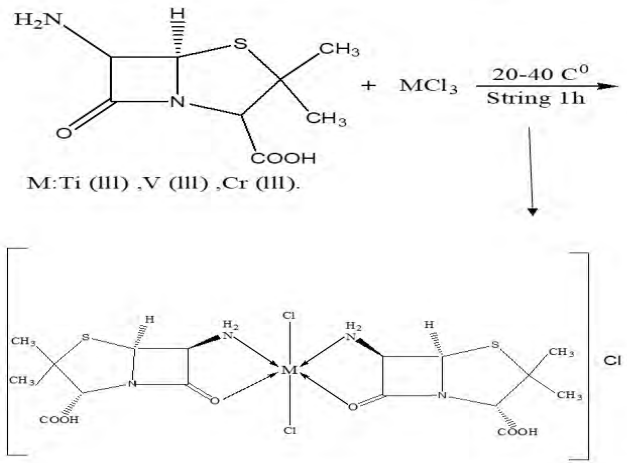

Figure 6. Suggested Prepared Ti(III), V(III), and Cr(III) Complexes with 6-APA Ligand

Biological Activity for the Complexes

Several factors influence the biological activities of ligands and metal ion complexes. These factors include the type of ligand, the specific metal ion, the electron configuration of the metal ions, the transition series, and the geometry of the complexes. The results of the biological activity tests for the prepared metal complexes are presented in Table 6. For each treatment, we measured the diameter of the inhibition zone

(including the disk diameter) in millimeters. The complexes demonstrated maximum antibacterial activity against all the organisms used in this study [36].

Table 6. Biological Activity for the Complexes

Complexes	Inhibition Zone			
	Staphylococcus aureus (+)		Pseudomonas aeruginosa (-)	
	1×10^{-6} M	1×10^{-3} M	1×10^{-6} M	**1×10^{-3} M**
TiL	-	8mm	-	**6mm**
CrL	4mm	15mm	4mm	**5mm**
VL	5mm	17mm	5mm	**14mm**

A: At a lower concentration, such as 1×10^{-6} M, the inhibition of bacterial growth was found to be minimal. This suggests that the complex has a limited ability to prevent the growth of bacteria at this concentration. However, B: when the concentration was increased to 1×10^{-3} M, a stronger inhibitory effect was observed against both Gram-positive and Gram-negative bacteria [37], as shown in Figures 7 and 8.

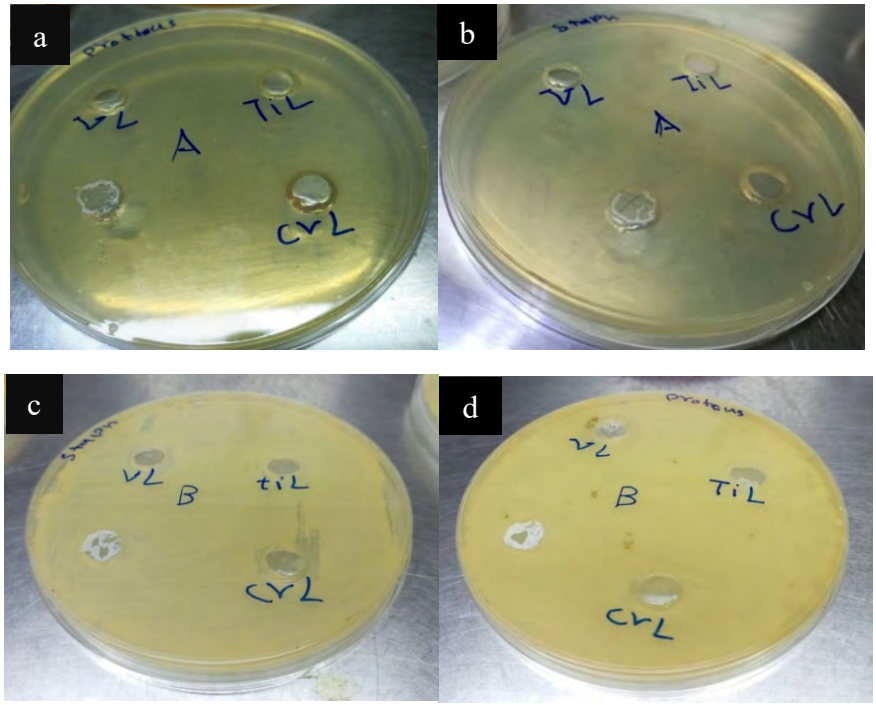

Figure 7. Effect of Metal Complexes on a) control, c) *Pseudomonas aeruginosa* at concentration 1×10^{-6} M and b) control, d) *Staphylococcus aureus* at concentration 1×10^{-6} M

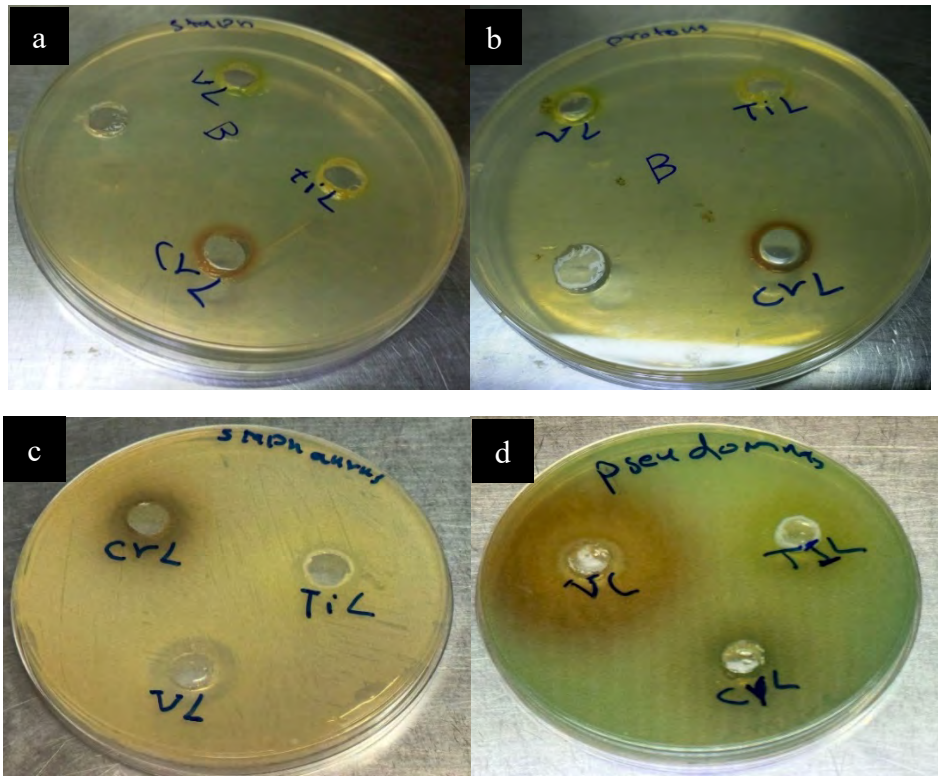

Figure 8. Shows the Effect of Metal Complexes on a) control, c) *Pseudomonas aeruginosa* at concentration 1×10^{-3} M, and b) control, d) *Staphylococcus aureus* at concentration 1×10^{-3} M

Molecular Docking

This study aims to understand how the ligand 6-aminopenicillin acid inhibits the enzymes and transcriptional regulatory receptor proteins of *Salmonella typhi* through molecular docking analyses. Initially, a model protein was created, allowing for the evaluation of its geometric conformations and stereochemical quality using various structural validation algorithms. The VADAR tool was utilized to assist in calculations for generating the Ramachandran plot. Auto Dock 4.2.6 was employed to simulate the molecular docking of all target compounds with 6-aminopenicillin acid [31]. This powerful *in silico* approach modeled atom-level interactions between the ligand (6-aminopenicillin acid) and the receptor proteins, elucidating their behavior within the binding sites. A total of 50 active sites were identified, with the largest one selected for further analysis of its docking interactions with each protein. Active sites are the pockets or grooves that serve as functional indicators of a protein's role. Typically constituting only 10%–20% of a protein's volume, these sites are crucial as they directly facilitate binding reactions. The docking results (see Figure 9) indicated that one enzyme, 5I5F from *Salmonella typhi*, exhibited energy values of -5.02 [32].

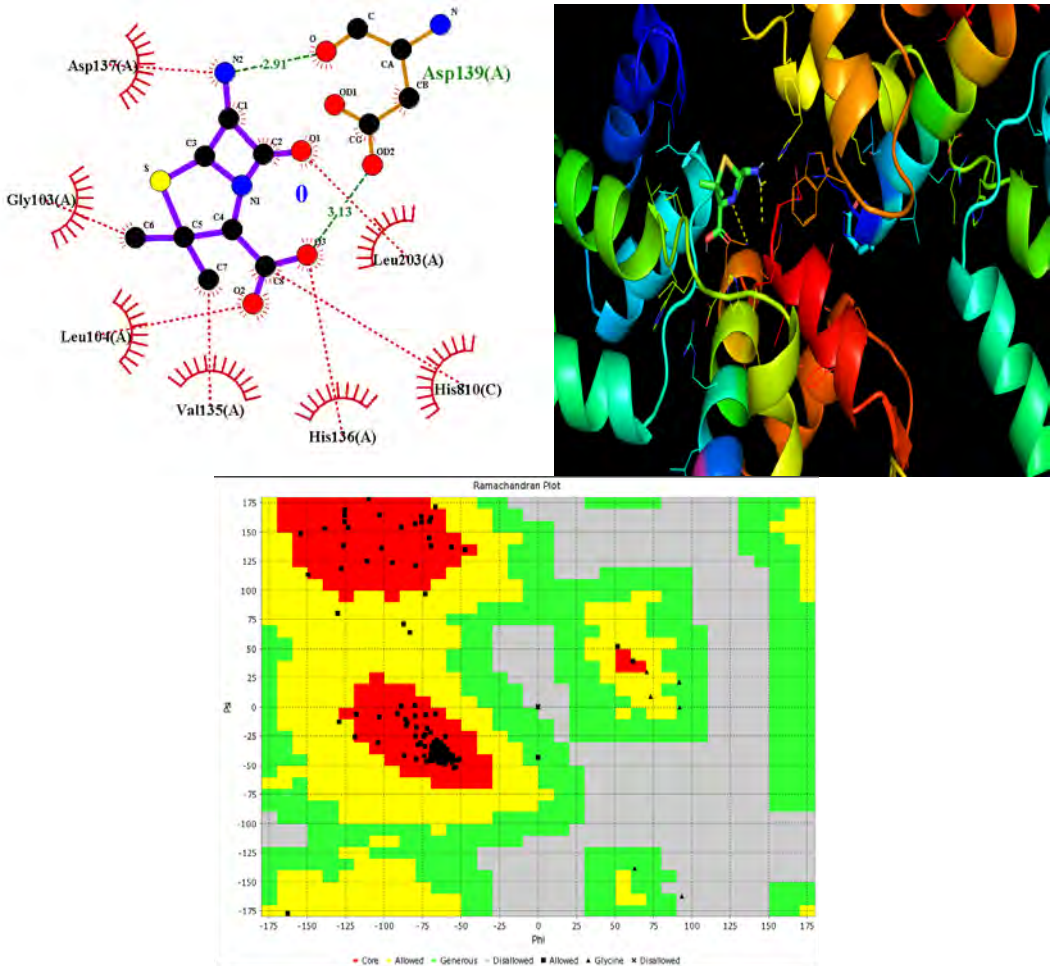

Figure 9. 2D Structure of 6-Aminopenicillin Acid and Protein Interaction (a) ID: 5I5F (A); b) e binding mode simulation of 6-aminopenicillin acid to the *S. typhi* active sites in ID: 5I5F (A); c) Ramachandran plot of 5I5F (A) with 6-aminopenicillin acid

4. Conclusion

The synthesis of titanium, vanadium, and chromium ion complexes using 6-aminopenicillin acid as a ligand resulted in the formation of novel compounds with unique chemical structures. These complexes were characterized through various analytical techniques, which confirmed their successful synthesis. Furthermore, they demonstrated significant biological activity against both *Staphylococcus aureus* (Gram-positive bacteria) and *Pseudomonas aeruginosa* (Gram-negative bacteria), indicating their potential as effective antibacterial agents. This research opens avenues for the development of new metal-based antimicrobial drugs, particularly in response to the increasing resistance of bacteria to traditional antibiotics. The findings suggest that 6-aminopenicillanic acid is a promising candidate for multiple applications, such as biofilm control, antimicrobial treatment, antioxidant activity, and environmental pollution mitigation. To explore the molecular interactions of 6-amino-

penicillanic acid, molecular docking studies were conducted to evaluate its binding with Salmonella global domain 191 proteins.

5. References

1. Aiyelabola TO, Okunade IE, Jordaan JH, Otto DP. Syntheses of coordination compounds of 2-amino-3-methylbutanoic acid their mixed ligand complexes and antibacterial activities. *Adv. Biol. Chem.*, 2020, 10(3), 67-85.
2. Grazul M, Budzisz E. Biological activity of metal ions complexes of chromones, coumarins and flavones. *Coord. Chem. Rev.*, 2009, 253(21-22), 2588-2598.
3. Muthusamy S, Natarajan R. Pharmacological activity of a few transition metal complexes: A short review. *J. Chem. Biol. Ther*., 2016, 1(2), 1-17.
4. Ma Z, Jacobsen FE, Giedroc DP. Coordination chemistry of bacterial metal transport and sensing. *Chem. Rev.*, 2009, 109(10), 4644-4681.
5. Beiraghi TR, Hakimi M, Dadmehr M. Synthesis and identification of chromium (III) complex with 2-amino-3-(1-hydrogen-indol-3-yl) propanoic acid ligand. *Chem. Methodol.*, 2024, 8(4), 234-240.
6. Liu X, Dong S, Lin L, Feng X. Chiral amino acids-derived catalysts and ligands. *Chin. J. Chem.*, 2018, 36(9), 791-797.
7. Ali BQ, Said MH, Jasim RH. Synthesis, characterization and antibacterial study of novel Schiff base ligand with some metal ion Co (II), Ni (II), Cu (II) and Zn (II). *Int. J. Chem. Sci*., 2016, 14(4).
8. Lima LM, da Silva BNM, Barbosa G, Barreiro EJ. β-lactam antibiotics: An overview from a medicinal chemistry perspective. *Eur. J. Med. Chem.*, 2020, 208, 112829.
9. Ahsaie FG, Pazuki G. Separation of phenyl acetic acid and 6-amino-penicillanic acid applying aqueous two-phase systems based on co-polymers and salts. *Sci. Rep.*, 2021, 11(1), 3489.
10. Favre A, Grugier J, Brans A, Joris B, Marchand-Brynaert J. 6-Aminopenicillanic acid (6-APA) derivatives equipped with anchoring arms. *Tetrahedron*, 2012, 68(52), 10818-10826.
11. Thakar DM, Ph.D. Studies of penicillin acylase immobilization using membranes for the production of 6-aminopenicillanic acid (6-APA). Thesis, University of Pune, 2009.
12. Alabdali AJ, Sabah YH, Mohsien RA. Synthesis, characterization and biological evaluation of penicillin derivatives complexes with some transition metal ions. *Int. J. Curr. Microbiol. App. Sci*., 2016, 5(12), 321-332.
13. Jasim RH, Said M, Ali BQ. Preparation, characterization and biological evaluation of β-lactam derived from 6-amino penicillinic acid and salicyldehyde. *Pharm. Anal. Chem.*, 2017, 2(3), 1-7.
14. Ali I, Said MH, Al-Wazn W. Preparation, characterization, and study of complexes containing beta-lactam group with some transitional elements and their biological activity. *Egypt. J. Chem.*, 2021, 64(10), 5703-5712.
15. Kareem NG, Said MH. Syntheses, and characterization of complexes containing beta-lactam group with some transitional elements and study their bio-

logical activity. *NeuroQuantology*, 2021, 19(11), 72-84.
16. AI-Janahi ZF, Said MH. Preparation and characterization using a new Schiff base ligand derived from benzoyl isothiocyanate with their complexes and study of their biological activity. *Al-Mustaqbal J. Pharm. Med. Sci.*, 2024, 2(3), 3.
17. Hussein HS, Said MH, Shantaf AH. Preparation and characterization of cadmium (ll), zinc (ll) and copper (ll) ion complexes using new triazene ligands and study of their biological activity. *Caspian J. Environ. Sci.*, 2024, 22(3), 663-672.
18. Wadood A, "Titanium and Titanium Alloys," Higher Education Commission, Islamabad, Pakistan, 2018, pp. 1-144.
19. Tebaldo V, Gautier di Confiengo G, Duraccio D, Faga MG. Sustainable recovery of titanium alloy: From waste to feedstock for additive manufacturing. *Sustainability*, 2023, 16(1), 330.
20. Huang JH, Huang F, Evans L, Glasauer S. Vanadium: Global (bio) geochemistry," *Chem. Geol.*, 2015, 417, 68-89.
21. Pessoa JC, Etcheverry S, Gambino D. Vanadium compounds in medicine. *Coord. Chem. Rev.*, 2015, 301, 24-48.
22. Aydia M, Ph.D. Radiochemical Study on the Separation of Chromium-51 from the Irradiated Target by Using Commercial and/or Synthesized Ion Exchanger. Thesis, Ain Shams University, 2012.
23. Khamir TM, Said MH. Synthesis, characterization and biological activity of novel triazene ligand and its nanocomplexes with some transition metal ion based on 2-amino-4-nitrobenzoic acid. *J. Nanostruct.*, 2024.
24. Anthony O, Henry EC. Photochemical and Antimicrobial Activity of Turmeric Rhizome Extract Against Some Selected Microorganisms. *Int. J. Adv. Multidiscip. Res. Stud.,* 2023, 3(2), 1158-1161.
25. Youssef YM, Azab ME, Elsayed GA, El-Sayed AA, Hassaballah AI, El-Safty MM, Soliman RA, El-Helw EAE. Synthesis and antioxidant, antimicrobial, and antiviral activity of some pyrazole-based heterocycles using a 2 (3 H)-furanone derivative. *J. Iran. Chem. Soc.*, 2023, 20(9), 2203-2216.
26. Strateva T, Yordanov D. *Pseudomonas aeruginosa* – A phenomenon of bacterial resistance. *J. Med. Microbiol.*, 2009, 58(9), 1133-1148.
27. Wu W, Jin Y, Bai F, Jin S. in Molecular Medical Microbiology, Elsevier, 2015, "Pseudomonas aeruginosa," pp. 753-767.
28. Álvarez-Fernández E, Cancelo A, Díaz-Vega C, Capita R, Alonso-Calleja C. Antimicrobial resistance in *E. coli* isolates from conventionally and organically reared poultry: A comparison of agar disc diffusion and Sensi Test Gram-negative methods. *Food Control*, 2013, 30(1), 227-234.
29. Ţucureanu V, Matei A, Avram AM. FTIR spectroscopy for carbon family study. *Crit. Rev. Anal. Chem.*, 2016, 46(6), 502-520.
30. Jia Y, Xiao B, Thomas K. Adsorption of metal ions on nitrogen surface functional groups in activated carbons. *Langmuir*, 2002, 18(2), 470-478.
31. Tiwari A, Mishra A, Mishra S, Mamba B, Maji B, Bhattacharya S. Synthesis and DNA binding studies of Ni (II), Co (II), Cu (II) and Zn (II) metal complexes of N1, N5-bis [pyridine-2-methylene]-thiocarbohydrazone Schiff-base ligand. *Spectrochim. Acta, Part A*, 2011, 79(5), 1050-1056.

32. Hussen NH, Hamid SJ, Sabir MN, Hasan AH, Mohammed SJ, Shali AA. Novel penicillin derivatives against selected multiple-drug resistant bacterial strains: Design, synthesis, structural analysis, in silico and *in vitro* studies. *Curr. Org. Synth.*, 2024, 21(5), 684-703.
33. Perkampus H-H. UV-VIS Spectroscopy and its Applications, Springer Science & Business Media, 2013.
34. Issa RM, Khedr AM, Rizk HF. UV–vis, IR and 1H NMR spectroscopic studies of some Schiff bases derivatives of 4-aminoantipyrine. *Spectrochim. Acta, Part A*, 2005, 62(1-3), 621-629.
35. Delol H. Modified method for preparation of aurintricarboxylic acid and prepare of its chromium (III) complex: Study its interaction with some human serum proteins. *J. Kerbala Univ.*, 2007, 3(2), 65-76.
36. Aljeboree AM, Albdairi HK, Jawad MA, Hamood SA, Abdulrazzak, FH., Alkaim AF. Synthesis, characterization, and biological activity of a novel SA-g-p(AAc-co-AM)/ZnO NP hydrogel composite †. *Eng. Proc.*, 2023, 59(1), Art no. 192. doi: 10.3390/engproc2023059192.
37. Aljeboree AM, Hussein UA-R, Jawad MA, Abdulridui HA, Shaheen BS, Ibraheam IA, Alkaim AF. Role of *Ricinus communis* plants: As highly adsorbent surface for removal of dyes from aqueous solutions and its role of biological activity. *Asian J. Water, Environ. Pollut.*, 2024, 21(6), 69-76. doi: 10.3233/AJW240074.

The Chemist
Journal of the American Institute of Chemists

Antimicrobial and Antioxidant Properties of Extracts from the Leaves of Syrian *Juniperus excelsa* M.Bieb.

Manar Abdullah Abou Hassan[1], Mariam Abdul Razak Drakli[2]

[1,2] *Department of Chemistry, Faculty of Medicine, Syrian Private University, Syria*

[2] *(Email: Mariamdarakli44@gmail.com)*
[1]*Corresponding author (E-mail: manarhassan330@gmail.com)*

Abstract: This study explores the chemical and biological properties of dried leaves of Syrian *Juniperus excelsa* M.Bieb., highlighting their potential applications in the pharmaceutical and functional food industries. Two types of extracts—aqueous and 70% ethanol—were prepared. Proximate analysis revealed moisture, protein, fat, carbohydrate, crude fiber, and ash contents of 7.94%, 5.7%, 10.6%, 22.2%, 49.1%, and 4.5%, respectively. Mineral analysis (ppm) showed concentrations of calcium (2500), potassium (830), sodium (125), and iron (0.1). Total phenolic content was measured using the Folin–Ciocalteu method, and antioxidant activity was evaluated via the DPPH radical scavenging assay. The ethanol extract exhibited higher phenolic content and antioxidant activity than the aqueous extract. Antimicrobial activity, assessed using the disc diffusion method, demonstrated effectiveness against Gram-negative bacteria (*E. coli*, *P. aeruginosa*), Gram-positive bacteria (*S. aureus*, *B. subtilis*), and yeast (*Candida albicans*). These findings suggest that *J. excelsa* leaf extracts hold promising therapeutic potential for developing treatments for various diseases.

Key Words: *Juniperus excelsa* M.Bieb., antioxidant activity, antimicrobial, extract, total phenol content, DPPH

1. Introduction

Over the past two centuries, extensive investigations into the chemical and biological activities of plants have catalyzed advancements in synthetic organic chemistry, giving rise to the field of medicinal chemistry. This evolution has paved the way for the development of more potent therapeutic agents [1]. As observed in recent

years, multiple drug resistance in human pathogenic microorganisms have developed due to indiscriminate use of commercial antimicrobial drugs commonly used in the treatment of infectious diseases. This situation forced scientists to search for new antimicrobial substances from various sources, like medicinal plants, which are good sources of novel antimicrobial chemotherapeutic agents [2]. Medicinal plants have been used for centuries as remedies for human diseases because of their biochemical constituents, which have therapeutic significance [3]; also because of their ability to biosynthesize a diverse array of chemical compounds with profound physiological significance. They are harnessed for human use across various domains including perfumery, culinary arts, cosmetics, and pharmaceuticals. These plants can synthesize a large variety of chemical substances that are of physiological importance [1,4].

This paper is concerned with studying the plant *Juniperus*, classified as a conifer plant within the Cupressaceae family. It is estimated that 70 species of *Juniperus* are distributed throughout the world, primarily North America, Europe, and Asia [5,6]. *Juniperus* represents the third largest genus among global conifers, characterized by its monophyletic nature. Remarkably long-lived, some *Juniperus* specimens have demonstrated a lifespan of up to 2000 years and have shown a variety of sizes from small shrubs to towering forest giants [6,7]. Notably, *Juniperus* exhibits a unique resilience to extreme temperature fluctuations, enabling its growth in arid environments that prove inhospitable to many other flora [8]. In addition, the wood derived from *Juniperus* is distinguished by its aromatic qualities and its resistance to decay. This unique combination of attributes has made it highly sought after for a variety of applications, including the manufacture of furniture, panels and barriers. Conifers such as *Juniperus* are an excellent source of firewood, and tend to produce minimal ash and smoke when burned [6]. Moreover, the genus *Juniperus* has earned recognition for its prominent role in traditional medicine [9].

J. excelsa: this medicinal plant has been historically employed in the treatment of various conditions including dysmenorrheal, cough, bronchitis and colds, jaundice and tuberculosis, and to induce menses and expel fetuses [2,5], abdominal spasm, asthma, diarrhea, fever, headache, gonorrhea, and leucorrhoea. It is also considered useful as an antihypertensive, appetizer, diuretic, carminative, and stimulant [10]. *Juniperus excelsa* M.Bieb. is a large shrub or tree, spread mainly throughout the eastern Mediterranean, starting from north-eastern Greece and southern Bulgaria, across Turkey, to the Middle East countries (Syria and Lebanon) and the Caucasus Mountains. Its presence is also noted in Iran, Pakistan and Oman [11]. *J. excelsa* is rich in phenolic compounds and demonstrates various biological effects, such as antimicrobial, antifungal, antioxidant, anti-inflammatory, anticancer, antiviral, and cytotoxic activities. Phytochemical analyses have unveiled the presence of sterols, flavonoids, lignans, polysaccharides, some aromatic compounds, and fatty acids across various anatomical components of the *Juniperus* genus [12].

Since antioxidants were discussed, it must be mentioned that it has recently been observed that reliance on synthetic antioxidants in food production leads to a deterioration of the taste and biologically active qualities of food and may lead to conditions suitable for the occurrence of food allergies. This has spurred researchers to seek alternative sources of reactive components capable of counteracting oxidative

processes, which have negative effects on cellular metabolism. Knowledge of the antioxidant properties of many plant species allows their usage as a means of preserving food quality by slowing down or preventing lipid oxidation processes. The pursuit of novel and safe antioxidants from natural sources has garnered substantial interest in their application for natural antioxidants, functional foods, and nutraceuticals [12-14].

Based on the above, the goals of the present study were to assess the antimicrobial potential of aqueous and ethanolic extracts *Juniperus excelsa* M.Bieb. against Gram-positive bacteria, Gram-negative bacteria, and yeast; to evaluate the antioxidant activity of plant extracts; and to determine the total phenolics content of plant extracts and perform the phytochemical screening of dried leaves of the plant studied.

2. Materials and Methods

The study was conducted in the laboratories of Syrian Private University, Atomic Energy Commission of Syria, and the National Commission for Biotechnology in Damascus.

Plant sample

The leaves of *Juniperus excelsa* M.Bieb. were collected in July 2023 from the al-Khusha in the mountains of al-Qalamoun, Ras al-Ma'arra village, Yabroud area, Damascus countryside, Syria. The fresh leaves were separated from the bark and then washed with water thoroughly and dried for 24 hours at room temperature in shadow. The leaves were stored at -20°C until use, then crushed immediately before using into small pieces using an electric grinder, where the particle dimensions were less or equal to 0.2 mm. Figure 1 shows *Juniperus excelsa* M.Bieb. trees with the taxonomy of the plant [15].

Figure 1. *Juniperus excelsa* M.Bieb. Trees in the Qalamoun Mountains in Syria with Their Taxonomy [15]

Proximate Composition Analysis

The proximate analysis of dried leaves of *Juniperus excelsa* M.Bieb. was carried out for moisture content, protein, fat, carbohydrate, crude fiber and ash content as described by the Association of Official Analytical Chemists (AOAC) (2000). All chemical analysis results were calculated relative to the oven dry sample weight [16].

Mineral Composition Analysis

Dried leaves of *Juniperus excelsa* M.Bieb. were mineralized at 450°C. The residue was first dissolved in concentrated HCl and evaporated to dryness, then the remainder was dissolved in 0.1 mol/L HNO_3 solution. Mineral contents were determined on an atomic absorption spectrophotometer (AAS) Perkin Elmer/ HGA 500 (Norwalk, USA), under the following instrumental parameters for the flame AAS: sodium (Na) 589.6 nm; potassium (K), 766.5 nm; calcium (Ca), 317.0 nm; and iron (Fe), 238.3 nm. Identification of metals was carried out by comparison to a standard solution of metal salts, and metal concentrations were calculated from a calibration curve, built by using a standard ppm solution [17].

Preparation of Plant Extracts

50 g of dried *Juniperus excelsa* M.Bieb. leaf powder was extracted with 200 mL of water or ethanol with continuous stirring by a magnetic stirrer at 25°C and 6 rpm for 6 hours; after which, each mixture was soaked for 24 hours at 4°C and then was filtered using Whitman No. 1 filter paper. Each supernatant was evaporated using a vacuum rotary evaporator to concentrate the extracts.

The volume of the resulting aqueous extract was 3.5 mL, while the volume of the ethanolic extract was 3 mL.

Total content of phenolic compounds

Phenolics are secondary metabolites that are omnipresent in plants. They are a large group of bioactive compounds comprising about 8000 compounds [18]. The two major classes of phenolic compounds include flavonoids and phenolic acids [19]. The total phenolics of *Juniperus excelsa* M.Bieb. extracts were determined by the Folin–Ciocalteu method with some modifications commensurate with laboratory work. 0.0025 mL of each extract was mixed with 0.5 mL of Folin–Ciocalteu reagent in complete darkness for 10 min, and then 1 mL of sodium carbonate solution 15% was added. The extracts were kept in the dark for 30 min and the absorbance was measured at 740 nm. A calibration curve with gallic acid (1 mg/mL) was established, where (0.01, 0.03, 0.06, 0.125, 0.25, 0.5, 1) mg/mL of gallic acid solution were used instead of the studied sample, and the total phenolic content was expressed in milligrams of gallic acid per mL of Plant extract. Figure 2 shows the standard curve of gallic acid [20,21].

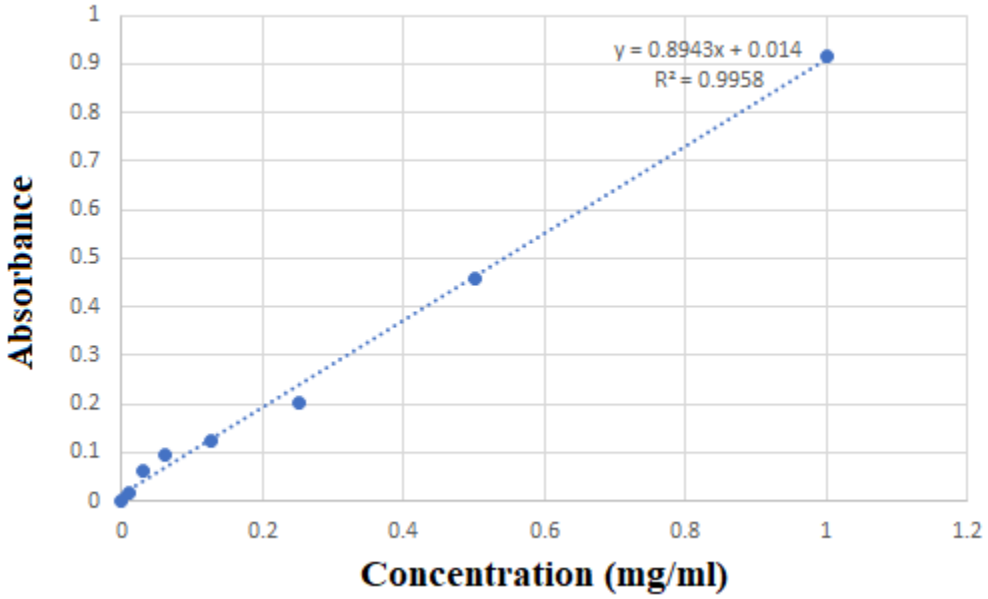

Figure 2. Standard Curve of Gallic Acid

Determination of DPPH-Free Radical Scavenging Ability

The antioxidant activity of extract samples was assessed on the basis of radical scavenging effect of the stable DPPH (1,1-diphenyl-2-picrylhydrazyl) free radical. The DPPH• test is based on the ability of the stable 2,2-diphenyl-1-picrylhydrazyl free radical to react with hydrogen donors. The DPPH• radical displays an intense UV-VIS absorption spectrum. In this test, a solution of radical is decolourized after reduction with an antioxidant (AH) or a radical (R•) in accordance with the following scheme:

$$DPPH\bullet + AH \rightarrow DPPH\text{-}H + A\bullet$$
$$DPPH\bullet + R\bullet \rightarrow DPPH\text{-}R$$

This method is very simple and quick for manual analysis [20]. In a test tube, 1 mL of ethanolic DPPH solution (4 mg/100 mL absolute ethanol) was combined with 50 µL of each extract. After that, the tubes were kept in darkness for 30 min. The absorbance was therefore determined at 517 nm. The scavenging rate of a DPPH-free radical was calculated according to the following formula:

$$\text{Inhibition of free radical DPPH in percent (I\%)} = 100 \times (A_{Control} - A_{Sample}) / A_{Control}$$

where, $A_{Control}$ is the absorbance of the control reaction (containing all reagents except the test compound), and A_{Sample} is the absorbance of the test compound [23].

Antimicrobial activity

Screening of the antimicrobials was investigated on Gram-negative bacteria (*E. coli*, *K. pneumoniae*, *Citro. freundii*, *P. aeruginosa*), Gram-positive bacteria (*St. aureus*, *B. subtilis*, *St. epidermidis*) and yeast (*C. albicans*). The disc diffusion method was employed to determine the antimicrobial activities of the studied extracts. The parent cultures of each microorganism were set up to 24 hours before the assays to reach the stationary phase of growth. Briefly, a suspension of the tested microorganism that contained 10^6 colony-forming unit/mL was prepared and then spread on a solid medium (nutrient agar) by a swab. Paper disks (diameter 6 mm) were impregnated with different amounts of each extract (50 and 100 µL), placed on inoculated plates and left for 15 minutes at room temperature. The plates were incubated at 37°C for 24 hours for bacteria and at 27°C for 48 hours for the yeasts. The diameters of inhibition zones were measured in millimeters [5]. The sensitivity to the extracts was determined by the diameter of the inhibition zones: not sensitive for diameters <8 mm; sensitive for diameters 9–14 mm; very sensitive for diameters 15–19 mm: and extremely sensitive for diameters >20 mm [10].

3. Statistical Analysis

Statistical analysis was carried out using the STATISTICA 12.0 version (StatSoft, Inc., USA). Each experiment was conducted 3 times; all data were presented as mean values with their standard deviations (mean±SD). The analysis of variance (ANOVA) was performed, with a confidence interval of 95% ($P < 0.05$). Means were compared by Duncan multiple range test.

4. Results and Discussion

Knowledge of proximate, micronutrients and phytochemical composition is fundamental to the understanding of modes and mechanisms of action of medicinal plants in general and play a crucial role in assessing its nutritional value and significance (<0.05) [24].

The main chemical, nutritional and mineral composition of *J. excelsa* M.Bieb. dried leaves was determined, and the data pertaining to various chemical and mineral composition are illustrated in Table 1 and Table 2.

Table 1. Proximate Composition of *J. excelsa* M.Bieb Dried Leaves

Sample	% protein	% fat	% fibre	% ash	% carbohydrate	% moisture
J. excelsa M.Bieb. leaves	5.7±0.22	10.6±0.05	49.1±0.23	4.5±0.09	22.2 ± 0.02	7.94±0.19

Values are mean±SD; n = 3

Table 2. Mineral Constituents of *J. excelsa* M.Bieb. Dried Leaves

Sample (ppm)	Ca	Na	K	Fe
J. excelsa M.Bieb. leaves	2500± 4.23	830± 0.64	125± 1.02	0.1± 0.21

Values are mean±SD; n = 3.

Results given in Table 1 indicated that the plant is a rich source of basic food nutrients such as proteins, fats, fibre, and carbohydrates. The values of these substances amounted to 5.7%, 10.6 %, 49.1%, and 22.2%, respectively, while the moisture and ash contents were 7.94% and 10.6%, respectively. All these substances have an important place in human nutrition. Dietary fibres are constituents of many fruits and vegetables. Clinical studies suggest fiber can exert a wide range of benefits in areas such as bowel function, gut health, immunity, blood glucose control, and serum lipid levels [25]. On the other hand, high fibre content for the leaves of the plant is usually a major drawback in human nutrition as it can cause intestinal irritation and it is low in nutrient availability as humans cannot digest them easily [26]. Additionally, dietary fibre delays gastric emptying or increases viscosity of GIT content thereby suppressing digestion and carbohydrate absorption. This mechanism is selectively advantageous in that the threat or risk of hypoglycaemia, hyperinsulinemia and undue weight-gain is absolved [24].

Carbohydrates are useful as they supply energy to cells such as brain, muscles and blood. They contribute to fat metabolism and spare proteins as an energy source and act as a mild laxative for human beings. They generally add to the bulk of the diet [26,27]. The protein content of the leaves shows the plant is a good protein supplement for animal feed [26], however, the content is not as high as the 12.5% reported for *Nauclea latifolia* leaves, 20.42% for *Moringa* leaves and 14.73% for *Ageratum conyzoides* leaves [25-27]. The fat content (10.6% for the leaves of *J. excelsa* M.Bieb.) is low and compares with the results for Agbafor *et al.* (2015) and Eze *et al.* (2014), who concluded that the leaves of *Ageratum conyzoides* are poor sources of lipids [25,26]. Our results agree with Dike *et al*. (2016) [28]. The total moisture content is considered low, and this low moisture content of the leaves indicates that the plant materials can be stored over a long period with lesser susceptibility to microbial attack [28]. The total ash content of the plant materials is low (4.5%) indicating low total mineral elements in the plant materials [29].

Minerals have an important place in human nutrition. The importance of these minerals, also known as trace elements, has been well understood in recent years, since when missed, causes diseases and major disorders in the human body [30]. The mineral composition of *J. excelsa* M.Bieb. dried leaves was analyzed and the results revealed that iron was 0.1, calcium 2500, potassium 830, and sodium 125 ppm. These minerals play significant roles in several biological processes. Bone growth and turnover are influenced and regulated by the metabolism of Ca and other minerals, in addition to its role in muscle contraction and blood clotting. Iron is an essential trace element for normal functioning of the central nervous system. It is known to be a component of some metalloenzymes, myo-globin and hemoglobin, which is needed in the transport of oxygen and carbon dioxide during respiration or cellular metabolism. This hemoglobin (containing iron) also serves as a buffer to regulate changes in blood. Potassium and sodium, which are presented in the intracellular and extracellular fluid, help to maintain electrolyte balance and membrane fluidity pH [29]. Also, potassium is involved in inducement of calmness [25]. The amount of Ca was close to its content in *Momordica charantia* leaves while the amount of Na, K, and Fe was lower [29]. The balanced nutritional composition of *J. excelsa* M.Bieb. makes it a potential source of nutrients that can be included in a number of foods.

Total Content of Phenolic Compounds

The amounts of the total polyphenols in the aqueous and ethanol extracts of *J. excelsa* M.Bieb. leaves are shown in Table 3. The total phenolic content found in water and ethanol extracts was 0.631 and 1.27 mg/mL, respectively. The values were reported as mg of gallic acid equivalent (GAE) per 1 mL of extract with reference to gallic acid standard curve.

Table 3. Total Phenolic Content of *J. excelsa* M.Bieb. Leaves Extracts

extract	aqueous	ethanol
Total phenolic content (mg/ml)	0.631^{a}±0.15	1.27^{b}±0.44

Values are mean±SD; n = 3.
Values with different superscripts are significantly different (P<0.05).

Results given in Table 3 indicate that the ethanol extract shows high total phenol content. The result is similar to those reported by Rebaya *et al.* (2014) and Do *et al.* (2014) [13, 31]. Phenolics are the most predominant phytochemicals present in nature, and to date, about 10,000 different structures are currently described [32]. Phenolic components represent the largest class of secondary metabolites which are known as exceptional antioxidants, and their antioxidant activity is based on their redox potential. They include phenolic acids, flavonoids, tannins, stilbenes, curcuminoids, coumarins, lignans, quinones and others. Various bioactivities of phenolic compounds are responsible for their biological properties, like antimicrobial, anticarcinogenic, anti-inflammatory and therapeutic effects [33], and also play a major role in modifying gene expression [18]. Phenolic substances have important contributions to human health. These compounds have been reported to play an effective role in preventing cancer and cardiovascular diseases by preventing free radical formation in the body [30].

The presence of phenolic compounds enables the plants to act as reducing agents, hydrogen donators and singlet oxygen quenchers. During cell metabolism, all living cells generate free radicals as part of normal cellular functions that are highly reactive may cause oxidative stress, leading to cellular damage and subsequently various diseases, such as atherosclerosis, diabetes mellitus, arthritis, ischemic heart disease, gastritis, immunosuppression, neurodegenerative diseases, ageing, and cancer [19].

DPPH Radical Scavenging Activity

Determining antioxidant activity as radical scavenging activities are critically important due to the detrimental role of free radicals in foods and biological systems. Plants rich in secondary metabolites such as phenolics and flavonoids exhibit antioxidant activity attributable to their oxidative properties and chemical compositions. The DPPH assay is one of the indispensable tests when assessing the antioxidant activity of extracts and is widely used to test the free radical-scavenging activity of several natural products. The results of the antioxidants for aqueous and alcoholic extracts of *J. excelsa* were demonstrated in Table 4.

Table 4. DPPH Free Radical Scavenging Activity of *J. excelsa* M.Bieb. Leaves Extracts

extract	aqueous	ethanol
DPPH test	27.63^{a}±0.23	65.13^{b}±0.11

Values are mean±SD; n = 3.
Values with different superscripts are significantly different (P<0.05).

DPPH reacted, as a stable free radical, interacting with any molecule capable of donating an electron or hydrogen to it, which lead to DPPH bleaching (color change from violet to yellow). The absorbance was measured at 517 nm [34]. The data presented in this study supports the prevailing mechanism which designates DPPH• as a primary, if not exclusive, hydrogen acceptor [35]. The enhanced DPPH scavenging activity observed may be attributed to higher phenolic contents [34]. The results also indicate that the ethanolic extract exhibits greater activity compared to the aqueous extract. That is due to the phenolic compounds' major contribution to antioxidant properties of the used plant. This may be explained by the fact that different types of phenolic compounds possess different antioxidant capacities which is related to their chemical structure. The results of this study are in agreement with the results of many studies that reported that the plant extracts with high total phenolic content showed high radical scavenging activity, formed from very complex mixtures of different molecules, and the proton donating hydroxyl groups with a particular position in the structure of molecules might be controlling the radical scavenging properties of these extracts [36]. The results could be explained by the sensitivity of the Folin-Ciocalteu reagent towards a wide range of phenolic compounds, whereas DPPH free radicals display varying sensitivity to different antioxidants. The Folin-Ciocalteu reagent reacts with both free and bound phenolics present in the extracts and other samples, whereas the DPPH assay exclusively quantifies free antioxidants and phenolics [14]. The existing literature provides evidence of a significant correlation between total phenolic content and antioxidant activity, suggesting that phenolic compounds make a substantial contribution to the antioxidant properties of the respective plant materials [36].

Antimicrobial Activity Assay

In the present study, the antimicrobial compounds from the leaves of *J. excelsa* M.Bieb. were extracted against wide range of microorganisms on the basis of disc-diffusion assay using a suspension containing contained 10^6 colony-forming unit/mL microorganism spread on nutrient agar. The discs (6 mm in diameter) were impregnated with 50 and 100 µL separately of each extract and placed on the inoculated agar. The antimicrobial activities of *J. excelsa* M.Bieb. ethanol and aqueous extracts against microorganisms were examined in the present study, and their potency was quantitatively assessed by the presence or absence of inhibition zones and zone diameters. The inhibition zone, measured in millimeters, including the diameter of the well, was used as the criterion for measuring the antimicrobial activity.

The results are as shown in Table 5 showed that the ethanol and aqueous extracts have an inhibition effect on the growth of all microorganisms tested with varying degrees of inhibition, depending on the bacterial strains and volume of extract applied.

Table. 5 Antibacterial Activities (inhibition zone measured in mm) of the Ethanol and Aqueous Extracts of *J. excelsa* M.Bieb. Leaves

Microorganisms		Ethanol extract 50	Aqueous extract 50	Ethanol extract 100	Aqueous extract 100
Gram-negative bacteria	*E. coli*	15±0.24	15±0.32	20±0.28	20±0.15
	K. pneumoniae	18±0.56	16±0.17	23±0.31	19±0.49
	Citro freundii	19±0.44	18±0.52	25±0.11	23±0.34
	P. aeruginosa	18±0.13	15±0.46	21±0.58	18±0.27
Gram-positive bacteria	*St. aureus*	20±0.45	18±0.38	28±0.71	25±0.36
	B. subtilis	18±o.11	15±0.19	20±0.23	30±0.08
	St. epidermidis	20±0.29	18±0.09	30±0.28	27±0.62
yeast	*C. albicans*	20±0.53	15±0.22	30±0.61	25±0.18

Values are mean±SD; n = 3. Sensitivity – not sensitive for diameters < 8 mm; sensitive for diameters 9–14 mm; very sensitive for diameters 15–19 mm; and extremely sensitive for diameters >20 mm.

The diameter of inhibition zones was obtained in the range of 15 to 30 mm. The ethanol extracts of the leaves showed the highest activity on all microorganisms, except *B. subtilis* at 100 µL, probably because of more efficient extraction by ethanol. Behbahani *et al.* (2013) reported that alcoholic extract of *Eucalyptus camaldulensis* leaves has a greater impact on all strains compared to aqueous extract [37]. Also, extracts (100 µL) showed higher activity than extracts (50 µL). For Gram-positive, the most sensitive microorganisms were *St. aureus*, *St. epidermidis* with 20 mm inhibition for ethanol extract (50 µL), and *St. epidermidis* with 30 mm inhibition for ethanol extract (100 µL), *St. aureus* and *St. epidermidis* with 18 mm inhibition for aqueous extract (50 µL), and *B. subtilis* with 30 mm for aqueous extract (100 µL). On the other hand, the most sensitive Gram-negative bacteria was *Citro. freundii* at all extracts with the range 18-33 mm inhibition. This bacterial inhibition is mainly related to the chemical composition of the extracts [4].

These kinds of differences in susceptibility among the microorganisms against anti-microbial substances in the plant extracts may be explained by the differences in cell wall composition and/or inheritance genes on plasmids that can be easily transferred among bacterial strains [2].

Our data indicate that Gram-positive bacteria are the most sensitive tested strain to the different extracts; the tendency of polyphenols, flavonoids, tannins, and anthocyanins to react could be explained by that. The structures of the cell envelope, including cytoplasmic membrane and cell-wall component, are different between Gram-positive and Gram-negative bacteria. Gram-negative bacteria possess an outer membrane surrounding the cell wall, which restricts diffusion of hydrophobic compounds through its lipopolysaccharide covering. Without the outer membrane, the cell wall of Gram-positive bacteria can be permeated more easily and disturb the cytoplasmic membrane, disrupting the proton motive force, electron flow, active

transport, and coagulation of cell contents. Therefore, the structural difference of bacteria plays an important role in their susceptibility [9]. In many studies, the mechanism of the cell wall is considered. Kotzekidou *et al.* (2008) find that the antimicrobial compounds in the plant extract have interaction with the phospholipids' two layers membrane, and affect the permeability of the bacterial cell membrane, and released the intracellular components. Also, they have reported that cell wall and cell membrane affected and changed their permeability, causing the release of intracellular contents, which can be associated with impaired membrane function, such as electron transfer, enzyme activity or nutrient uptake [37,38]. In conclusion, it can be suggested that *J. excelsa* M.Bieb. leaves extract *in vitro* have considerable antimicrobial ability over the studied strains. More studies are needed to identify the effective dose of the extract on the microorganisms, and introduce the extract as a natural and novel antimicrobial compound. Therefore, using *J. excelsa* M.Bieb. as a natural antimicrobial compound *in vitro* requires further research on the mechanism of the pharmacy plant on microorganisms.

5. Conclusion

Medicinal plants are useful and economically essential. *J. excelsa* M.Bieb. is a plant of medicinal importance due to its activity against microorganism. The extracts obtained by *J. excelsa* M.Bieb. plant showed significant antimicrobial and antioxidant activities, which can be used as anti-microbial agents in new drugs for therapy to treat many infectious diseases. Two extracts were obtained, i.e. ethanolic extract and aqueous extract from *J. excelsa* M.Bieb. leaves. The quantitative analysis of *J. excelsa* M.Bieb. showed that the phenol content was 1.27 and 0.631 mg/mL and antioxidant activity was 65.13 and 27.63% for ethanolic and aqueous extract, respectively.

6. Author Contributions

Investigation, Project administration, Supervision, and Software; D, Mariam. Writing–review & editing, Formal analysis, and Methodology; A. H, Manar. All authors have read and agreed to the published version of the manuscript.

Funding:
This research received no external funding.

Data Availability Statement:
Data is contained within the article.

Conflicts of Interest:
The authors declare no conflict of interest.

7. References

1. Smith YA. Determination of chemical composition of *Senna-siamea* (Cassia leaves). *Pak. J. Nutr.*, 2009, 8(2), 119-121.
2. Karaman I, Şahin F, Güllüce M, Öğütçü H, Şengül M, Adıgüzel A. Antimicrobial activity of aqueous and methanol extracts of *Juniperus oxy-cedrus* L. *J. Ethnopharmacol.*, 2003, 85(2-3), 231-235. doi:10.1016/S0378-8741(03)00006-0
3. Elidrissi AE, Mssillou I, Agour A, Tourabi M, Nouioura G, Lyoussi B, Derwich E. Phytochemical analysis and evaluation of antifungal and antioxidant activities of essential oil of fruits from *Juniperus oxycedrus* L. obtained from Morocco. *Braz. J. Pharm. Sci.*, 2023, 59,e21088.doi: http://dx.doi.org/10.1590/s2175-97902023e21088
4. Djelloul R, Mokrani K, Hacini N. Study of the antibacterial activity of the extract from the essential oil of *Eucalyptus globulus* and *Rosmarinus officinalis* on three bacterial strains. *Int. J. Appl. Environ. Sci*, 2017, 12(1), 47-56.
5. Moein MR, Ghasemi Y, Moein S, Nejati M. Analysis of antimicrobial, antifungal and antioxidant activities of *Juniperus excelsa* M. B subsp. Polycarpos (K. Koch) Takhtajan essen-tial oil. *Pharmacogn. Res.*, 2010, 2(3), 128. doi**:** 10.4103/0974-8490.65505
6. Kashani SA, Ali I, Hasni MS, Asrar M, Ahmad J, Shahzad MZ. Nutritional and anti-nutritional study of *Juniperus excelsa* (M. Bieb) of Ziarat, Balochistan, Pakistan. *Environ. Sci. Ecol.: Curr. Res. (ESECR)*, 2020, 1(0008).
7. Weli AM, AL-Hinai JR, Al-Mjrafi JM, Alnaaimi JR, Hossain MA, Saeed S, Aktar MS. Effect of different polarities leaves crude extracts of *Omani juniperus* excels on antioxidant, antimicrobial and cytotoxic activities and their bio-chemical screening. *Asian Pac. J. Reprod.*, 2014, 3(3), 218-223.
8. El-Juhany L. The magnitude of dieback on *Juniperus procera* trees in the nat-ural forests in the southwestern region of Saudi Arabia. *Biosci., Biotechnol. Res. Asia*, 2015, 12(1), 219-230.
9 Ennajar M, Bouajila J, Lebrihi A, Mathieu F, Abderraba M, Raies A, Romdhane M. (2009). Chemical composition and antimicrobial and anti-oxidant activities of essential oils and various extracts of *Juniperus phoenicea* L.(Cupressacees). *J. Food Sci.*, 2009, 74(7),M364-M371. doi: http://dx.doi.org/10.1111/J.1750-3841.2009.01277.X
10. Eryigit T, Yildirim B, Ekici K. Chemical composition, antioxidant and antibacterial properties of *Juniperus excelsa* M. Bieb. leaves from Türkiye. *Acta Sci. Pol., Hort. Cult.*, 2023,22(1),11-17. doi:https://doi.org/10.24326/asphc.2023.4577
11. Sela F, Karapandzova M, Stefkov G, Cvetkovikj I, Kulevanova S. Chemical composition and antimicrobial activity of essential oils of *Juniperus excelsa* Bieb. (Cupressaceae) grown in R. Macedonia. *Pharmacogn. Res.*, 2015, 7(1), 74.
12. Stankov S, Fidan H, Petkova Z, Stoyanova M, Petkova N, Stoyanova A, Semerdjieva I, Radoukova T, Zheljazkov VD. Comparative study on the phytochemical composition and antioxidant activity of Grecian juniper (*Juniperus excelsa* M. Bieb) unripe and ripe galbuli. *Plants*, 2020, 9(9), 1207. doi: https://doi.org/10.3390/plants9091207

3. Do QD, Angkawijaya AE, Tran-Nguyen PL, Huynh LH, Soetaredjo FE, Ismadji S, Ju YH. Effect of extraction solvent on total phenol content, total flavonoid content, and antioxidant ac-tivity of *Limnophila aromatica*. *J. Food Drug Anal.*, 2014, 22(3), 296-302. doi: http://dx.doi.org/10.1016/j.jfda.2013.11.001
4. Afshar FH, Delazar A, Nazemiyeh H, Esnaashari S, Moghadam SB. Com-parison of the total phenol, flavonoid contents and antioxidant activity of methanolic extracts of *Artemisia spicigera* and *A. splendens* growing in Iran. *Pharm. Sci.*, 2019, 18(3), 165-170.
5. Nabi S, Kaleemullah, Al-Kahraman YM, Tahira B, Hajira B, Rasool A, Muhammad A. A review on *Juniperus excelsa*: Description, distribution and ecology, ethnobotany and biological activities. *Indo Am. J. Pharm. Sci.*, 2017, 4(3), 636-644.
6. Association of Official Analytical Chemists (AOAC) in Official Methods of Analysis of Association of Analytical Chemists International, 17th Ed., ed. W. Horwitz, AOAC Inter-national Publs., Maryland, USA, 2000, vol I and II, ch. 45, pp 12-20. doi: http://doi.org/10.5281/zenodo.495471
7. Stankov S, Fidan H, Petkova N, Stoyanova M, Radoukova T, Stoyanova A. Phytochemical profile of ripe *Juniperus excelsa* M. Bieb. Galbuli from Bulgaria. *Int. J. Nutr. Food Eng.*, 2020, 14(9), 109-112.
8. Pamulaparthi A, Prathap VR, Banala M, Nanna RS. Total phenolic, flavo-noid contents and antioxidant assays in leaf extracts of *Senna alata* (L.) Roxb. *J. Pharm. Sci. Res.*, 2016, 8(9), 981-985.
9. Fattahi S, Zabihi E, Abedian Z, Pourbagher R, Ardekani AM, Mostafazadeh A, Akhavan-Niaki H. Total phenolic and flavonoid contents of aqueous extract of stinging nettle and *in vitro* antiproliferative effect on Hela and BT-474 cell lines. *Int. J. Mol. Cell. Med.*, 2014, 3(2), 102.
20. Siddiqui N, Rauf A, Latif A, Mahmood Z. "Spectrophotometric determination of the total phenolic content, spectral and fluorescence study of the herbal Unani drug Gul-e-Zoofa (*Nepeta brac-teata* Benth). *J. Taibah Univ. Med. Sci.*, 2017, 12(4), 360-363.
21. Folin O, Ciocalteu V. On tyrosine and tryptophane determinations in pro-teins. *J. Biol. Chem.*, 1927, 73(2), 627-650.
22. Sochor J, Ryvolova M, Krystofova O, Salas P, Hubalek J, Adam V, Trnkova L, Havel L, Beklova M, Zehnalek J, Provaznik I, Kizek, R. Fully automated spectrometric protocols for deter-mination of antioxidant activity: Advantages and disadvan-tages. *Molecules*, 2010, 15(12), 8618-8640. doi: 10.3390/molecules15128618
23. Goze I, Alim A, Tepe AS, Sokmen M, Sevgi K, Tepe B. Screening of the antioxidant activity of essential oil and various extracts of *Origanum rotun-difolium* Boiss. from Turkey. *J. Med. Plants Res.*, 2009, 3(4), 246-254.
24. Atangwho IJ, Ebong PE, Eyong EU, Williams IO, Eten MU, Egbung GE. Comparative chemical composition of leaves of some antidiabetic medicinal plants: *Azadirachta indica*, *Vernonia amyg-dalina* and *Gongronema latifo-lium*. *Afr. J. Biotechnol.*, 2009, 8(18).
25. Agbafor KN, Engwa GA, Obiudu IK. Analysis of chemical composition of leaves and roots of *Ageratum cony-zoides*. *Int. J. Curr. Res. Acad. Rev.*, 2015, 3(11), 60-65.
26. Eze SO, Ernest O. Phytochemical and nutrient evaluation of the leaves and fruits of *Nauclea latifolia* (Uvuru-ilu). *Commun. Appl. Sci.*, 2014, 2(1).

27. Rajput H, Prasad SGM, Srivastav P, Singh N, Suraj L, Chandra R. (2017). Chemical and phytochemical properties of fresh and dried *Moringa oliferiea* (PKM-1) leaf powder. *Chem. Sci. Rev. Lett.*, 2017, 6, 1004-1009.
28. Dike IP, Ibojo OO, Daramola FY, Omonhinmin AC. Phytochemical and proximate analysis of foliage and seed of *Bixa orellana* Linn. *Int. J. Pharm. Sci. Rev. Res.*, 2016, 36(2), 247-251.
29. Bakare RI, Magbagbeola OA, Akinwande AI, Okunowo OW. Nutritional and chemical evaluation of *Momordica charantia*. *J. Med. Plants Res.*, 2010, 4(21), 2189-2193. doi: 10.5897/JMPR10.274
30. Odabaş-Serin Z, Bakir O. Some chemical, nutritional and mineral properties of dried juniper (*Juniperus drupacea* L.) berries growing in Turkey. *Appl.Ecol.Environ.Res.*, 2019,17 (4).doi: http://dx.doi.org/10.15666/aeer/1704_81718178
31. Rebaya A, Belghith SI, Baghdikian B, Leddet VM, Mabrouki F, Olivier E, Cherif JK, Ayadi MT. Total phenolic, total flavonoid, tannin content, and antioxidant capacity of *Halimium halimifolium* (Cistaceae). *J. Appl. Pharm. Sci.*, 2015, 5(1), 052-057. doi: 10.7324/JAPS.2015.50110
32. Gonçalves AC, Flores-Félix JD, Coutinho P, Alves G, Silva LR. (2022). Zimbro (*Juniperus communis* L.) as a promising source of bioactive compounds and biomedical activities: A review on recent trends. *Int. J. Mol. Sci.*, 2022,23(6),3197.doi: https://doi.org/10.3390/ijms23063197
33. Živić, N, Milošević S, Dekić V, Dekić B, Ristić N, Ristić M, Sretić, L. Phytochemical and antioxidant screening of some extracts of *Juniperus communis* L. and *Juniperus oxycedrus* L. *Czech J. Food Sci.*, 2019, 37(5), 351-358.doi: https://doi.org/10.17221/28/2019-CJFS
34. Bakchiche B, Habati M, Benmebarek A, Gherib A. Total phenolic, flavonoid contents and antioxidant activities of honey and propolis collected from the region of Laghouat (South of Algeria). *World News Nat. Sci.*, 2017, 11.
35. Ahmed D, Khan MM, Saeed R. Comparative analysis of phenolics, flavonoids, and antioxidant and antibacterial potential of methanolic, hexanic and aqueous extracts from *Adiantum-caudatum* leaves. *Antioxidants*, 2015, 4(2), 394-409. doi: 10.3390/antiox4020394
36. Osman MA, Mahmoud GI, Shoman SS. Correlation between total phenols content, antioxidant power and cytotoxicity. *Biointerface Res. Appl. Chem.*, 2020, 11, 10640-10653. doi: https://doi.org/10.33263/BRIAC106401065 3
37. Alizadeh Behbahani B, Tabatabaei Yazdi F, Mortazavi SA, Zendeboodi FATEMEH., Gholian MM, Vasiee A. Effect of aqueous and ethanolic extract of *Eucalyptus camaldulensis* L. on food infection and intoxication microorganisms *in vitro*. *J. Paramed. Sci.*, 2013, 4.
38. Kotzekidou P, Giannakidis P, Boulamatsis A. Antimicrobial activity of some plant extracts and essential oils against foodborne pathogens *in vitro* and on the fate of inoculated pathogens in chocolate. *LWT-Food Sci. Technol.*, 2008, 41(1), 119-127.

The Chemist
Journal of the American Institute of Chemists

Reactions of $C_2H_5O_2$ and C_2H_5 Radicals on Acidic and Basic Surface

Astine S. Martirosyan, Irma A. Vardanyan

Nalbandyan Institute of Chemical Physics, National Academy of Sciences of the Republic of Armenia; P. Sevak 5/2; Yerevan 0014, RA

(E-mail: astine@ichph.sci.am)

Abstract: The analysis and discussion of the kinetic data obtained by studying the effect of the nature of the reactor surface (H_3BO_3, KCl) on the oxidation of C_2H_5CHO allowed us to provide experimental evidence for the heterogeneous reaction of $C_2H_5O_2$ radicals with aldehyde and the heterogeneous formation of ethylene and hydroperoxide through the involvement of C_2H_5 radicals. In this context, elucidating the possibility of heterogeneous reactions involving $C_2H_5O_2$ and C_2H_5 radicals is important for advancing our understanding of the oxidation and ignition reactions of aldehydes. It was also concluded that the interaction of peroxy radicals with an organic compound is more general and not limited to CH_3O_2 radicals.

Key Words: reaction mechanism, radicals, oxidation and ignition reactions, surface

1. Introduction

The possibility, of heterogeneous interactions between CH_3O_2 radicals with aldehydes and hydrocarbons has been established in recent studies [1−9]. However, there is no direct evidence of such heterogeneous reactions concerning $C_2H_5O_2$ and C_2H_5 radicals. In this study, we sought to provide such evidence by analyzing and discussing the kinetic data obtained from the investigation of the influence of the reaction vessel surface (H_3BO_3, KCl) on the oxidation process of propionaldehyde at atmospheric pressure in air flow [10,11]. This reaction proceeds *via* a chain degenerate branching mechanism [12].

$$C_2H_5CO_3H \rightarrow C_2H_5CO_2 + OH \quad (1)$$
$$C_2H_5CO_2 \rightarrow C_2H_5 + CO_2 \quad (2)$$
$$C_2H_5 + O_2 \rightarrow C_2H_5O_2 \quad (3)$$

Eq. 1-3, where the branching stage at relatively low temperatures, involves the heterogeneous radical decay of $C_2H_5CO_3H$ (Eq. 1). The leading active centers in this process are $C_2H_5CO_3$ radicals (Eq. 1-3). As the oxidation process develops, the contribution of $C_2H_5O_2$ radicals, formed as a result of the heterogeneous decay of peracid, increases (Eq. 1).

Based on the dependence of the yields of such reaction products as ethylene and ethyl hydroperoxide on the nature of the reactor surface [10,11], it was possible to identify their heterogeneous formation with the participation of C_2H_5 radicals (Eq. 2, 3).

Gas-phase oxidation reactions of aldehydes, proceeding *via* a chain degenerate branching mechanism, are a source of valuable oxygen-containing compounds. Depending on the nature of the reaction vessel, both the rate and the direction of the process can change [12]. For example, during the oxidation of C_2H_5CHO in the boric acid-treated reactor, peroxypropionic acid ($C_2H_5CO_3H$) can be formed with high selectivity (80%), while in the potassium chloride-treated reactor, the selectivity for propionic acid ($C_2H_5CO_2H$) is 90%.

The heterogeneous reactions of peroxy radicals such as CH_3O_2 play a crucial role in the combustion of $CH_3CHO + O_2$ mixtures, initiated by peroxy radicals formed during the heterogeneous radical decay of RCO_3H [13].

Thus, investigating the possibility of heterogeneous reactions involving $C_2H_5O_2$ (Eq. 3) and C_2H_5 (Eq. 2) radicals is essential for understanding the mechanism of oxidation and combustion reactions of aldehydes.

2. Results and Discussion

Reaction of $C_2H_5O_2$ Radical with Aldehyde on Solid Surface

Figures 1 and 2 demonstrate the kinetic curves of the consumption of C_2H_5CHO and the accumulation of some reaction products including peroxy radicals, $C_2H_5CO_3H$ and $C_2H_5O_2H$, obtained in the aforementioned two reactors at 291°C [11].

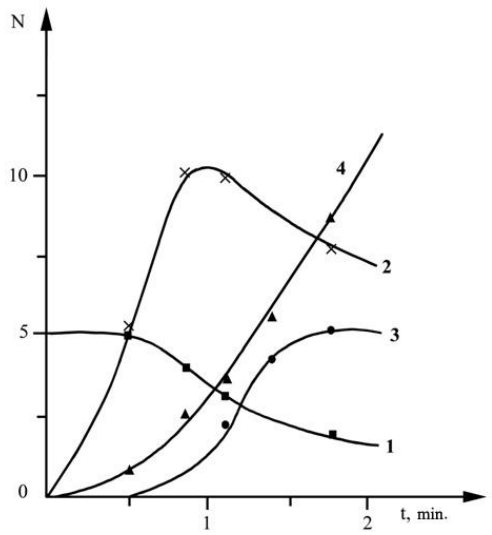

Fig. 1. Kinetic Curves of C_2H_5CHO Consumption (1) and of Accumulation of Peroxy Radicals (2), RCO_3H (3), RO_2H (4) at T = 291°C in the Reactor, Treated by Boric Acid. $[C_2H_5CHO] = N \times 10^{17}$, [radical] = $N \times 10^{12}$, $[RCO_3H]$ and $[RO_2H] = N \times 10^{16}$ part.cm^{-3}.

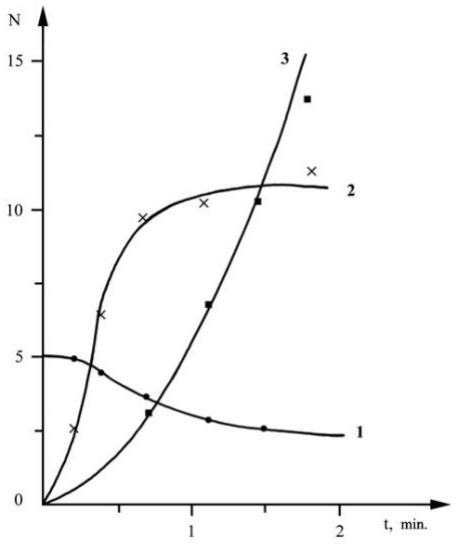

Fig. 2. Kinetic Curves of C_2H_5CHO Consumption (1) and of Accumulation of Peroxy Radicals (2), RO_2H (3) at T = 291°C in a Reactor Treated by KCl. $[C_2H_5CHO] = N \times 10^{17}$, [radical] = $N \times 5 \times 10^{11}$, $[RO_2H] = N \times 2 \times 10^{16}$ part.cm^{-3}.

Table 1 shows the concentrations of reaction products at 291°C and 1 minute of reaction time in reactors treated by boric acid and potassium chloride.

Table 1. Concentrations of Reaction Products at 291°C and t = 1 min (reaction time) in Reactors Treated by Boric Acid and Potassium Chloride; $[C_2H_5CHO]_0 = 5 \times 10^{17}$ part.cm^{-3}

Surface	KCl (part.cm^{-3})	H_3BO_3 (part.cm^{-3})
$[C_2H_5CHO]_t$	3×10^{17}	3.6×10^{17}
$[RCO_3H]$	–	1.5×10^{16}
$[RO_2H]_t$	1.07×10^{17}	3.2×10^{16}
$[RCO_3 + RO_2]_t$	5.2×10^{12}	1.02×10^{13}
$[C_2H_4]_t$	2.3×10^{16}	–
$[CO_2]_t$	2.04×10^{17}	3×10^{16}

This data indicates that the process characteristics strongly depend on the nature of the surface. This applies both to the composition of the reaction products and to the absolute values of products concentrations. Notably, $C_2H_5CO_3H$ is absent in the reactor treated with KCl. This is attributed to a higher rate of heterogeneous radical decay of the peracid on the KCl surface in compared to the H_3BO_3 surface [14]. The high yield of CO_2, formed during the decay of peracid in the reactor, further supports this. Consequently, the process in the KCl-treated reactor begins earlier than in the H_3BO_3-treated reactor, and even at t = 1 min the aldehyde consumption is 1.4 times greater than that in a boric acid-treated reactor. It is noteworthy that the concentration of peroxy radicals in the volume is less by approximately 2 times. This clearly indicates that a significant portion of the aldehyde in the KCl-treated reactor is consumed on the reactor surface. The yield of hydroperoxide is almost three times higher than in the reactor treated with boric acid.

Apparently, a significant contribution to the formation of hydroperoxide is linked to the heterogeneous interaction of $C_2H_5O_2$ radicals with propionaldehyde. The presence of ethylene in the KCl-treated reactor and its absence in the boric-acid reactor, also suggests that more C_2H_5 radicals were formed in the first reactor. It is important to note that the reactions of C_2H_5 radicals are the source of both ethylene and $C_2H_5O_2$ radicals.

Regarding the H_3BO_3 surface, since it is known that the rate of $C_2H_5CO_3H$ heterogeneous radical decomposition on this surface is much slower than that on the KCl surface, it is evident that the amount of formed $C_2H_5O_2$ radicals on the H_3BO_3 surface should be significantly lower. Therefore, the yield of hydroperoxide is also lower.

A comparison of the kinetic curves for the accumulation of peroxy radicals in both reactors and, considering the significant

amounts of $C_2H_5CO_3H$ in the boric acid-treated reactor, shows that the ratio of $C_2H_5CO_3$ and $C_2H_5O_2$ radical concentrations is higher in the boric acid-treated reactor.

Analysis of the kinetic data on propionaldehyde oxidation depending on the nature of the surface, reliably indicates the possibility of heterogeneous interaction between $C_2H_5O_2$ radicals and aldehyde-C_2H_5CHO. Thus, we conclude that the interaction of peroxy radicals with organic compounds is more general and is not limited to CH_3O_2 radicals.

Heterogeneous Reaction Pathways of C_2H_5 Radicals on a Solid Surface

This work presents data on the heterogeneous formation of several reaction products, such as C_2H_4 and $C_2H_5O_2H$, during the low-temperature oxidation of propionaldehyde. These results were obtained by analyzing the kinetic patterns of the process in reactors treated with boric acid and potassium chloride [10].

Fig. 3 and 4 illustrate the kinetics of peroxy radicals formation and the initial aldehyde consumption while the concentrations of some reaction products for a fixed reaction time are shown in the Table 2.

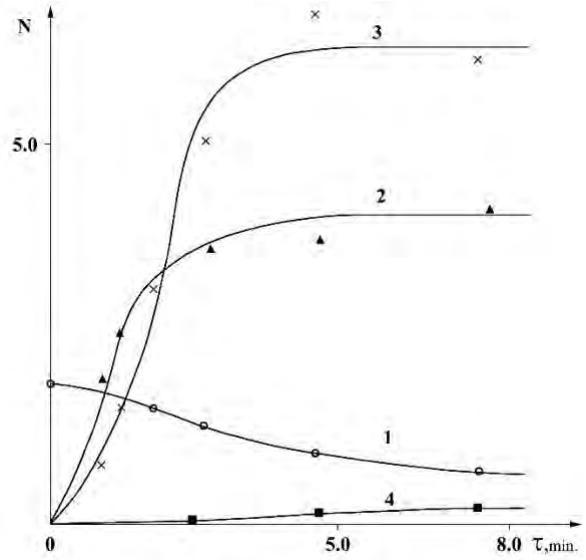

Fig. 3. Kinetic Curves of C_2H_5CHO (1) Consumption and of Peroxy Radicals (2), $C_2H_5CO_3H$ (3), C_2H_4, CO (4) Accumulation at 175°C in a Boric Acid Treated Reactor. $[C_2H_5CHO] = N \times 10^{18}$, $[RCO_3H] = N \times 2 \times 10^{16}$, $[RO_2] = N \times 4 \times 10^{12}$, $[C_2H_4] = N \times 10^{17}$, part.cm^{-3}.

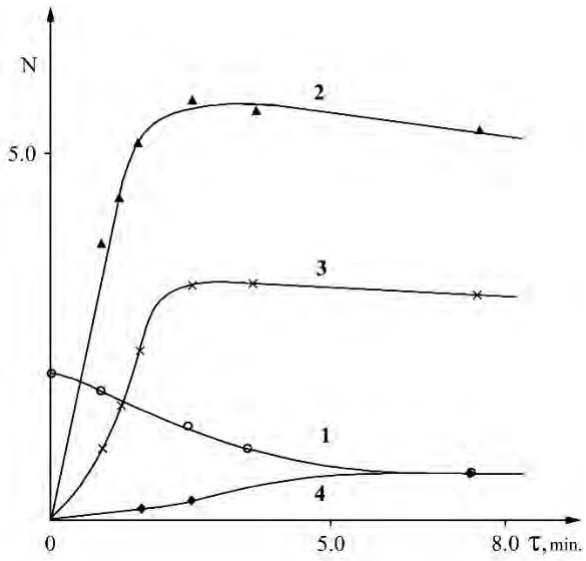

Fig. 4. Kinetic Curves of C_2H_5CHO (1) Consumption and of Peroxy Radicals (2), $C_2H_5CO_3H$ (3), $C_2H_5O_2H$ (4) Accumulation at 175°C in a Reactor Treated by KCl. $[C_2H_5CHO] = N \times 10^{18}$, $[RCO_3H] = N \times 2 \times 10^{16}$, $[RO_2] = N \times 4 \times 10^{12}$, $[C_2H_5O_2H] = N \times 10^{17}$, part.cm^{-3}.

Table 2. The Concentrations of the Reaction Products at 175°C and at Reaction Time t = 5 min in Reactors Treated by H_3BO_3 and KCl; $[C_2H_5CHO]_0 = 1.9 \times 10^{18}$ part.cm^{-3}

Surface	KCl (part.cm^{-3})	H_3BO_3 (part.cm^{-3})
$[C_2H_5CHO]_t$	7.5×10^{17}	9.3×10^{17}
$[C_2H_5CO_3H]_t$	6.2×10^{16}	1.3×10^{17}
$[C_2H_5CO_2H]_t$	8.4×10^{17}	3.9×10^{17}
$[RO_2]_t$	2.1×10^{13}	1.6×10^{13}
$[C_2H_4]_t$	-	1.7×10^{16}
$[CO_2]_t$	8.5×10^{16}	6×10^{16}
$[CH_3CHO]_t$	1.8×10^{17}	9.3×10^{15}

Comparison of the results obtained in the two reactors reveals that the rate of the process in the potassium chloride-treated reactor is higher than in the boric acid-treated reactor, while the yield of $C_2H_5CO_3H$ product responsible for the branching is much lower. This was not unexpected, as the rate of heterogeneous radical decay of peracids is greater in a reactor treated with potassium chloride [14].

The data indicates that the concentration of peroxy radicals such as $C_2H_5CO_3$ and $C_2H_5O_2$ [10] in the given volume, correlates

with the rate of oxidation in these reactors, and is higher in the reactor treated by potassium chloride.

An important feature of the process is the detection of ethylene and the absence of hydroperoxide in the boric acid-treated reactor. Conversely, in the potassium chloride-treated reactor, hydroperoxide is detected while ethylene is absent. This suggests that there are heterogeneous pathways for the formation of these compounds. Possible pathways for the formation of these compounds are:

1. $RCO_3H \rightarrow RCO_2 + OH \rightarrow R + CO_2 + OH$
2. $R + O_2 \rightarrow RO_2$
3. $RO_2 + RCHO \rightarrow RO_2H + RCO$
4. $R \rightarrow C_2H_4 + H$
5. $R + O_2 \rightarrow C_2H_4 + HO_2$, where R is a C_2H_5 radical

It is noteworthy that comparison of the yields of ethylene and hydroperoxide with those obtained during the oxidation of C_2H_5CHO in the same reactors at 291°C [11], reveals that the concentration of hydroperoxide is higher in the reactor treated with potassium chloride, although a certain amount of it is also already registered in the reactor treated with boric acid. As for ethylene, it is formed at higher temperatures in the potassium chloride-treated reactor. The obtained data show that the competition between reactions 2. and reactions 4. and 5. favor of 2. on the KCl surface.

3. Conclusion

Thus, this study allows us to conclude that the heterogeneous reactions of $C_2H_5O_2$ and C_2H_5 radicals play a crucial role in the gas-phase oxidation of C_2H_5CHO, contributing to the formation of several reaction products.

Declaration of competing interest: The authors declare that they have no known competing financial interests or personal relationships that could have appeared to influence the work reported in this paper.

4. References

1. Manucharova LA, Tsarukyan SV, Vardanyan IA. Reactions of CH_3O_2 radicals on solid surface. *Int. J. Chem. Kinet.*, 2004, 36, 591−595.
2. Jalali HA, Manucharova LA,Tsarukyan SV, Vardanyan IA. Reaction of peroxide radicals with methane on the titanium oxide surface: Effects of the composition of the initial mixture. *Russ. J. Phys. Chem. A*, 2011, 85, 483−485.
3. Christopher R. Reactive radicals on reactive surfaces: Heterogeneous processes in catalysis and environmental pollution control. *Prog. React. Kinet. Mech.*, 2005, 30, 145−213.
4. Martirosyan AS, Tsarukyan SV. Investigation of a model of interaction between organic compound and CH_3O_2 radicals in the presence of oxygen on the active and passive surfaces. *Reports NAS RA*, 2016, 116,

219−224.
5. Biggs P, Canosa-Mass CE, Fracheboud J-M, Shallcross DE, Wayne RP. Rate constants for the reactions of C_2H_5, C_2H_5O and $C_2H_5O_2$ radicals with NO_3 at 298 K and 2.2 torr. *J. Chem. Soc., Faraday Trans.*, 1995, 5, 817−825.
6. Zhang P, Wang W, Zhang T, Chen L, Du Y, Li Ch, Lü J. Theoretical study on the mechanism and kinetics for the self-reaction of $C_2H_5O_2$ radicals. *J. Phys. Chem. A*, 2012, 116, 4610−4620.
7. Goldman MJ, Green WH, Kroll JH. Chemistry of simple organic peroxy radicals under atmospheric through combustion conditions: Role of temperature, pressure, and NO_x level. *J. Phys. Chem A*, 2021, 125, 10303−10314.
8. Orlando JJ, Tyndall GS. Laboratory studies of organic peroxy radical chemistry: an overview with emphasis on recent issues of atmospheric significance. *Chem. Soc. Rev.*, 2012, 41, 6294−6317.
9. Arutyunyan AA. The conversion of SO_2 by hydrogen oxidation branching chain reaction. *Global NEST J.*, 2022, 24, 590−593.
10. Oganesyan EmA, Vardanyan IA, Nalbandyan AB. Investigation of low temperature propionaldehyde oxidetion kinetics in vessels, treated with boric acid and potassium chloride. *Arm. Chem. J.*, 1977, 30, 107−113.
11. Oganesyan EmA, The Influence of the Nature and Surface Condition of the Reaction Vessel on the Kinetics of Propionaldehyde Oxidation, Ph.D. Thesis, Institute of Chem. Physics, Arm. Acad. of Sciences, Arm. SSR, Yerevan, 1978.
12. Nalbandyan AB, Vardanyan IA, Modern State of Problem of Gas Phase Oxidation of Organic Compounds, Arm. Acad. Sciences Arm. SSR, Yerevan, 1986.
13. Vardanyan IA, Arustamyan AM, Martirosyan AS, Tsarukyan SV. Interaction between peroxy radicals and acetaldehyde on solid surfaces and its role in the oxidation of aldehydes. *Russ. J. Phys. Chem. A*, 2016, 90, 744−747.
14. Baghdasaryan GO, Oganesyan EmA, Vardanyan IA, Sachyan GA, Nalbandyan AB. The effect of the reaction vessel surface on the kinetics of the heterogeneous radical decomposition of perpropionic acid. *Arm. Chem. J.*, 1976, 29, 899−903.

The Chemist
Journal of the American Institute of Chemists

Preparation, Characterization and Anti-inflammatory Evaluation of Fortified Cosmeceutical Emollient from the Seed Oil of *Azadirachta indica* A. Juss

Olubunmi Atolani [*a], Funmilayo C. Oladapo [a], Olubunmi C. Olupade [a], Glory C. Ekejiuba [a], Emmanuel A. Taiwo [a,b]

[a] *Medicinal Chemistry Unit, Department of Chemistry, University of Ilorin, PMB 1515 Ilorin, Nigeria*
[b] *Department of Chemistry, Kogi State University, PMB 222 Kabba, Nigeria*

[*]*Correspondence (E-mail: atolani.o@unilorin.edu.ng)*

Abstract: The need for a green process in the preparation of cosmeceuticals cannot be overemphasized, as many synthetic skincare and hair-care products are reportedly carcinogenic or toxic to humans. The aim of this study was to prepare and characterize an organic-fortified cosmeceutical emollient from neem seed oil (*Azadirachta indica* A. Juss) and determine the *in vitro* anti-inflammatory potential. The air-dried seeds were de-shelled, pulverized and extracted with n-hexane, then trans-esterified to obtain the Fatty Acid Methyl Esters (FAMEs) which were characterized using Gas Chromatography Mass Spectrometry (GC-MS). The anti-inflammatory potential was determined using the albumin denaturation assay. The result from the GC-MS analysis showed the presence of major fatty acids which include elaidic acid (37.7%), oleic acid (20.23%), palmitic acid (14.62%), eicosanoic acid (9.49%), linoleic acid (6.95%) and stearic acid (4.08%). The oil emollient exhibited significant albumin denaturing activity. The seed oil, often discarded as waste holds tremendous promise as a renewable source of pharmacological oil for affordable organic cosmetic formulations.

Key Words: neem seed, cosmeceutical(s), emollient, antioxidant, cytotoxicity, fatty acid

1. Introduction

Plants parts, which include flowers, leaves, roots, stems, fruits, or seeds, are used widely for therapeutic purposes due to low accessibility and high cost of orthodox medicine. While some are used as prophylaxis, others are adopted for curing many types of illnesses.

The remarkable number of reports on the therapeutic properties of medicinal plants, together with long-term experience in folk medicine, has led to a growing interest in the use of natural products [1]. Medicinal plants still hold promise as therapeutic agents because of the enormous number of plants around the world yet to be explored for their pharmacological potential. These plants produce a number of secondary metabolites as chemical compounds with important biological activities, such as antimicrobial, anti-inflammatory, anticancer, anti-aging, antiviral, antioxidant, enzyme inhibitory, antihypertensive, and anticoagulant effects [2,3].

Cosmetics, on the other hand, defined by the European Commission (2015) as any substance or mixture intended to be placed in contact with the external parts of the human body (epidermis, hair system, nails, lips and external genital organs) or with the teeth and the mucous membranes of the oral cavity with a view exclusively or mainly to cleaning them, perfuming them, changing their appearance, protecting them, keeping them in good condition or correcting body odors, play an essential role in our society today.

Medicinal plants are used extensively today in drugs, cosmetics, and the formulation of skin care products for their reduced toxicity and ability to enhance natural beauty [4-6]. The application of seeds in food [7], health [8,9] and industrial sectors [10] cannot be overemphasized. *Azadirachta indica*, also known as neem, Indian lilac or Margosa, belong to the family Meliaceae, subfamily Meloideae and tribe Melieae [11]. Neem is the most versatile, multifarious trees of the tropics, with immense potential in herbal medicine and pharmacotherapy. It is widely distributed in the arid areas of several tropical and subtropical countries; it often grows to a height of 15–20 m with pinnate leaves of average 30 cm long and asymmetric leaflets often reaching 8 cm (Figure 1).

Figure 1. (a) Neem Plant Showing the Leaves at the Flowering Stage; (b) Neem Fruits on Plant; (c) Neem Tree Showing Stem in its Natural Habitat (d) Neem Tree Showing Extensive Branching

Neem leaves are medium to large in size and elongated to oblong in shape, averaging 20–40 cm in length. The vibrant green leaves are smooth and glossy with sharp serrated edges. Neem leaves grow on the branches of neem trees in groups of two and each branch produces approximately eight pairs. The fruit is smooth, ellipsoidal drupe, sometimes up to 1.5 cm long, comprising of sweet pulp enclosing a seed.

Neem possesses more useful non-wood products (leaves, bark, flowers, fruit, seeds, gum, oil and neem cake) than any other tree species. These non-wood products are known to have antiallergenic, antidermatic, antifeedant, antifungal, anti-inflammatory, antipyorrhoeic antiscabic, cardiac, diuretic, insecticidal, larvicidal, nematicidal, spermicidal and other biological activities. Neem

and its products have been widely reported to control insect pests [12]. The seed is composed of a shell and a kernel which is the source of the oil that is highly medicinal in nature. The seed oil is used directly as an insect and mite repellent, worm expellant, insecticide, and fungicide when diluted to various concentrations and mixed with other substances [13]. Neem is used to treat dermatitis, eczema, acne, bacterial and fungal infections, and other skin disorders. The paste made from the neem or seed oil is used for treating acne, eczema, impetigo, ulcers, pustules, snake and scorpion bites, chicken pox, measles, scaly scalp, psoriasis, pruritus, dermato-phytosis, leprosy, pediculosis, and scabies [14]. The leaves are dried and burnt as insect repellant. The extract is used to improve the immune system and also as an anti-inflammatory agent in skin disorders [15]. The use of seed oils and other organic products in green cosmetics has gained more attention recently. This is because many scientific outputs reportedly have linked rashes, skin discoloration and allergic skin irritation to many synthetic additives used in cosmetics [16]. Hence, the need for green preparation of cosmetics cannot be over-emphasized. This work reports the characterization of neem seed oil, the formulation of an organic cosmetic product and anti-inflammatory evaluation.

2. Materials and Methods

The high purity reagents were obtained from SigmaAldrich, Inc. (Missouri, USA) and were used as received without further purification. Other chemical and reagents used were analytical grade, while solvents which include n-hexane, ethyl acetate, chloroform and methanol were re-distilled before use when required.

Collection and Preparation of Plant Samples

The seeds of the neem plant were collected from fruiting trees within the Ilorin metropolitan area and were authenticated by a taxonomist at the herbarium of Plant Biology Department at the University of Ilorin. The seeds were dried at am-bient temperature, de-shelled, pulverized and were kept in a cool dark place for further work. The oleoresin used for the fortification of the seed oil was obtained as a gift for the Medicinal Chemistry Research group of the Department of Chemistry.

Solvent Extraction of Neem Seed Oil

The pulverized neem seed was weighed (413.53g) and subjected to Soxhlet extraction using n-hexane until exhaustion, then filtered and concentrated to obtain the oil.

Lipid Transesterification

The oil obtained was trans-esterified by treating 2 g with 0.2 M methanolic HCl (60 mL) [17]. The mixture was refluxed for an hour and allowed to cool. The organic layer

was separated from the aqueous layer using a separating funnel. The organic phase was washed with water, dried over anhydrous magnesium sulphate, and then concentrated to afford the fatty acid methyl esters (FAMES) and stored for GC–MS analysis. The percentage yield (% w/w) of oil obtain (30.02%) of the trans-esterified oil was determined using the formula (equation 1):

$$\text{Percentage Yield} = \frac{weight\ of\ transesterified\ oil}{weight\ of\ oil} \text{ x } 100 \quad (1)$$

Saponification Value

One (1) gram of each oil was weighed into a conical flask containing 25 mL of methanolic KOH and mixed together. The mixture was warmed in a water bath for 5 min, 3 drops of phenolphthalein were added to it, and the content titrated against 0.5 M HCl until the pink colour disappeared. The discolouration indicates the end point. The saponification value was calculated using the equation (2):

$$\text{SV} = \frac{S(-B)\times M\times 56.1 gmol}{(WEIGHT\ OF\ SAMPLE)\ g} \quad (2)$$

where SV = saponification value; B = blank titre value (mL); S = sample titre value (mL); M = Molarity of KOH, taking the molecular weight of KOH to be 56.1 g/mol.

Acid Value

One (1) gram of the oil was weighed into a flask with 25 mL of methanol and 3 drops of phenolphthalein indicator was added to it. The mixture was warmed in a water bath for 5 min and titrated against 0.1 M KOH until the pink colour disappeared, which indicates the end point. Acid value was calculated using the equation (3):

$$\text{AV} = \frac{Ml\ OF\ KOH \times N \times 56.1\ g\ mol}{(Weight\ of\ sample)\ g} \quad (3)$$

where AV = acid value; M = Molarity of KOH.

Peroxide Value

The oil (0.5 g) was weighed into a conical flask containing 1 g potassium iodide. The mixture of glacial acetic acid (13.5 mL) and chloroform (6.5 mL) was added to it. The solution warmed in water bath for a minute, 20 mL of 5% potassium iodide and 25 mL of water was added to the mixture. Sodium thiosulphate solution (0.002 M) was titrated against the content to colourless using freshly prepared starch as indicator. The results were expressed in mMol/Kg. The

peroxide value was calculated using the formula:

$$\text{Peroxide value} = \frac{(V_s - V_b) \times M \text{ of titrant}}{(\text{Weight of sample}) \text{ g}} \quad (4)$$

where V_b = titre for blank; V_s = titre for sample; M = Molarity.

Green Seed Oil Fortification with Oleoresin

The seed oil was fortified with oleoresin originally obtained from the stem bark of the *Danielli oliveri* plant using the formulation indicated in Table 1.

Table 1. Fortification of Neem Seed Oil with Oleoresin

Sample Code	Neem Seed Oil (g)	Oleoresin (g)
NE	5	0
NE1	5	1
NE2	5	2
NE3	5	3
NE4	5	5

3. Results

Neem Seed Oil Chemical Profiling

The results obtained from GC-MS analysis of the trans-esterified neem seed oil are as depicted in Table 2.

Table 2. Chemical Composition of Neem Oil FAMEs

S/N	Retention Time	Compound Name	Molecular Formula	% Relative Abundance
1	11.41	Lauric acid	$C_{12}H_{24}O_2$	0.15
2	12.19	7-Hexadodecanoic acid	$C_{16}H_{30}O_2$	0.05
3	14.41	Tridecanoic acid	$C_{13}H_{26}O_2$	0.14
4	16.88	Palmitoleic acid	$C_{16}H_{30}O_2$	1.05
5	17.33	Palmitic acid	$C_{16}H_{32}O_2$	14.62
6	18.49	Margaric acid	$C_{17}H_{34}O_2$	0.42
7	19.35	Linoleic acid	$C_{18}H_{32}O_2$	6.95
8	19.64	Elaidic acid	$C_{18}H_{34}O_2$	37.70
9	20.07	Oleic acid	$C_{18}H_{34}O_2$	20.23
10	19.88	Eicosanoic acid	$C_{20}H_{40}O_2$	9.49
11	20.07	6-Octadecenoic acid	$C_{18}H_{34}O_2$	1.53
12	20.62	Stearic acid	$C_{18}H_{36}O_2$	4.08
13	21.43	7-Hexadecanoic acid	$C_{16}H_{30}O_2$	1.22
14	21.92	Cis-11-eicosenoic acid	$C_{20}H_{38}O_2$	0.44
15	22.71	8,11,14-dodecatrienoic acid	$C_{18}H_{30}O_2$	0.49
16	24.84	Behenic acid	$C_{22}H_{44}O_2$	0.90
17	28.20	Lignoceric acid	$C_{24}H_{48}O_2$	0.45

In vitro Anti-inflammatory Activity

The anti-inflammatory activity of the oil was evaluated using the albumin denaturation assay. The results obtained are as depicted in Table 3.

Table 3. Inhibition of Albumin Denaturation Activity

Concentration (mg/mL)	NE (I%)	NE1 (I%)	NE2 (I%)	NE3 (I%)	NE4 (I%)	Oleo (I%)	Quercetin (I%)
25	38.06±1.74	26.64±3.3	27.77±1.45	39.60±2.18	32.20±0.14	22.42±0.29	59.46±1.45
50	31.58±0.14	25.92±3.49	24.48±1.74	21.81±1.74	32.15±0.87	13.16±2.03	40.94±1.45
75	25.41±0.43	31.58±0.43	36.11±4.51	23.25±2.32	38.88±2.9	14.30±0.14	34.15±1.16
100	28.49±14	59.15±0.14	45.88±0.58	30.34±0.14	51.02±2.3	12.13±0.58	34.67±1.60

I - Inhibition; NE - Neem Seed Oil; Oleo - Oleoresin

4. Discussion

The GC-MS analysis of the neem seed oil confirms the presence of constituents which are known to exhibit medicinal as well as physiological activity [18]. Characterization of the fatty acid profile of neem seed oil is vital for industrial and economic purposes. The GC-MS results showed the presence of major fatty acids including palmitic acid (14.62%, 17.33), a saturated fatty acid, elaidic acid (37.7%, 19.64), oleic acid (20.23%, 20.07), linoleic acid (6.95%, 19.35), eicosanoic acid (9.49%, 19.88), and stearic acid (4.08%, 20.62). The profile revealed the presence of more long chain fatty acids than the short chain fatty acids. The lower amounts of stearic acid and linoleic acid observed in this study could be attributed to different factors such as seasonal variation, time of harvesting, growing conditions and other biotic and abiotic factors. Eicosanoic acid is known to be useful in cosmetics formulations while docosanoic acid, also called behenic acid ($C_{22}H_{44}O_2$), is often used as hair conditioners and moisturizers, giving them smoothing properties [19].

The anti-inflammatory properties of the oil and the fortified products revealed a dose-dependent albumin denaturation inhibition potential comparable to the standard, quercetin. While the oleoresin showed low dose-dependent activity, the fortified products exhibited better activities reflecting potential synergistic activity of the oleoresin with the oil.

The composition of the neem oil indicates a rich mixture of saturated, monounsaturated, and polyunsaturated fatty acids. This diverse composition makes neem oil suitable for various applications in cosmetics and skincare due to the presence of oleic and linoleic acids which are required for skin moisturizing and nourishment. The presence of the lauric acid will enhance the antimicrobial properties in cases acne and other skin infection conditions. Moreover, the pharmaceuticals potential will be enhanced due to the presence of significant amount of linoleic acid known to possess anti-inflammatory properties. Fatty acids are crucial components of oils and fats, and their composition can significantly influence the properties and applications of the oil.

5. Conclusion

Neem seed oil, investigated for its chemical composition, has been formulated into a green cosmeceutical product with potential anti-inflammatory activity. The formulated product, devoid of all synthetic and artificial additives, revealed the potential application of the oil in organic cosmetics. As most cosmetic consumers now prefer herbal, organic, or green cosmetic products which are less toxic and more environmentally friendly, the application of the seed oil for use in cosmeceuticals is hereby reinforced. Neem seed oil, often discarded as waste, holds tremendous promise as a viable and sustainable source of bioactive oil for affordable organic cosmetic formulation. Owing to the results obtained in this study, coupled with the abundance of neem seeds in the study area, production of viable oil from neem seeds is highly recommended for further investigation as a source of raw material for cosmeceutical industries. The chemical composition of the neem seed oil highlights its versatility and potential for various applications. Its rich blend of fatty acids not only supports its traditional uses but also opens up new possibilities in modern industries.

6. Conflict of Interest:

Authors declares no conflict of interest.

7. References

1. Tlili N, Sarikurkcu C. Bioactive compounds profile, enzyme inhibitory and antioxidant activities of water extracts from five selected medicinal plants. *Ind. Crops Prod.*, 2020, 151, Article 112448. doi: 10.1016/j.indcrop.2020.112448
2. Ali MC, Chen J, Zhang H, Li Z., Zhao L, Qiu H. Effective extraction of flavonoids from *Lycium barbarum* L. fruits by deep eutectic solvents-based ultrasound-assisted extraction. *Talanta*, 2019, 203, 19-22. doi:10.1016/j.talanta.2019.05.02
3. Lesellier E, Lefebvre T, Destandau E. Recent developments for the analysis and the extraction of bioactive compounds from *Rosmarinus officinalis* and medicinal plants of the *Lamiaceae* family TrAC. *Trends Anal. Chem.*, 2021, 135. doi: 116158, 10.1016/j.trac.2020.116158.
4. Oguntoye SO, Ezennaya OL, Yusuff OK, Atolani O (). Eco-Friendly Formulation, Characterizations, Bioactivity studies and *in silico* evaluation of cosmetic prepared from the seed oils of *Carica papaya*, *Dacryodes edulis* and *Raphia hookeri. The*

Chemist, 2023, 94(2). Accepted - *In Press*

5. Zubair MF, Ibrahim SO, Atolani O, Hamid AA, Ibukun OJ, Abdulrahim HA. Chemical characterization, preparation of biosurfactant and biochemical evaluation of seed oil of *Luffa aegyptiaca. The Chemist*, 2022, 93(1).
6. Atolani O, Areh ET, Oguntoye OS, Zubair MF, Fabiyi OA, Oyegoke RA, Tarigha DE, Adamu N, Adeyemi OS, Kambizi L, Olatunji GA in Chemical Characterization, Antioxidant, Cytotoxicity, Anti-Toxoplasma gondii and Antimicrobial Potentials of the *Citrus sinensis* Seed Oil for Sustainable Cosmeceutical Production, Heliyon (Elsevier), 2020a, 6:2 e03399. https://doi.org/10.1016/j.heliyon.2020.e03399
7. Adeyemi KD, Abdulrahman A, Ibrahim SO, Zubair MF, Atolani O, Badmos AA. Dietary supplementation of *Tetracarpidium conophorum* (African walnut) seed enhances muscle n-3 fatty acids in broiler chickens. *Eur. J. Lipid Sci. Technol.*, 2020,1900418. doi.org/10.1002/ejlt.201900418
8. Atolani O, Oguntoye H, Areh ET, Adeyemi OS, Kambizi L. Chemical composition, anti-toxoplasma, cytotoxicity, antioxidant, and anti-inflammatory potential of *Cola gigantea* seed oil. *Pharm. Biol.*, 2019, 57(1),154-160. doi:10.1080/13880209.2019.1577468
9. Atolani O, Areh ET, Oguntoye OS, Zubair MF, Fabiyi OA, Oyegoke RA, Tarigha DE, Adamu N, Adeyemi OS, Kambizi L, Olatunji GA. Chemical composition, antioxidant, anti-lipooxygenase, antimicrobial, anti-parasite and cytotoxicity of *Polyalthia longifolia* seed oil. *Med. Chem. Res*., 2019, 22(12). https://link.springer.com/article/10.1007/s00044-019-02301-z
10. Zubair MF, Ibrahim SO, Stephen K, Hamid AA, Ibukun O, Atolani O. Synthesis and chemical characterization of alkyd resins using maleic and phthalic anhydrides and seed oil of *Luffa aegyptiaca*. *J. Turk. Chem. Soc., Sect. A*, 2023. https://dergipark.org.tr/tr/pub/jotcsa/issue/78393/1256237
11. Tomoko I, Asukai N, Konishi T, Inamoto E, Kageyama T. Mental health effects of child sexual victimization in Japan. *J. Mental Health*, 2002, *48,* 23-28.
12. Simon Ascher KR. Nonconventional insecticidal effects of pesticides available from the Neem tree, *Azadirachta indica. Insect Biochem. Physiol*., 1993, 22(3-4), 433-449.
13. Bina S, Javadi I, Iravani O. Evaluation of the repellency effect of Neem (*Melia azedarach*) plant extracts based on the Mittler & Dadd Method. *J. Agric. Chem. Environ.*, 2017,6,65-174. doi: 10.4236/jacen.2017.64011
14. Gopinath H, Karthikeyan, K. Neem in dermatology: Shedding light on the traditional panacea. *Indian J. Dermatol.*, 2021, 66(6), 706. doi: 10.4103/ijd.ijd_562_21
15. National Research Council (US) Panel on Neem. Neem: A Tree for Solving Global Problems, National Academies Press, Washington (DC), 1992, 7, Medicinals. Available from: https://www.ncbi.nlm.nih.gov/books/NBK234637/
16. Atolani O, Olabiyi ET, Issa AA, Azeez HT, Onoja EG, Ibrahim SO,

Zubair MF, Oguntoye OS, Olatunji GA. Green synthesis and characterisation of natural antiseptic soaps from the oils of underutilised tropical seed. *Sustainable Chem. Pharm.*, 2016,4,32-39. https://doi.org/10.1016/j.scp.2016.07.006

17. Atolani O, Omere J, Otuechere CA, Adewuyi A. Antioxidant and cytotoxicity effects of seed oils from edible fruits. *J. Acute Dis.*, 2012, 1, 130-134.
18. Sofowora A in Medicinal Plants and Traditional Medicine in Africa, Spectrum Books Ltd., Ibadan, Nigeria, 1993, pp 191-289.
19. Warra AA. Physico-chemical and GC/MS analysis of wild castor (*Ricinus communis*) seed oil. *Appl. Sci. Rep.*, 2015, 32(4), 55-37

The Chemist
Journal of the American Institute of Chemists

The Determination of Cefadroxil by Using Organic Reagent NQS

Hind AbdulWhaab Abdulateef[1], Dheyaa H. Ibrahim[1], Zaid H. Mahmoud[*2]

[1] Department of Chemistry, College of Education for Pure Sciences University of Diyala, Iraq
[2] Department of Chemistry, College of Sciences University of Diyala, Iraq

(E-mail: hhindabd@gmail.com, dheyaahus@gmail.com)
**Corresponding author (E-mail: zaidhameed_91@yahoo.com)*

Abstract: A simple spectrophotometric method to determine the cefadroxil has been investigated. The method is based on Schiff's base reaction of cefadroxil with 1,2-naphthoquinone-4-sulfonic acid (NQS) in an aqueous solution to give a dark yellow product for maximal absorption of 460 nm. It complied with Beer's Law with a range of 0.1 – 20 µg/ml. The limit of detection (LOD) and the limit of quantitation (LOQ) were 0.0339 and 0.169 ppm, respectively. It was found that the average recovery percent was 99.89% and 1:1 product. As the stability constant was 2.7×10^6 L/mol, this method was successfully applied for the determination of cefadroxil in the pharmaceutical formulations. The results obtained using this method are compatible with the method of the British Pharmacopoeia method.

Key Words: cefadroxil, Shiff's base

1. Introduction

Cefadroxil is an antibiotic [1] consumed and used to treat mild to moderate infections caused by susceptible microorganisms [2]. It is used to treat bacterial infection of the skin and strep throat for the urinary tract [3,4]. Figure 1 shows the structure of the drug.

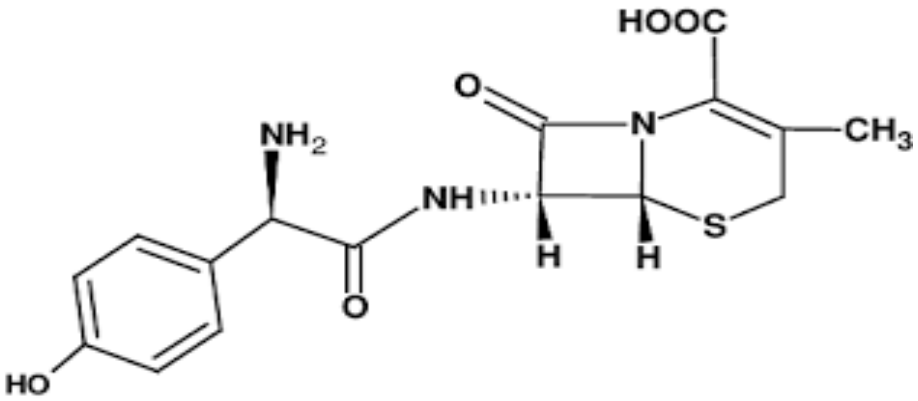

Figure 1. Structure of Cefadroxil [5]

Several scientific methods of analysis were available in the literature for the determination of cefadroxil in their pharmaceutical preparations, including fluorimetry [6] and polarography [7,8]. Thin layer chromatography [9], HPLC [10,11], sequential injection analysis [12], chemiluminescence [13,14], capillary electrophoresis [15], and spectrophotometric methods have been described to determine cefadroxil using various reagents based on the formation of complexes with copper (II) [16] Flow injection analysis (FIA) [17]. Additionally, another method is based on the liberation of hydrogen sulfide and followed by the reaction with N,N-diethyl-p-phenylenediamine [18]. Other spectrophotometric methods are reported for the determination of cefadroxil based on its reactivity with iodine [19]. Nitrosation and subsequent metal chelation reaction with 2,6-dichloro-quinone-4-aminoantipyrene in the presence of potassium hexacyanoferrate [20] or by oxidation in an acid medium [21].

These methods are time-consuming and required extraction steps or required indirect procedures. This work describes a simple and sensitive spectrophotometric method for the determination of cefadroxil. This method is based on the reaction of the drug with NQS and the formation of Schiff's base.

2. Experimental Apparatus

- Spectrophotometer using Ajena model 1100 (Germany) with a quartz cell with 1 cm path length, PW "9421" pH meter for a common glass electrode.

A meter electrical balance was used to weigh the sample. The reagent was supplied by BOH and Fluka. The standard solution of 100 ppm cefadroxil was prepared by dissolving 0.01 g in 2 ml of de-ionized water and then diluted to 100 ml. Also, 5×10^{-3} M of 1,2-naphthoquinone reagent was made by dissolving 0.06 g in 50 ml de-ionized water.

3. Results and Discussion

In a primary test, the NQS reagent reacted with cefadroxil in the presence of sodium hydroxide NaOH and formed a red color product with the highest absorption peak at 465 nm, where the reagent blank showed low absorbance at this wavelength.

4. Study of Optimal Reaction Conditions

Impact of NQS Reagent

The impact of changing the reagent 1,2-naphthoquinone solution concentration on the absorbance of cefadroxil was performed. It was noticed that the absorbance increased and reached a maximum when 1 ml of 5 × 10^{-3} M 1,2 - naphthoquinone solution was used (Figure 2).

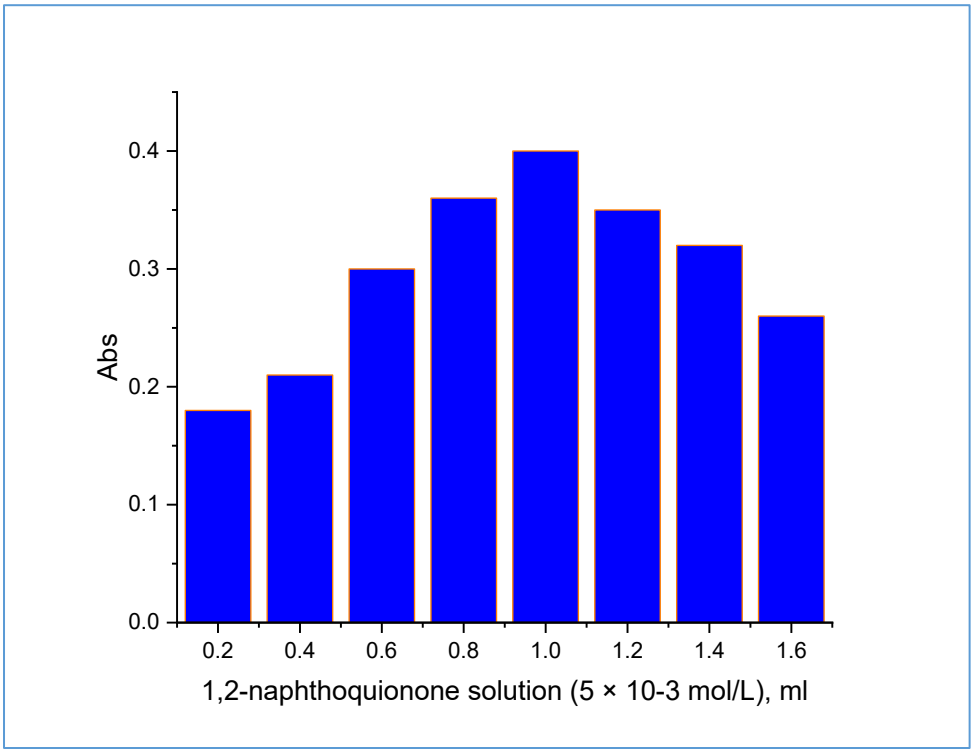

Figure 2. Impact of NQS Reagent Conc.

Impact of Base

The impact of bases (sodium hydroxide NaOH, potassium hydroxide KOH, ammonium hydroxide NH_4OH, and sodium carbonate Na_2CO_3) was investigated. It was found that potassium hydroxide gave maximum absorption at 460 nm (Figure 3).

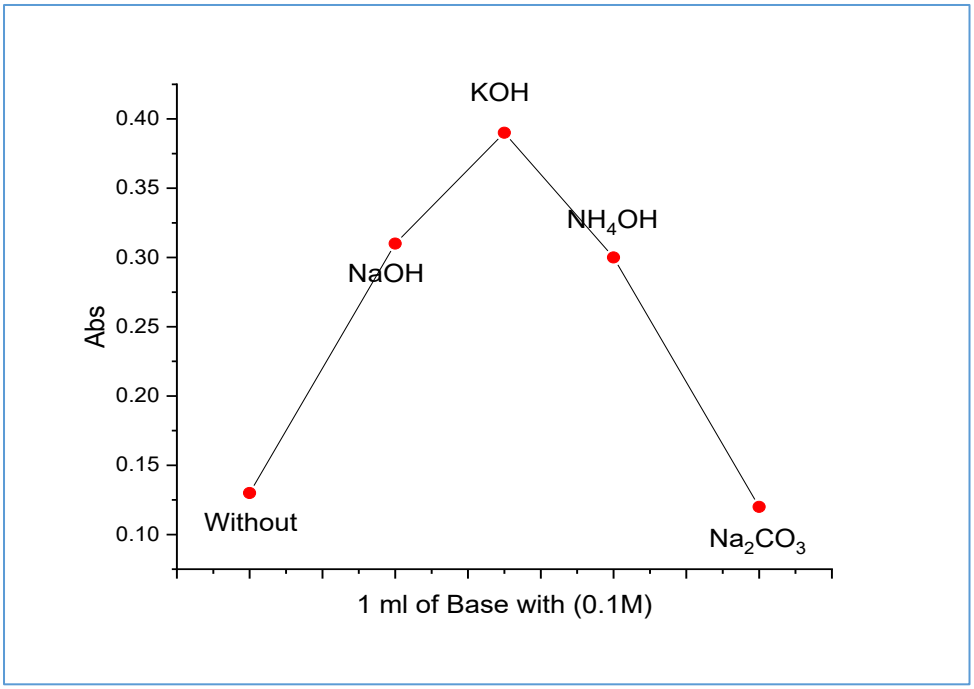

Figure 3. Bases (1 ml of 0.1M)

Furthermore, the impact of the potassium hydroxide volume and pH were studied. Maximum absorbance was observed when 1.5 ml of 0.1M KOH at pH 11.31 was used.

Table 1. The Impact of Increasing pH and the Volume of KOH 0.1 M on the Absorption of the Mixture (8 ppm Cefadroxil, NQS, KOH)

KOH V(ml)	0.5	1	1.5	2
pH	6.5	10.3	11.31	12.15
Absorbance	0.23	0.41	0.45	0.40

Impact of Surfactants

The impact of Tween 80 (TW-80), Triton X-100 (TX-100), and cetyltrimethyl ammonium bromide (CTAB) of 0.1% concentration was studied. However, the absorbance was decreased when CTAB was used (Figure 4). Therefore, it was excluded from the experiment.

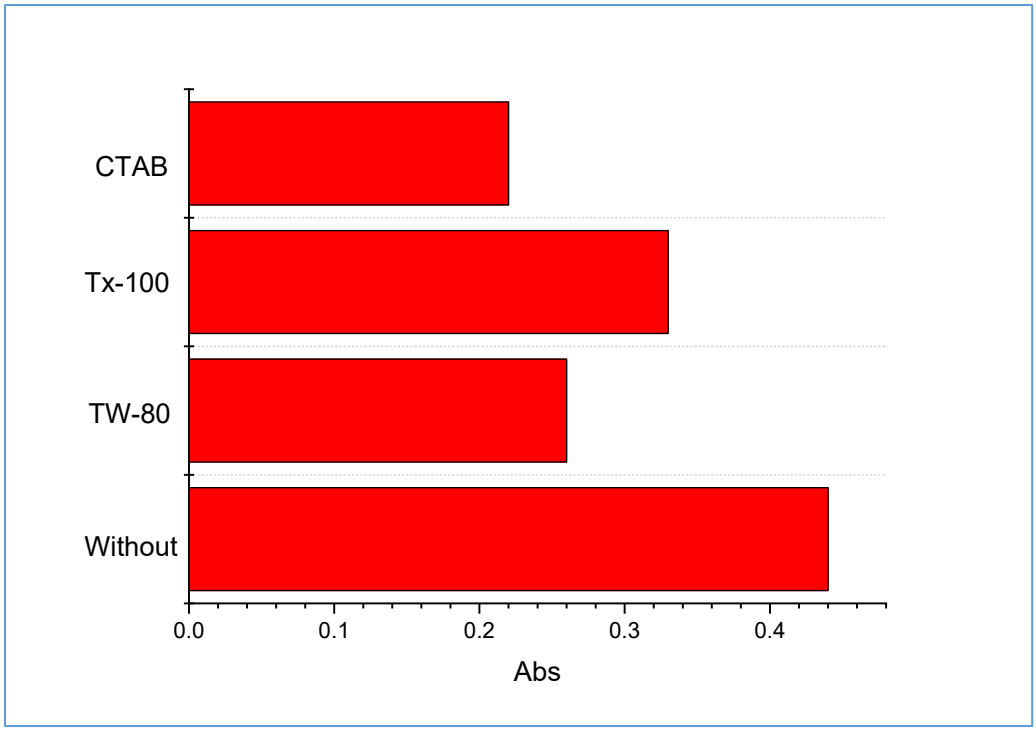

Figure 4. Impact of Surfactant on the Absorption of the Product

Impact of Temperature Versus Time on the Absorbance of the Complex

The effect of reaction time was performed at different temperatures. Figure 5 shows a decrease in the absorbance when time increased, attributed to the dissociation of the complex. It was found that the optimum time and temperature for the complex was 15 min at 40°C, respectively.

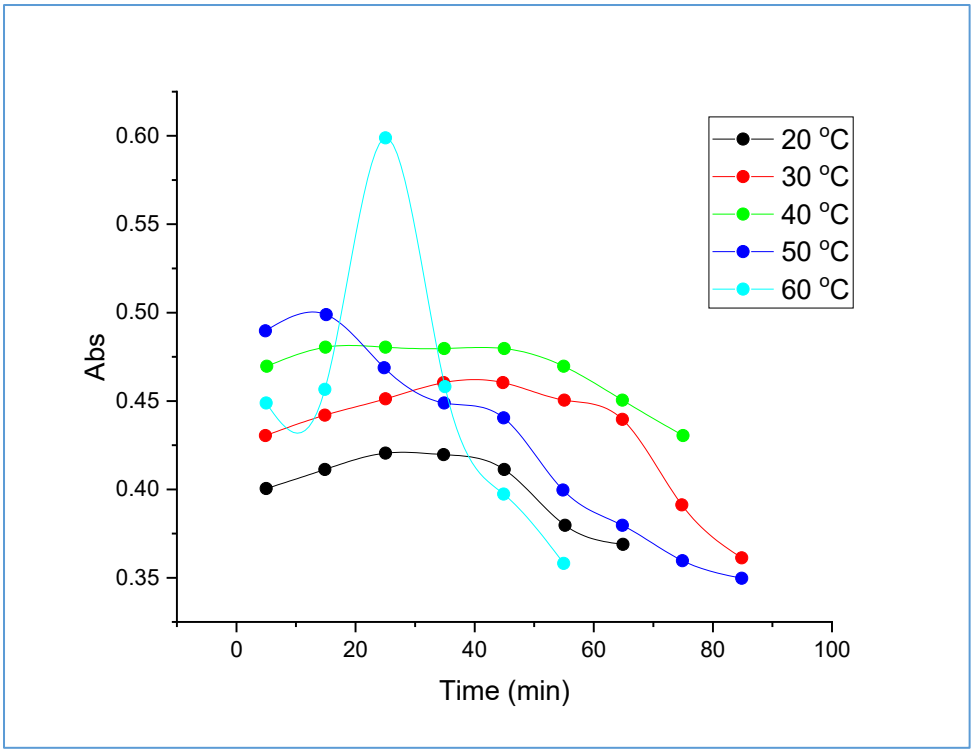

Figure 5. The Impact of Temperature Development and Time on the Stability of the Complex

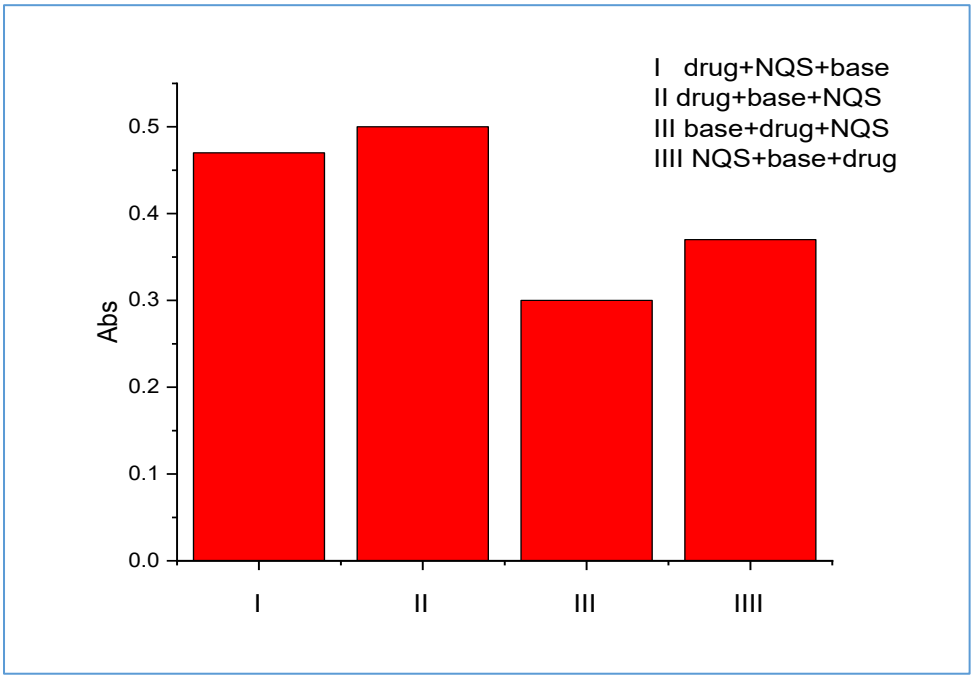

Figure 6. Impact of the Order of Addition on the Absorption

Impact of the Order of Addition

Under the optimum conditions, the order of addition was investigated. Figure 6 shows that in the order of addition, no. II was the best.

Absorption Spectra

Figure 7 shows the absorption spectra for the best condition that has been confirmed above.

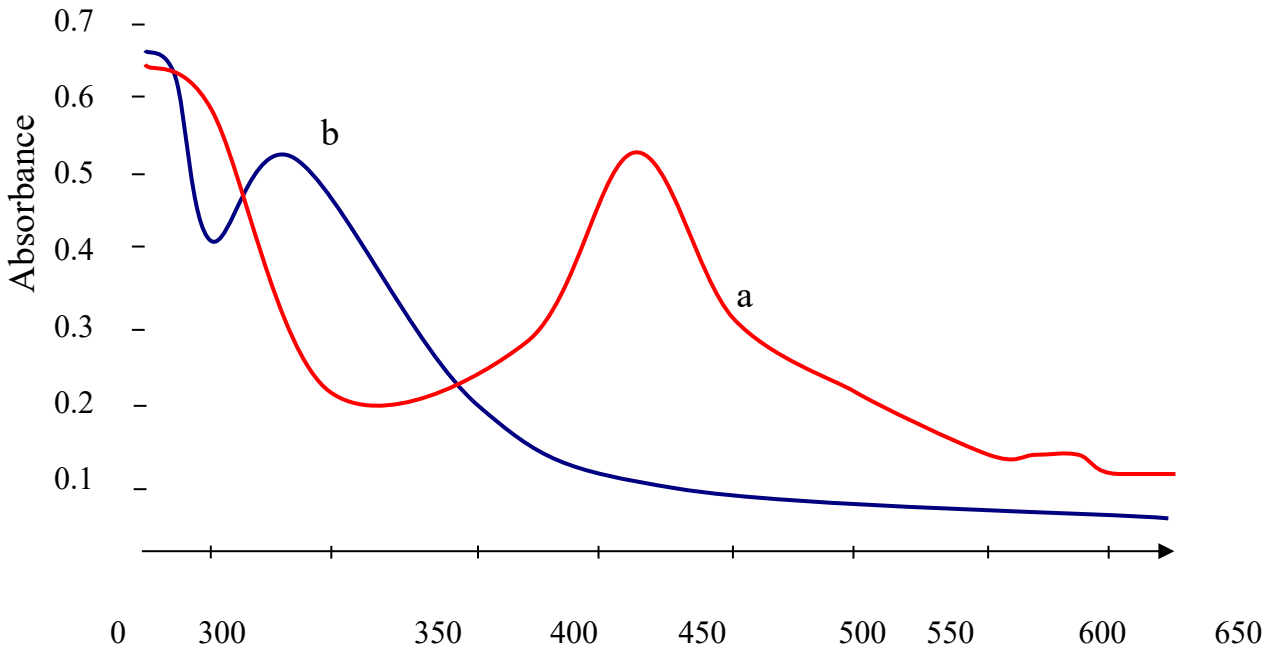

Figure 7. (a) The absorption Spectra of Cefadroxil with 1,2-Naphthoquinone Versus Reagent Blank at 460nm (b) Reagent Blank Versus Distilled Water

The Details of the Statistical Data and Optical Characteristics of the Suggested Method

The absorbance of the complex was measured at 460 nm. Beer's law limits and molar absorptivity values are shown in Table 2. In addition, the relative standard deviation (RSD) and the accuracy of analysis on six replicates for three different concentrations of cefadroxil indicate that the method is valid. Also, the limit of detection (LOD) is accepted as well.

Table 2. The Summary of Optical Characteristics

Parameter	Cefadroxil
Beer law limit (ppm)	0.1-20
Molar abs (L/mol . cm)	3.152×10^3
LOD (ppm)	0.0399
LOQ (ppm)	0.169
Average recovery percent (%)	99.89
Correlation Coefficient	0.989
Slop a	0.122
Intercept b	0.0169
R.S.D.	≤ 0.44

Analytical Implementation

The results showed that the experimental F-Test and T-Test were less than the theoretical value (t = 2.50, f = 6.41). However, it was observed that there was no significant variation between the suggested method and the formal method [22].

Quantities and Stability Constant

Quantities of a reaction of cefadroxil for NQS were studied through the molar ratio as well as job method [23,24].

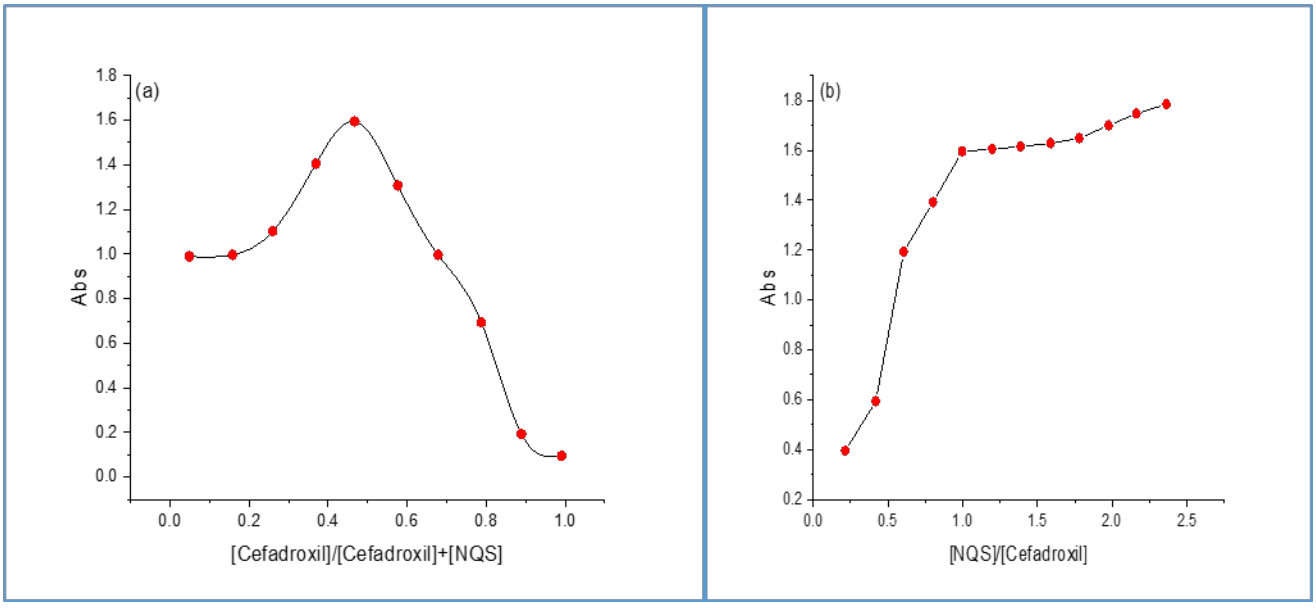

Figure 8. (a) Continuous Variations (b) Mole Ratio

Figure 8 (a) and (b) showed that the results were 1:1 and the average conditional stability constant for the resulting complex was calculated using the equation (1) below:

$$K_{st} = 1 - \propto / (\propto^2 C)$$
$$\propto = (Am - As) / (Am) \quad (1)$$

where K_{st}: the stability constant (L/mol), (∝): the dissociation degree, and (C): the concentration of the resulting complex. The average K_{st} is 2.7×10^6 which illustrates that the resulting product is stable.

Mechanism of the Reaction

Under the experimental conditions, the mechanism of the reaction is shown in Scheme 1.

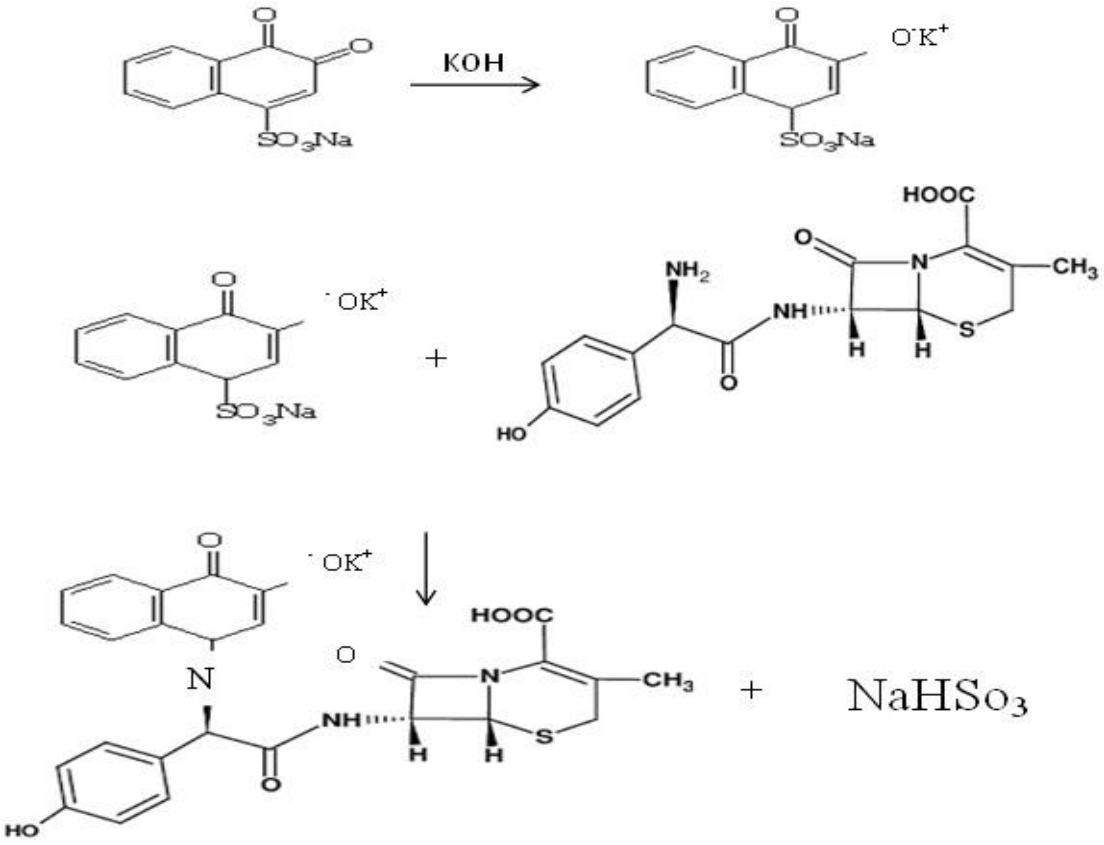

Scheme 1. The Suggested Mechanism of the Product

The mechanism suggests that the NQS was converted into a quinoidal which reacts with phenol amine via the replacement of the hydrogen atom of the primary aromatic amine group to produce paraquinoidimide-condensation (Schiff's base) $NaHSO_3$.

5. Conclusion

The suggested spectrophotometric method is simple, sensitive, and low cost. In addition, this method does not involve a solvent extraction step. Also, it gives accurate and precise results. The calibration curve shows high linearity. The coefficient correlation was higher than 0.99. The limit of detection and limit of quantitation values were very acceptable as well. Finally, the suggested mechanism of the product formation shows the NQS was converted to a quinoidal that reacts with phenol amine to produce paraquinoidimide-condensation (Schiff's base) and $NaHSO_3$.

6. References

1. Buck RE, Price KE. Cefadroxil, a new broad-spectrum cephalosporin. *Antimicrob. Agents Chemother.*, 1977, 11, 324-330.
2. Abdulrahaman AA, Metwally FH, Al-Tam ASI. Spectrophotometric assay of certain cephalosporins based on formation of ethylene blue. *Anal. Lett.*, 1993, 26, 2619-2635.
3. Badawy SS, Abdul-Gawad FM, Ibrahim MM. Spectrophotometric studies on determination of cefadroxil with copper (II) and vanadium (V) in sulphuric acid medium, *Anal. Lett.*, 1993, 26, 487-497.
4. Anjum A, Shetty SKA, Ahmed M, Sridhar BK, Vijaya KML. Development and validation of RP-HPLC method for the quantitative estimation of cefadroxil monohydrate in bulk and pharmaceutical dosage forms. *Int. J. Chem. Sci.*, 2012, 10(1), 150-158.
5. Devaliya R, Jain UK. Noval estimation of cefadroxil in tablet dosage forms by RP-HPLC. *Orient. J. Chem.*, 2009, 25(4), 1053.
6. Yang J, Zhou G, Jie N, Han R, Lin C, Hu J. Simultaneous determination of cephalexin and cefadroxil by using the coupling technique of synchronous fluorimetry and H-point standard additions method. *Anal. Chim. Acta*, 1996, 325, 195-200.
7. Abdel Gaber AA, Ghandour MA. Polarographic studies of some metal (II) complexes with cephalosporins selected from the first generation. *Anal. Lett.*, 2003, 36, 1245-1260.
8. Özkan SA, Erk N, Uslu B, Yilmaz N, Biryol İ. Study on electrooxidation of cefadroxil monohydrate and its determination by different pulse voltammetry. *J. Pharm. Biomed. Anal*., 2000, 23, 263-273.
9. Shabadi CV, Shelar BA, Shelab AR. Simultaneous determination of cephalexin acid cefadroxil in pharmaceutical preparation by quantitative thin layer chromatography. *Indian Drugs*, 1998, 35, 766-770.
10. Shinde VM, Shabadi CV. Simultaneous determination of cefadroxil and cephalexin from capsule by reverse phase HPLC. *Indian Drugs*, 1997, 34, 399-402.
11. Kano EK, Serra CHR, Koono EEM, Fukuda K, Porta V. An efficient HPLC-UV method for the quantitative determination of cefadroxil in human plasma and its application in pharmacokinetic studies. *J. Liq. Chromatogr. Relat. Technol.*, 2012, 35(13), 1871-1881.
12. Feng S, Jiang J, Fan J, Chen X.

Sequential injection analysis with spectrophotometric detection of cefadroxil and amoxicillin in pharmaceuticals. *Chem. Anal. (Warsaw, Pol.)*, 2000, 135, 191-196.
13. Sun. Y. Tang. YH. Yao H, Zheng XH. "Potassium permanganate-glyoxal chemiluminescence determination of cefadroxil antibiotics: Cefalexin, cefadroxil, and cefazolin sodium in pharmaceutical preparations. *Anal. Chim. Acta*, 2001, 422, 201-202.
14. Thongpoon, C, Liawruangrath, B, Liawruangrath S, Wheatley RA, Townshend A. Flow injection chemiluminescence determination of cefadroxil using potassium permanganate and formaldehyde system. *J. Pharm. Biomed. Anal*., 2006, 42(2), 277-282.
15. Andrasi M, Buglyo P, Zekany L, Gaspar A. A comparative study of capillary zone electrophoresis and pH-potentiometry for determination of dissociation constants. *J. Pharm. Biomed. Anal*., 2007, 44(5), 1040-1047.
16. Issopoulos PB. Spectrophotometric determination of cephalexin cephradine, ampicillin and amoxicilling using copper (II) acetate as a completing agent. *J. Pharm. Biomed. Anal.*, 1988, 6, 321-328.
17. Ródenas V, García MS, Sánchez-Pedreño C, Albero MI. Spectrophotometric methods for the determination of cephradine or ceftazidine in human urine using batch and flow-injection procedures. *J. Pharm. Biomed. Anal.*, 1997, 15, 1687-1693.
18. Abdalla MA, Fogg AG, Burgess C. Selective spectrophotometric method determination of cephalosporins by alkaline degradation to hydrogen sulphide and formation of methylene blue. *Analyst*, 1982, 107, 213-217.
19. Sastry CSP, Rao SG, Naidu PY, Srinivas KR. New spectrophotometric method for the determination of some drugs with iodine and wool fast blue BL. *Talanta*, 1998, 45, 1228-1235.
20. Salem H. Selective spectrophotometric determination of phenolic B-lactan antibiotic in pure forms and in their pharmaceutical formulation. *Anal. Chem. Acta*, 2004, 515, 333-341.
21. Sasty CS, Rao KR, Prasad DS. Determination of cefadroxil by three simple spectrophotometric methods using oxidative coupling reactions. *Microchim. Acta*, 1997, 126, 167-172.
22. British Pharma Copoeia, Version 4-CD ROM, Her Majesty's Stationery Office, 2000, pp 8-33.
23. Saurina J, Hemandez-Cassos S, Taular R. *Anal. Chem.*, 1995, 67, 3722.
24. Renny JS, Tomasevich LL, Tallmadge EH, Collum DB. Method of continuous variations: Application of job plots to the study of molecular associations in organometallic chemistry. *Angew. Chem., Int. Ed.*, 2019, 52(46), 11998-12013.

The Chemist
Journal of the American Institute of Chemists

Comparative Analysis of Graphene, Graphene Oxide, and Carbon Nanotubes as Nano-Fillers in Polymeric Anti-Corrosion Coatings: Enhancing Protection Effectiveness in Industrial Applications

M. T. A. Al-Khalidi*, A. N. Blokhin

Department of Technique and Technology for the Production of Nanoproducts
Tambov State Technical University, Leningradskaya, 1, Tambov, 392036, Russia

**Corresponding author (E-mail: mustafa_alkhalidi@mail.ru)*

Abstract: The issue of metal corrosion presents one of the most formidable challenges for various industrial sectors, including construction, marine, and oil industries. The significant risks associated with the corrosion of metals used in these applications can lead to catastrophic failures, necessitating substantial expenditure to maintain these facilities in optimal operating conditions. In response to this issue, researchers have developed numerous methods to mitigate corrosion; one of them was the use of polymeric coatings reinforced with various nano-fillers, such as carbon-based nanomaterials, being particularly prominent. This study conducted a comparative analysis to evaluate the effectiveness of graphene, graphene oxide, and carbon nanotubes in enhancing the anti-corrosion properties of polymeric coatings. The objective was to identify the most effective nano-additive based on its average anti-corrosion protection performance. The comparative results indicated that carbon nanotubes exhibited the highest performance in terms of average protection effectiveness against corrosion, followed by graphene oxide and graphene.

Key Words: anti-corrosion coatings, carbon nanotube, corrosion, graphene, graphene oxide, nano-filler

1. Introduction

The issue of corrosion of steel reinforcement and structural steel is considered one of the most important problems facing several industries, such as construction, marine, and oil industries [1,2]. Solving this issue entails large maintenance expenditures because it creates a major threat to the safety of facilities. Engineers used several solutions to tackle this issue including cathodic protection [3], concrete permeability reduction to block

corrosion agents [4], and applying anticorrosion coatings to metal surfaces [5].

Because of the significance of the corrosion problem, there have been mathematical models that predict it. For instance, Asmara and Kurniawan [6] researched the predictive models and methods of corrosion rate for carbon steel, which is a major problem in oil and gas. They also examined the environmental conditions affecting corrosion, i.e., temperature, pressure, and chemical composition, while assessing predictive models derived from experimental data and computer simulation in their research. Other researchers [7] addressed the topic of interest to most industrial processes, i.e., corrosion in mild steel when exposed to acidic environments. The researchers investigated the possibility of using readily available eco-friendly imidazolium-based ionic liquids as corrosion inhibitors. They employed both experimental techniques and theoretical models to explore inhibition mechanisms. The results show that these ionic liquids are efficient in inhibiting corrosion and that some molecular interactions are important in the process. Similarly, how metals corrode in different industry environments was explored [8]. The corrosion resistance of AISI304 stainless steel and copper when immersed in alkali (KOH and NaOH) and saline (NaCl) solutions under the electrolysis process was the subject of the experiment. They performed electrochemical tests to determine the corrosion rate of this alloy and found that it was more prone to corrosion when immersed in NaCl because of the aggressive chloride ions. Conversely, the rates of corrosion of KOH and NaOH were lower, but KOH offered more protection to the stainless steel. The authors underlined the need to select material for the intended purpose in a given industrial environment. Coatings are an intricate multi-step process rooted in basic chemistry and physics to coat metal surfaces against corrosion. In its simplest manifestation, this process is designed to create a barrier that prevents corrosive substances like chlorine, oxygen, and water ions from making contact with the metal surface and triggering destructive interactions [9,10]. Coatings like these work partly because they mechanically block electrons from the metal surface, but they also establish a barrier to the transfer of charge in general. This keeps electronic oxidation, the first stage of corrosion, from happening [11]. Through the combination of these two principles, anti-corrosion coatings can strengthen the corrosion barrier in a way that neither of them could do alone. The coating protects the corrosive chemical substances from the exposed metal surface by forming a physical barrier. At the same time, corrosion-causing electron flow is blocked by its high electrical resistance. On the surface of the metal, the coating effectively inhibits electronic oxidation reactions from starting by blocking charge transfer.

The discovery of nanomaterials and their use to improve physical and chemical properties of materials revolutionized the field of materials science since nanomaterials have more superior mechanical properties compared to their bulk counterparts. For instance, carbon nanotubes (CNTs) and graphene have superior strength, stiffness, and flexibility [12], which make them able to reinforce polymers, ceramics, and metals in composites. This results in materials of higher hardness and strength and resistance to corrosion and fatigue. At the chemical properties level, nanomaterials have a high surface-to-volume ratio, which provides more surface area for interaction with their surrounding environments [13]. It should be remembered that nanomaterials have played a very important role in improving the physical properties of many coatings, for example, improving thermal conductivity

and optical absorption [14] in solar collector coatings, resistance to ultraviolet radiation [15], fungi and bacteria resistance [16], and corrosion resistance [17].

In this regard, collective research endeavors have been made to explore the intricate dynamics among various nano-additives and how they enhance the anti-corrosion properties of the coating. A core research interest in this regard is nanoparticles (NPs) developed from metals or their oxides. These NPs have been comprehensively studied to determine their role in enhancing the anti-corrosion properties of coatings [18]. Also, the work includes nanoparticles from carbon-based materials, i.e., graphene and carbon nanotubes, which are greatly prized for their excellent mechanical, electrical, and chemical properties. The work has included both these pure carbon materials and their oxides, i.e., graphene oxide. Following our earlier work [18], we investigated the influence of adding metal or metal oxide nanoparticles on the anti-corrosion behavior of coatings.

This work intends to compare the impact of integrating diverse carbon-based NPs, namely graphene, graphene oxide, and carbon nanotubes, on the anti-corrosion capabilities of polymeric coatings. We aim to determine the most effective nano-additive for increasing corrosion resistance by assessing its impact on barrier characteristics, mechanical reinforcement, and overall protective efficacy. The results will yield remarkable insights into the ideal selection of nano-fillers for the formulation of sophisticated anti-corrosion coatings.

2. Experimental

In our study, a comparative analytical methodology was used to examine the results obtained from previous studies conducted by researchers in the field of anti-corrosion coatings research, specifically those involving the effect of carbon nanomaterials on anti-corrosion properties. In order to compare the protection effectiveness resulting from coatings modified with different carbon nanomaterials, the protection effectiveness provided by these coatings was calculated based on the corrosion current values before and after applying the modified coating (these values are mentioned in the studies we discussed in this review or in the supplementary materials attached to those studies).

3. Results and Discussion

The incorporation of carbon NPs into polymeric coatings has demonstrated huge potential in the enhancement of corrosion resistance, which leverages the distinctive physical and chemical properties of materials such as graphene, carbon nanotubes (CNTs), and graphene oxide (GO). Graphene, characterized by high electrical conductivity, exceptional mechanical strength, and a large surface area, enhances corrosion resistance through its impermeable nature and effectively blocks the diffusion of corrosive agents like water and oxygen. Similarly, CNTs improve anti-corrosion properties by

forming a reinforcing network within the polymer matrix due to their outstanding tensile strength and flexibility. Thereby, the structural integrity and hindering the movement of corrosive substances are increased. Overall, it can be stated that carbon-based NPs introduce a more tortuous path for corrosive agents that reduce their penetration rate and modify the electrochemical properties of the coating to enhance corrosion resistance. Additionally, the mechanical properties of the coating are improved, which gives more resilience to physical damage that could expose the underlying metal. The following sections explore the materials mentioned above.

Graphene

Graphene-modified anti-corrosion coatings have emerged as a highly effective solution to enhance the durability and longevity of materials exposed to corrosive environments. Incorporating graphene into polymeric coatings enhances its physical and chemical properties; this leads to noticeable improvements in wear resistance. The incorporation of graphene into the polymeric coating matrix increases its corrosion resistance through two mechanisms. The first mechanism is termed the barrier effect, which is one of the strongest mechanisms for corrosion protection. On this basis, the impermeable nature of graphene prevents the diffusion of corrosion-causing agents such as water, oxygen, and salts. This decreases the rate with which these agents seep down to the supporting mineral substrate markedly. The other is mechanical strengthening, where the polymer matrix receives a reinforcement through the addition of graphene to augment its mechanical stiffness. Here, the possibility for cracks and faults that expose metal to corrosive substances is curbed.

In another study by Gao et al. [19], an oil-based epoxy resin (OEP) coating modified with graphene (G/OEP) was synthesized to enhance corrosion resistance of AZ31 magnesium alloy. In this study, the potential benefits of using graphene in epoxy resin coatings in surface finish, structure, and protection were taken into consideration. AZ31 magnesium alloy was coated with G/OEP, i.e., graphene-modified oil-based epoxy resin, for this study. For comparison of the coatings that had been modified using graphene with the unmodified coatings, as well as for detecting surface defects, scanning electron microscopy (SEM) observations were also conducted. Surface finish of the coating and defect reduction were both enhanced by the addition of graphene, as revealed through SEM micrographs. FTIR spectroscopy analysis of the coating composition ensured that the coatings were primarily composed of epoxy (polyurethane) resin and its curing agent, with the addition of graphene incorporated in the matrix successfully. The corrosion resistance of the coatings was also assessed using electrochemical measurements. The results indicated that the G/OEP coatings provide excellent corrosion protection, as the corrosion current density of the magnesium alloy reduced from 6.20×10^{-7} A/cm^2 (0 wt.% graphene) to 6.96×10^{-12} A/cm^2 (0.6 wt.% graphene) upon the application of the G /OEP coatings, which increased the protective efficiency to 99.99%. Finally, a post-corrosion morphology analysis was performed to examine the structural integrity of the coating after being subjected to electrochemical corrosion. The analysis aimed to assess the extent of structural damage and determine the role of graphene in enhancing the protective nature of the coating against corrosive media. The results indicated that graphene significantly

improved the corrosion resistance of the coating by reducing structural damage. The incorporation of graphene effectively sealed micro-defects in the coating upon curing, hence inhibiting the uptake of corrosive materials and enhancing the durability and protective efficacy of the coating as a whole.

In a study by Xu et al. [20] for enhanced anticorrosion properties of composite coatings, E44 waterborne epoxy resin was used as the matrix material, and graphene was incorporated as a nano-filler. The investigation focused on studying the structure and electrochemical response of such composite coatings with a view to studying the contribution of graphene toward increased corrosion resistance. To characterize the graphene, X-ray diffraction (XRD) and transmission electron microscopy (TEM) were used. The resulting structure is a thin pile of graphite sheets with many wrinkles, and it improves the coating performance. Graphene-epoxy coatings were found to have a flawless surface according to SEM. This was attributed to the ability of the graphene to effectively fill micro-pores and internal micro-cracks, thus strengthening the coating and making it more protective. The FTIR test results indicated that the composite coatings were primarily composed of epoxy resins with polyamide curing, in which the characteristic peaks according to the materials used. Finally, the result of electrochemical testing, particularly the Tafel polarization curves, indicated that it raised the corrosion potential and reduced the corrosion current when more graphene was incorporated. Therefore, the corrosion resistance was ultimately enhanced. The intensity of the corrosion current decreased from 1.2×10^{-3} A·cm^{-2} in the case of pure epoxy to 7.6×10^{-5} A·cm^{-2} in the case of epoxy with 0.6 wt.% nano-filler, which means an increase in the effectiveness of protection by 93.67%. However, the electrochemical impedance spectroscopy (EIS) results showed that graphene increased the impedance arc in Nyquist plots and impedance modulus at low frequencies, confirming the improvement in corrosion resistance. The study concluded that the improved mechanism of corrosion protection by graphene is attributed to the improved barrier performance of the coating because graphene clogs the pores in the coating matrix. Thus, penetration of the corrosive substance was avoided, and the general long-term stability of the coating was improved.

Suharyadi et al. [21] studied the effect of graphene and epoxy coatings as corrosion inhibitors on carbon steel plate substrates used in heat exchangers in the oil and gas industries. Several coating samples were prepared with different mass concentrations of graphene/epoxy (0%, 2%, 5%, and 10%), and the coating was applied to the substrates using the bath method. The corrosion behaviors of substrates immersed in 1 M sulfuric acid solution at room temperature were studied using dynamic polarization. Experimental results indicated that graphene and epoxy coatings are effective in inhibiting corrosion. The dynamic polarization potential curves showed that the corrosion potential of coated carbon steel turned to more positive values than that of uncoated carbon steel. The study also found that corrosion current densities and corrosion rates decreased by up to 36 times. This improvement was attributed to the enhanced barrier effect of the coating, achieved by filling its pores with well-dispersed graphene nanoparticles. This modification reduced the permeability of the graphene-epoxy coating to ions and other corrosive species in acidic solutions, ultimately increasing its protective effectiveness to 97.23%.

In another study [22], an anticorrosion coating composed of a polyeugenol/graphene

(PE/G) composite was developed, and its effectiveness in protecting metals from corrosion was evaluated. Here, several methodologies were used to synthesize and evaluate the PE/G composite. Polyeugenol was synthesized via cationic addition polymerization using $BF_3O(C_2H_5)_2$ as a catalyst, while graphene was produced through the chemical reduction of GO using the Hummers' method. The PE/G composite was prepared at various weight concentrations (0.25 wt.%, 0.5 wt.%, 0.75 wt.%, 1 wt. %, and 1.25 wt.%.) using a solution mixing method and applied to metal substrates via drop-casting. To assess the anticorrosion performance, the researchers used potentiodynamic polarization techniques, which involved measuring the electrochemical behavior of the coated metals in a 3.5% sodium chloride solution. The PE/G composite exhibited superior corrosion resistance compared to unmodified polyeugenol, as the addition of graphene reduced the corrosion current density from 4.0239 $\mu A \cdot cm^{-2}$ at 0 wt.% to 1.3854 $\mu A \cdot cm^{-2}$ at 1.25 wt.% of graphene, leading to a protection efficiency increase of up to 78.42%. Morphological analyses were conducted using SEM which revealed that the PE/G coated metals had a defect-free surface and the graphene was effectively filled within the micro-pores and micro-cracks. XRD analysis was also performed, and the obtained results confirmed the absence of corrosion products on the PE/G-coated metals after exposure to the corrosive environment.

Accordingly, the studies reviewed clearly show that graphene has a great ability to improve corrosion-resistant properties, as the average protection effectiveness is about 96.963%.

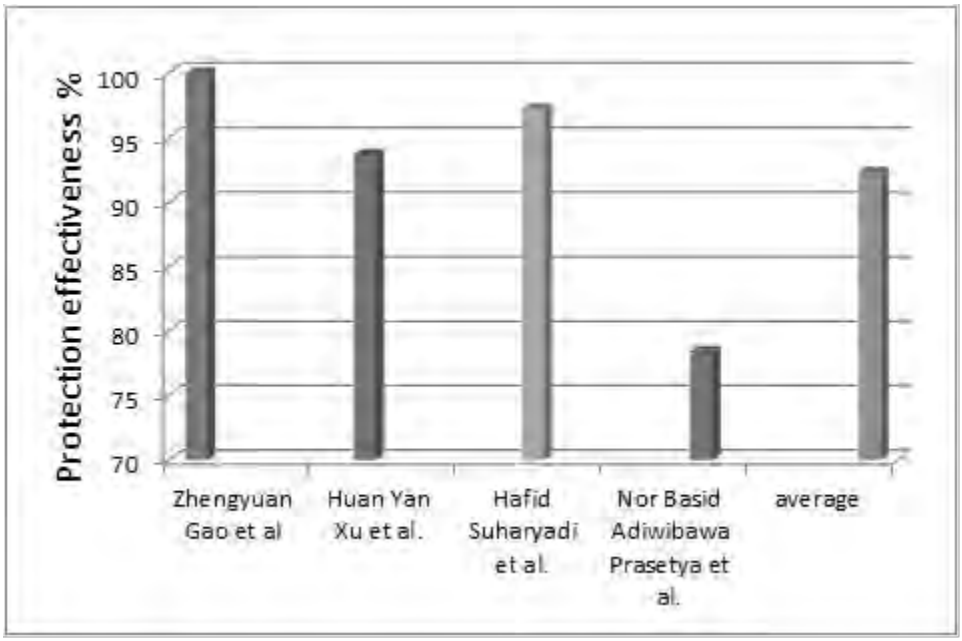

Fig. 1. The Values of the Corrosion Protection Effectiveness of Graphene-containing Coatings in Reviewed Studies and the Average Value

Figure 1 shows the values of the corrosion protection effectiveness of graphene-containing coatings and the average value of selected studies.

Graphene Oxide (GO)

Due to the unique properties of graphene oxide (GO), such as high surface area, excellent mechanical strength, and excellent barrier properties, it has been one of the most promising additives to enhance the performance of corrosion-resistant coatings. GO is a graphene derivative that contains oxygen functional groups, such as hydroxyl, epoxide, carbonyl, and carboxyl groups, which enhances its dispersibility in water and organic solvents. These functional groups also allow GO to form strong interactions with polymer matrices and make it an excellent candidate for composite coatings. The high aspect ratio of GO creates tortuous paths that impede the diffusion of corrosive agents, greatly improving the barrier properties of the coating.

Regarding corrosion resistance mechanisms, the effectiveness of GO in corrosion-resistant coatings can be attributed to several mechanisms. The first one is the barrier effect, where the layered structure of GO increases the diffusion of corrosive species. Here, a delay in the penetration of water, oxygen, and ions occurs. The second mechanism is its self-healing properties, as some studies [23-25] indicate that combining GO with some polymers can contribute to repairing small cracks independently and prolong the life of the coating. The third is the synergistic effects with polymers, where GO can interact with polymer matrices to enhance their mechanical properties and adhesion to substrates, and the coating failure is possibly reduced.

In their study, Jiang et al. [26] investigated the corrosion resistance behaviors of epoxy composite coatings reinforced with GO. They focused on understanding how varying aspect ratios of GO influence the corrosion resistance properties of the coatings. To achieve this, the researchers prepared epoxy composite coatings by incorporating GO with different aspect ratios. The study sought to understand better how GO's structural properties affect its ability to improve composite coatings' anti-corrosion performance. As a result, valuable insights that can be used to optimize the design of advanced protective coatings were gained. The researchers used a modified Hammers method to synthesize GO in different aspect ratios. They then mixed it with an epoxy resin matrix at a concentration of 0.1 weight percent. The composite coatings were applied to sandblasted carbon steel metal substrates. To evaluate the corrosion resistance performance, a series of electrochemical tests were performed, including dynamic polarization and EIS, the results of which indicated that the aspect ratio of GO highly affected the corrosion resistance of epoxy composite coatings, where coatings with a higher aspect ratio of GO had superior corrosion resistance. The corrosion current densities decreased significantly from 3.115×10^{-7} $A \cdot cm^{-2}$ for GO-c to 1.164×10^{-8} $A \cdot cm^{-2}$ for GO-a, which demonstrates a substantial improvement in protection effectiveness of approximately 97.71% compared to the neat epoxy coating. Concurrently, the complex impedance values increased from 2×10^6 to 4×10^7, further confirming the enhanced barrier properties and corrosion resistance of the GO-reinforced epoxy composite coatings. In addition, the surface morphology and structural properties of the coatings were examined using SEM and TEM. These analyses determined that there was a rise in the uniformity and defect-free surface of the coating as the GO aspect ratio was greater. This increased structural integrity signifi-

cantly contributed to the barrier nature of the coatings, which ensured that the corrosive agents were not able to penetrate and added further to the overall corrosion resistance of the composite coating. The study concluded that increasing the aspect ratio of GO in epoxy composites is vital in order to make the corrosion resistance more efficient.

In another research conducted by Yang et al. [27], the *in situ* polymerization method was used for preparing GO/polyaniline (GO/PANI) nanocomposites with unique anti-corrosion properties. In this research, epoxy/GO coating samples were prepared. In order to characterize the different samples, surface morphology of the materials was studied using SEM, whose images revealed that pure GO had flaky structure with a folded and smooth surface. For understanding corrosion resistance, EIS measurements and dynamic polarization curves were carried out. The findings of these tests indicated that the incorporation of graphene caused E_{corr} to rise from −0.704 volts for the neat epoxy to −0.548 volts for the epoxy/GO. Additionally, corrosion current density (I_{corr}) was decreased from 3.64×10^{-4} A/cm^2 for pure epoxy to 1.79×10^{-8} A/cm^2 for epoxy/GO, which can be an indication of 99.99% improvement in protection efficiency.

In another study, Irfan et al. [28] explored the performance of a new anti-corrosion and environmentally friendly coating was developed and evaluated. The study focused on the utilization of a hybrid nanocomposite coating that includes composite green NPs and biopolymers to enhance corrosion resistance on metal substrates. The methodology involved the NPs synthesis process using plant extracts as reducing agents, and then nano-hybrid coatings were prepared by dispersing the composite NPs in a biopolymer matrix. Electrochemical methods, including dynamic polarization and EIS, evaluated the corrosion resistance of the coatings. Experimental results showed that nano-hybrid coatings improved the corrosion resistance of metal substrates, where electrochemical tests revealed that the coatings effectively reduced the I_{corr}, as its value decreased from 1.767×10^{-7} A·cm^{-2} for the coating without nano-filler to 7.736×10^{-9} A·cm^{-2} for the coating with nano-filler, which means the effectiveness of protecting the coating against corrosion increased by 95.62%, and the impedance value (E_{corr}) increased from -0.476 volts for the paint without nano-filler to -0.191 volts for the coating with the NPs filler, indicating enhanced protective properties. SEM and TEM analyses showed that the NPs were well dispersed within the polymer matrix, which contributed to a uniform and defect-free coating surface.

In a study by Huang et al. [29], waterborne epoxy coatings with enhanced wear resistance were developed by incorporating NPs of aluminum oxide (Al_2O_3), GO, and hybrid Al_2O_3@GO. In order to prepare composite coatings, the modified NPs were dispersed in waterborne epoxy resin, where different concentrations of these NPs (1.5 wt.% for Al_2O_3, 0.2 wt.% for GO, and 0.4 wt.% for Al_2O_3@GO) were used to create different composite layers. Then, to characterize the samples, the researchers used several techniques to characterize the surface morphology and the morphology of NPs. The SEM images showed the presence of ripples in a large area of the GO sheets, which represents a stacked state, where the GO sheets were strongly assembled into a stacked shape with a width of micrometers. Regarding corrosion resistance tests, dynamic polarization tests and electro-chemical impedance spectroscopy were conducted to evaluate the coatings in a 3.5% sodium chloride solution. The results showed that coatings that contain GO showed

superior corrosion resistance compared to neat epoxy coatings. The value of the corrosion potential E_{corr} increased from −0.760 V in the case of neat epoxy to −0.354 V in the case of 0.4% epoxy/GO coating. Also, the value of the I_{corr} decreased from 1.235×10^{-5} A·cm^{-2} in the case of neat epoxy to 1.697×10^{-6} A·cm^{-2} in the case of 0.4% epoxy/GO coating. These results indicate an increase in protection effectiveness by 86.26%. The improved performance is attributed to the better barrier properties and lower permeability provided by the well-dispersed NPs.

Accordingly, the studies reviewed clearly show that GO has a great ability to improve corrosion-resistant properties, as the average protection effectiveness is about 94.895%. Figure 2 below shows the values of the corrosion protection effectiveness of GO-containing coatings and the average value of selected studies.

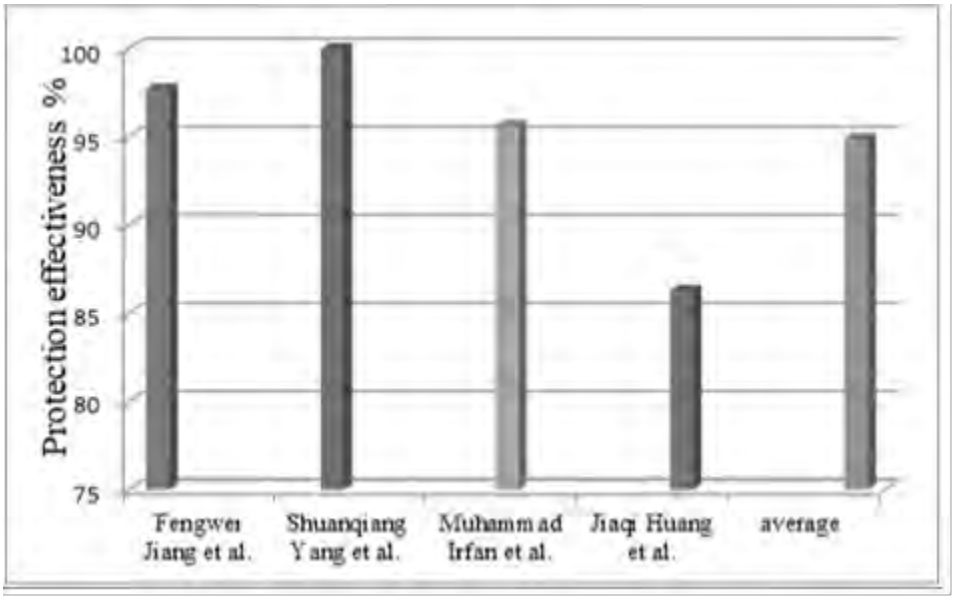

Fig. 2. The Values of the Corrosion Protection Effectiveness of GO-containing Coatings in Reviewed Studies and the Average Value

Carbon Nanotubes

Carbon nanotubes (CNTs) show promise as an additive in anti-corrosion paints due to their high mechanical properties due to their high tensile strength and better chemical properties like chemical inertness. These features make CNTs suitable candidates to enhance the performance of anti-corrosion coatings. CNTs aid corrosion protection by multiple mechanisms, for which the most important one is the barrier effect. CNTs create a dense and impermeable network within the coating matrix, which increases the diffusion of corrosive species such as water, oxygen, and chloride ions to the substrate.

The mechanical strengthening mechanism is another critical parameter in which CNTs enhance the corrosion resistance of the coating. By enhancing the mechanical

properties of the coating, CNTs become physically more robust and reduce the risk of exposing the metal substrate to corrosive conditions. In a study by Kong et al. [30], a corrosion-resistant polymeric coating composed of polyurethane and CNTs was prepared. The study was focused on the effectiveness of using NPs in improving the mechanical and anti-corrosion properties of such coatings. In preparation of the coating, the researchers incorporated NPs into the polymeric matrix, with varying concentrations of NPs used to find the optimal formulation for optimal performance. SEM analysis was performed to examine the surface morphology, and dispersion of NPs within the coatings. The NPs were homogenously dispersed in the images, adding to the global properties of the coating. They were uniformly distributed in the polymeric matrix and formed defect-free coatings. Corrosion protection of the coatings for electrochemical tests was analyzed using methods such as Tafel polarization and EIS. Electrochemical analysis showed that the addition of CNTs caused an increase in the E_{corr} from −0.54 V for the plain coating to −0.38 volts for the 3% CNTs-containing paint. The value of the I_{corr} decreased from 5.24×10^{-7} A·cm^{-2} in the case of coating without nano-fillers to 8.94×10^{-9} A·cm^{-2} in the case of the coating of 3.0% of CNTs, which means an increase in protection effectiveness of 98.29%.

In another study [31], a corrosion-resistant coating composed of epoxy coating and functionalized CNTs was developed and evaluated to enhance the corrosion resistance of aluminum alloys. The primary goal was to explore the effectiveness of incorporating these NPs into epoxy coatings to improve their mechanical properties and protect aluminum substrates from corrosive environments. To prepare the coating, the researchers incorporated functionalized CNTs into an epoxy matrix by dispersing the modified NPs in epoxy resin. The mechanical stirring and ultrasonic dispersion techniques were used after these NPs had been modified with appropriate chemical treatments to enhance their dispersion and compatibility with the epoxy resin. Finally, the resulting nanocoatings were applied to aluminum alloy substrates using spray coating processes. Also, SEM was used to characterize the surface morphology and ensure uniform dispersion of the NPs within the coatings. The SEM images showed that running the NPs led to their excellent dispersion within the epoxy matrix, as the nanocomposite coatings had a uniform surface free of defects. For electrochemical tests, techniques such as Tafel polarization and EIS have been used to evaluate the corrosion resistance of the coating. These tests were performed in a 3.5% sodium chloride solution to simulate a corrosive environment. Electrochemical tests indicated a significant improvement in the corrosion resistance of the nanocoatings compared to the unmodified epoxy coatings. The Tafel polarization curves showed a huge decrease in the corrosion current density, as its value decreased from 7.155×10^{-7} A·cm^{-2} in the case of the neat epoxy coating to 4.050×10^{-9} A·cm^{-2} in the case of the coating containing 0.25% CNTs, where the effectiveness of corrosion protection reached 99.43%. The EIS results also showed an increase in impedance, as the E_{corr} value increased from −0.594 V in the case of the neat epoxy coating to −0.001 V in the case of the coating containing 0.25% CNTs, which indicates better barrier properties of the coatings.

In a similar context, Al-Gamal et al. [32] developed a polymeric coating made of polyaniline (PANI) and alkyd resin containing multi-wall carbon nanotubes (MWCNTs) to enhance their corrosion resistance properties. To prepare the coating, the

researchers chemically modified CNTs to improve their dispersion and compatibility with polyaniline resins. Then, different concentrations of functionalized CNTs were then incorporated into the PANI resin matrix. After this, coatings were prepared by mixing short alkyd resin as a binder with selective dyes for several pigment/binder mixing ratios, and then the solvent, which is xylene, was added at a rate of 15% by weight. Finally, the paint was applied to the carbon steel with a brush to prepare the samples. The SEM images confirmed the uniform distribution of CNTs in the coating matrix. Additionally, the corrosion resistance of the coating was characterized by electrochemical tests, in which Tafel polarization was performed. The results of this test indicated an improvement in the corrosion resistance of the coating containing the nanocomposite PANI/MWCNTs compared to the unmodified coating, where Tafel polarization curves showed a significant decrease in the I_{corr}, as its value decreased from 5.99 μA in the case of PANI/alkyd coating to 1.030 μA in the case of (PANI-MWCNTs)/alkyd 3% coating, which indicates enhanced protection against corrosion as it was protection effectiveness of 82.81%.

A corrosion-resistant coating was prepared to protect aluminum surfaces [33]. The coating consisted of a sol-gel of N-propyl-trimethoxy-silane filled with different amounts of MWCNTs. The coating was applied to aluminum substrates by drop casting. The SEM images showed that a uniform gel coating with a content of 0.4 wt.% CNT was obtained. Low or high nanotube contents cause non-homogeneity of nano-filler distribution in the coating. The corrosion resistance using dynamic polarization and electrochemical impedance analysis when immersed in 3.5 wt.% sodium chloride was also characterized. The results of the analysis of dynamic polarization curves indicated a decrease in the I_{corr}, as its value decreased from 0.8×10^{-2} mA/cm^2 in the case of the coating without nano-fillers to 1.0×10^{-5} mA/cm^2 in the case of AS3-CNT6 nano-fillers, which means increased protection effectiveness by 99.875%. The electrochemical impedance analysis results indicated a decrease in the E_{corr} value from -1.210 volts for the paint without nano-fillers to −0.220 volts for the AS3-CNT6 nano-fillers.

Accordingly, the studies reviewed clearly show that CNTs can improve the corrosion-resistant properties of coatings, as the average protection effectiveness value is about 95.10%.

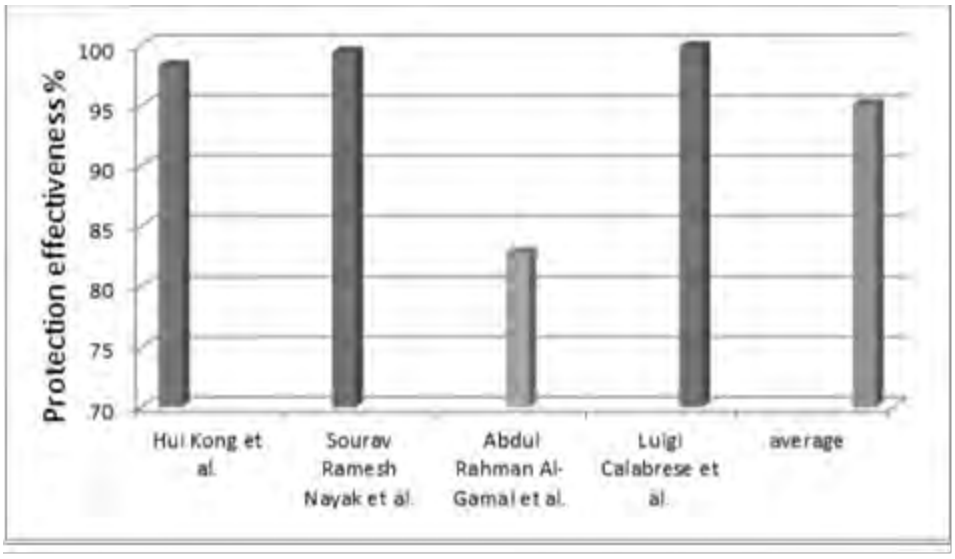

Fig 3. The Values of the Corrosion Protection Effectiveness of CNTs-containing Coatings in Reviewed Studies and the Average Value

Figure 3 shows the corrosion protection effectiveness of CNT-containing coatings and the average value.

It is worth noting that the results of the studies showed that the modification of polymeric coatings using CNTs provided the highest performance in reducing corrosion, followed by GO and, finally, graphene. The average improvement in protection effectiveness supports this finding. This can be attributed to the unique structure of carbon nanotubes (CNTs), which, as one-dimensional (1D) particles, can occupy spaces in the polymer matrix that two-dimensional (2D) graphene oxide (GO) or graphene particles cannot. As a result, CNTs exhibit a greater ability to enhance the barrier effect compared to GO or graphene particles.

On the other hand, the dispersion of GO could be better than the dispersion of graphene in the polymer matrix. This can be attributed to several reasons, the most important of which is that GO contains different oxygen functional groups, such as hydroxyl and carboxyl groups, which enhance its interaction with polymer matrices. The absence of functional groups in graphene could also lead to large van der Waals forces between individual graphene sheets and cause aggregation in the polymer matrix. These forces are greatly weakened when graphene is oxidized, which improves its dispersion in the coating matrix. This, in turn, improves the barrier effect, which leads to improved protection effectiveness of the coating.

4. Conclusion

This research presents a comprehensive review of the impact of incorporating carbon nanomaterials, specifically graphene, GO, and CNTs, as fillers within polymer-based corrosion-resistant coatings on the corrosion resistance properties of these coatings. Based on data from the relevant literature, the average protection effectiveness of each type of nanomaterial was determined. The analysis revealed that CNTs offered the highest

corrosion reduction performance, followed by GO and graphene. The variation in protection effectiveness for the same type of additive can be attributed to several factors, primarily the type of polymer forming the host matrix. Differences in polymer composition influence its bonding with the nano-additive, while the polymer matrix density affects the amount of nano-filler that can be incorporated without causing agglomeration. Achieving a stable, homogeneous coating enhances its ability to form an effective barrier against corrosive agents. This study provides researchers with insights for selecting the most suitable type of nano-filler for the host coating matrix.

5. References

1. Corrosion Science: Theoretical and Practical Applications, eds. Savas Kaya, Ime Bassey Obot, Demet Özkir, Goncagül Serdaroglu, Ambrish Singh, CRC Press, Florida, 2023. https://doi.org/10.1201/9781003328513
2. Al-Moubaraki AH, Obot IB. Corrosion challenges in petroleum refinery operations: Sources, mechanisms, mitigation, and future outlook. *J. Saudi Chem. Soc.*, 2021, 25(12), 101370. https://doi.org/10.1016/j.jscs.2021.101370
3. Solovyeva VA, Almuhammadi KH, Badeghaish WO. Current downhole corrosion control solutions and trends in the oil and gas industry: A review. *Materials*, 2023, 16(5), 1795. https://doi.org/10.3390/ma16051795
4. Mohtasham MM, Rahmati K, Saradar A, Moon J, Karakouzian M. A critical review examining the characteristics of modified concretes with different nanomaterials. *Materials*, 2024, 17(2), 409. https://doi.org/10.3390/ma17020409
5. Figueira RB. Hybrid sol–gel coatings for corrosion mitigation: A critical review. *Polymers*, 2020, 12(3), 689. https://doi.org/10.3390/polym12030689
6. Asmara YP, Kurniawan T. Corrosion prediction for corrosion rate of carbon steel in oil and gas environment: A review. *Indones. J. Sci. Technol.*, 2018, 3(1),64-74. http://dx.doi.org/10.17509/ijost.v3i1.10808
7. Ech-Chihbi E, El Hajjaji F, Titi A, Messali M, Kaya S, Serdaroğlu G, Hammouti B, Taleb M. Towards understanding the corrosion inhibition mechanism of green imidazolium-based ionic liquids for mild steel protection in acidic environments. *Indones. J. Sci. Technol.*, 2024, 9(2), 395-420. https://doi.org/10.17509/ijost.v9i2.68764
8. Hamidah I, Solehudin A, Setiawan A, Hamdani A. Corrosion study of AISI 304 on KOH, NaOH, and NaCl solution as an electrode on electrolysis process. *J. Eng. Sci. Technol.*, 2018, 13(5), 1345-1351.
9. Isecke B, Schütze M, Strehblow HH in Springer Handbook of Metrology and Testing, eds. Horst Czichos, Tetsuya Saito, Leslie Smith, Springer, Berlin, 2011, Corrosion, p 667. https://doi.org/10.1007/978-3-642-16641-9_12
10. Mousa OI, Al-Luaibi SS, Al-Mubarak AS, Lgaz H, Hammouti B, Chaouiki A,

Ko YG. On the development of an intelligent poly(aniline-co-o-toluidine)/Fe_3O_4/alkyd coating for corrosion protection in carbon steel. *Appl. Sci.*, 2023, 13(14), 8189. https://doi.org/10.3390/app13148189

11. Ghaderi M, Bi H, Dam-Johansen K. Advanced materials for smart protective coatings: Unleashing the potential of metal/covalent organic frameworks, 2D nanomaterials and carbonaceous structures. *Adv. Colloid Interface Sci.*, 2023, 323(1), 103055. https://doi.org/10.1016/j.cis.2023.103055
12. Papageorgiou DG, Li Z, Liu M, Kinloch IA, Young RJ. Mechanisms of mechanical reinforcement by graphene and carbon nanotubes in polymer nanocomposites. *Nanoscale*, 2020, 12(4),2228-2267. https://doi.org/10.1039/C9NR06952F
13. Altammar KA. A review on nanoparticles: Characteristics, synthesis, applications, and challenges. *Front. Microbiol.*, 2023, 14(1), 1155622. https://doi.org/10.3389/fmicb.2023.1155622
14. Procter P, Solc J, "Improved Thermal Conductivity in Microelectronic Encapsulants", 1991 Proceedings 41st Electronic Components & Technology Conference, Atlanta, GA, 1991, pp 835-842 https://doi.org/10.1109/ectc.1991.163976
15. Yousefi F, Mousavi SB, Heris SZ, Naghash-Hamed S. UV-shielding properties of a cost-effective hybrid PMMA-based thin film coatings using TiO_2 and ZnO nanoparticles: A comprehensive evaluation. *Sci. Rep.*, 2023,13(1),7116. https://doi.org/10.1038/s41598-023-34120-z
16. Ganguli P, Chaudhuri S. Nanomaterials in antimicrobial paints and coatings to prevent biodegradation of man-made surfaces: A review. *Mater. Today: Proc.*, 2021, 45(1), 3769-3777. https://doi.org/10.1016/j.matpr.2021.01.275
17. Nazari MH, Zhang Y, Mahmoodi A, Xu G, Yu J, Wu J, Shi X. Nanocomposite organic coatings for corrosion protection of metals: A review of recent advances. *Prog. Org. Coat.*, 2022, 162(1), 106573. https://doi.org/10.1016/j.porgcoat.2021.106573
18. Ezzeddin B, Al-khalidi MTA. An investigation into the effect of using different metal oxide nanoparticles on the anti-corrosion properties of coatings: A comparative study. *Moroccan J. Chem.*, 2023, 12(2), 657-675. https://doi.org/10.48317/IMIST.PRSM/morjchem-v12i2.43008
19. Gao Z, Sun C, Du L, Yang D, Zhang X, An Z. The corrosion resistance of graphene-modified oily epoxy coating on AZ31 magnesium alloys. *Front. Mater.*, 2021, 8(1), 739334. https://doi.org/10.3389/fmats.2021.739334
20. Xu HY, Lu D, Han X. Graphene-induced enhanced anticorrosion performance of waterborne epoxy resin coating. *Front. Mater. Sci.*, 2020, 14(1),211-220. https://doi.org/10.1007/s11706-020-0507-7
21. Suharyadi H, Soegiarto TS, Wardhana AS, Umam MF. The effect of graphene-epoxy coatings on anti-corrosion performance for heat exchanger. *J. Eng. Sci. Technol., Spec. Issue*, 2023, 18(4), 179-187. https://jestec.taylors.edu.my/Special%

20Issue%20ICIST%202022_2/ICIST_2_14.pdf
22. Prasetya NB, Ajizan AI, Widodo DS, Ngadiwiyana N, Gunawan G. A polyeugenol/graphene composite with excellent anti-corrosion coating properties. *Mater. Adv.*, 2023, 4(1), 248-55. https://doi.org/10.1039/D2MA00875K
23. Chen Y, Wu L, Yao W, Chen Y, Zhong Z, Ci W, Wu J, Xie Z, Yuan Y, Pan F. A self-healing corrosion protection coating with graphene oxide carrying 8-hydroxyquinoline doped in layered double hydroxide on a micro-arc oxidation coating. *Corros. Sci.*, 2022, 194,109941. https://doi.org/10.1016/j.corsci.2021.109941
24. Li B, Xue S, Mu P, Li J. Robust self-healing graphene oxide-based superhydrophobic coatings for efficient corrosion protection of magnesium alloys. *ACS Appl. Mater. Interfaces*, 2022,14(26),30192-30204. https://doi.org/10.1021/acsami.2c06447
25. Wu W, Chu L, Garcia SJ, van der Zwaag S, Li M, Shen L, Bao N. Fabrication of graphene oxide-modified self-healing microcapsules for Cardanol-based epoxy anti-corrosion coatings. *Prog. Org. Coat.*, 2023,183,107777. https://doi.org/10.1016/j.porgcoat.2023.107777
26. Jiang F, Zhao W, Wu Y, Dong J, Zhou K, Lu G, Pu J. Anti-corrosion behaviors of epoxy composite coatings enhanced via graphene oxide with different aspect ratios. *Prog. Org. Coat.*, 2019, 127, 70-79. https://doi.org/10.1016/j.porgcoat.2018.11.008
27. Yang S, Zhu S, Hong R. Graphene oxide/polyaniline nanocomposites used in anticorrosive coatings for environmental protection. *Coatings*, 2020,10(12),1215. https://doi.org/10.3390/coatings10121215
28. Irfan M, Bhat SI, Ahmad S. Reduced graphene oxide reinforced waterborne soy alkyd nanocomposites: Formulation, characterization, and corrosion inhibition analysis. *ACS Sustainable Chem. Eng.*, 2018, 6(11), 14820-14830. https://doi.org/10.1021/acssuschemeng.8b03349
29. Huang JQ, Liu K, Song X, Zheng G, Chen Q, Sun J, Jin H, Jiang L, Jiang Y, Zhang Y, Jiang P. Incorporation of Al_2O_3, GO, and Al_2O_3@GO nanoparticles into water-borne epoxy coatings: Abrasion and corrosion resistance. *RSC Adv.*, 2022, 12(38), 24804-24820. doi: 10.1039/d2ra04223a
30. Kong H, Luo X, Zhang P, Feng J, Li P, Hu W, Wang X, Liu X. Self-healing, solvent-free, anti-corrosion coating based on skin-like polyurethane/carbon nanotubes composites with real-time damage monitoring. *Nanomaterials*, 2022,13(1),124. https://doi.org/10.3390/nano13010124
31. Nayak SR, Mohana KN, Hegde MB, Rajitha K, Madhusudhana AM, Naik SR. Functionalized multi-walled carbon nanotube/polyindole incorporated epoxy: An effective anti-corrosion coating material for mild steel. *J. Alloys Compd.*, 2021, 856, 158057. https://doi.org/10.1016/j.jallcom.2020.158057
32. Al-Gamal AG, Farag AA, Elnaggar EM, Kabel KI. Comparative impact of doping nano-conducting polymer with carbon and carbon oxide composites in alkyd binder as anti-corrosive coatings. *Compos. Interfaces*, 2018, 25(11), 959-

980. https://doi.org/10.1080/09276440.2018.1450578
33. Calabrese L, Khaskoussi A, Proverbio E. Wettability and anti-corrosion performances of carbon nanotube-silane composite coatings. *Fibers*, 2020, 8(9), 57. https://doi.org/10.3390/fib8090057

The AIC Code of Ethics

Approved by the AIC Board of Directors, April 29, 1983

The profession of chemistry is increasingly important to the progress and the welfare of the community. The Chemist is frequently responsible for decisions affecting the lives and fortunes of others. To protect the public and maintain the honor of the profession, the American Institute of Chemists has established the following rules of conduct. It is the Duty of the Chemist:

1. To uphold the law; not to engage in illegal work nor cooperate with anyone so engaged;

2. To avoid associating or being identified with any enterprise of questionable character;

3. To be diligent in exposing and opposing such errors and frauds as the Chemist's special knowledge brings to light;

4. To sustain the institute and burdens of the community as a responsible citizen;

5. To work and act in a strict spirit of fairness to employers, clients, contractors, employees, and in a spirit of personal helpfulness and fraternity toward other members of the chemical profession;

6. To use only honorable means of competition for professional employment; to advertise only in a dignified and factual manner; to refrain from unfairly injuring, directly or indirectly, the professional reputation, prospects, or business of a fellow Chemist, or attempting to supplant a fellow chemist already selected for employment; to perform services for a client only at rates that fairly reflect costs of equipment, supplies, and overhead expenses as well as fair personal compensation;

7. To accept employment from more than one employer or client only when there is no conflict of interest; to accept commission or compensation in any form from more than one interested party only with the full knowledge and consent of all parties concerned;

8. To perform all professional work in a manner that merits full confidence and trust; to be conservative in estimates, reports, and testimony, especially if these are related to the promotion of a business enterprise or the protection of the public interest, and to state explicitly any known bias embodied therein; to advise client or employer of the probability of success before undertaking a project;

9. To review the professional work of other chemists, when requested, fairly and in confidence, whether they are:
    a. subordinates or employees
    b. authors of proposals for grants or contracts
    c. authors of technical papers, patents, or other publications
    d. involved in litigation;

10. To advance the profession by exchanging general information and experience with fellow Chemists and by contributing to the work of technical societies and to the technical press when such contribution does

not conflict with the interests of a client or employer; to announce inventions and scientific advances first in this way rather than through the public press; to ensure that credit for technical work is given to its actual authors;

11. To work for any client or employer under a clear agreement, preferable in writing, as to the ownership of data, plans, improvements, inventions, designs, or other intellectual property developed or discovered while so employed, understanding that in the absence of a written agreement:
    a. results based on information from the client or employer, not obtainable elsewhere, are the property of the client or employer
    b. results based on knowledge or information belonging to the Chemist, or publicly available, are the property of the Chemist, the client or employer being entitled to their use only in the case or project for which the Chemist was retained
    c. all work and results outside of the field for which the Chemist was retained or employed, and not using time or facilities belonging to a client or employer, are the property of the Chemist;

12. Special data or information provided by a client or employer, or created by the Chemist and belonging to the client or employer, must be treated as confidential, used only in general as a part of the Chemist's professional experience, and published only after release by the client or employer;

13. To report any infractions of these principles of professional conduct to the authorities responsible for enforcement of applicable laws or regulations, or to the Ethics Committee of The American Institute of Chemists, as appropriate.

The Chemist
Journal of the American Institute of Chemists

Manuscript Style Guide

The Chemist is the official online refereed journal of The American Institute of Chemists (AIC). We accept submissions from all fields of chemistry defined broadly (e.g., scientific, educational, socio-political). *The Chemist* will not consider any paper or part of a paper that has been published or is under consideration for publication anywhere else. The editorial office of *The Chemist* is located at: The American Institute of Chemists, Inc. 315 Chestnut Street Philadelphia, PA 19106-2702, Email: aicoffice@theaic.org.

Categories of Submissions

RESEARCH PAPERS

Research Papers (up to ~5000 words) that are original will only be accepted. Research Papers are peer-reviewed and include an abstract, an introduction, up to 5 figures or tables, sections with brief subheadings and a maximum of approximately 30 references.

REPORTS

Reports (up to ~3000 words) present new research results of broad interest to the chemistry community. Reports are peer- reviewed and include an abstract, an introductory paragraph, up to 3 figures or tables, and a maximum of approximately 15 references.

BRIEF REPORTS

Brief Reports (up to ~1500 words) are short papers that are peer-reviewed and present novel techniques or results of interest to the chemistry community.

REVIEW ARTICLES

Review Articles (up to ~6000 words) describe new or existing areas of interest to the chemistry community. Review Articles are peer-reviewed and include an abstract, an introduction that outlines the main point, brief subheadings for each section and up to 80 references.

LETTERS

Letters (up to ~500 words) discuss material published in The Chemist in the last 8 months or issues of general interest to the chemistry community.

BOOK REVIEWS

Book Reviews (up to ~ 500 words) will be accepted.

Manuscript Preparation

RESEARCH PAPERS, REPORTS, BRIEF REPORTS & REVIEW ARTICLES

- **The first page** should contain the title, authors and their respective institutions/affiliations and the corresponding author. The general area of chemistry the article represents should also be indicated, i.e. General Chemistry, Organic Chemistry, Physical Chemistry, Chemical Education, etc.

- **Titles** should be 55 characters or less for Research Papers, Reports, and Brief Reports. Review articles should have a title of up to 80 characters.

- **Abstracts** explain to the reader why the research was conducted and why it is important to the field. The abstract should be 100-150 words and convey the main point of the paper along with an outline of the results and conclusions.

- **Text** should start with a brief introduction highlighting the paper's significance and should be understood to readers of all chemistry disciplines. All symbols, abbreviations, and acronyms should be defined the first time they are used. All tables and figures should be cited in numerical order.

- **Units** must be used appropriately. Internationally accepted units of measurement should be used in conjunction with their numerical values. Abbreviate the units as shown: cal, kcal, µg, mg, g (or gm), %, ^{o}C, nm, µm (not m), mm, cm, cm^{3}, m, in. (or write out inch), h (or hr), min, s (or sec), ml [write out liter(s)], kg. Wherever commonly used units are used their conversion factors must be shown at their first occurrence. Greek symbols are permitted as long as they show clearly in the soft copy.

- **References and notes** should be numbered in the order in which they are cited, starting with the text and then through the table and figure legends. Each reference should have a unique number and any references to unpublished data should be given a number in the text and referred to in the references. References should follow the standards presented in the AIC Reference Style Guidelines below.

REFERENCE STYLE GUIDELINES

References should be cited as numbers within square brackets [] at the appropriate place in the text. The reference numbers should be cited in the correct order throughout the text (including those in tables and figure captions, numbered according to where the table or figure is designated to appear). The references themselves are listed in numerical order at the end of the final printed text along with any Notes. Journal abbreviations should be consistent with those presented in Chemical Abstracts Service Source Index (CASSI) (http://www.cas.org) guide available at most academic libraries.

- **Names** and initials of all authors should always be given in the reference and must not be replaced by the phrase *et al*. This does not preclude one from referring to them by the first author, et al in the text.

- **Tables** should be in numerical order as they appear in the text and they should not duplicate the text. Tables should be completely understandable without reading the text. Every table should have a title. Table titles should be placed above the respective tables.

  Table 1. Bond Lengths (Å) of 2-aminophenol

- **Figure legends** should be in numerical order as they appear in the text. Legends should be limited to 250 words.

  Figure 1. PVC Melt Flow Characterized by Analytical Structural Method

- **Letters and Book Reviews** should be clearly indicated as such when being submitted. They are not peer-reviewed and are published as submitted. Legends should be placed after/under the respective figures.

- **Journals -** The general format for citations should be in the order: **author(s), journal, year, volume, page**. Page number ranges are preferred over single values, but either format is acceptable. Where page numbers are not yet known, articles may be cited by DOI (Digital Object Identifier). For example:

  Booth DE, Isenhour TL. *The Chemist*, 2000, 77(6), 7-14.

- **Books -** For example:

  Turner GK in *Chemiluminescence: Applications*, ed. Knox Van Dyke, CRC Press, Boca Raton, 1985, vol 1, ch. 3, pp 43-78.

- **Patents** should be indicated in the following form:

  McCapra F, Tutt D, Topping RM, UK Patent Number 1 461 877, 1973.

- **Reports and bulletins, etc. -** For example:

  Smith AB, Jones CD, *Environmental Impact Report for the US*, final report to the National Science Foundation on Grant AAA-999999, Any University, Philadelphia, PA, 2006.

- **Material presented at meetings -** For example:

  Smith AB. Presented at the Pittsburgh Conference, Atlantic City, NJ, March 1983, paper 101.

- **Theses -** For example:

  Jones AB, Ph.D. Thesis, Columbia University, 2004.

- For material presented at a meeting, congress or before a Society, etc., but not published, the following form should be used:

  Jones AB, presented in part at the 20th American Institute of Chemists National Meeting, Philadelphia, PA, June, 2004.

- For material accepted for publication, but not yet published, the following form should be used:

  Smith AB. *Anal. Chem*., in press

- For material submitted for publication but not yet accepted the following form should be used:

  Jones AB, *Anal. Chem*. submitted for publication.

- For personal communications the following should be used:

  Smith AB, personal communication.

- If material is to be published but has not yet been submitted the following form should be used:

  Smith AB, unpublished work.

Reference to unpublished work should not be made without the permission of those by whom the work was performed.

Manuscript Selection

The submission and review process is completely electronic. Submitted papers are assigned by the Editors, when appropriate, to at least two external reviewers anonymously. Reviewers will have approximately 10 days to submit their comments. In selected situations the review process can be expedited. Selected papers will be edited for clarity, accuracy, or to shorten, if necessary. The Editor-in-Chief will have final say over the acceptance of submissions. Most papers are published in the next issue after acceptance. Proofs will be sent to the corresponding author for review and approval. Authors will be charged for excessive alterations at the discretion of the Editor-in-Chief.

Conditions of Acceptance

When a paper is accepted by *The Chemist* for publication, it is understood that:

- Any reasonable request for materials to verify the conclusions or experiments will be honored.

- Authors retain copyright but agree to allow *The Chemist* to exclusive license to publish the submission in print or online.
- Authors agree to disclose all affiliations, funding sources, and financial or management relationships that could be perceived as potential conflicts of interest or biases.
- The submission will remain a privileged document and will not be released to the public or press before publication.
- The authors certify that all information described in their submission is original research reported for the first time within the submission and that the data and conclusions reported are correct and ethically obtained.
- The Chemist, the referees, and the AIC bear no responsibility for accuracy or validity of the submission.

Authorship

By submitting a manuscript, the corresponding author accepts the responsibility that all authors have agreed to be listed and have seen and approved of all aspects of the manuscript including its submission to *The Chemist*.

Submissions

Authors are required to submit their manuscripts, book reviews and letters electronically. They can be submitted via email at aicoffice@theaic.org with "Submission for consideration in *The Chemist*" in the subject line. All submissions should be in Microsoft® Word format.

Copyright Assignment & Warranty Form for The Chemist

It is the policy of *The Chemist* to require all contributors to transfer the copyright for their contributions (hereafter referred to as the manuscript) to The American Institute of Chemists, Inc. (hereafter referred to as The AIC) the official publisher of *The Chemist*. By signing this agreement you assign to The AIC to consider publishing your manuscript the exclusive, royalty-free, irrevocable copyright in any medium internationally for the full term of the copyright. This agreement shall permit The AIC to publish, distribute, create derivative works, and otherwise use any materials accepted for publication in *The Chemist* internationally. A copy of the Copyright and Warranty Form for *The Chemist* will be sent to the author(s) whose manuscript is accepted for publication. The AIC will not publish any accepted manuscript in *The* Chemist without its author(s) fully complying with this requirement.

For further information or if you can any questions please contact the Publisher of *The Chemist* at (215) 873-8224 or via email at publications@theaic.org.

Website: http://www.theaic.org/ Email: aicoffice@theaic.org Phone: 215-873-8224

Announcements

INVITATION TO AUTHORS

Authors are invited to submit manuscripts for ***The Chemist,*** the official online refereed journal of The American Institute of Chemists (AIC). We accept submissions from all fields of chemistry defined broadly (e.g., scientific, educational, socio-political). *The Chemist* will not consider any paper or part of a paper that has been published or is under consideration for publication anywhere else.

Research Papers (up to ~5000 words) that are original will only be accepted. Research Papers are peer-reviewed and include an abstract, an introduction, up to 5 figures or tables, sections with brief subheadings and a maximum of approximately 30 references.

Reports (up to ~3000 words) present new research results of broad interest to the chemistry community. Reports are peer- reviewed and include an abstract, an introductory paragraph, up to 3 figures or tables, and a maximum of approximately 15 references.

Brief Reports (up to ~1500 words) are short papers that are peer-reviewed and present novel techniques or results of interest to the chemistry community.

Where to Send Manuscripts?

Please submit your manuscripts by email (aicoffice@theaic.org) to the attention of:

The Editor-in-Chief, The Chemist
The American Institute of Chemists, Inc.
315 Chestnut Street,
Philadelphia, PA 19106-2702
Email: aicoffice@theaic.org

Review Articles (up to ~6000 words) describe new or existing areas of interest to the chemistry community. Review Articles are peer-reviewed and include an abstract, an introduction that outlines the main point, brief subheadings for each section and up to 80 references.

Letters (up to ~500 words) discuss material published in *The Chemist* in the last 8 months or issues of general interest to the chemistry community.

Book Reviews (up to ~ 500 words) will be accepted.

American Institute of Chemists

www.TheAIC.org

From its earliest days in 1923 to the present, the American Institute of Chemists has fostered the advancement of the chemical profession in the United States.

The Institute has a corresponding dedication "to promote and protect the public welfare; to establish and maintain standards of practice for these professions; and to promote the professional experience through certification as to encourage competent and efficient service."

The AIC engages in a broad range of programs for professional enhancement through the prestigious Fellow membership category, awards program, certification programs, meetings, publications and public relations activities.

Advertising: Send insertion orders and advertising materials to AIC.
Visit The AIC Web Site for additional information at www.TheAIC.org

The American Institute of Chemists, Inc.
315 Chestnut Street, Philadelphia, PA 19106-2702.
Phone: (215) 873-8224 | Fax: (215) 629-5224 | E-mail: aicoffice@TheAIC.org